Luminescence dating of eolian and fluvial archives in the Middle and Lower Danube catchment and the paleoenvironmental implications

From the Faculty of Georesources and Materials Engineering of the
RWTH Aachen University

Submitted by

Janina Johanna Bösken M.Sc.
from Düsseldorf

in respect of the academic degree of
Doctor of Natural Sciences
approved thesis

Advisors: Univ.-Prof. Dr. rer. nat. Frank Lehmkuhl
Univ.-Prof. Dr. rer. nat. Helmut Brückner

Date of the oral examination: 19th July 2017

Contents

List of Figures

List of Tables

List of Abbreviations

AC	alternating current
$A-CN-K$-diagram	$Al_2O_3-(Na_2O+CaO^*)-K_2O$ - diagram
ALPCAPA	Alpine-Carpathian-Pannon (Mega-unit)
AMH	anatomically modern human
AMS	Anisotropy of magnetic susceptibility
BKT	Bodrogkeresztúr
BP	years before present (refers to radiocarbon ages)
cal BP	calibrated years before present (refers to radiocarbon ages)
CAM	Central Age Model
CBD	Carpatho-Balkan-Dinaric (region)
χ	magnetic susceptibility
χ_{fd}	frequency dependence of magnetic susceptibility
CIA	Chemical Index of Alteration
C-L	sample code Cologne-Luminescence Laboratory
COM	Common Age Model
CPA	Chemical Proxy of Alteration
CW	countinous-wave
D_0	characteristic saturation dose
D_{cosmic}	cosmic dose rate
D_e	equivalent dose
DIN	Deutsches Institut für Normung (German Organization for Standardization)
DR	dose rate
DRAC	Dose Rate and Age Calculator
DRC	dose response curve
DRT	dose recovery test
D_{total}	total dose rate
EDPXRF	dispersive X-ray fluorescence polarization energy
exp	exponential fitting
exp+lin	exponential plus linear fitting
FWHM	full width at half maximum
GS	grain size
Gy	Gray
hrs / h	hours
IRSL	infrared stimulated luminescence
ISO	International Organization for Standardization
ka	thousand years
KFS	kalifeldspar
L1-L3	loess layers
LED	light emitting diodes
LGM	last glacial maximum
L_n	natural luminescence signal
LPS	loess-paleosol sequence
L_x	luminescence signal
MAR	mass accumulation rates
MIS	marine isotope stage
MS	magnetic susceptibility

MS_{fd}	frequency dependence of magnetic susceptibility
MZ	Mollusc Zone
N	particle number
N	natural luminescence signal
n	amount (of aliquots)
NE	northeast
OD	overdispersion
OSL	optically stimulated luminescence
PHT	preheat plateau test
pIRIR	post-infrared infrared stimulated luminescence
PM	polymineral samples
ppm	parts per million
Q	quartz samples
R	regenerated luminescence signal
R	R programm
S0	recent soil
S1-S3	paleosols
SAR	Single Aliquot Regenerative dose protocol
SE	southeast
SI	International System of Units
σ_{fast}	photoionization cross section of the fast component
σ_{medium}	photoionization cross section of the medium component
σ_{slow}	photoionization cross section of the slow component
SRTM	Shuttle Radar Topography Mission (remote sensing data)
TL	thermoluminescence
T_n	testdose response after measurement of the natural signal
T_x	testdose response
W	water content
W_m	measured water content
wt. %	percentage by weight
W_{used}	used water content

Summary

The presented doctoral dissertation uses luminescence dating techniques to reconstruct the paleoenvironmental and paleoclimatic conditions in the Middle and Lower Danube catchments, especially during the period of anatomically modern human emergence. It is embedded in the Collaborative Research Center 806 "Our Way to Europe - Culture-Environment Interaction and Human Mobility in the Late Quaternary". To increase ones understanding of the environmental conditions during the last 150 ka, four loess-paleosol sequences and one fluvial section were investigated. The research area is located at the junction of Atlantic, Mediterranean and continental climatic regimes, which makes it sensitive to climatic changes. Moreover, the geographical position between Asia, Near East and Central Europe and the vast river network connecting these regions, make the area a favorable pathway for anatomically modern human migration. The sediments of the five investigated sites cover various time frames from the penultimate interglacial (MIS 7) to the Holocene. The methodological approach focused on optically stimulated luminescence dating, but for some of the sections the geochronological methods were combined with physical, biological, and geochemical proxy data to reconstruct the paleoenvironmental conditions.

In the Middle Danube Basin three sites were investigated. The Ságvár loess-paleosol sequence is located in the central basin and its sediments accumulated during the last glacial maximum from approximately $25 - 17$ ka. The sequence can be correlated to two Gravettian occupation layers. Paleoenvironmental conditions changed from short grassland ($25 - 24$ ka), to a mosaic of mammoth steppe, forest steppe, continental steppe, and tundra ($25 - 18$ ka), towards continental grassland (< 18 ka). The data indicates that the Gravettian occupation took place during a typically cold LGM phase.

The Bodrogkeresztúr loess-paleosol sequence is located in the foothills of the Carpathians in the northern part of the Middle Danube Basin. It is located in the vicinity of the Gravettian Bodrogkeresztúr-Henye site. The chronological data indicates rather high sediment accumulation rates, in particular between 33.5 ± 2.5 and 28.0 ± 2.1 ka. Moreover, generally more humid conditions during late MIS 3 and early MIS 2 in comparison to other regions in the Carpathian Basin were deduced. Nevertheless, two loess layers with high sand abundance in the profile suggest colder and dryer conditions with increased eolian dynamics during short periods within MIS 2. The findings highlight the unique microclimatic conditions at the foothills of the Carpathian Mountains, which may have offered a favorable environment for Upper Paleolithic populations.

Another research site investigated in the Middle Danube Basin is the Crvenka-At site. This site contains fluvial sediments and Aurignacian artifacts. Investigations here focused on the reconstruction of a geochronology for the Early Upper Paleolithic occupation. The Aurignacian artifacts were found in sediments with an age between 33.9 ± 2.9 ka and 41.3 ± 3.6 ka. This age range fits well to other dated Aurignacian findings in the Banat region and points to a more widespread occurrence of anatomically modern humans in the Banat region during this time frame than previously thought. It demonstrates that not only the upland regions, but also

lowland areas were attractive for early modern human occupation.

Moving to the southern part of the Middle Danube catchment, the Stalać section was investigated. It is located in the interior of the Central Balkan region, south of the typical loess distribution, in a zone of paleoclimatic shifts between continental and Mediterranean climate regimes. Detailed investigations on the luminescence signal of a quartz sample, which is unsuitable for dating, are presented. A firm chronology framing the last two glacial cycles was established using fine-grained polyminerals and the post-infrared infrared stimulated luminescence (pIRIR) protocol. The characteristics of the dated paleosols indicate similar climatic conditions during the last interstadial and interglacial phases, which were different from the penultimate interglacial period.

Finally, the Urluia loess-paleosol sequence in the Lower Danube Basin was investigated. This 16 m long sequence contains one paleosol at the bottom of the profile and a vast accumulation of loess above. The section was dated from 20.98 ± 1.6 ka to 144.9 ± 12.2 ka. While the chronology of the upper 7 m of the section is supported by independent age control in form of the Campanian Ignimbrite / Y-5 tephra, the lower part of the sequence remains less well constrained. A rapid increase in ages between ~7 and 9 m is followed by rather constant ages > 130 ka in the lower 7 m of the profile. These ages are in contrast with the expectation of a well developed MIS 5 paleosol in the lowermost part of the section. Several hypothesis trying to explain these findings were explored, but could not be solved satisfactorily.

The doctoral dissertation demonstrates that a detailed investigation is necessary in order to build robust age models. For quartz samples, the importance of preheat plateau and dose recovery tests are pointed out. Some samples of Stalać and Urluia, that have high equivalent doses, show falling preheat plateaus, while the quartz samples of Crvenka-At are already in saturation at very low doses. These findings indicate that these samples cannot be dated reliably using the SAR protocol. Most samples of this dissertation were dated with the pIRIR protocol. The necessary first IR stimulation temperature tests, dose recovery tests, fading experiments and residual dose measurements are presented. It is demonstrated that polymineral and kalifeldspar samples can be dated with higher doses than quartz. However, it remains unclear up to which dose range age estimates are reliable. E.g. at Urluia, the lowermost samples approach saturation even within the polymineral fraction and at Stalać the lowermost two ages underestimate the accepted correlative stratigraphy.

Overall, this doctoral dissertation highlights the importance of luminescence dating in paleoenvironmental and geoarcheological studies. It demonstrates how the combination of multiple proxy data enhances the paleoenvironmental interpretations, and identifies remaining challenges. The paleoclimatic dynamics in the research area at the junction of Atlantic, Mediterranean and continental climatic regimes are discussed. Finally, paleoenvironmental conditions during phases of Upper Paleolithic occupation were equally diverse highlighting anatomically modern humans' ability to adapt to changing paleoenvironments.

Zusammenfassung

In der vorliegenden Doktorarbeit werden Lumineszenzdatierungsmethoden für die Rekonstruierung der Paläoumwelt- und Paläoklimabedingungen des Einzugsgebiets der mittleren und unteren Donau angewendet. Dies ist besonders für die Migrationsphase des modernen Menschen von Interesse. Die Doktorarbeit ist eingebunden in den Sonderforschungsbereich 806 „Our Way to Europe - Culture-Environment Interaction and Human Mobility in the Late Quaternary“. Um die Umweltbedingungen der letzten 150 *ka* besser zu verstehen, wurden vier Löss-Paläoboden Sequenzen und ein Standort mit fluvialen Sanden untersucht. Im Untersuchungsgebiet herrschen atlantische, mediterrane und kontinentale klimatische Einflüsse vor. Hierdurch eignet sich das Gebiet für die Erforschung vergangener Klimaschwankungen besonders gut. Aufgrund seiner geographischen Position zwischen Asien, Nahost und Mitteleuropa, befindet sich das Untersuchungsgebiet auf einem möglichen Migrationsweg des frühen modernen Menschen. Die Sedimente der fünf untersuchten Standorte wurden in verschiedenen Zeitabschnitten zwischen dem vorletzten Interglazial (MIS 7) und dem Holozän abgelagert. Die methodische Herangehensweise konzentrierte sich auf optisch stimulierte Lumineszenzdatierung. Für einige Standorte wurden diese geochronologischen Methoden mit physikalischen, biologischen und geochemischen Daten kombiniert, um die Paläoumweltbedingungen zu rekonstruieren.

Im mittleren Donaubecken – dem Karpatenbecken – wurden drei Standorte untersucht. Die Löss-Paläoboden Sequenz von Ságvár befindet sich im zentralen Teil des Beckens. Die untersuchten Sedimente wurden während des letzteiszeitlichen Maximums (LGM) von ca. $25 - 17$ *ka* abgelagert und können zu zwei Schichten mit Funden aus dem Gravettien korreliert werden. Die Paläoumweltbedingungen änderten sich von kurzem Grasland ($25 - 24$ *ka*) zu einer Kombination aus Mammutsteppe, Waldsteppe, kontinentaler Steppe und Tundra ($25 - 18$ *ka*), bis zu kontinentalem Grasland (< 18 *ka*). Die Daten zeigen, dass die Kulturschichten des Gravettien während einer typisch kalten LGM-Phase abgelagert wurden.

Die Löss-Paläoboden Sequenz von Bodrogkeresztúr befindet sich im nördlichen Teil des Karpatenbeckens auf den südlichen Ausläufern der Karpaten. In der Nähe findet sich Bodrogkeresztúr-Henye mit Funden aus dem Gravettien. Hohe Sedimentationsraten lassen sich aus den geochronologischen Daten ableiten, vor allem zwischen 33.5 ± 2.5 und 28.0 ± 2.1 *ka*. An diesem Standort herrschten allgemein feuchtere Bedingungen zwischen dem späten MIS 3 und dem frühen MIS 2 im Vergleich zum zentralen und südlichen Teil des Karpatenbeckens. Nichtsdestotrotz zeigen auch zwei grobkörnigere Lössphasen trockenere und kältere Bedingungen mit erhöhter äolischer Aktivität während kurzer Perioden innerhalb des MIS 2 an. Die Untersuchungen heben die einzigartigen mikroklimatischen Bedingungen der Gebirgsausläufer am nördlichen Rand des Karpatenbeckens hervor, welche wahrscheinlich auch für den frühen modernen Menschen vorteilhaft war.

Im Karpatenbecken wurden außerdem noch Sedimente bei Crvenka-At untersucht. Hier lassen sich fluviale Sande und Artefakte aus dem Aurignacien finden. Die Untersuchungen konzentrierten sich auf die Erstellung einer Geochronologie der paläolithischen Funde. Die

Artefakte wurden in Sedimenten mit einem Alter zwischen 33.9 ± 2.9 *ka* und 41.3 ± 3.6 *ka* gefunden. Diese Altersspanne passt gut zu anderen datierten Funden aus dem Aurignacien in der Banatregion. Das spricht für eine weitere Verbreitung des frühen modernen Menschen während dieser Zeit im Banat als vorher angenommen. Außerdem zeigen die Untersuchungen, dass der *Homo sapiens* nicht nur auf geomorphologisch erhöhten Positionen, sondern auch im Flachland lebte.

Weiter im Süden des mittleren Donaueinzugsgebietes wurde die Löss-Paläoboden Sequenz von Stalać untersucht. Sie befindet sich im zentralen Balkan, südlich der typischen Lössverteilung. Das Gebiet ist von paläoklimatischen Wechseln zwischen kontinentalem und mediterranem Klima geprägt. Detaillierte Untersuchungen der Lumineszenzeigenschaften einer problematischen Quarzprobe werden vorgestellt. Für die finale Geochronologie wurden polimineralische Feinkornproben und das pIRIR-Protokoll (post-infrared infrared stimulated luminescence) verwendet. Die Datierungen zeigen, dass die Sequenz die letzten beiden Glazialzyklen umfasst. Die untersuchten Paläoboden deuten auf ähnliche Klimabedingungen während des letzten Interstadials und Interglazials hin und heben hervor, dass während des vorletzten Interglazials deutlich andere Klimabedingungen vorherrschten.

Letztendlich wurde die Löss-Paläoboden Sequenz von Urluia im unteren Donaubecken untersucht. Die 16 Meter hohe Sequenz enthält einen Paläoboden im unteren Teil, der von mehreren Lössschichten bedeckt ist. Die Sequenz wurde auf 20.98 ± 1.6 *ka* bis 144.9 ± 12.2 *ka* datiert. Die Chronologie der oberen 7 m ist durch das Vorhandensein der kampanischen Ignimbrit/Y5-Tephra als unabhängige Alterskontrolle gestützt. Der untere Teil der Sequenz weist allerdings einen starken Altersanstieg zwischen 7 und 9 m und konstante Altersschätzungen in den unteren 7 m des Profils auf. Diese Datierungen widersprechen jedoch der Pedostratigraphie, da der letzte Interglazialboden im unteren Teil des Profils erwartet wird. Mehrere Hypothesen werden dargelegt, aber die Diskrepanz konnte bisher nicht zufriedenstellend geklärt werden.

Die vorliegende Doktorarbeit erläutert, dass detaillierte Untersuchungen nötig sind, um robuste Altersmodelle zu erstellen. Für Quarzproben sind besonders Preheat-Plateau-Tests und Dose-Recovery-Tests von Bedeutung. Einige Proben mit hohen Äquivalenzdosen aus Stalać und Urluia besaßen fallende Vorheiztemperaturplateaus, während andere Proben aus Crvenka-At schon bei sehr geringen Dosen gesättigt waren. Diese Ergebnisse belegen, dass die Proben nicht verlässlich mit dem SAR-Protokoll datiert werden können. Die meisten Proben dieser Doktorarbeit wurden mit dem pIRIR-Protokol untersucht. Hierfür sind First-IR-Stimulation-Temperatur-Tests, Dose-Recovery-Tests, Fadingexperimente und die Messung der Residualdosis von Nöten. Obwohl polimineralische und Kalifeldspatproben mit höheren Dosen als Quarz datiert werden können, wurde auch gezeigt, dass es nicht sicher ist, bis zu welchen Dosen die Altersbestimmungen zuverlässig sind. Beispielsweise unterschätzen die unteren zwei Proben der Stalać-Sequenz die akzeptierte korrelative Stratigraphie. Auch in der Urluia-Sequenz sind die unteren Proben problematisch, weil sie Anzeichen von Sättigung aufweisen.

Insgesamt hebt die Doktorarbeit die Bedeutung von Lumineszenzdatierung in Paläoumwelt- und geoarchäologischen Studien hervor. Es wird gezeigt, wie die Kombinierung von verschiedenen Proxidaten die Interpretation der Paläoumweltbedingungen verbessert und bestehende Schwierigkeiten identifiziert. Die paläoklimatische Dynamik im Untersuchungsgebiet zwischen atlantischen, mediterranen und kontinentalen Klimaeinflüssen wird diskutiert. Letztendlich waren die Paläoumweltbedingungen während der Migrationsphasen des frühen modernen Menschen ebenso divers, welches die Fähigkeit des *Homo sapiens*, sich an unterschiedliche Umwelt- und Klimabedingungen anzupassen, untermalt.

1. Introduction

1.1. Paleoenvironmental research

Paleoenvironmental research investigates the geomorphological, environmental, and climatological conditions of the past. The better these conditions are understood, the more precise predictions of future climate developments can be made. Climate change is one of the global challenges of the 21st century, and therefore it is essential to increase ones understanding of atmospheric circulation patterns, climate responses and feedbacks, and their effects on humans. Different kinds of archives serve for paleogeographic investigations, e.g. terrestrial, marine, glaciological, and biological records. Those records can give insights into past environmental and climatic conditions by evaluating the information gained by physical, chemical, and biological analyses. One possible terrestrial archive for paleoclimatological reconstruction of the Quaternary are loess deposits. Loess-paleosol sequences can be several tens of meters thick and are widely distributed, as they cover ~10% of the Earth's surface (Pécsi, 1990). Physical and geochemical changes within those profiles may give information on pedogenesis, transport dynamics, weathering processes, sediment variability and provenance, among others.

For a chronological placement of this information, different dating techniques are available. Radiocarbon, Argon-Argon, and luminescence dating are among the most applied absolute dating methods, while paleopedological stratigraphy is an example for relative age determination. The method of choice depends on the available material and its characteristics. For terrestrial sediments such as loess or sands, luminescence dating and occasionally radiocarbon dating are the used absolute dating techniques. While radiocarbon dating is a very precise dating technique, luminescence dating is applicable to a wider range of materials and a longer time frame.

In loess deposits, the research of environmental and climatic conditions during the Quaternary is often combined with archeological studies. It is generally assumed that environmental and climatic conditions influence human migration, but the extent of which is a matter of debate. As a contribution to paleoenvironmental research in connection with modern humans' dispersal in Europe, the presented doctorate dissertation concentrates on luminescence dating of loess-paleosol sequences. It is part of a collaborative research center, which is presented in the next section, followed by the research goal and questions, and an outline of the dissertation.

1.2. CRC806 "Our Way to Europe"

This PhD dissertation is embedded in the Collaborative Research Center 806 “Our Way to Europe – Culture-Environment Interaction and Human Mobility in the Late Quaternary”. The project investigates population dynamics and dispersal processes of anatomically modern humans from northeast Africa to central Europe during the last 190 ka. To investigate past anatomically modern human (AMH) migration, but also the past predominant environmental and climatic conditions, archeological and geoscientific methods are combined. One of the key questions is how climatic conditions and changes in predominant climatic conditions affected AMH migration.

The project is divided into several clusters dealing with the ‘source’ area of AMH emergence in Africa (cluster A), the eastern corridor of AMH migration (Middle East, southeastern Europe, cluster B), a possible western corridor of AMH migration (northwest Africa, Iberian Peninsula, cluster C), and central Europe as ‘sink’ area of AMH migration (cluster D). Moreover, cluster E focuses on contextual change and climate modeling, and cluster F combines several dating facilities.

The presented PhD dissertation is part of the B1 project, but is also connected to the Cologne Luminescence Laboratory (project F2). It focuses on the eastern trajectory of AMH dispersal, especially on the Middle Danube Basin (Carpathian Basin) and the Lower Danube Basin. A close collaboration between archeologists and geoscientists allows detailed investigations. This PhD research concentrates on loess-paleosol sequences as paleoenvironmental archive, but also one fluvial archive has been investigated. Five research sites were studied combining luminescence dating with different paleoenvironmental proxies, such as malacology, grain size, geochemistry, rock magnetism, and color. The focus lies in the geochronological aspects of three of the sites, while two sites were investigated with a multi-proxy approach.

1.3. Research goal and questions

The overall aim of the presented doctorate study is to increase ones understanding of the environmental conditions in the Middle and Lower Danube catchments during the last 150 *ka*. For this purpose, four loess-paleosol sequences and one fluvial section have been investigated throughout the research area (Figure 1.1). The doctorate dissertation has a strong focus on the geochronological aspects. Those aspects have been combined with physical, biological, and geochemical proxy data to reconstruct the paleoenvironmental conditions. In one section Aurignacian artifacts were found, and two other sections were correlated to Gravettian findings from previous excavations, allowing a linkage of archeological and geoscientific aspects. In order to approach the overall research goal of understanding the environmental conditions in the Middle and Lower Danube Basins during the last 150 *ka*, the following questions are targeted:

- How can luminescence dating techniques aid reconstructions of the paleoenvironment? Where are its limitations and challenges?

- Which local paleoenvironmental and paleoclimatological conclusions can be drawn from the studied sections?
- What are the overall environmental and climatological implications for the Middle and Lower Danube catchments and how do these relate to anatomically modern human occupation?

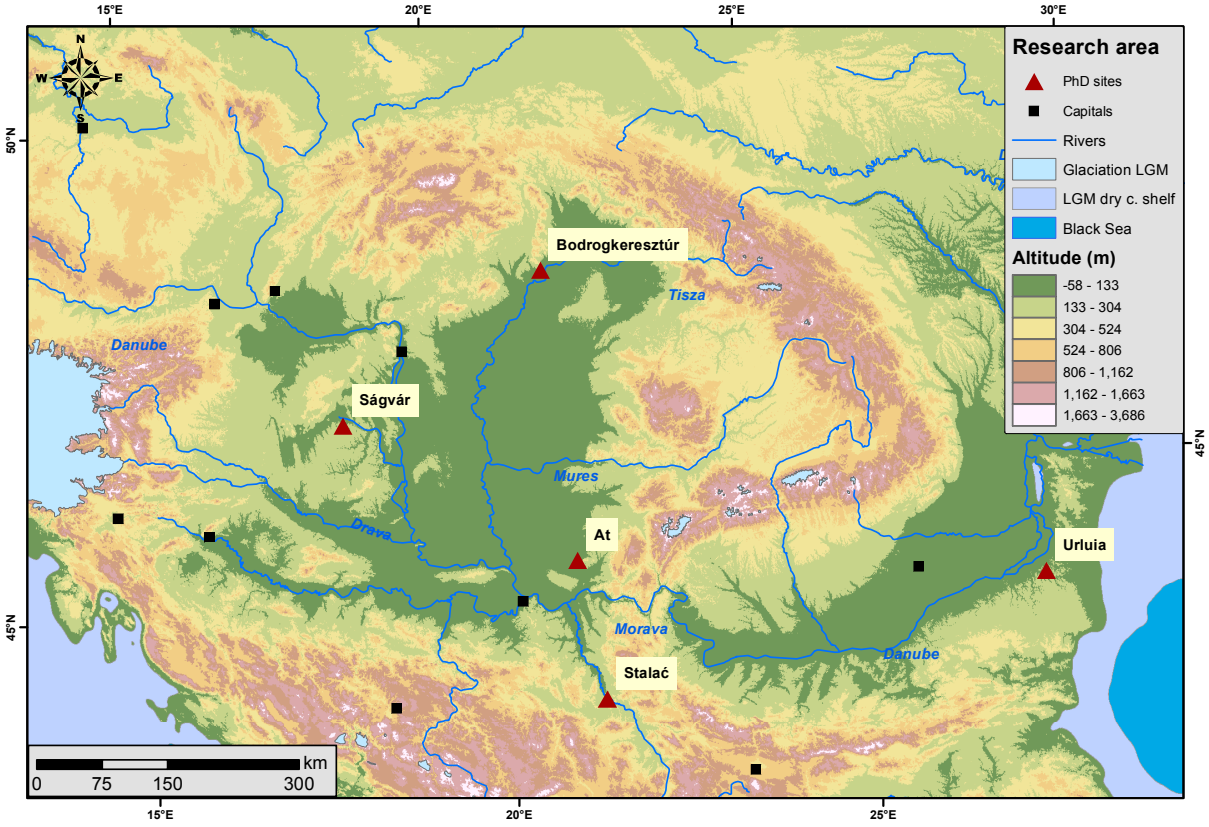

Figure 1.1.: Topographical map showing the location of the research sites Ságvár, Bodrogkeresztúr, At, Stalać, and Urluia. The extent of ice sheets and the dried out continental margins during the last glacial maximum are also indicated. Digital elevation model based on SRTM data available from U.S. Geological Survey (Farr et al., 2007).

1.4. Outline of the dissertation

The dissertation begins with an overview of the geological and geomorphological setting of the research area, and presents the present-day climatological conditions in Chapter 2. Chapter 3 introduces loess research and the distribution of loess deposits. Moreover, a historical overview of definitions on loess is given. Additionally, the chapter gives a short overview of research on anatomically modern humans in the research area. The methodological approaches used in this doctorate dissertation are presented and explained in the fourth chapter.

Chapters 5 - 9 present and discuss the research conducted at the the five investigated sites. Following a northwestern-southeastern gradient the first presented site is Ságvár. Here, the

geoarcheological context of a loess-paleosol sequence close to Lake Balaton in Hungary is investigated. The research focus lies in the environmental variability within the Gravettian settlement during the last glacial maximum and its paleoclimatic conditions. Another loess-paleosol sequence with archeological context is investigated in Chapter 6. It examines the paleoenvironmental conditions in northeastern Hungary at the Bodrogkeresztúr loess-paleosol sequence. This site is located close to the Gravettian Bodrogkeresztúr-Henye site at the foothills of the Carpathian Mountains. The investigated time-frame covers the MIS 3/2 transition and highlights an unique microclimate, which may have offered a favorable environment for Upper Paleolithic populations.

Chapter 7 presents the geochronology of the Crvenka-At site, where numerous Upper Paleolithic artifacts were found, giving it special importance for the collaborative research center. Due to a problematic behavior of the samples, several measurement protocols were tested before a final geochronology was established, putting the artifacts in a chronological context to other findings in the Banat region.

Further to the south of the Middle Danube Basin another loess-paleosol sequence was investigated. Chapter 8 presents the new geochronology of the Stalać sequence and demonstrates the challenges in dating rather old sediments. First paleoenvironmental implications for this research site are also given, which lies in a zone of paleoclimatic shifts between continental and Mediterranean climate regimes. The occurrence of two tephras give further time markers for the geochronology of the section. The fifth research site is presented in Chapter 9. The Urluia site is located in the Dobrogea region, thereby extending the research area to the Lower Danube Basin. The geochronological challenges in the investigation of the 16 m long loess-paleosol sequence are shown by investigating polymineral and quartz samples and their saturation characteristics.

A synthesis of the doctoral dissertation can be found in Chapter 10.

2. Regional setting

The investigated research sites are located in the Middle and Lower Danube catchments in southeastern Europe. The Carpathian Basin or Middle Danube Basin is surrounded by several mountains ranges: the Alps in the West, the Carpathians in the North and East, and the Dinarids and Balkan Mountains in the South. The Lower Danube Basin is located in the East of the Middle Danube Basin between the Arc of the Carpathian Mountains and the Black Sea. Both Basins are connected by the Danube River as main discharge system. The Danube River is the second largest river in Europe with a total length of approximately 2800 km from its source in the Black Forest to its delta at the Black Sea. The landscape of the research area is highly affected by the orogenic and fluvial systems. Therefore, the main geological and geomorphological characteristics are presented in the following. First, the geology is described briefly within the borders of the Carpathian-Balkan-Dinaric mountain systems as main geological units. Due to the size of the research area, the description of the geomorphology in the subsequent section concentrates on Hungary, Serbia, and Romania, as all research sites are located within these countries.

2.1. Geology and tectonics

The Carpatho-Balkan-Dinaric (CBD) region is part of the Mediterranean mountain system and formed during the Alpine orogeny (Haas, 2012). The evolution of the Atlantic and Tethys ocean systems played a major role during this formation. The main stages of this formation according to Haas (2012) were:

1. Pre-alpine: large parts of the Variscan Belt disjointed from the plate margins and were integrated into the Alpine orogenic system;
2. Oceanic basins opened in the early stages of the Alpine plate tectonic cycle (Middle Triassic – Early Cretaceous): the Neotethys ocean basin and the Penninic branch of the Atlantic Ocean formed;
3. Orogeny: closure of Neothetys and the Penninic branch during Jurassic-Miocene;
4. Formation of molasse basins in the foreland of alpine nappe stacks and in back-arc setting (related to subduction of the European plate) in the Late Tertiary.

The structural units of the Carpatho-Balkan-Dinaric region comprise the Alpine-Carpathian foredeep molasse basins, the Alpine Mountain system (Alps, Carpathians, Balkanides), the Dinaric Mountain System (Appenides, Southern Alps, Dinarides, Hellenides) that formed along the margin of the Adriatic microplate, and the internal molasse basins (Haas, 2012). The

Carpathian Basin, which is one of the focus regions in this dissertation, consists of several basins that are separated by smaller ranges. The basement of the basin contains the Tisza and ALPCAPA (Alpine-Carpathian-Pannon) Mega-units with very different geological structures (see Haas, 2012, for more detail). The Early Tertiary in the Carpathian Basin was characterized by strike-slip movement and opposed rotation of the Mega-units (Csontos et al., 1992; Fodor et al., 1999; Haas, 2012; Márton and Fodor, 2003). The basins formed through subsidence of the Adriatic microplate and rollback of the European subduction slaps causing crustal thinning (Haas, 2012; Horváth et al., 2006). This crustal thinning lead to volcanism and further subsidence accompanied by basin infill during the Miocene. Through the uplift of the Carpathian arc, the connection to the Black Sea was blocked, leading to the formation of Lake Pannon (Haas, 2012; Magyar et al., 1999). The Lake was consequently filled up through Alpine and Carpathian deltas (Juhász et al., 2007) until these fluvial-lacustrine systems were replaced by swamps and wetlands in the Pliocene (Haas, 2012). Further subsidence of the basins began ~5 Ma (Haas, 2012). The Pleistocene and Holocene are characterized by thick fluvial sediments that developed through this subsidence and further uplift of Transdanubia, the western Danube-Tisza Interfluve, and the present day mountain ranges.

2.2. Geomorphology and the Danube River system

The landscape has been determined greatly by the Danube River and its tributaries. The Danube River can be divided into the Upper Danube River from its source in the Black Forest to the Devín Gate (close to Bratislava); the Middle Danube River between the Devín and Iron Gates (Serbian Romanian border); and the Lower Danube River from the Iron Gate to the Black Sea. The focus of this dissertation lies on the Middle and Lower Danube Basins and the description will focus upon these. The water and sediment discharge of the Danube River originates mainly from Austria and Romania due to an increased precipitation in the Alps and Carpathians. Although the solid load of the river contains mainly quartz, different tributaries can be distinguished by their sediments' geochemical composition (Miklánek, 2012). The Middle Danube River has many tributaries, e.g. Váh, Hron, Tisza, Drava, Velika Morava. East of Győr the Danube flows in a braided river system and cuts into deposits of shoal and loess (Miklánek, 2012). Ongoing uplift of the Carpathian Mountains during Pleistocene and Holocene lead to extensive erosion $>$ 250 m at the Iron Gate (Miklánek, 2012). The landscape of the Lower Danube Basin is characterized by the Romanian and Bulgarian lowlands, (loess) plateaus and mountain ranges. Major tributaries of the Lower Danube River are the Timok, Iskar, Olt, Siret, and Prut Rivers. The Lower Danube Basin is bordered by the Southern Carpathians, the Bessarabian upland plateau, the Dobrogea massif and the Balkan Mountains (Miklánek, 2012). Alluvial fans deposited bedload sediments on the footslopes, while suspended load reached the valleys (Miklánek, 2012). This is also reflected in the large amounts of loess deposited in eastern Romania (see Chapter 3.1). The Quaternary was characterized by tectonic and eolian processes: tectonic uplift of the Dobrogea region in the Pleistocene changed the course of the Danube River from south of the plateau to north of it (Miklánek, 2012; Sommerwerk et al., 2009). Nowadays, the Danube River flows in wide, braided river channels before reaching its delta at the Black Sea. The main geomorphological features of the Hungarian, Serbian, and

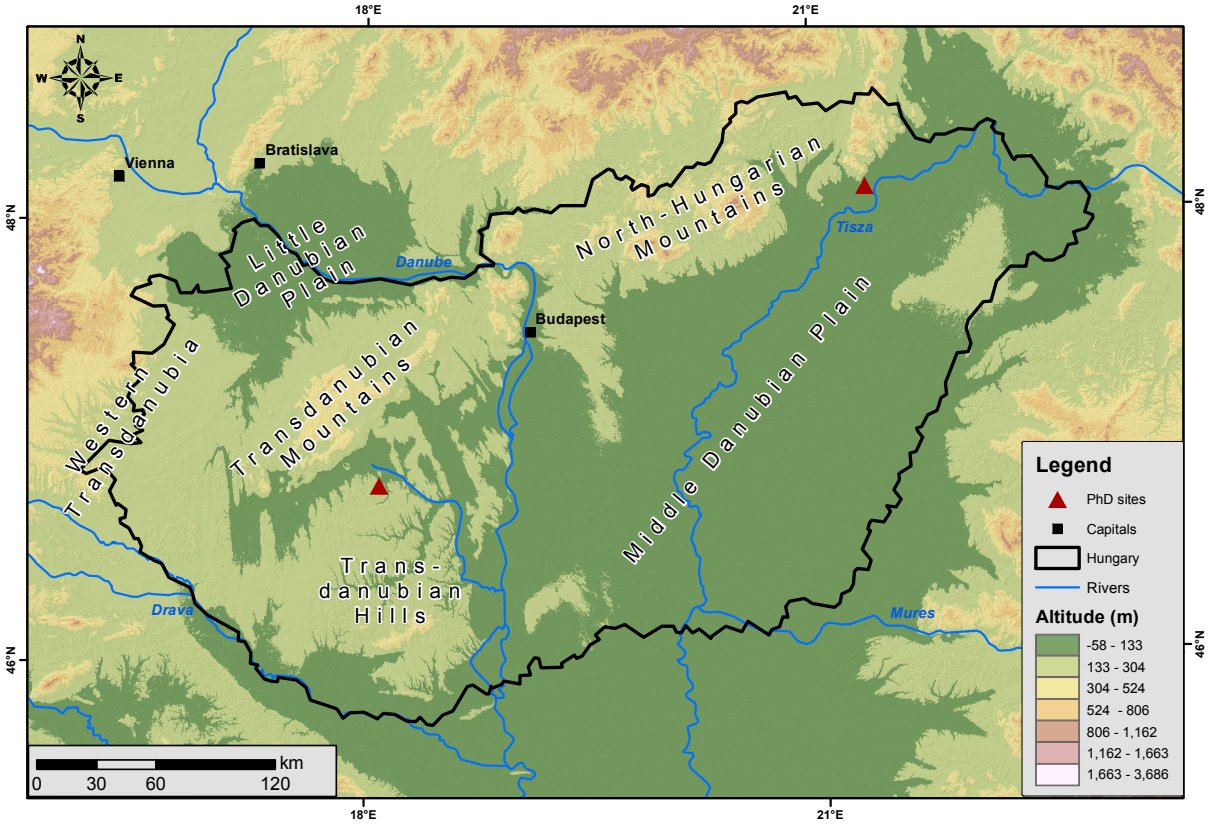

Figure 2.1.: Topographical map of Hungary showing the geomorphological units presented in the text. Digital elevation model based on SRTM data available from U.S. Geological Survey (Farr et al., 2007).

Romanian landscape are presented in the following paragraphs. For more detailed information the reader is referred to the quoted literature.

Hungary comprises six geomorphological units according to Lóczy et al. (2012): 1. the Middle Danubian Plain; 2. the Little Danubian Plain; 3. Western Transdanubia; 4. the Transdanubian Hills; 5. the Transdanubian Mountains; and 6. the North-Hungarian Mountains with intramontane basins (Fig. 2.1). The geomorphology of Hungary is mainly a result of fluvial processes, especially in the lowlands, that led to the formation of the present channels and floodplains. Nowadays water erosion is a large problem on agricultural fields, in particular through the formation of gullies on loess deposits (Lóczy et al., 2012). Features of past wind erosion and dune fields are other important geomorphological landforms. The landscape of mountainous areas in Hungary is characterized by processes of mass movement and karstification (Lóczy et al., 2012).

Serbia is generally divided into the plain of Vojvodina, which is part of the Carpathian Basin, and a hilly-mountainous area south of the Sava and Danube Rivers (Pavlović et al., 2012). Interesting geomorphological features of this hilly-mountainous region are for example paleoabrasion surfaces of the Miocene Pannonian Sea, and north to south oriented graben structures, like the one that carries the Velika and Južna Morava Rivers (Figure 2.2). Moreover, geological units

comprise the tectonically fragmented Serbian-Macedonian Massif, the Carpathian Mountains, the Vadar zone, and the Dinarides (for more detail see Pavlović et al., 2012). Major recent geomorphological processes contain sheet wash (deluvial-proluvial processes), gully erosion, landslides, rock falls, fluvial processes, and karstification (cf. Pavlović et al., 2012). Past geological and geomorphological processes that still influence the landscape today are mainly tectonics and volcanism (see Chapter 2.1). Tectonic processes lead to the formation of horst and graben structures, and depressions. The Fruška Gora (F.G. in Figure 2.2) and the Vršački Breg (V.B.) are examples of horst structures in the Vojvodina region. Other landscape features are conical hills, volcanic necks and calderas, which were formed by late Cretaceous to Pliocene volcanic activity. Furthermore, glacial and eolian processes played a role during the Pleistocene. Eolian activity has formed several loess plateaus and sand dunes (Pavlović et al., 2012), such as the northern Serbian dune fields Deliblatska Peščara (D.P.) and Subotička Peščara (S.P.). These are of Holocene age and were likely still active some centuries ago (Pavlović et al., 2012).

The main geomorphological units of **Romania** are the Eastern and Southern Carpathians, the Banat and Apuseni Mountains, and the Transylvanian Depression (Figure 2.3). Geomorphological processes in Romania comprise mass movements, such as rock fall, debris flows, landslides, and karstic features in the mountains. The rivers are characterized by high discharge and intensive erosional force, while riverbank accumulation is only locally observed (Bălteanu et al., 2012). The Transylvanian depression shows sheet and gully erosion, and the Moldavian Plateau contains features of soil erosion, gullying and landslides (Bălteanu et al., 2012).

2.3. Present climatic conditions

The climate is generally regarded as temperate warm with different subtypes (Niedźwiedź, 2012). However, it is very diverse in the CDB region. This is related to the great extent of the region, that influences the amount of solar irradiation and hours of sunshine, and the orogenic differences that affect temperature, precipitation, and snow cover (Niedźwiedź, 2012). The Western Carpathians are transitional between Atlantic and continental climatic regimes (January temperature -10 – 0°C, summer temperature 15 – 20°C). In the Eastern Carpathians a continental climate with summer temperatures >20°C and a temperature range of 25 K is present (Niedźwiedź, 2012). Generally, continentality increases eastwards while the Atlantic influence diminishes (Marković et al., 2016). The Lower Danube Basin is characterized by dry continental climate (Niedźwiedź, 2012), making the Dobrogea and Danube River delta region one of the driest in Europe with precipitation ~350 mm (Richard et al., 2000, in Marković et al., 2016). The inner Carpathian Basin exhibits warm intermediate climate, while further to the south subtropical climate with mean temperatures > 10°C in the coolest month can be found.

Next to these regional differences, Hess (1965, 1971) also differentiates vertical climatic zones. These zones are further connected to the vegetation belts: the upper tree and snow lines for example correspond to the +2°C and -2°C annual isotherms respectively (Niedźwiedź, 2012). The snow line is lower in the Eastern Carpathians than in all other mountain ranges

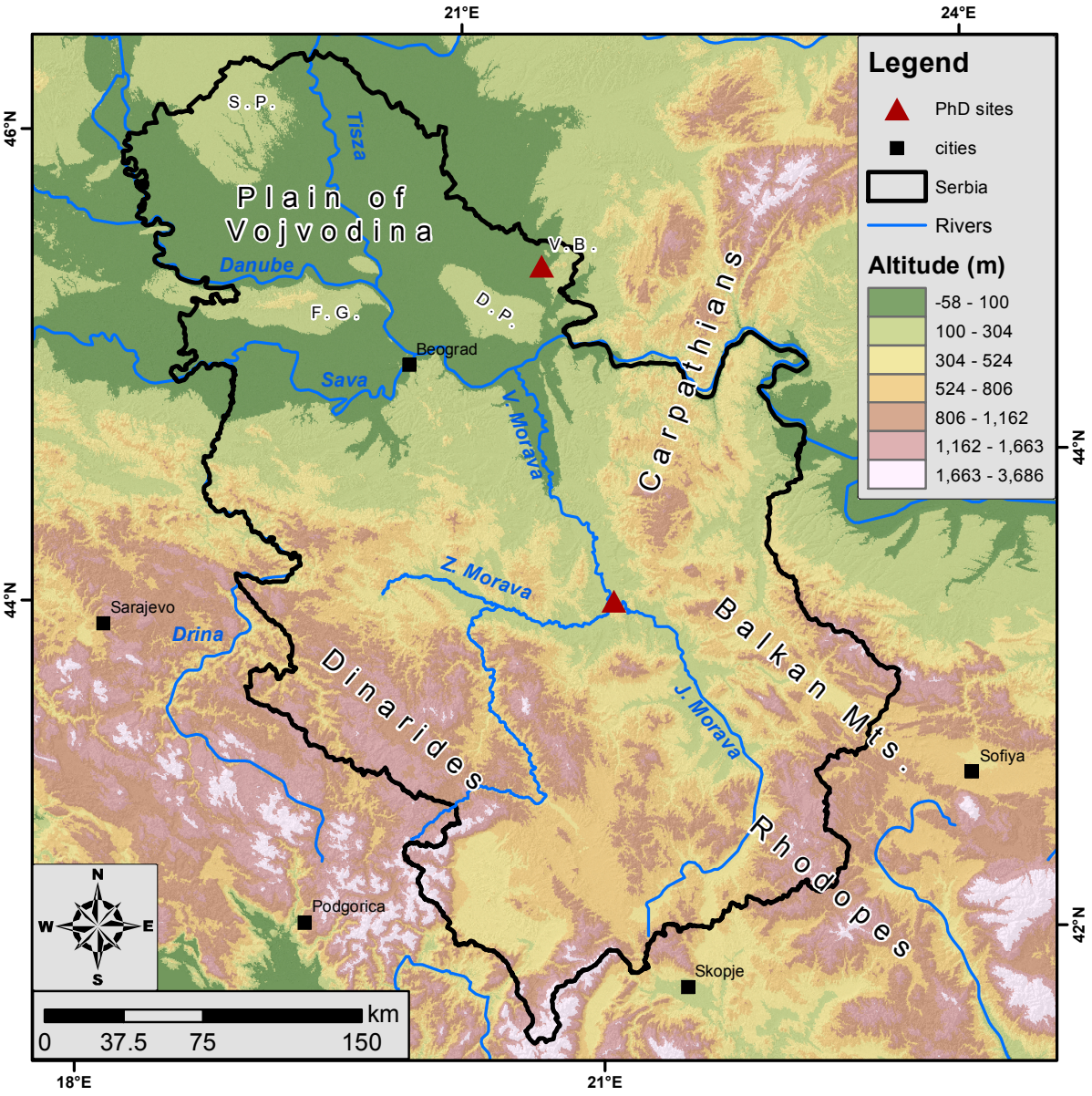

Figure 2.2.: Topographical map of Serbia showing the geomorphological units presented in the text. Digital elevation model based on SRTM data available from U.S. Geological Survey (Farr et al., 2007).

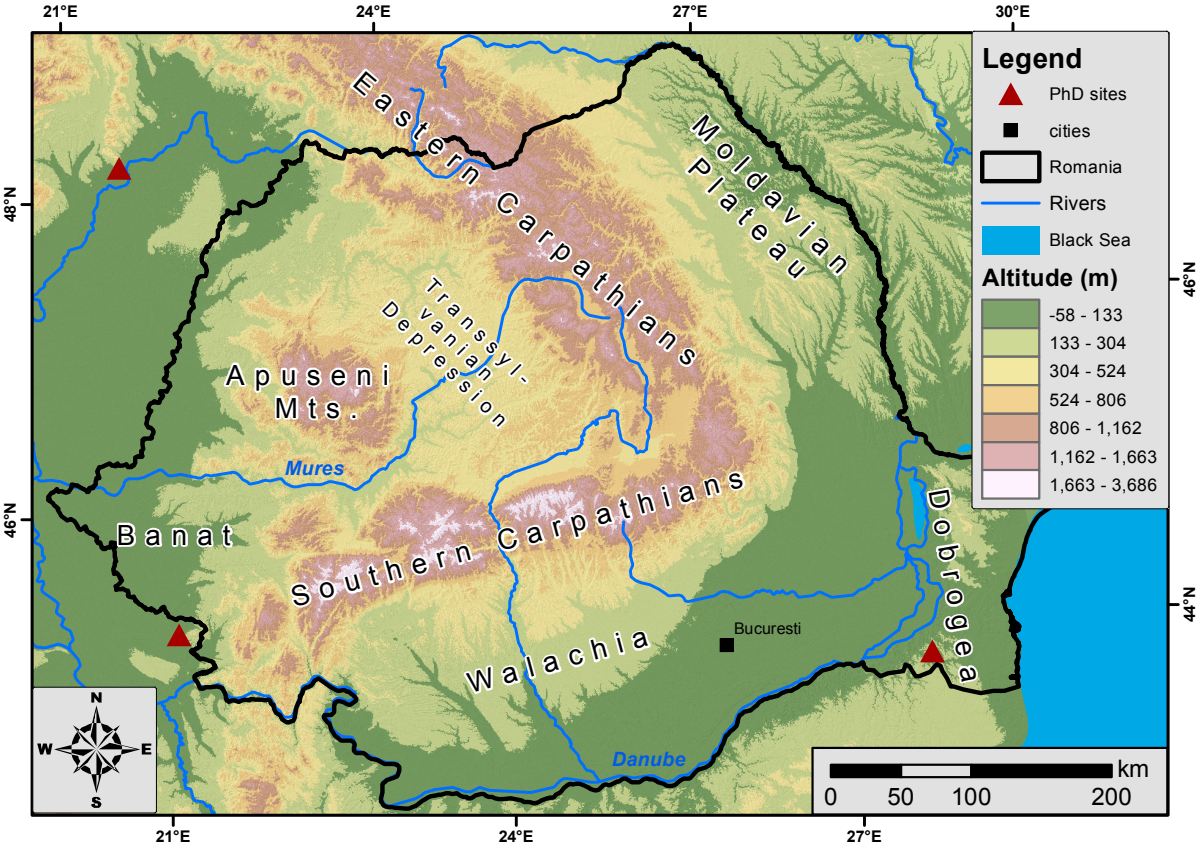

Figure 2.3.: Topographical map of Romania showing the geomorphological units presented in the text. Digital elevation model based on SRTM data available from U.S. Geological Survey (Farr et al., 2007).

of the research area. Contrarily, the upper tree line is lowest in the Northern Carpathians and highest in the Rhodopes. Moreover, the precipitation regimes are rather diverse in the CBD region. The mountains exhibit higher precipitation due to enhanced cloud cover and orographic convection (Barry, 2008; Niedźwiedź, 2012). An exceptionally high precipitation of ~4600 mm encounter the Dinaric Mountains in Montenegro (Furlan, 1977; Niedźwiedź, 2012). Basins located in the rain-shadow of the mountain belts, such as the Niš Basin, receive less precipitation (~500 mm). Also, the Middle Danube Basin and Transylvania are relatively dry with only ~500 mm (Niedźwiedź, 2012).

The current climate in the Middle and Lower Danube Basins between Atlantic, Continental, Mediterranean, and possibly Asian (cf. Marković et al., 2016) climatic influence make the region very interesting for paleoclimate research. Arguably, even small changes in these atmospheric systems might have great impact on the prevailing regional climate (Stevens et al., 2011). This is used in studies that try to reconstruct the past climatic and environmental conditions (see Chapter 3.1.4).

3. State of the art concerning loess and archeological research in the study area

3.1. Overview of loess research

3.1.1. Historical definitions of loess

There are numerous definitions of loess and up to now, none are generally accepted. In the early 19^{th} century, loess was regarded as loamy soil-like sediment of alluvial origin containing mainly silt (Leonhard, 1823; Lyell, 1834). Only later, Richthofen (1882) published the classical eolian theory of loess formation. In the 20^{th} century definitions of loess included weathering or pedogenetic processes, and the term 'loessification' was used to describe the processes that result in the development of the typical structure of loess (Berg, 1916; Russell, 1944), although these are hardly explained in the literature. In the second half of the 20^{th} century, Ložek (1965) emphasized that both eolian and in situ processes are important for its formation, and that loess deposits only developed in glacial times (Sprafke and Obreht, 2016). Later research on ice cores confirmed significantly higher dust deposition rates during glacials (Lambert et al., 2008; Smalley et al., 2011; Thompson and Mosley-Thompson, 1981). These are explained by increased wind speeds, changes in the hydrological cycle, expansion of dust source areas, and effects of low atmospheric carbon dioxide on plant productivity (Harrison et al., 2001; Mahowald et al., 1999; Smalley et al., 2011; Tegen, 2003). Contrarily, G. Kukla (1987) highlights that loess deposits undergo eolian accumulation and certain pedogenetic processes, mainly related to semi-arid continental climates. Further to its eolian deposition, post-depositional processes, such as secondary carbonate formation or other weathering processes, are discussed (Liu, 1988, in Sprafke and Obreht, 2016). Even in more recent years there is a still an ongoing debate about whether 'loess is just the accumulation of dust' (Pye, 1995; Smalley et al., 2011) or not (Pécsi, 1990), its transport processes prior to accumulation (fluvial, eolian), and if it is restricted to periglacial environments (Iriondo and Kröhling, 2007). These are often in reference to the very detailed definition by Pécsi (1990). He defined ten criteria describing loess as a "deposit with coarse silt predominant in grains size, unstratified, porous, permeable, stable in steep walls, easily erodible by water, 'structured light loam' of pale yellow color due to finely dispersed limonite (iron hydroxides), quartz as main mineral constituent (40-80%), subordinate feldspar content, variable amounts of clay minerals (5-20%) and carbonates (1-20%)". According to Pye (1995) there are only three requirements for its formation: a permanent dust source, adequate wind energy for dust transportation, and a suitable site for deposition. He concedes some degree of modification by weathering, reworking and bioturbation, but rejects the process of loessification. Sprafke and Obreht (2016) give an overview of the historic definitions of loess.

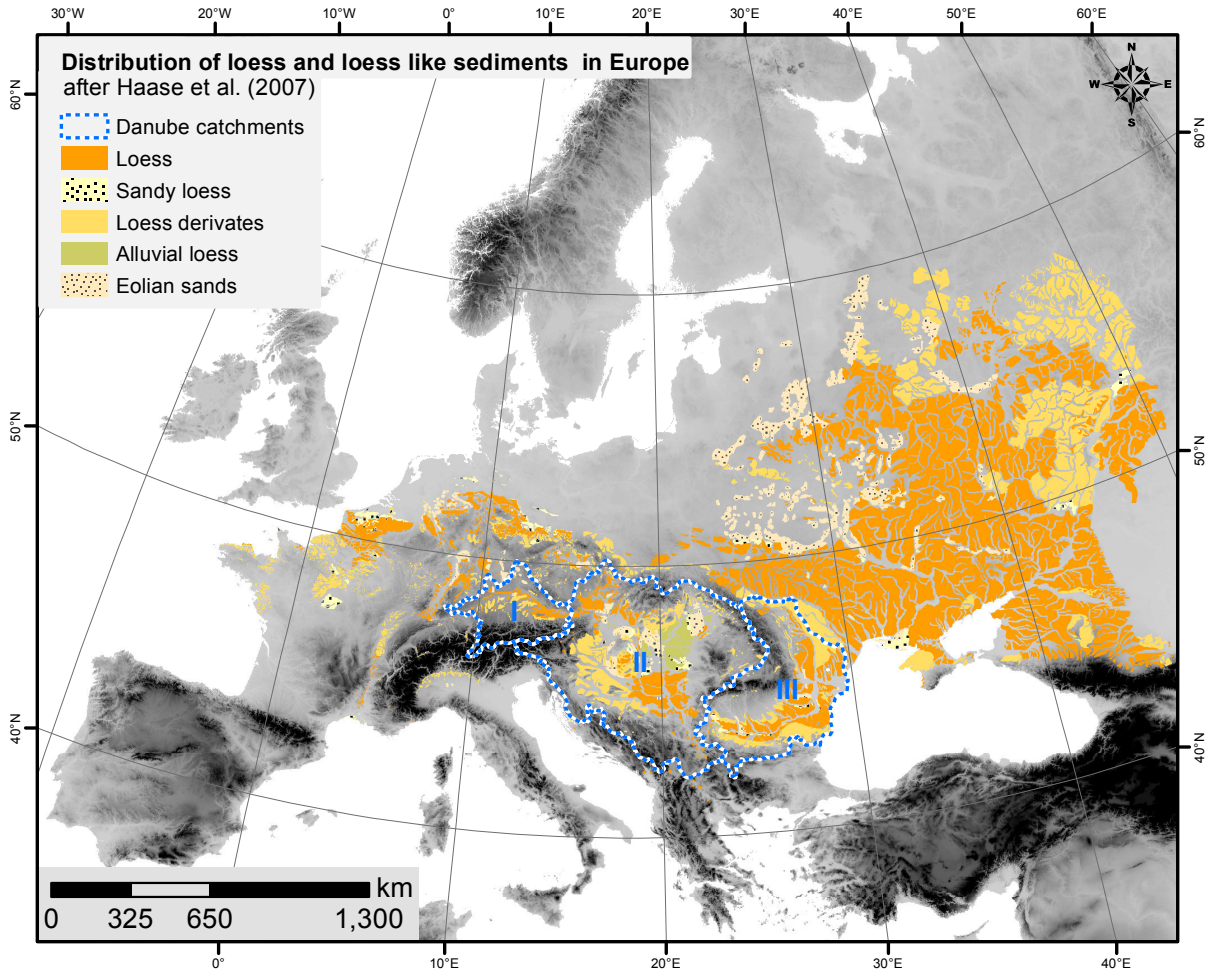

Figure 3.1.: European loess map according to Haase et al. (2007) showing the Upper (I), Middle (II), and Lower (III) Danube catchments. This doctoral dissertation focuses on II and III. Digital elevation model based on SRTM data available from U.S. Geological Survey (Farr et al., 2007).

Nowadays, multidisciplinary research focuses on biological factors of loess formation. Also Svirčev et al. (2013) point out that the essential abiotic factors controlling loess formation are the source dust material, the atmospheric circulation, suitable surface and trapping conditions of the eolian material and the following processes related to typical loess formation. They propose that biological crusted surfaces might be a possible explanation for trapping, accumulation and preservation of the sediments, especially in semi-arid regions.

3.1.2. Distribution of loess deposits

Loess covers ~10% of the Earth's surface (Pécsi, 1990), and is found mainly in former semi-arid, steppe and forest steppe environments that were ice-free during the last glaciation. Most loess deposits formed during Pleistocene glaciations (Pécsi, 1990), but there is also evidence of Miocene Chinese loess deposition (Guo et al., 2002). Loess is not only found in former periglacial areas as so called 'cold loess', but also in semiarid-subhumid zones around deserts as 'warm loess' (or desert loess) after Pécsi (1990). Figure 3.1 shows the distribution of loess and loess-like sediments in Europe according to Haase et al. (2007). Loess occurs often in major river

basins, e.g. along the Rhine and Danube Rivers, implying the importance of loess distribution by rivers (e.g. Smalley et al., 2009). Especially in the Middle and Lower Danube Basins (see Figure 3.1) thick loess deposits are found. Smalley et al. (2009) argue that this is connected to the vast river network that distributes large amounts of alpine sediments, as one of the suggested major sediment sources.

3.1.3. Loess deposits in the research area

The loess deposits in the Middle and Lower Danube Basin are among the thickest and most complete in Europe (e.g. Marković et al., 2016). Figure 3.2 shows their distribution. They have been the focus of recent paleoclimatic research offering quasi-continuous and detailed archives for environmental reconstructions (Frechen et al., 2003; Marković et al., 2005; Stevens et al., 2011). It has been proposed that loess contains local and distant sources that reflect the typical bimodel grain size distribution of mainly silt-sized particles. A possible distant source area of windblown dust in southeastern Europe is the Saharan desert. Modelled values of North African deflation suggests a dust flux around $3.2 - 5.4\ g/m^2a$ into the Carpathian Basin (G. Varga et al., 2016). The authors postulated that interglacial paleosols contain ~20-30% of North African dust. Another discussed source for Danubian loess are reworked Pliocene-Pleistocene Pannonian deposits (B. J. Smith et al., 1991; Stevens et al., 2011).

Loess paleosol sequences (LPS) in the Middle and Lower Danube Basins entail more complete archives than deposits in the Upper Danube Basin, which are often very complex and of minor thickness (cf. Marković et al., 2016). Among the most famous sections are the Hungarian type locations Basaharc, Mende and Paks. The Paks section comprises ~60 m and is classically divided into 'Younger Loess Series' and the 'Older Loess Series' reaching the Brunhes-Matuyama boundary in the latter one (cf. Pécsi, 1979; Thiel et al., 2014). Thiel et al. (2014) correlated the so-called Basaharc Double soil complex to MIS 7, while the underlying sediments could not be dated accurately. In northeastern Hungary, Schatz et al. (2011, 2012, 2015a,b) undertook detailed investigations on the Tokaj section, highlighting the advantages in combining different disciplines and methodologies in a multi-proxy approach. They confirmed a trend of decreasing dust sedimentation from North to South in the Carpathian Basin, and quantified mean annual temperature and precipitation indicating lower temperatures and drier climate during MIS 2 in comparison to MIS 3. Eastern Croatian loess deposits along the Danube are up to 30 m thick and contain 3-4 paleosols. The Zmajevac, Erdut and Šarengard section cover the last ~200 ka, but the sections were also subject to fluvial activity (Galović, 2016). Numerous sections in the Vojvodina region in northern Serbia have been investigated. Here, around 60% of the area is covered by loess deposits, which build thick loess plateaus along the rivers (e.g. Basarin et al., 2014). Among the LPS are the Crvenka (e.g. Stevens et al., 2011), the Ruma (Vandenberghe et al., 2014), the Titel (e.g. Basarin et al., 2014), the Stari Slankamen (e.g. Murray et al., 2014), and the Orlovat (Obreht et al., 2015) sections. Following the Danube downstream, one can find several LPS in the Dobrogea region in eastern Romania. At the Rasova section (Zeeden et al., 2016b) semi-cyclic behavior in the frequency dependent magnetic susceptibility points to millenial-scale climatic variability since the last glacial. Furthermore, a continuous eolian sedimentation was also shown during the Holocene. Particularly thick loess deposits can be

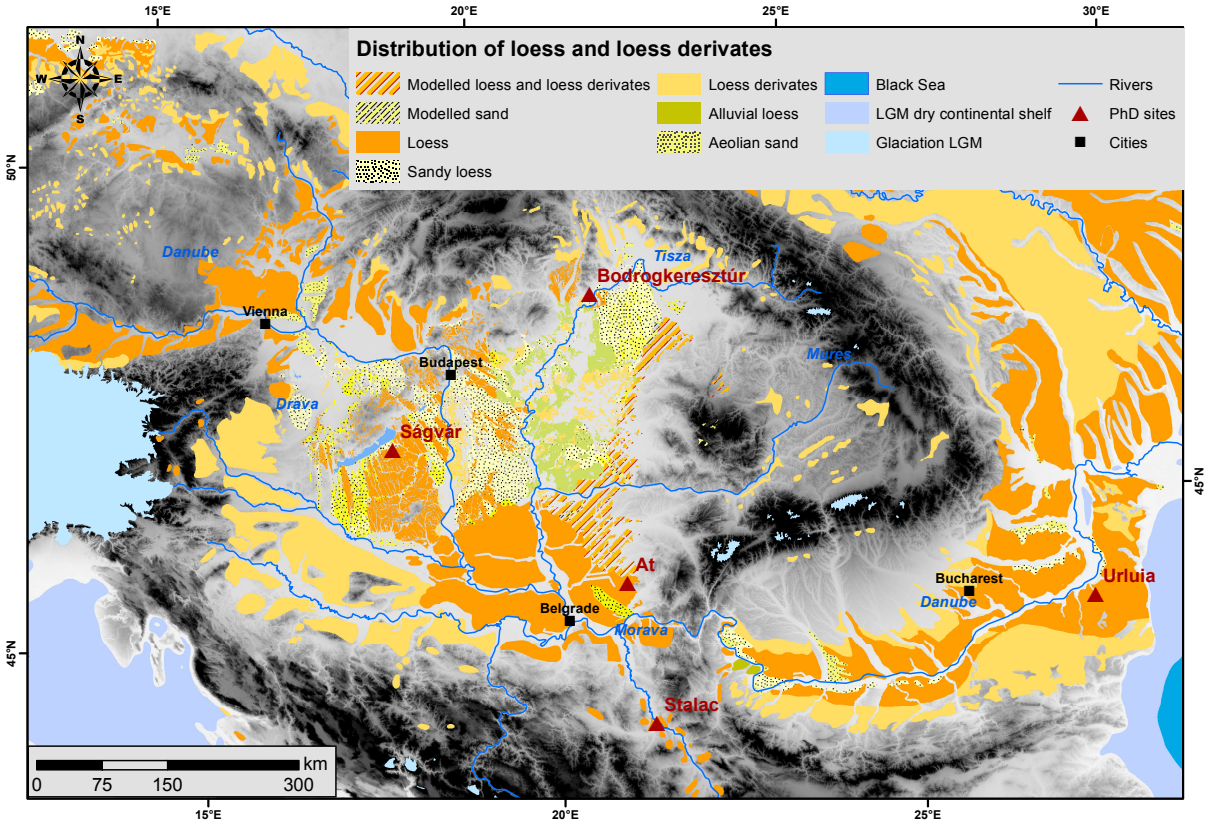

Figure 3.2.: Loess map of the research area showing different types of loess (modified after Gyalog and Síkhegyi, 2005; Haase et al., 2007; Lindner et al., 2017; Vandenberghe et al., 2014) and the location of the research sites. Digital elevation model based on SRTM data available from U.S. Geological Survey (Farr et al., 2007).

found at the Urluia section (Fitzsimmons and Hambach, 2014) that contains the Campanian Ignimbrite tephra. The tephra is widely spread in the region and serves as excellent time-marker; it is dated to 39.28 ± 0.11 ka (De Vivo et al., 2001). Moreover, many Romanian LPS comprise detailed geochronological context by luminescence dating (e.g. Constantin et al., 2015; Timar-Gabor et al., 2012; Vasiliniuc et al., 2013). On the other side of the Danube in Bulgaria LPS have been investigated as well (e.g. Jipa, 2014; Jordanova et al., 2007b). For a historic overview of Danubian loess research the reader is referred to Marković et al. (2016).

3.1.4. Loess-paleosol sequences as terrestrial archive for paleoenvironmental studies

The wide distribution of loess and its thick accumulation in the research area serve as ideal hunting grounds for paleoenvironmental and paleoclimatological research. The alteration of paleosols and loess deposits gives a first direct indication of different climatological conditions. Generally, one assumes that higher temperatures and increased humidity are necessary for the formation of paleosols. However, also within the pale looking loess, variations in environmental proxy data can be detected suggesting changes in paleoclimate. By looking at grain size alteration throughout the loess-paleosol profile, valuable information on sediment variability, transport dynamics, and weathering processes is gained (e.g. Buggle et al., 2011; Újvári et al., 2008). One proxy is for example the U-ratio that compares medium and coarse-grained ($16 - 44$ μm) to fine-grained ($5.5 - 16$ μm) silts and can be used as indicator for wind strength (Vandenberghe, 2013). Moreover, the geochemical composition and its changes within loess-paleosol sequence shed light on the origin or provenance of the sediments, but give also indication on the degree of weathering and pedogenesis. Different elemental ratios (e.g. Ba/Sr) and indices, like the Chemical Index of Alteration (CIA) are used to analyze the geochemistry. These chemical weathering indices build upon the concept of mineral alteration, where the depletion of 'mobile' elements is compared to the enrichment of 'immobile' elements (e.g. Buggle et al., 2011; Nesbitt and Young, 1989). Next to these physical and chemical proxies, also biological proxies can be used for paleoenvironmental studies, such as palynology and malacology. While pollen is often not preserved in loess, mollusks are more commonly found. Malacology - the study of mollusks – gains biological proxy data by analyzing the abundance and compositions of mollusk fauna with regard to their environmental preferences (e.g. Bösken et al., 2017b; Sümegi et al., 2016).

Furthermore, magnetic susceptibility is a frequently used proxy in loess research. It is controlled by the amount of iron-bearing paramagnetic and ferromagnetic minerals (Thompson and Oldfield, 1986). Conversion of less-magnetic minerals to magnetic magnetite (Fe_3O_4) and maghemite ($\gamma - Fe_2O_3$) through pedogenic oxidation processes leads to magnetic enhancement. Therefore, increased magnetic susceptibility is often an indicator for increased weathering (and pedogenesis) or increased moisture conditions (Buggle et al., 2014; Marković et al., 2009; Necula et al., 2013). Finally, it is also used for correlation between different geoarchives (e.g. Basarin et al., 2014; Buggle et al., 2009; Marković et al., 2015).

3.2. Brief overview of anatomically modern humans in the research area

The geographical position of the Middle and Lower Danube Basins between Asia, Near East and Central Europe and the vast river network connecting these regions, make the area a favorable pathway for anatomically modern human (AMH) migration. Migration routes from Africa over the Near East, as well as from Asia over the Caucasus and Ukraine, towards central and Western Europe have been proposed (cf. Iovita et al., 2014). Nevertheless, findings of human occupation have been scarce within the Middle and Lower Danube Basins, which is probably related to the thick cover of loess deposits in this area (cf. Chapter 3.1). The 'Danube corridor' (Conard and Bolus, 2003) has also been proposed by Iovita et al. (2014) for the rather rapid expansion of anatomically modern humans into central Europe. They further propose another corridor of human migration from eastern Romania towards the Dniestr and Dniepr valleys in the Northeast. Another pathway, outside the study area, was probably located along the Mediterranean coastline towards southern and western Europe (Mellars, 2011).

Humans migrated into the research area long before the arrival of the first AMH populations. The Dealul Guran site for example confirmed hominin presence during the Middle Pleistocene (MIS 11, Iovita et al., 2012). However, here, we only want to give a short overview and focus on two Upper Paleolithic industries - the Aurignacian and the Gravettian.

The research area has drawn international interest since the discovery of a human mandible in the Peştera cu Oase (Cave with Bones) in southwestern Romania (Trinkaus et al., 2003). The mandible was dated directly by accelerator mass spectrometry radiocarbon to $34-36$ *ka BP* ($37-42$ *ka cal BP*), which makes it the oldest directly dated human fossil in Europe. Moreover, its DNA shows that $6-9\%$ of its genome is of Neanderthal origin, with a direct ancestor only $4-6$ generations back. However, the Oase population did not contribute substantially to the later *Homo sapiens* population in Europe (Fu et al., 2015). Other AMH sites in southwestern Romania are the Peştera Muierii (~$29-30$ *ka BP*, ~35 *ka cal BP*) and the Peştera Cioclovina Uscată (~28.5 *ka BP*, ~33 *ka cal BP*, Gheorghiu and Haas, 1954; Rainer and Simionescu, 1942; Rougier et al., 2007; Soficaru et al., 2006, 2007; Trinkaus et al., 2009, 2003). Processes of migration and dispersal are very complex and not yet fully understood. E.g. Hervella et al. (2016) demonstrated a migration from Western Eurasia back to Northern Africa by means of a mitogenome found in the Peştera Muierii individual that nowadays is only present in the Northafrican population. With the increasing research interest, also other sites in the Banat region were recently reinvestigated. Léonard (2016) evaluated the Early Upper Paleolithic finds at the sites Tincova, Coşava, and Romaneşti-Drumbrăviţa (40.6 ± 1.5 *ka*, C. Schmidt et al., 2013) that resembles the Early Aurignacian Krems-Hundsteig site in Austria. A prior investigation by Sitlivy et al. (2012, 2014) indicated that the Protoaurignacian ('archaic stage of the Aurignacian technocomplex') and the Early Aurignacian industries couldn't be separated in these records, suggesting a syncretism of both technological traditions. Kels et al. (2014) investigated the genesis of the sediments at these sites. The paleosol complex that contains the Paleolithic finds

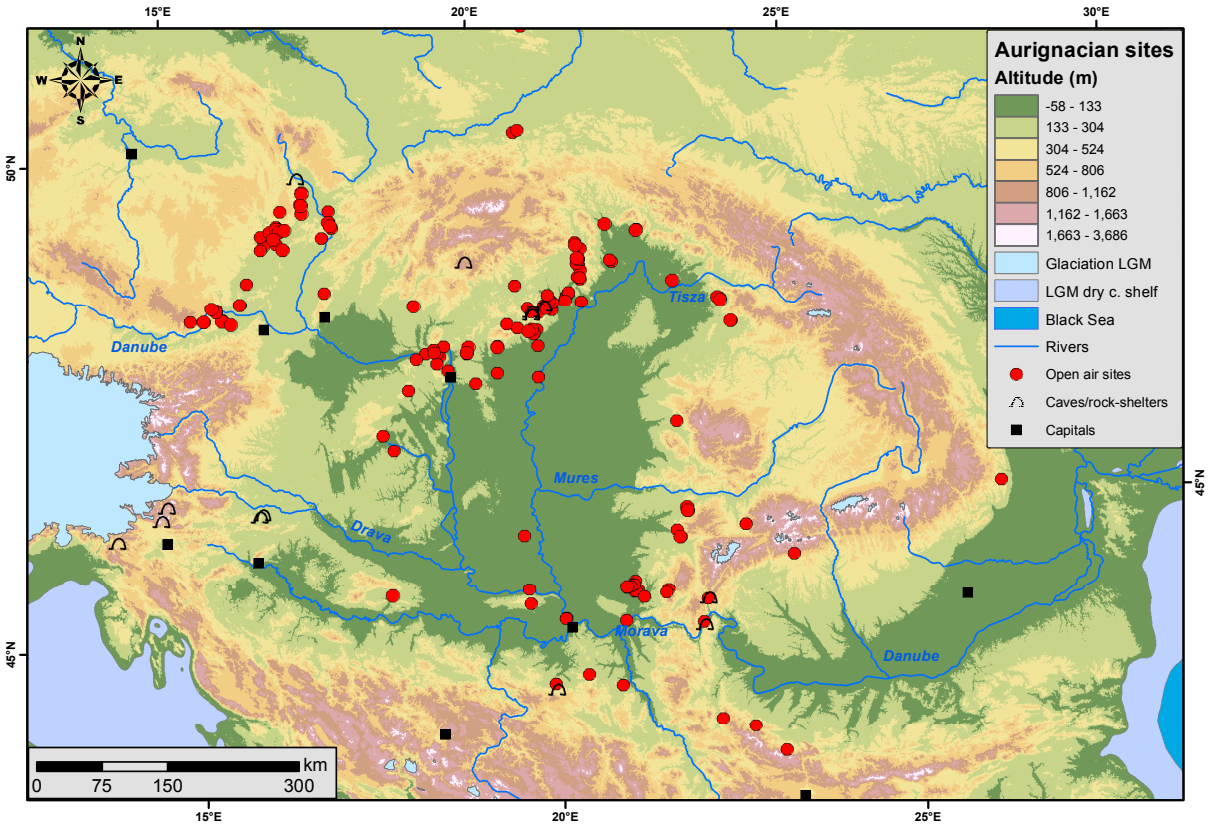

Figure 3.3.: Map demonstrates the find density of Aurignacian open-air sites, caves and rock-shelters in the Middle Danube Basin. Most sites are located at elevated positions in the landscape (cf. Hauck et al., 2017). Digital elevation model based on SRTM data available from U.S. Geological Survey (Farr et al., 2007).

hints at a forest steppe environment with higher vegetation during MIS 3. Léonard (2016) divided the lithic records of Tincova, Coşava, and Romaneşti-Drumbrăviţa into two groups. While the artifacts of Coşava I-II indicate high residential mobility and core, blank and tool portability, the lithics of Romaneşti-Drumbrăviţa I-II and Tincova do not (Léonard, 2016). What is more, the position within the same soil complex argues for chronological differences between the assemblages. Léonard (2016) proposed that the two groups represent different behavioral adaptations corresponding to changes in the paleoclimate, if the stratigraphy is not disturbed. Other possibilities are larger settlement systems or different camps with seasonal differences in resource distributions.

Most of the Upper Paleolithic finds in the Middle Danube Basin are located in higher landscape positions, such as foothills, terraces or caves (cf. Hauck et al., 2017). Figure 3.3 gives an overview. In the Lower Danube Basin sites are either located along the Danube River or close to the mountain ranges (cf. Floss et al., 2016). One example from the Banat lowlands, is the Crvenka-At site, close to Vršac (Serbia, Chu et al., 2014). The sites was only discovered due to former sand exploitation, as the artifacts are found in a depth of ~5 m. Thus, it is possible that more unknown sites are located in the lowlands, covered by loess. Chu et al. (2014) re-excavated the Aurignacian Crvenka-At site. Preliminary data indicates two levels containing

possibly Aurignacian finds at multiple locations. Further chronological investigations will be presented in Chapter 7. Another noteworthy site is the Hungarian Szeleta Cave that is believed to comprise a transitional industry – the Szeletian industry – between Middle and Upper Paleolithic or a local Early Upper Paleolithic Aurignacian (cf. Adams, 2007). Unfortunately, published radiocarbon ages are highly problematic (Lengyel and Mester, 2008).

Examples of the younger Gravettian industry in the Middle Danube Basin are Bodrogkerezstúr and Ságvár. At the Bodrogkerezstúr-Henye site, the Gravettian finds are located within a podzol that formed on top of a previously decarbonated paleosol (Sümegi and Hertelendi, 1998; Sümegi and Rudner, 2001). The site yields an exotic stone assemblage indicating that the Gravettian lithic procurement strategy was opportunistic and exotic stone tools were taken as mobile toolkit (Lengyel, 2015). At Ságvár, numerous excavations were undertaken in the 20^{th} century yielding lithic artifacts, hearths, faunal remains, charcoal, and hut basements from two archeological layers (Gábori, 1959, 1965, 1969, 1989; Gábori and Gábori-Csánk, 1957; Gábori-Csánk, 1978; Gáboriné Csánk, 1960; Vöros, 1982). There has been some discussion if the two layers actually belong to one occupation; further details are presented in Chapter 5. A summary of archeological and paleoenvironmental research at these two Hungarian sections is given in Chapters 5 and 6.

A noteworthy example from the Dniester region is the Doroshivtsy section. It contains seven Upper Paleolithic levels within a 12 m loess-paleosol sequence (Kulakovska et al., 2015). Most artifacts belong to the Gravettian industry. Klasen et al. (2017) compared quartz OSL, $pIRIR_{290}$ and radiocarbon ages of the section, yielding ages for the Gravettian layers within the expected period $\sim 22 - 28\ ka$.

4. Methodological approach of luminescence dating

4.1. Basic principle of optically stimulated luminescence dating

Optically stimulated luminescence (OSL) dating, as well as thermoluminescence (TL) dating and electron spin resonance dating belong to the techniques of trapped charge dating (Grün, 2001). Luminescence dating techniques exploit the property of certain minerals, such as quartz and feldspar, to act as natural dosimeters, i.e. their ability to store information on deposited energy or dose (cf. Ankjærgaard, 2010). These minerals are subject to low levels of radiation by naturally occurring radioactive isotopes of elements like uranium (U), thorium (Th), rubidium (Rb) and potassium (K). This radiation leads to ionization of the minerals' atoms during which electrons may be excited and trapped in defects in the crystal lattice (cf. Walker, 2005). Through time, the minerals record the amount of radiation they have been exposed to by storing an increasing amount of energy in the form of trapped electrons (Duller, 2015b). These electrons can be released in the laboratory by light or heat leading to a recombination of the trapped charge in luminescence centers (i.e. a type of structural defect), and emission of light (hence termed luminescence) that is proportional to the amount of electrons trapped (e.g. Walker, 2005). When the release is effected through the application of light it is termed optically stimulated luminescence; the application of heat is subject in thermoluminescence methods. Both methods date the event of last signal resetting. The signal is reset, i.e. the trapped charged is released, by exposure to high temperatures or (sun)light. For dating purposes it is therefore important to determine whether the luminescence signal has been completely reset (or bleached) prior to deposition, hence dating the timing of sedimentation.

Optically stimulated luminescence dating is a widely applicable dating method for the Quaternary covering the last few hundred thousand years. Quartz and feldspar are mainly used, but there are also studies on zircon and volcanic glasses (e.g. Berger, 1991; Biswas et al., 2013; Smith, 1988; B. W. Smith et al., 1991). It is appropriate especially for sediments that have been bleached during transport, particularly eolian sediments like loess deposits and dunes (cf. Roberts, 2008). Nevertheless, also other sediments such as fluvial, marine, limnic, and colluvial deposits have been dated successfully (e.g. Bartz et al., 2017; Brill et al., 2015). For the calculation of the luminescence age, one needs to determine the paleodose, i.e. the energy accumulated since burial, and the dose rate, i.e. the amount of radiation the sample receives each year:

$$Age(ka) = \frac{Paleodose\ (Gy)}{doserate\ (Gy/ka)} \tag{4.1}$$

The unit of the equivalent dose is the Gray (Gy), which is the S.I. unit of absorbed radiation. 1 Gy corresponds to 1 J/kg. The dose measured in the laboratory is termed equivalent dose (D_e) because it is an estimate of the 'natural dose' produced by using solely beta (or gamma) irradiation and much higher dose rates than are found in nature. The D_e serves as an estimate for the paleodose.

4.1.1. Physical background

The physical processes behind luminescence are usually explained by the band gap energy model. Figure 4.1 presents the band structure of a semiconductor or insulator such as the minerals under study, in which the valence band is fully occupied by electrons, while none are located in the conduction band (cf. Duller, 2015b). Within the two bands exists a so called 'forbidden gap', where electrons are unable to reside. Due to chemical impurities and structural defects in the crystal lattice, traps are occasionally located within this forbidden gap (orange lines on Fig. 4.1). By means of energy induced by ionizing radiation, an electron is 'excited' and moves into the conduction band. This leaves an empty 'hole' (charge deficit) in the valence band. Since the electron is unable to remain in the conduction band, it will either immediately de-excite back into the valence band (releasing the energy absorbed through the radiation), or become trapped in the forbidden gap (thereby losing a small amount of energy, cf. Duller, 2015b). At the same time, the charge deficit can diffuse through the crystal and might also become trapped at another type of defect called 'luminescence or recombination center' (a). The more electrons become trapped over burial time, the more energy is stored. The stability of a trap is related to its depth from the conduction band; only trap depths $> 1.6\ eV$ are stable over geologically relevant timescales (Aitken, 1998). The stability of the charge within the trap depends on the amount of energy that is required to empty the trap. For dating purposes, it is important that the life span of the electrons in a trap is longer than the age span of the sample (e.g. several million years for dating purposes; Aitken, 1998). If sufficient energy is applied by light or heat (e.g. within the laboratory during OSL measurements or during sunlight exposure in nature), the electrons stored within the forbidden gap are excited into the conduction band and may recombine with the hole stored at the luminescence center (b). This results in the emission of light that can be recorded during the D_e measurement by means of a photomultiplier tube.

The model for feldspar is more complex and still not well understood. Figure 4.1 only shows a simplified version; for more details the reader is referred to the literature (cf. Jain and Ankjærgaard, 2011). IR excitation of feldspars moves the trapped electron into the excited state, from where it can either immediately get retrapped, or transitions from band tail states and recombines with the 'hole' (c). Other possibilities are ground state tunneling and excited state tunneling, where the electron recombines directly. This process is connected to loss of trapped charge, also known as anomalous fading, which may lead to underestimation of age (more details in Chapter 4.2.1).

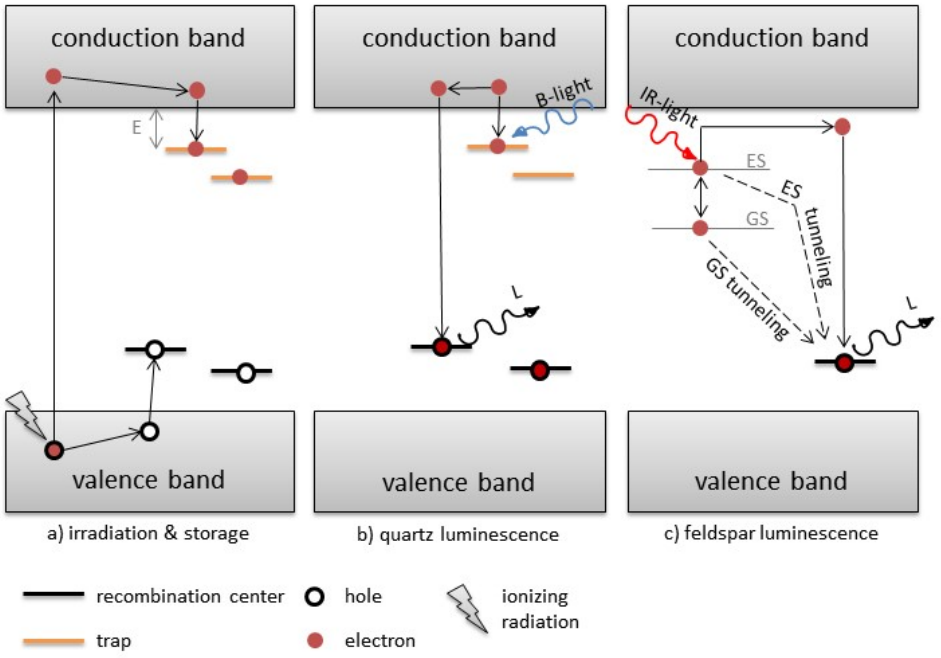

Figure 4.1.: Simplified band gap energy model of luminescence showing the processes during radiation and storage (a), quartz luminescence (b), and feldspar luminescence (c). Modified after Aitken (1998) and Jain and Ankjærgaard (2011). More details in the text.

4.1.2. A note on historic developments

First scientific investigations of luminescence began in 1663 when Robert Boyle demonstrated that certain varieties of diamonds ('carbuncle') are able to emit cold light (cf. Aitken, 1998). After some geological research on e.g. crystal structures and defects and early applications of thermoluminescence dating in the 20^{th} century (e.g. Aitken, 1985b, 1997, 1998; Curie, 1963; Laverenz, 1950; McKeever, 1985), the dawn of OSL dating was the discovery that visible light could also be used for stimulation (Huntley et al., 1985). First, blue-green light from an argon-ion laser was used, later infrared stimulated luminescence (IRSL) methods for feldspar dating were developed (Hütt et al., 1988). Nowadays, green lasers and blue LEDs are mostly used to date quartz, and infrared LEDs for investigations on feldspars or polymineral samples. Another breakthrough in OSL dating was the development of the single aliquot regeneration (SAR) method (Wintle and Murray, 2000). This approach employs the D_e measurements on one subsample (termed aliquot) instead of using multiple aliquots for the determinations. Prior to this development it was necessary to use numerous aliquots and therewith bigger sample sizes for D_e determination, either by applying the additive or the regenerative dose method (more details in Fig. 4.2). The development of the SAR protocol, nowadays applied to quartz and feldspars (using IRSL), has decreased sources of error deriving from e.g. grain-to-grain variation or aliquot-to-aliquot scatter (Walker, 2005). Another methodological development has been the possibility to date single mineral grains, especially useful in environments where post-depositional mixing processes or incomplete bleaching cannot be excluded (e.g. Duller, 2004; Galbraith et al., 1999; Jacobs et al., 2003; Roberts et al., 1999).

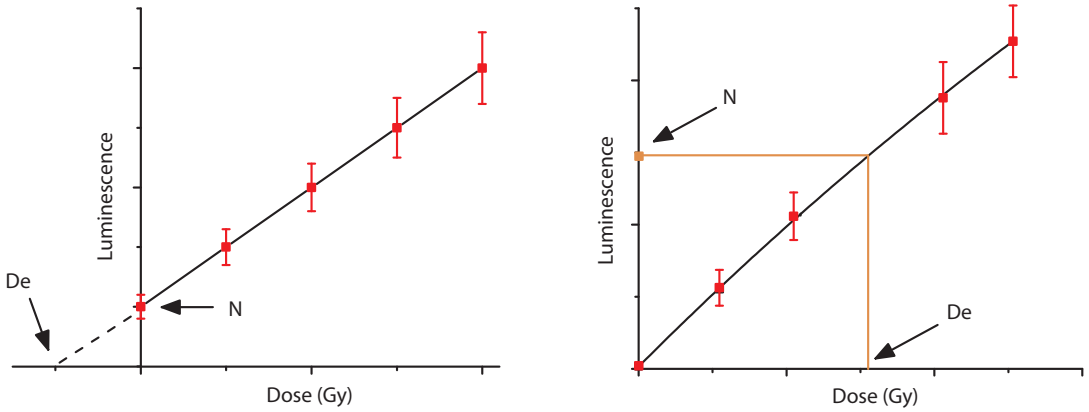

Figure 4.2.: General approaches for D_e determination include the additive dose method (left) and the regeneration dose method (right). Each point on the curve shows an average of several aliquots (multiple aliquot approach). The natural luminescence signal is marked on the y-axis and its dose is determined by extending the line onto the x-axis (left) or by extrapolation onto the curve (right). Modified according to Aitken (1998).

4.2. Equivalent dose

4.2.1. Measurement equipment and general considerations

All measurements for this doctorate dissertation were conducted on a Risø TL/OSL DA 20 reader at the Cologne Luminescence Laboratory. The reader is equipped with a $^{90}Sr/^{90}Y\,\beta$-source that is used for artificial beta irradiation during the measurement (cf. Chapter 4.2), as well as blue and infrared light emitting diodes (LEDs). Generally, electrons of both quartz and feldspars are excited by blue light, while only electrons of feldspars are excited by IR light. Therefore, for measurements on quartz, samples are etched to remove other minerals and are stimulated by blue LEDs. Consequently, feldspar measurements use IR LEDs. To test whether the etching of quartz was successful, IR stimulation can be used (IR depletion ratio, Duller, 2003). Moreover, different detection windows by using filters in front of the photomultiplier tube make sure that only the luminescence signal is recorded and not the light emitted by the LEDs during stimulation. For measurements of quartz a Hoya U-340 filter and for measurement of feldspars and polymineral samples a 410 nm interference filter is used. The luminescence signal itself is finally collected in the photomultiplier tube. All measurements conducted were continuous-wave OSL measurements. The reader is referred to the literature for other types of measurements such as linear-modulation or pulsed OSL (e.g. Bøtter-Jensen et al., 2003). More explanations on the used protocols will be given in the following sections.

General consideration during sampling, sample preparation, and data analysis comprise the differences between the used minerals, and the measurement protocols used. Quartz grains bleach faster than feldspar grains, but they also saturate earlier (i.e. traps are filled and further radiation does not increase the dose, e.g. Murray et al., 2012; Thomsen et al., 2008). Therefore,

the upper dating limit of feldspars is usually higher, but due to smaller bleaching rates, dating feldspars might be problematic in non-eolian environments. Moreover, feldspar suffers from a signal loss, termed 'anomalous fading', especially when the $IRSL_{50}$ signal is used. To circumvent age underestimation, fading tests need to be conducted to correct the measured D_e and therewith age (Auclair et al., 2003; Huntley and Lamothe, 2001). Another possibility to minimise the influence of fading is the use of elevated temperature protocols that measures a signal that is less affected by anomalous fading, such as the post-infrared infrared stimulated luminescence (pIRIR) protocol (Buylaert et al., 2009; Thiel et al., 2011b) that was mainly used in this doctorate dissertation. The protocol is presented in Chapter 4.2.3).

4.2.2. Blue stimulated luminescence dating of quartz

To date quartz, commonly the single-aliquot-regenerative-dose protocol (Murray and Wintle, 2000, 2003) is applied. Table 4.1 pictures the measurement scheme. All steps are conducted on a single aliquot to decrease errors by inter-aliquot-scatter. After a preheat (step 2) that empties shallow traps, the aliquot is stimulated, while the natural luminescence signal (L_n) is recorded (step 3). Sensitivity changes are monitored by repeatedly measuring the luminescence response to a constant test dose (T_n, T_x) in steps 4-6. After this first cycle, a dose is given and steps 2-7 are repeated, while determining the following L_x and T_x. By means of a plot of the sensitivity corrected luminescence signal (L_x/T_x) against dose, the equivalent dose can be determined by extrapolating L_n/T_n onto the dose response curve (often referred to as growth curve, similar to Fig. 4.2). For fine-grained eolian samples a sample size of 10 aliquots is often sufficient.

In order to assess the quality of the measurement the SAR criteria (Murray and Wintle, 2000) were developed. These include a minimum signal intensity (signal $>$ 3 sigma above background), and a minimum precision in test dose determination (test dose error $\leq$ 10%). What is more, repeated measurements of L_x after the same dose should be reliable (recycling ratio of 1.0 ± 0.1), and sensitivity changes between first and last measurement should be minimal (recuperation $< 5\%$). To check whether the quartz sample is free of feldspar grains, an infrared stimulation is used (IR depletion ratio of 1.0 ± 0.1). Finally the paleodose error must be $< 10\%$ and the signal must not be in laboratory saturation ($D_e < 2 * D_0$). D_0 is a mathematical value describing the shape of the curve. If a criterion is not fulfilled, the measured aliquot is rejected.

For determination of the proper preheat temperature a so-called preheat plateau test (Murray and Wintle, 2000) needs to be applied prior to D_e measurements. Here, different preheat temperatures are tested with otherwise constant measurement settings. If there is a plateau in a plot of preheat temperature against D_e, one of the preheat temperatures within the plateau can be used for the subsequent measurements. Finally, it is also tested whether a given laboratory dose can be recovered (i.e. the same dose is measured as was added to the aliquot prior to measurement) in a dose recovery test (Murray and Wintle, 2003).

Table 4.1.: The measurement protocols mainly used in this doctoral dissertation. For quartz a modified SAR protocol according to Murray and Wintle (2000, 2003) was used. For feldspar and polymineral samples the pIRIR$_{290}$ protocol according to Thiel et al. (2011b) was used. For one section also a pIRIR$_{225}$ protocol was applied (see Chapter 7).

SAR protocol for quartz		**pIRIR$_{290}$ protocol for feldspar**	
1	Give dose, D_i	1	Give dose, D_i
2	Preheat (180-280°C for 10 s)	2	Preheat (320°C for 60 s)
		3	IR stimulation for 200 s at 50-180°C
3	Blue stimulation for 40 s at 125°C → $\mathbf{L_i}$	4	IR stimulation for 200 s at 290°C → $\mathbf{L_i}$
4	Give test dose, D_t	5	Give test dose, D_t
5	Cutheat (160-260°C for 10 s)	6	Cutheat (320°C for 60 s)
		7	IR stimulation for 200 s at 50-180°C
6	Blue stimulation for 40 s at 125°C → $\mathbf{T_i}$	8	IR stimulation for 200 s at 290°C → $\mathbf{T_i}$
		9	IR stimulation for 100 s at 325°C
7	Return to 1	10	Return to 1

4.2.3. Post-infrared infrared stimulated luminescence (pIRIR) dating of feldspars and polymineral samples

For the measurement of feldspar, the same principle as for quartz is used, but stimulation is done by infrared light. In order to circumvent anomalous fading, the sample is stimulated twice. The first stimulation empties unstable 'shallow' traps, while the second stimulation is used as luminescence signal. Table 4.1 shows the steps of the protocol. The same SAR-criteria are used to ensure measurement quality. Instead of a preheat plateau test, a prior IR stimulation temperature test is conducted to decide on the best first IR stimulation temperature. Once a plateau in a plot of prior IR stimulation temperature against D_e is present, one can be sure to gain the same result independent of the first IR stimulation temperature used. Moreover, dose recovery tests are conducted after bleaching the aliquots for 24 h in a solar simulator. Feldspars that are measured with the pIRIR protocol sometimes exhibit a residual signal that cannot be bleached. This is determined by bleaching the sample for 24 h in a solar simulator and determining the remaining D_e. There has been some debate whether this 'unbleachable signal' ought to be subtracted from the final D_e or not, but most applicable seems to be a subtraction for dose recovery tests, but not for equivalent dose measurements (Kars et al., 2014).

4.3. Dose rate

4.3.1. Radioactive decay

Radioactive decay causes changes in the number of protons and neutrons within atoms leading to a transformation from so-called mother isotopes into daughter isotopes following known decay chains. The energy that is released during this transformation is emitted as α, β, and γ-rays (cf. Aitken, 1985b; Duller, 2015b), which will be further explained in the following. The term 'ionization', which is often used in luminescence, refers to the interaction of these rays with a medium, while 'excitation' refers to a transfer of electrons to higher energy levels within the atom (cf. Hilgers, 2007).

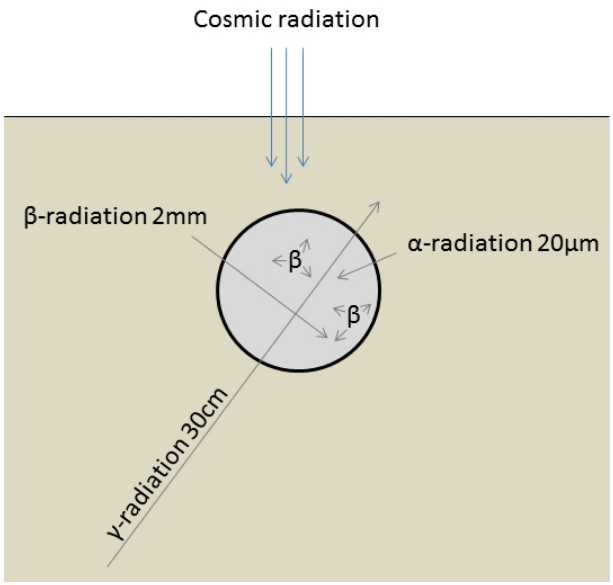

Figure 4.3.: Sketch of different penetration depths of alpha, beta, gamma, and cosmic radiation (Aitken, 1998).

Alpha particles contain two neutrons and two protons and are therefore a twice positively charged helium ion. Due to their size, alpha particles are absorbed after very short distances reaching e.g. only ~20 μm in sediments with a density of 2.5 g/cm^3 (Grün, 1989). Alpha particles travel along so-called fission tracks, while they ionize adjacent atoms losing their energy rapidly (cf. Aitken, 1998; Grün, 1989). Due to these short transport distances, they are less efficient in comparison to beta and gamma rays, which reach further. Therefore, an alpha efficiency factor needs to be considered (cf. following section). **Beta particles** consist of electron or positrons emitted during beta decay. Beta particles are smaller than alpha particles, thereby penetrating ~2mm into sediments with a density of 2.5 g/m^3 (Aitken, 1998; Grün, 1989). At the same time they are less ionizing than alpha particles and lighter, which means that they do not travel in straight lines, but rather get scattered (Aitken, 1998). **Gamma radiation** consists of electromagnetic waves that get emitted during the transformation of protons into neutrons (Aitken, 1985b). These also get scattered during penetration and reach ~30 cm in sediments with a density of 2.5 g/cm^3 because of little interaction with the penetrated material. All three types of radiation produce secondary electrons that might get trapped in the crystal lattice (Aitken, 1998). Figure 4.3 shows the different penetration powers of alpha, beta, and gamma radiation after Aitken (1998).

Cosmic radiation contains a soft and a hard component. While the soft component is only relevant for samples taken with the upper half meter of sediment, the hard component penetrates deeper (Aitken, 1998). Generally, the cosmic dose rate makes up only a small proportion of the total dose rate in luminescence dating. The cosmic dose rate can be calculated by the geographical position, altitude and depth of each sample below the surface (following Prescott and Hutton, 1994).

4.3.2. Dose rate determination

The dose rate is determined by measuring the radionuclide concentrations of U, Th, and ^{40}K in the sediment surrounding the sample in a radius of approximately 30 cm. The radionuclide concentrations are assessed in a high-purity germanium gamma-ray spectrometer. The effect of rubidium is often regarded as negligible and might be added into the calculations by means of a literature value. These concentrations are subsequently converted into dose rates by different conversion factors. These external dose rates are further complemented by giving an estimate of the internal dose rates. More specifics are given in Chapters 5-9 particular to each section. The cosmic proportion of the total dose rate is calculated considering Prescott and Hutton (1994). A complication in dose rate determination can be the presence of water and organic matter in the sediment matrix (Walker, 2005) because these influence the absorption of radiation. Therefore, it is useful to avoid organic matter accumulation while sampling. In case of the water content a precise estimate of average water content since time of deposition is necessary. As this is rather complicated, an estimate of water content can be assumed by considering the current and the saturation water content and applying an error range covering possible water contents. Additionally, one can also use possibly available paleoenvironmental data to estimate the potential range of the paleo-water content. Moreover, stratigraphical information should be included in the estimation as well, e.g. higher water contents can be assumed for pedogenic horizons and lower ones for calcareous horizons.

A useful tool for final dose rate and age calculation is the **D**ose **R**ate and **A**ge **C**alculator by Durcan et al. (2015). It allows easy and transparent calculation using different input variables like conversion factors, mineral types, internal and external dose rates, grain sizes, attenuation factors and many more. DRAC was applied for all samples measured in this doctorate thesis except for the Crvenka-At samples, which were complicated due to stratigraphic layers < 30 cm. In this case, the Adele software was used.

4.3.3. Alpha efficiency

As explained in the previous section, the α-efficiency needs to be accounted for when calculating the dose rate for fine-grained samples. Different systems were presented quantifying the α-efficiency (for an overview see Aitken, 1985a). From these the a-value system has been most widely used. For quartz, the a-value is calculated by the ratio of luminescence induced by an α-dose (in Gy) to that induced by a β-dose (in Gy). For other minerals a correction factor 'r' needs to be used, which relates the mineral-specific a-value to the quartz a-value (Aitken, 1985a).

Only a few studies have determined the a-value individually for the investigated samples. Many authors use an a-value of 0.08 ± 0.02 referring to Rees-Jones (1995). However, this value is only based on three samples, whose mean a-value is 0.086, and it was determined for an IRSL multiple-aliquot protocol. Biswas et al. (2013) reported a-values ranging between 0.036 ± 0.003 and 0.055 ± 0.002 for volcanic ash samples using the pIRIR_{290} protocol. They determined the values by administering a known α-dose to a bleached sample and recovering the equivalent β-dose using a single-aliquot regeneration dose protocol. The authors tested

the applicability of this measurement procedure by successfully applying dose recovery tests using solely α-regeneration or solely β-regeneration (and a fixed β-test dose for normalization). Furthermore, Kreutzer et al. (2014) determined a-values for five loess samples from Saxony (Germany) using the $pIRIR_{225}$ protocol and found systematic differences between $IRSL_{50}$ and $pIRIR_{225}$ a-values.

With regards to these varying α-efficiency values, it was necessary to determine the a-value for at least 1-2 samples per section, in order to avoid age discrepancies. The a-values were not corrected for by the 'r' factor because the factor depends largely on the density difference between feldspars and quartz, which seem negligible. Only for the samples of the Crvenka-At section (Chapter 7) a-values were not determined and the value given by Kreutzer et al. (2014) was used, since both investigations applied the $pIRIR_{225}$ protocol.

5. Investigating the last glacial Gravettian site 'Ságvár Lyukas Hill' (Hungary) and its paleoenvironmental and geochronological context using a multi-proxy approach

Janina Bösken[1], Pál Sümegi[2], Christian Zeeden[1], Nicole Klasen[3], Sándor Gulyás[2], Frank Lehmkuhl[1]
Published in Palaeogeography, Palaeoclimatology, Palaeoecology at http://dx.doi.org/10.1016/j.palaeo.2017.08.010.

5.1. Introduction

Geoarcheological investigations on loess have a long tradition in the Carpathian Basin and Europe since numerous (Paleolithic) archeological sites are embedded in loess and loess like sediments (e.g. Haesaerts et al., 2009; Händel et al., 2009; Iovita et al., 2014; Kels et al., 2014; Terhorst et al., 2013; Zeeden et al., 2015). Usually the aim is to understand the paleoenvironmental context of archeological finds at a specific site, which often brings the occurrence of finds into a wider context of human-climate and human-landscape interaction. The paleoenvironment is investigated by means of proxies like grain size, geochemistry, rock magnetism, color characteristics, and malacology (see e.g. Baumgart et al., 2013; Buggle et al., 2011, 2014; Heller et al., 1991; Hošek et al., 2015; Krauß et al., 2016; Obreht et al., 2014, 2015; Sümegi, 2005; Sümegi et al., 2015; Zeeden et al., 2016d). Grain size data may provide information on sediment variability, transport distance, dynamics, and pedogenesis (e.g. Bokhorst et al., 2011; Ding et al., 2002; Obreht et al., 2015, 2016; Újvári et al., 2016a; Vandenberghe et al., 2014; G. Varga et al., 2012); the geochemical composition can be used to infer origin and provenance of sediments, and degree of weathering (e.g. Buggle et al., 2011; Újvári et al., 2008, and references therein). Proxy data and especially magnetic susceptibility are commonly used for correlation between geoarchives, including correlation between terrestrial and marine records (e.g. Basarin et al., 2014; Buggle et al., 2009; Marković et al., 2015). Especially in loess, malacology provides a well understood paleoenvironmental framework for the interpretation of environmental conditions during the last glacial cycle (Marković et al., 2007, 2012a, 2015; Moine, 2014; Moine et al., 2005, 2008; Sümegi, 2005; Sümegi et al., 1998b, 2012a,b, 2013, 2015). Usually, several proxies are combined to a multi-proxy approach and linked to luminescence or radiocarbon dating to obtain

[1]Department of Geography, RWTH Aachen University, Templergraben 55, 52056 Aachen, Germany
[2]Department of Geology and Palaeontology, University of Szeged, Hungary
[3]Institute of Geography, University of Cologne, Albertus-Magnus-Platz, 50923 Cologne, Germany

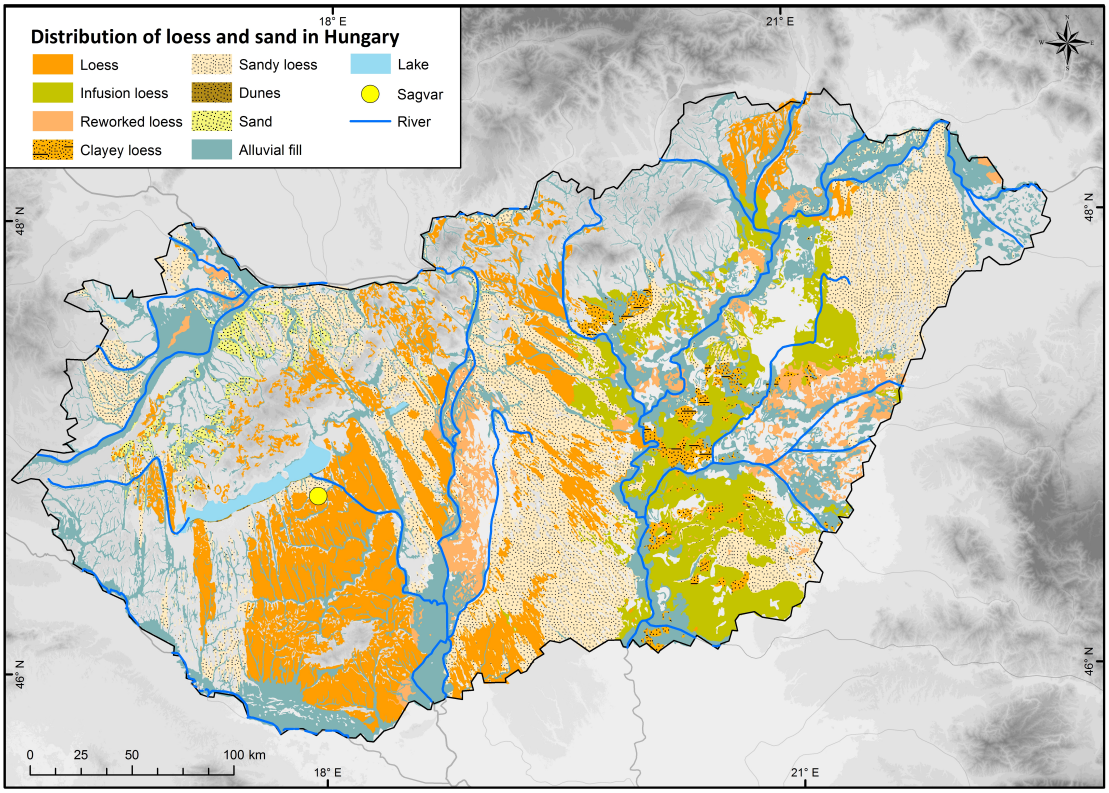

Figure 5.1.: Map showing the distribution of loess in Hungary (modified after Lindner et al., 2017) and the location of the sampled profile (yellow dot). Digital elevation model in the background based on SRTM data available from U.S. Geological Survey (Farr et al., 2007).

a temporal context for the proxy data or archeological finds (e.g. Kels et al., 2014; Újvári et al., 2014a, 2016b; Zeeden et al., 2009). In case of sediments, radiocarbon dating is often hindered due to a lack of datable material or the considered time-frame, whereas luminescence dating is widely applicable to sediment archives, but ages entail greater uncertainties. Optically stimulated luminescence (OSL) dating of quartz, feldspars or polymineral samples determines the time of last exposure to sunlight or heat (e.g. Duller, 2015b), and can be applied to sediments that have been bleached prior to deposition. Dating of fine-grained polymineral sediment samples with post-infrared infrared stimulated luminescence protocols (pIRIR, Thiel et al., 2011b) offers advantages over more conventional techniques and can be applied in regions (and time-frames) where dating of quartz might be considered problematic (e.g. glacial sediments, Lukas et al., 2007; glaciofluvial sediments, Klasen, 2008; equivalent doses > 100 Gy, Timar-Gabor et al., 2015a).

5.1.1. The research site 'Ságvár Lyukas Hill'

The studied loess sequence (46.824173°N, 18.092754°E) and its Upper Paleolithic site is situated in the Somogy Hills in Hungary, close to Lake Balaton (see Fig. 5.1). It represents one of few Gravettian settlements during the LGM and is therefore important for the understanding of the LGM occupation in southeastern Europe. It is located in a loess landscape with dominantly

northwest-southeast striking valleys and landforms suggested to be of eolian origin (Sebe, 2013; Sebe et al., 2011). The Upper Paleolithic site was first recognized in 1922 (Lazckó, 1929), and archeological excavations were performed in the 1930s (Gallus, 1936). Further fieldwork in the 1950s found lithic artifacts, hearths, faunal remains, charcoal, and hut basements from two archeological layers (Gábori, 1959, 1965, 1969, 1989; Gábori and Gábori-Csánk, 1957; Gábori-Csánk, 1978, 1984; Gáboriné Csánk, 1960; Vöros, 1982), which are related to one occupation, but may have been found separate due to taphonomic processes (Lengyel, 2010). The 'upper' occupation layer yielded a higher density of archeological finds, although reconstruction of the field context is problematic (Lengyel, 2010). Radiocarbon ages place the Paleolithic occupation into the last glacial: the upper occupation layer yielded an age of $17,760 \pm 150$ BP (GrN-1959); the lower one $18,900 \pm 100$ BP (GrN-1783) (Vogel and Waterbolk, 1964). After the archeological excavation a profile was opened for paleoenvironmental studies close to the previous archeological excavation surface (Sümegi and Krolopp, 2002). The occupation layers were correlated to this profile and two radiocarbon samples were taken, yielding ages of $18,510 \pm 160$ BP (Deb-8822, 25 cm depth) and $19,770 \pm 150$ BP (Deb-8821, 55 cm depth) from charcoal and mollusk shells (Sümegi and Krolopp, 2002). This profile was reinvestigated here (referred to as Ságvár I). To further supplement the investigation a second, longer profile close by was analyzed as well (Ságvár II).

5.1.2. Archeological context at 'Ságvár Lyukas Hill'

A detailed overview of the archeological studies conducted at Ságvár can be found in Lengyel (2010). Here, only a short summary will be given. The most remarkable finds were big hearths with diameters between 2 and 4.2 m containing charred pieces of pine wood. Other archeological finds were flint workshops, reindeer butchering areas, and basement structures with postholes (Lengyel, 2010). Hearths were distinguishable by their red colored sediment. Resemblance of the charcoal pieces to *Pinus rotundata* indicates the existence of wet woodland in the vicinity of the site. There were two levels of superimposed hearths, separated by varying thicknesses of loess (Lengyel, 2010). One of the hearths also yielded knapped flakes and animal bones. The faunal remains indicate reindeers, horses, and mammoth (Lengyel, 2010). Another site at the hill revealed a 'garbage heap' that contained further animal bones, knapped lithics, ash and charcoal. Prior to absolute dating, the site was assigned to the Magdalénian (Lengyel, 2010), while it is now considered to belong to the Gravettian. In the last excavations between 1957 and 1959 another garbage pit with two opposing holes came to light. Two distinct pit levels were distinguished, separated by clean sediment, and three dentalium beads were found (Lengyel, 2010). The pit was covered in and surrounded by well-preserved charcoal, dated to $17,760 \pm 150$ BP (GrN-1959; Gáboriné Csánk, 1960; Vogel and Waterbolk, 1964). While bones were found everywhere, knapped lithics were mainly found within the pit (Lengyel, 2010). The lower occupation layer yielded several hearths, but less artifacts. Charcoal samples date one hearth to $18,900 \pm 100$ BP (GrN-1783; Gábori, 1959; Vogel and Waterbolk, 1964). Gábori (1959, 1965) interpreted the pits and holes as dwelling remains with postholes. In the 1970s Gábori-Csánk (1978) interpreted organic rich levels at Ságvár to be equal to the Lascaux interstadial in France (Leroi-Gourhan, 1968) and called this period in Hungary the 'Lascaux–Ságvár

interstadial'. Later it was proposed to use the term 'Ságvár stage' for this period, as no interstadial features were evident (Lengyel, 2010; Vöros, 1982). Sümegi and Krolopp (2002) investigated this stage in several Hungarian loess deposits arguing for a connection between reindeer migration and Gravettian sites. The Gravettian hunters might have followed the reindeer herds from their winter spots in the Carpathian Basin (taiga) to their summer spots in the uplands of the mountain ranges (tundra). Recently, statistical analysis (Csongrádiné, 1997) and lithic refitting (Lengyel, 2010) of the artifacts of both layers showed that most likely only one single human occupation is found at Ságvár, possibly indicating post-depositional disturbances, which remained invisible in the excavations (cf. Lengyel, 2010).

5.1.3. The last glacial environment in the Carpathian Basin

Recent paleoclimatological investigations through pollen records indicate a high abundance of needle-leaved and cold-temperate tree vegetation in the western Carpathians, steppe herbs in the eastern Carpathians and fluctuations of arboreal pollen in the Carpathian Basin at the transition from MIS 3 to MIS 2 (Feurdean et al., 2014). Malacological studies show a dominance of boreal forest-steppe vegetation in the central Carpathian Basin during the LGM (Sümegi et al., 2012b). Also frequent fluctuations between mixed coniferous, broad-leaved open parkland and cold continental steppe vegetation are inferred, with infrequent contributions of boreal woodland and tundra-like vegetation (Sümegi and Krolopp, 2002; Sümegi et al., 2013). Sümegi and Krolopp (2002) reconstructed summer paleotemperatures and showed that the southeastern part of the Hungarian Plain was ca. $2-4°C$ warmer than the remaining basin. This allowed the survival of thermophilous broad-leaved temperate tree taxa (e.g. Rudner and Sümegi, 2001; Sümegi and Krolopp, 2002; Willis and Andel, 2004; Willis et al., 2000). The LGM in Hungary has been divided generally in a summer-warmer southern part with shrubs and open forest steppe, and a northern and colder part (Sümegi and Krolopp, 2002; Sümegi et al., 2011). At the end of the LGM *Pinus* and a low proportion of cold deciduous taxa was abundant in pollen records (Feurdean et al., 2014).

5.1.4. Research aim

The aim of this interdisciplinary study is to better understand the environmental variability within the Gravettian settlement at Ságvár during the LGM, and to determine the paleoclimatic conditions during human occupation at the end of the last glacial. Moreover, physical, chemical and biological proxy data will be compared to test their sensitivity towards paleoclimatic changes and anthropogenic disturbances. By integrating these different proxy data, not only the effects of external (climatic) factors on the proxies, but also the explanatory power of different proxy data is explored.

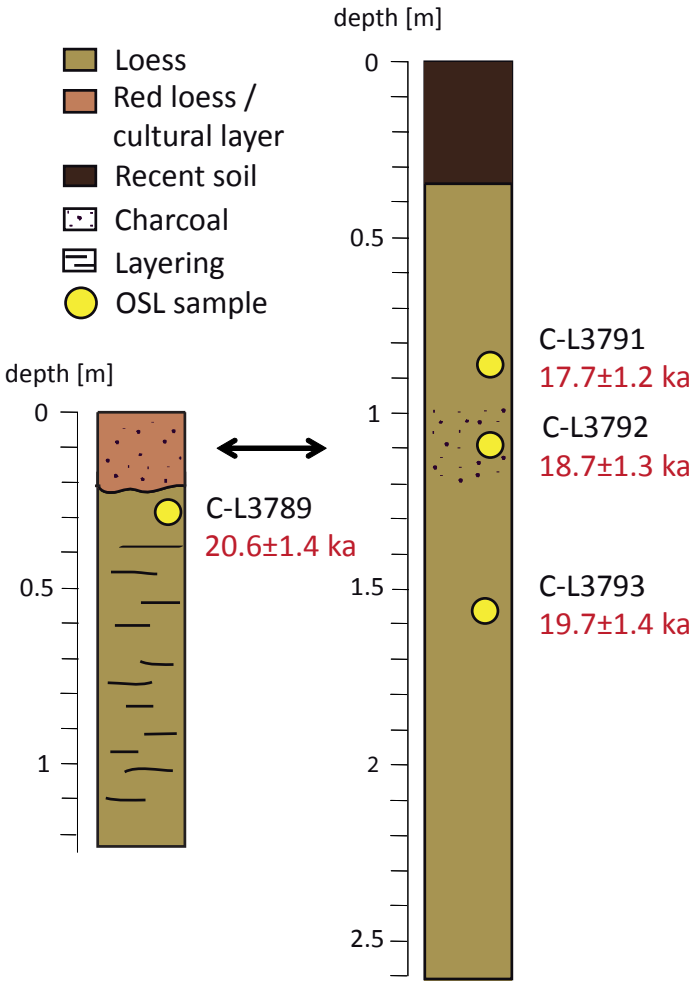

Figure 5.2.: Schematic drawing of the two sampled profiles Ságvár I (left) and Ságvár II (right) with luminescence samples indicated. The arrow indicates the correlation between the two profiles in the field.

5.2. Methods

5.2.1. Sampling and stratigraphy

At Ságvár, two profiles were sampled at a roadcut, near the hilltop and facing towards the north-west. The first 1.24 m profile covers a loess sequence that has been correlated to previous archeological investigations (see Chapter 5.1.1) that contained two visible cultural layers (further referred to as Ságvár I). Although it has been discussed that the two cultural layers belong to the same occupation, we continue our description with both layers, as these were described in the previous archeological and malacological fieldwork and serve as correlation to them. The second 2.6 m long profile (Ságvár II) is located ca. 20 m uphill; it was sampled because a longer outcrop of loess is available here, which involves more sample material for analysis and possibly also a longer timeframe. Correlation between profiles was done optically in the field (see below) and through physical proxy data (cf. Chapter 5.4.1).

The loess is represented by a greyish-ochre fine material without obvious changes in composition. The upper archeological layer (which was discussed to represent also the lower layer from a chronological point of view) contains burned material (easily visible by eye), including bone in the upper $20-25$ cm, likely related to the hearths found at the archeological site. At the bottom of this layer at a depth of ~25 cm, charcoal-rich sediment is present. The stratigraphically lower cultural layer of the archeological excavation is situated at a depth of ~55 cm, but this was not visible during the most recent fieldwork (but lithic artifacts have been found at the same site during fieldwork related to Sümegi and Krolopp, 2002). The loess at Ságvár II was sampled from below the recent soil, and it also represents greyish-ochre colored fine loess. It shows black spots from $1.0-1.2$ m, which may be used for correlation between these profiles, as indicated in Figure 5.2. Supplementary Figure A.1 shows photos of the two profiles.

Both profiles were sampled in 4 cm resolution for malacological, grain size, geochemical and rock magnetic analysis. Luminescence samples were taken by hammering and extracting 15 cm long metal tubes into the previously cleaned sediment wall, and by collecting the surrounding material in a radius of 30 cm for dose rate determination. At Ságvár I, the sediment 1.5 m above the profile was not sampled because of numerous roots in this part (not shown in Figure 5.2, see Supplementary Figure A.1).

5.2.2. Luminescence dating and recalibration of radiocarbon ages

Samples for D_e determination were extracted from metal tubes, the outer 2 cm were removed, samples were oven dried ($50°C$), and the water content over dry mass was determined. Work has been done under subdued red light conditions. The samples were subject to chemical treatment (10% HCl, 10% H_2O_2, and $0.01N$ $Na_2C_2O_4$) to remove carbonates, organic matter, and dissolve aggregates. Finally, samples were separated into the $4-11$ μm fraction using Stokes' Law and by removing the clay fraction (< 4 μm) via centrifugation.

Continuous wave optically stimulated luminescence measurements (CW-OSL) were carried out on a Risø TL/OSL DA 20 reader, equipped with a $^{90}Sr/^{90}Y\beta$-source and IR LEDs, emitting at 870 nm (FWHM = 40 nm). The $pIRIR_{290}$ SAR protocol by Thiel et al. (2011b) was followed. Signals of the polymineral samples were detected through a 410 nm interference filter. An investigation of a pure quartz fraction was not possible because of the small sample amount left after etching in H_2SiF_6. Prior IR stimulation temperature tests (cf. Buylaert et al., 2012) and dose recovery tests (24 h solar simulator) were performed on samples C-L3789 and C-L3793. Finally, the equivalent dose (D_e) was determined using the central age model (CAM) by Galbraith et al. (1999). The signal was integrated using the first 2.4 s minus a background of the last 25.6 s. Residual doses were assessed after bleaching the aliquots for 24 hours in a Hönle Sol2 solar simulator. Fading rates of two samples were measured after administering a dose of 85 Gy and using storage times between 100 and 800 minutes (following Auclair et al., 2003).

Samples for dose rate measurements were oven dried ($50°C$), homogenized and packed into

plastic cylinders after determination of the water content. Radionuclide concentrations were measured in a high-purity germanium gamma-ray spectrometer after a resting period of four weeks. The dose rate was calculated using DRAC v.1.1 (Durcan et al., 2015). The conversion factors of Liritzis et al. (2013) and an estimated water content of $15 \pm 5\%$ were used. The water content was obtained using a formula for Hungarian loess sections by Pécsi and Richter (1996). The internal beta dose rate contribution of the polymineral samples was calculated by assuming a potassium content of $12.5 \pm 0.5\%$ (Huntley and Baril, 1997). Attenuation factors of Bell (1980) and Guérin et al. (2012) were used. The cosmic dose rate was calculated according to Prescott and Hutton (1994) considering the geographical position, altitude and sample depth. The value of α-efficiency was determined by giving the samples an α-dose of ~80 Gy (after annealing to $480°C$) in a Freiberg Instruments Lexsyg Research device and repeating the D_e-measurements in a Risø-reader, similar to a dose recovery test. A minimum of three aliquots were used. It was ensured that the given dose was small enough to be fitted with a linear function. Furthermore, previously published ^{14}C bulk sediment samples (Krolopp and Sümegi, 2002) were recalibrated using the CALIB 7.0 software (Reimer et al., 2013). The samples originate from the archeological occupation layers at a depth of ca. 25 cm and 55 cm in profile Ságvár I.

5.2.3. Malacology

Samples of 1 dm^3 (5.7 kg) were dispersed in water and wet-sieved through 0.5 mm meshes. After sieving, the mollusk shells were dried, sorted and identified under a stereo dissecting microscope at a magnification of 6-50x. The shells were identified using the following classifications: Horsák et al. (2013), Kerney et al. (1983), Ložek (1964), Soós (1943), Welter-Schultes (2012). Shells were classified into ecological and biogeographical groups based on the system published by Krolopp and Sümegi (1995), and Sümegi and Krolopp (1995, 2002).

Relative frequencies of each taxa and the ecological groups were determined, calculated and plotted. Biozones were delineated via cluster analysis. Bray-Curtis similarity calculations (Southwood, 1979) were followed by Orlóci-Ward-type clustering (Podani, 1978, 1979). Numerical analyses were done with NUCOSA (Tóthmérész, 1993). Clusters on the dendograms were taken to represent a single biozone (MZ-1, MZ-2, etc., after Molnár and Sümegi, 1990, 1992). The malacological data was plotted using psimpoll (Bennett et al., 1991).

Climatic reconstruction was carried out using the malacothermometer method (Hertelendi et al., 1992; Sümegi, 1989, 1996, 2005; Sümegi and Krolopp, 2002). This method is based on the geographic pattern of 16 dominant gastropod species from a composite malacofauna (Sümegi, 1996, 2005). For selected gastropod species, the optimal climatic condition can be determined along with the minimum and maximum temperature values of tolerance (activity range of gastropods), with the help of data from meteorological stations. The malacothermometer method is based on equation 5.1 (Sümegi, 1989, 1996, 2005).

The estimated paleotemperature values gained by this method are only valid for the vegetation (growing) period, because the studied gastropod species are active only during certain periods

$$T = \frac{\sum_{i=1}^{n} A_i T_i}{\sum_{i=1}^{n} A_i} \tag{5.1}$$

T = Estimated July paleotemperature [$°C$]
A_i = The abundance of a given species i in the sample
T_i = The optimum temperature of a given species i in the sample
n = The number of species used for the estimation

of the year (Ant, 1963; Evans, 1972; Rousseau et al., 1994; Sólymos and Sümegi, 1999). The activation temperatures of the individual mollusk species is determined by the recent distribution of the forms under study and the measured temperatures of the growth season recorded at mesoclimatic stations (Sümegi, 1989). It should be noted though that mesoclimatic stations record temperatures at a height of 2 m, which are only distantly correlated to the actual activation temperatures of the mollusk species (Sümegi, 1989).

5.2.4. Grain size

For particle size analysis, all samples were dried at 35°C, homogenized and passed through a 2 mm sieve. Organic matter was removed by treating the samples with 0.70 ml 30% H_2O_2 at 70°C for several hours. This process is repeated until a bleaching of the sediment occurs (Allen and Thornley, 2004), however, lasts no longer than three days. To keep particles dispersed, the samples were treated with 1.25 ml $Na_4P_2O_7$ for 12 hours on an overhead shaker (DIN ISO 11277, 2002; Pye and Blott, 2004). Particle size was measured with a Laser Diffraction Particle Size Analyzer (Beckman Coulter LS 13320) calculating the percentaged size frequency of 116 classes within a size range of $0.04 - 2000$ μm with an error of 2%. Each sample was measured four times in two different concentrations to increase accuracy. The grain size distributions were determined applying the Mie theory (Fluid RI: 1.33; Sample RI: 1.55; Imaginary RI: 0.1; Özer et al., 2010; ISO International Standard 13320, 2009; cf. Schulte et al., 2016).

5.2.5. Rock magnetism

The rock magnetic measurements follow procedures outlined in Baumgart et al. (2013), Buggle et al. (2014), and Zeeden et al. (2011, 2015). Samples were dried and compressed into plastic boxes of 6.4 cm^3 volume. For measurement of the (frequency dependent) magnetic susceptibility (χ_{fd}) each specimen was measured twice at two different frequencies (0.3 and 3 kHz) in a magnetic AC field of 320 A/m using a MAGNON VFSM susceptibility bridge (sensitivity greater than 5×10^{-6} SI). Data were corrected for instrument drift and the susceptibility of the container. The frequency dependent magnetic susceptibility is calculated as follows:

$$\chi_{fd}\ [\%] = \frac{\chi_{0.3\text{kHz}} - \chi_{3\text{kHz}}}{\chi_{0.3\text{kHz}}} \times 100\ [\%] \tag{5.2}$$

χ_Δ as function of χ_{lf} is used to calculate the detrital background susceptibility of the unweathered parent loess (Buggle et al., 2014; Forster et al., 1994).

5.2.6. Geochemistry

For elemental determination by X-ray fluorescence (EDPXRF) a Spectro Xepos was used. These bulk sediment samples were sieved $< 63\ \mu m$, dried for 12 hours at $105°C$ and prepared for powder pellets. Measurements were conducted in the pre-calibrated mode (38 KeV, 10 W). All samples were measured twice; the arithmetic mean is presented here. For data evaluation, selected elements were used, especially those that reflect influences of weathering and redoximorphic features. Elemental ratios that give indications of weathering processes were built. The chemical index of alteration (CIA, Nesbitt and Young, 1989) and the Ba/Sr ratio, an indicator for immobile (Ba, bound to clay)/mobile (Sr, similar behavior as Ca and mainly associated with Ca) elements (see Buggle et al., 2011, and references therein) were determined.

5.2.7. Color

Color of dried and homogenized sediment samples was determined using a Konica Minolta CM-5 spectrophotometer. The L* a* b* values indicate the extinction of light, on a scale from L* 0 (absolute black) to L* 100 (absolute white), and express color as chromaticity coordinates on red-green (a*) and blue-yellow (b*) scales. Plotting of measured colors was done using the 'drawProfile.R' R script (Zeeden et al., 2016a,e), similar to Fitzsimmons et al. (2016) and Sprafke (2016).

5.3. Results

5.3.1. Chronological data

For one sample of each profile a prior IR stimulation temperature test and dose recovery tests (DRTs) were conducted on the luminescence samples (more extensive testing was restrained by the amount of sample material). Samples C-L3789 and C-L3793 show a plateau between $50 - 140°C$ (Fig. 5.3 top). For sample C-L3793 a DRT was conducted with a first IR stimulation temperature of $50°C$, which behaved satisfactorily with a recovered/given dose ratio of 0.95 ± 0.02 (n=4; Fig. 5.3 bottom). Accordingly, all samples of Ságvár II were measured with the $pIR_{50}IR_{290}$ protocol (cf. Buylaert et al., 2012). Contrarily, sample C-L3789 of Ságvár I showed greater inter-aliquot scatter for the prior IR stimulation temperature of $50°C$, which is why DRTs were performed for two higher prior IR stimulation temperatures ($pIR_{80}IR_{290}$, $pIR_{110}IR_{290}$). These delivered recovered/given dose ratios of 0.99 ± 0.03 (n=5) and 0.98 ± 0.03 (n=5; Fig. 5.3 bottom). Since the best DRT was achieved with a first IR stimulation temperature of $80°C$, D_e measurements of C-L3789 used the $pIR_{80}IR_{290}$ protocol. The abanico plots in Supplementary Figure A.2 show a high precision and a low relative standard error of samples C-L3789, C-L3791 and C-L3793. Sample C-L3792 behaved somewhat different, which is related to the limited amount of material left (only 8 aliquots could be measured). Overdispersion values were all $< 4\%$. All measurements show bright signals, negligible recuperation and desired recycling ratios. Supplementary Figure A.3 depicts exemplary growth and shine down curves. Residuals were $< 4.4\%$ of the D_e values and were subtracted for DRT, but not for D_e determination (cf. Kars et al., 2014; Murray et al., 2014). Measurements of

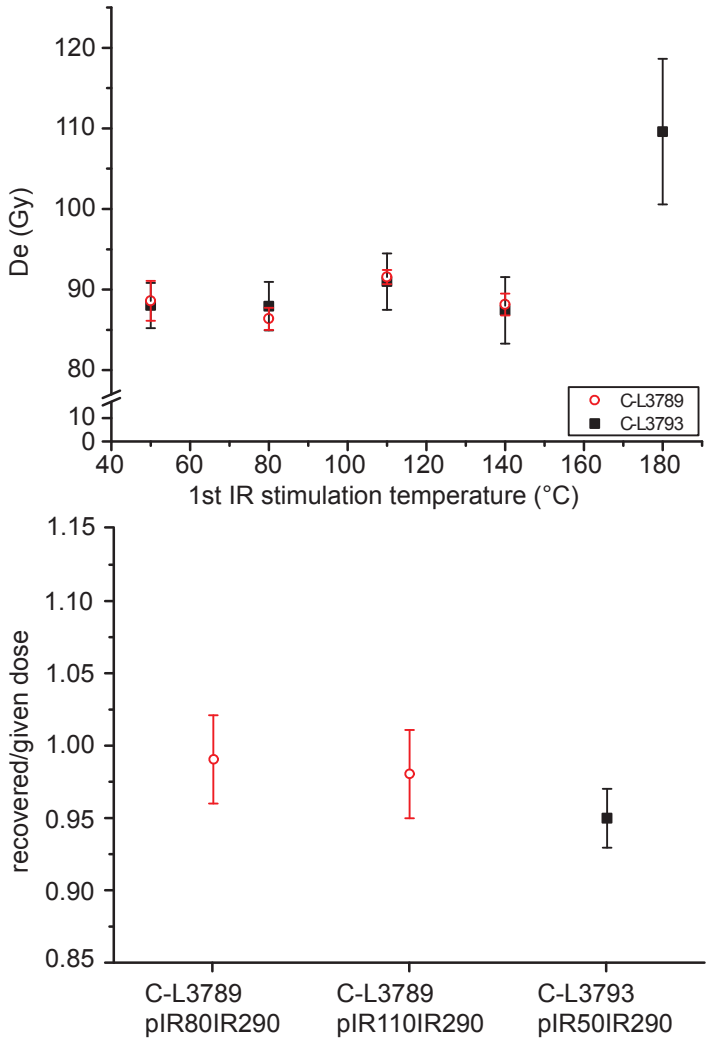

Figure 5.3.: First IR stimulation temperature tests (top) and dose recovery tests (bottom) of samples C-L3789 and C-L3793. Arithmetic mean and standard error are shown. For dose recovery ratios residual doses after 24 h solar simulator irradiation were subtracted.

α-efficiency were not straightforward, as signals within the linear part of the growth curve were quite dim. The α-efficiency measurements gave the following values: 0.13 ± 0.1 (C-L3789) and 0.15 ± 0.12 (C-L3793) and were used for the remaining samples. The samples do not exhibit any appreciable fading; measured fading rates were $g_{2days} = -1.2 \pm 0.9\%$/decade (C-L3789) and $g_{2days} = 0.00 \pm 0.7\%$/decade (C-L3793). Final age calculation gave ages between 20.6 ± 1.4 *ka* (C-L3789) and 17.7 ± 1.2 *ka* (C-L3791), placing the site in the last glacial maximum (see Table 5.1). Table 5.1 summarizes the geochronological data.

Furthermore, recalibration of the bulk radiocarbon data gave an age of 22.4 ± 0.4 *ka cal BP* for the upper sample and 23.8 ± 0.4 *ka cal BP* for the lower sample (cf. Krolopp and Sümegi, 2002).

5.3.2. Malacology

The Ságvár I profile yielded more than 25,000 specimens of 20 terrestrial mollusk taxa. According to the statistical analyses of the Quaternary mollusk fauna, six local malacological zones were distinguished. Supplementary Figure A.4 gives an overview of mollusk fauna abundances; Figure 5.4 shows their temperature-related, humidity-related, and vegetational indications.

The first local malacological zone ($120-112$ cm) was poor in species and the specimen number was likewise low ($13-14$ species). A clear prevalence of xerophilous, steppe-dweller elements like *Pupilla muscorum, Pupilla triplicata, Pupilla sterri, Chondrula tridens, Helicopsis striata* characterizes this zone (Fig. A.4). With cryophilous *Pupilla sterri* and thermophilous *Pupilla triplicata* being most abundant, a *Pupilla sterri* paleoassociation developed in this horizon. The reconstructed July paleotemperature was $< 14°C$ based on the malacothermometer method (Fig. 5.4). For comparison, the current July temperature at the Miskolc climatic station is $21.2 \pm 0.8°C$ (mean 2006-2014, NOAA, 2017).

The abundance of cryophilous species such as *Pupilla sterri* decreased in the second local malacological zone ($112-88$ cm), while the abundance of *Columella columella* gradually increased. Also, thermophilous *Pupilla triplicata* and *Helicopsis striata* became more abundant and formed a paleoassociation. The individual and species number decreased and the mean July paleotemperature were between $15-16°C$.

There is a marked and relatively rapid change in the mollusk fauna at about 88 cm. The concentration of thermophilous taxa declines resulting in the development of a new assemblage with a high dominance of cold-resistant and cryophilous taxa. This is characterized by the appearance of circumpolar, boreo-alpine elements. The presence of a *Columella columella – Vallonia tenuilabris* paleoassociation was inferred for this horizon. The malacothermometer suggests July paleotemperatures between $11.7-12.9°C$. Parallel to the formation of this cold phase the abundance of hygrophilous taxa increased. Besides the cryophilous taxa, the shade-loving *Clausilia dubia* was also abundant.

Table 5.1.: Luminescence data showing equivalent dose (D_e) including their standard error, residual signal with standard deviation, alpha efficiency used (measured for starred samples), dose rate data and calculated ages. 1σ-errors are indicated. As described in the methods the measured water content was not used for age calculation, instead an assumed value of $15 \pm 5\%$ was applied.

Sample Code	**Grain size (μm)**	**Depth (m)**	**No. of aliquots**	**D_e (Gy) CAM**	**Residual (Gy)**	**U (ppm)**	**Th (ppm)**	**K (%)**	**Alpha efficiency**	**Water cont.(%)**	**Total DR (Gy)**	**Age (ka)**
C-L3789	4-11	1.8	12/13	86.44 ± 4.41	3.76 ± 0.33	3.06 ± 0.14	9.64 ± 0.5	1.29 ± 0.03	0.13 ± 0.01*	1.29	4.21 ± 0.19	20.6 ± 1.4
C-L3791	4-11	1.35	10/10	79.3 ± 4.05	3.13 ± 0.24	3.08 ± 0.14	9.85 ± 0.51	1.31 ± 0.03	0.15 ± 0.02	3.02	4.49 ± 0.21	17.7 ± 1.2
C-L3792	4-11	1.65	8/9	83.45 ± 4.41	3.04 ± 0.2	2.96 ± 0.13	9.96 ± 0.5	1.35 ± 0.03	0.15 ± 0.02	4.53	4.47 ± 0.21	18.7 ± 1.3
C-L3793	4-11	2.25	13/13	85.68 ± 4.45	3.24 ± 0.26	3.08 ± 0.14	9.22 ± 0.49	1.28 ± 0.03	0.15 ± 0.02*	2.47	4.35 ± 0.21	19.7 ± 1.4

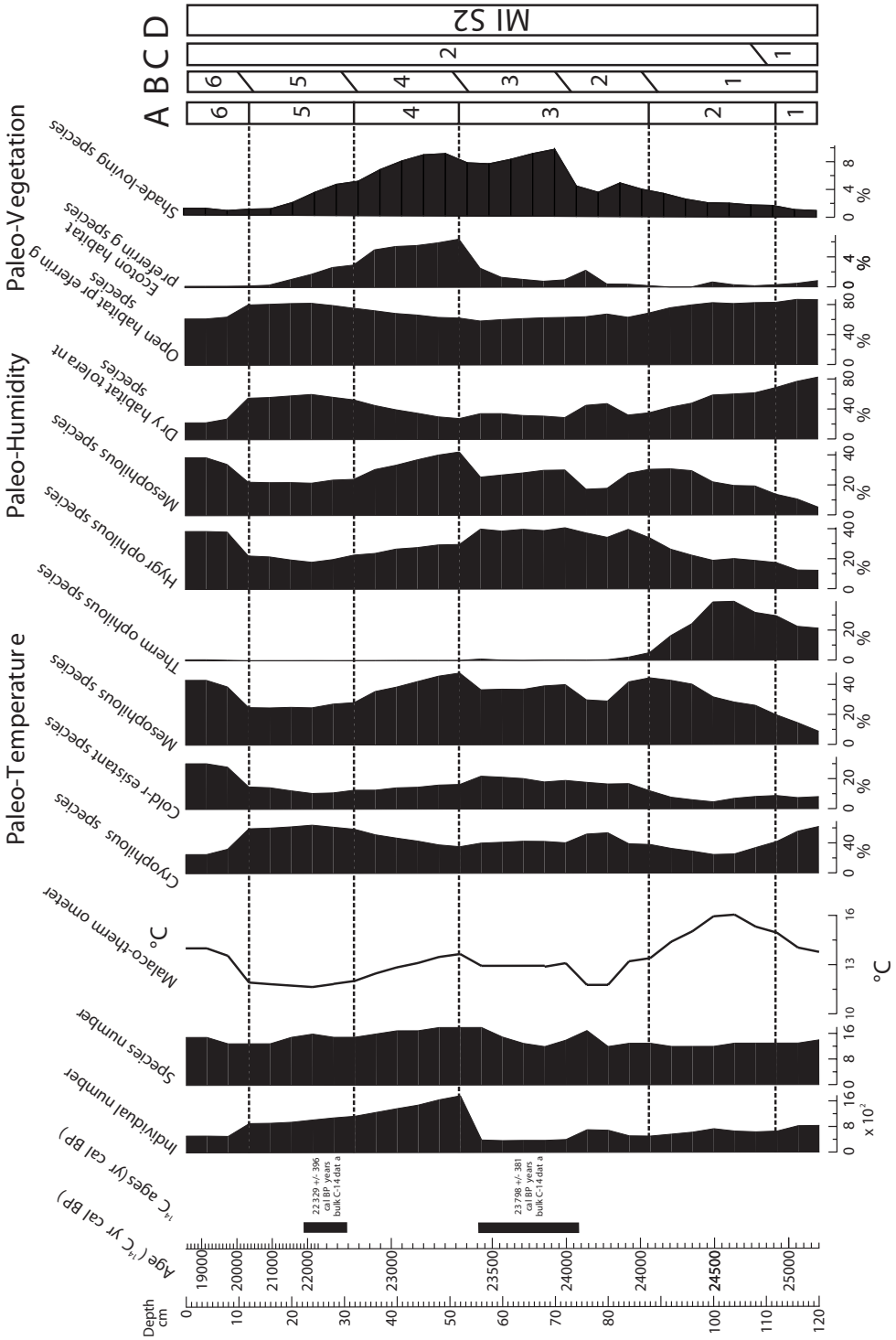

Figure 5.4.: The dominance of the different paleoecological groups and the reconstructed mean July paleotemperatures from Ságvár I showing A) local malacological zones; B) Hungarian Malacological Zones from the Late Quaternary, 1 = *Granaria frumentum – Vallonia enniensis* zone, 2 = *Pupilla triplicata* zone, 3 = *Vallonia tenuilabris* zone, 4 = *Vallonia costata* zone, 5 = *Columella columella* zone, 6 = *Vestia turgida – Punctum pygmaeum* zone; C) Hungarian Malacological Subzones from the Late Quaternary, 1 = *Catinella arenaria* subzone, 2 = *Semilimax kotulai* subzone; D = Marine Isotope Stages (Krolopp and Sümegi, 2002; Sümegi, 1995; Sümegi and Krolopp, 2000, 2002). For orientation a time-scale is given that is based on two radiocarbon ages (Krolopp and Sümegi, 2002) and a comparison to other radiocarbon-dated malacological sections in Hungary. Note that the radiocarbon samples were taken at a depth of ~25 and ~55 cm.

In the fourth malacological zone ($52-32$ cm) more shade-loving, forest-dwelling species, such as *Semilimax kotulai*, and *Arianta arbustorum* appear. In addition there is an increase in the number of the ecoton-habitat preferring mollusks (Figs. 5.4 and A.4). *Semilimax semilimax* occurs at a rather short interval at the transition between zones three and four. This refers to the emergence of a *Semilimax kotulai – Punctum pygmaeum - Arianta arbostrum* paleoassociation with mean July paleotemperatures ranging between 11 and 13°C.

There is a decrease in the number of taxa in zone 5 ($32-12$ cm), after this mollusk rich layer. The shade-loving and ecoton taxa declined gradually and cryophilous, xeromontane *Vallonia tenuilabris* became the most dominant mollusk species. This marks the development of a *Vallonia tenuilabris* paleoassociation characterized by mean July paleotemperatures ranging between $11-12°C$. The amount of cryophilous elements, such as *Columella columella* and *Vallonia tenuilabris* decreased in the sixth malacological zone ($12-0$ cm) and parallel to this decline, mesophilous *Pupilla muscorum* and hygrophilous *Trichia hispida* increased and became the dominant taxa of this horizon. Mean July paleotemperatures ranged here between 13 and 15°C.

5.3.3. Grain size properties

In the uppermost ca. 50 cm of Ságvár I, fine grain sizes < 5 μm contribute to ca. 11% of the overall grain size distribution. In the lower part, this percentage is higher and around 12%, with a decreasing trend in the lower ca. 40 cm (cf. Fig. 5.5). Grain sizes coarser than 63 μm contribute with ca. 22% in the upper ~80 cm, below they have a higher contribution with ca. $25-30$%. The mode follows the pattern of the > 63 μm fraction, and shows a coarsening trend from ca. 80 cm towards the bottom of the profile.

For Ságvár II the < 5 μm fraction shows a decreasing trend towards the bottom; maximum values (~18%) occur in the topmost ~40 cm, followed by a minimum from ca. $50-80$ cm (~12%). After an increase at $90-100$ cm towards values of ~14%, an almost linear trend towards lower values at the bottom of the profile (~12%) is evident. The > 63 μm fraction shows an opposite trend and highest values with ~24% in the topmost ca. 60 cm of the profile. After a maximum at ca. $60-80$ cm with values up to ~30%, another minimum follows from $\sim 80-160$ cm showing $\sim 22-24$% of coarse material. Below this level the > 63 μm fraction plays again a more important role with $24-28$%. The mode of grain size distributions shows no clear pattern, and varies around 51 μm.

Generally, clay does not show a pronounced second peak in granulometric volume % data, indicating no or only weak pedogenesis in some intervals for both profiles (Fig. A.5).

5.3.4. Rock magnetism

The loess at Ságvár shows a background magnetic susceptibility of ca. $30 \times 10^{-8} \frac{m^3}{kg}$ (Ságvár I) and $18 \times 10^{-8} \frac{m^3}{kg}$ (Ságvár II). The magnetic susceptibility (MS) is clearly elevated in the younger cultural layer sampled in the first profile (Fig. 5.5), and reaches values of more than 130×10^{-8} $\frac{m_3}{kg}$

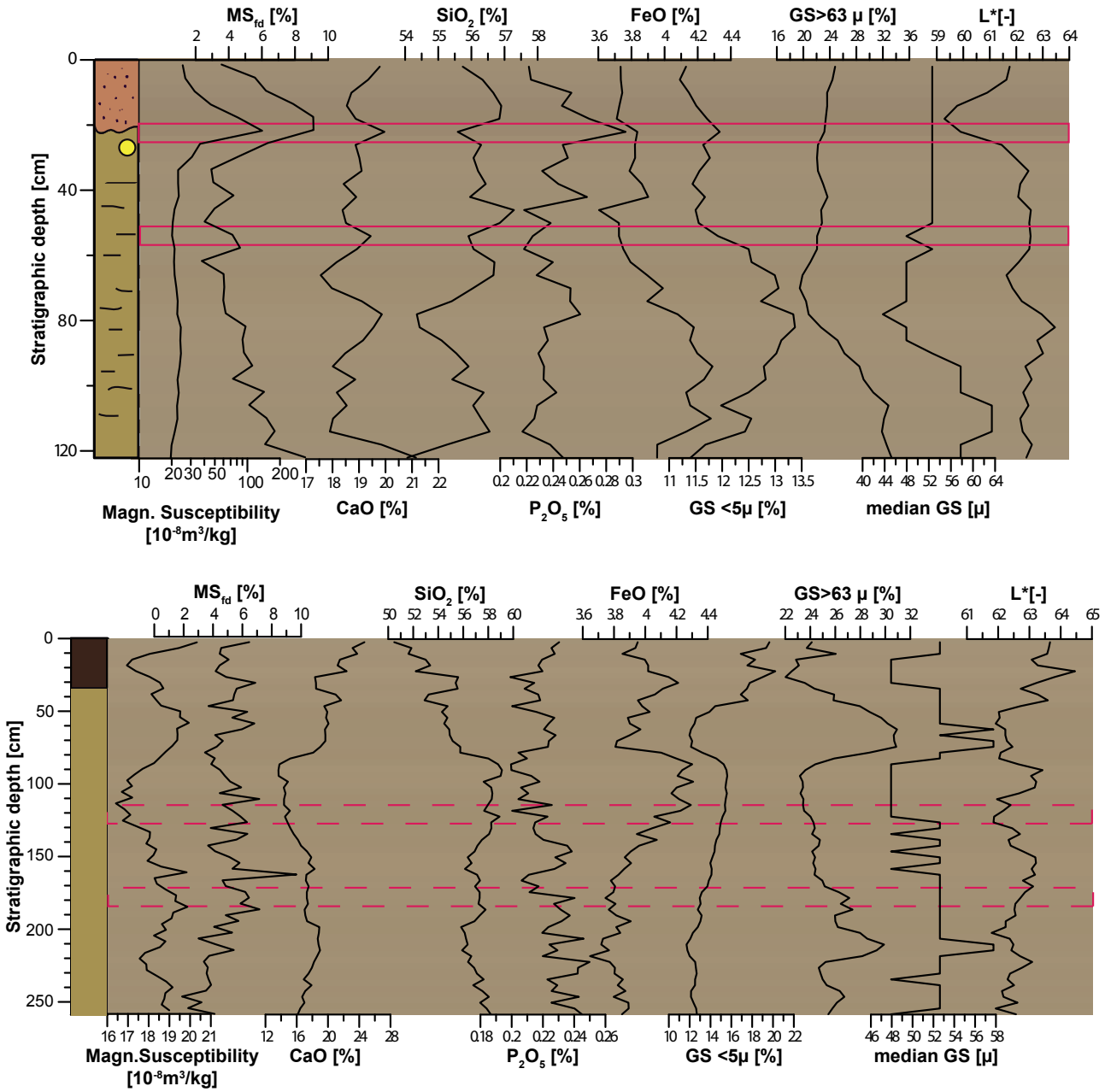

Figure 5.5.: Sediment properties from Ságvár I (top) and II (bottom), underlain by a representation of the measured dry color (Sprafke, 2016; Zeeden et al., 2016a). Note that magnetic susceptibility is presented on a logarithmic scale. The position of the cultural layers is indicated with red boxes.

in one sample. At Ságvár II, the MS follows a semi-sinusoidal pattern with maxima at ~60 and 190 cm, and minima around 110 and 220 cm. The susceptibility has frequency dependencies of around 6% in both profiles. At Ságvár I the younger cultural layer shows strong frequency dependence, and also the lowest part shows increased frequency dependence with values around 5%.

5.3.5. Geochemistry

The calcium oxide content at Ságvár I varies around 19% without a clear trend (Fig. 5.5); silica oxides, probably mainly quartz, contribute with ~55% to the loess and show a minimum at ~80 cm. The phosphorus pentoxide content peaks in the younger cultural layer and iron oxide shows a tendency to higher ($> 4\%$) contribution towards the profile base. FeO concentrations seem to follow the $< 5\ \mu m$ fraction. Weathering indices show an increasing trend towards the base of the profile, but do not show the younger cultural layer clearly (Fig. 5.6). The somewhat darker interval around $60 - 70$ cm depth on the other hand is visible in the Ba/Sr ratio and is located in the same depth as the lower cultural layer.

At Ságvár II, calcium oxide concentrations are highest (~20%) in the uppermost 70 cm, and minor below this level (~16%). The silica content follows the opposite pattern (Fig. 5.5), and is lowest (~54%) in the uppermost 70 cm, and higher thereafter (~58%). FeO concentrations follow the $< 5\ \mu m$ fraction as in Ságvár I, and have maxima at ca. 30 and 100 cm reaching ~4.2%. Minima at ~50 cm and at the bottom of the profile show values of ~3.8%. Also weathering indices show a pattern similar to the $< 5\ \mu m$ fraction (Fig. 5.6).

5.3.6. Color

For Ságvár I, plotted dry color variations (Sprafke, 2016; Zeeden et al., 2016a) are supplemented by plotting of L* (Figs. 5.5 and 5.6). The darker and more reddish cultural layer can be clearly distinguished from the loess at ~20 cm. The L* indicates a maxima at ~85 cm. A local minima of L* at ~65 cm likely corresponds to the lower cultural layer. For Ságvár II, the spectrophotometric measurements bring more information than was possible to observe by eye in the field, and show several changes from lighter to darker loess (Fig. 5.5). Three minima can be distinguished at $50 - 80$ cm, $110 - 140$ cm and around 200 cm.

5.4. Discussion

5.4.1. Correlation between profiles

The two profiles at Ságvár were correlated by means of the SiO_2 abundance and the lightness L* (see Fig. 5.7), mainly because we regard the silica content as a good proxy of quartz which is not easily weathered, and we regard the color as useful proxy to detect cultural remains (here: charcoal remains) and the presence of dark organic carbon (vs. light carbonate). We regard minima in lightness more robust than maxima, because maxima may be caused by carbonate (re)precipitation. The lightness shows two clear minima at 20 cm and 70 cm depth (Ságvár I),

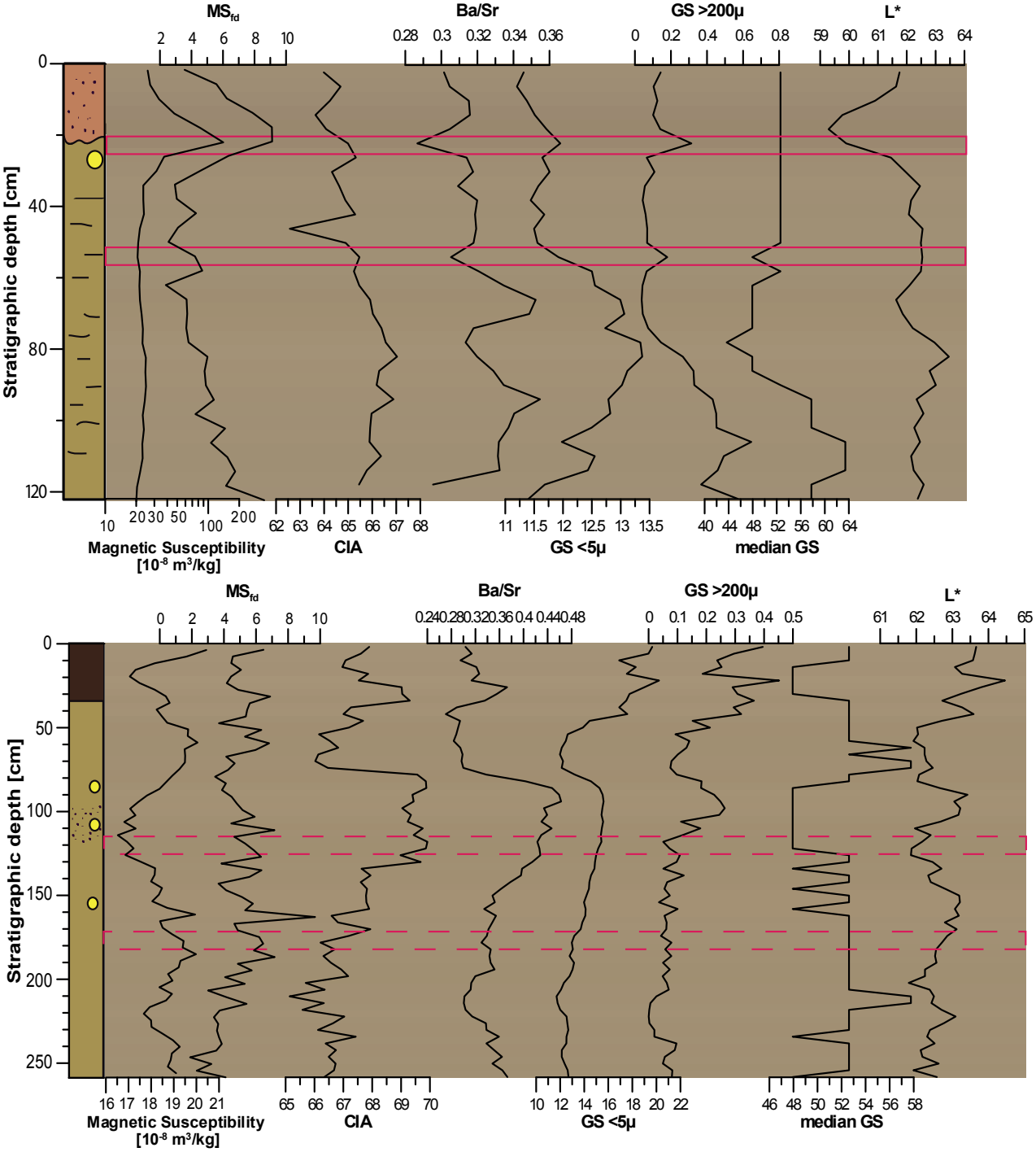

Figure 5.6.: Sediment properties of Ságvár I (top) and Ságvár II (bottom) including the chemical index of alteration (CIA) and the Ba/Sr ratio, both regarded weathering proxies in some environments. Note that magnetic susceptibility is presented on a logarithmic scale. The position of the cultural layers is indicated with red boxes. Both plots are underlain by a representation of the measured dry color (Sprafke, 2016; Zeeden et al., 2016a).

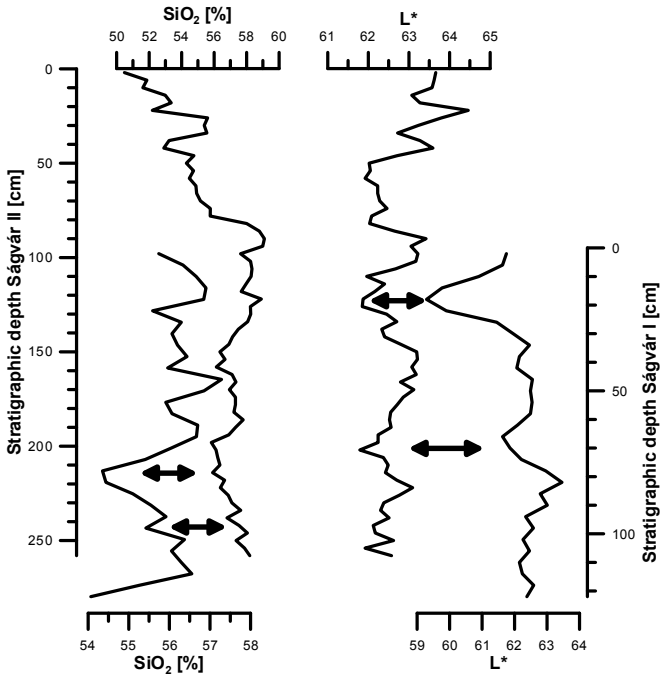

Figure 5.7.: Correlation between the two profiles at Ságvár using the abundance of SiO_2 and the lightness L*. Arrows indicate common features used for correlation.

and two maxima at ~30 cm and 80 cm depth (Ságvár I scale), which can be recognized in the Ságvár II profile (see Fig. 5.7). In general, both profiles show similar patterns of these proxies. The trends in SiO_2 are not as clear, but prominent minima in SiO_2 abundance can be observed at ~80 cm and ~100 cm, while two local maxima are shown around ~40 cm and ~60 cm depth. Generally, variations appear clearer for Ságvár I than for Ságvár II, maybe caused by the (recent) landscape position (slope vs. hilltop). Several other proxies do not directly fit the correlation (e.g. the grain size fraction $< 5\ \mu m$), which may be related to different local weathering intensities due to different solar irradiation and moisture on slopes. The correlation between the profiles confirms our observation in the field, where we correlated a clearly visible archeological layer in Ságvár I with a layer containing charcoal flitters at Ságvár II.

5.4.2. Age model

Prior IR stimulation temperature tests, dose recovery tests and residual measurements show that the measurements perform well and that the samples are suitable for measurement with the pIRIR protocol. Although the samples of the two sections were not measured with the exact same protocol (differing in their prior IR stimulation temperature), we do not expect any difference in age, since both temperatures used are within the plateau region. Moreover, the differing protocols allowed all samples to be measured with the protocol that delivered the most reliable results.

One of the major concerns in pIRIR measurements are possible age overestimations in young samples due to high residual doses. It has been shown that this is not always the case (e.g.

Klasen et al., 2017; Murray et al., 2014). Also at Ságvár age overestimation due to high residuals can be excluded, as residual doses are $< 5\%$ of $D_e s$ (i.e. < 1 *ka* possible age difference). As expected for this protocol, no fading was detected (cf. Buylaert et al., 2012; Thiel et al., 2011b). The α-efficiency measurements showed a clear deviation from the often used literature value (e.g. Buylaert et al., 2012). This indicates how important those measurements are and impacts the age result (also cf. Kreutzer et al., 2014). In case of Ságvár, the luminescence ages are $> 15\%$ younger using the measured α-efficiency instead of the commonly used value of 0.08 ± 0.02.

Although pIRIR ages increase with depth for Ságvár II, all age data overlap within 1σ. Therefore, correlation between profiles was achieved by using physical and chemical proxy data, as described in Chapter 5.4.1. This correlation provides furthermore the opportunity to transfer the age data from Ságvár II to Ságvár I, which helps us further constrain the malacological zones (see Chapter 5.4.3). What is more, the pIRIR age of Ságvár I (20.6 ± 1.4 *k*a) agrees within 1σ with the upper radiocarbon age of 22.3 ± 0.4 *ka cal BP* (18.5 ± 0.2 *ka BP*). The luminescence sample was taken just a few cm below the radiocarbon sample. Another ^{14}C age of 23.8 ± 0.4 *ka cal BP* (19.8 ± 0.2 *ka BP*) is further used as time-marker for Ságvár I (cf. Krolopp and Sümegi, 2002).

Taphonomic issues have been raised for the 1950s excavation. These cannot be excluded here due to the proximity of the two profiles and the averaging of the multigrain approach used for pIRIR dating. Due to a lack of material, it was not possible to investigate single coarse grain data. However, sample ages increase with depth, compare well to radiocarbon ages, and show little scatter, thus we disregard this concern. To conclude, the performance of the luminescence measurements and the agreement with the ^{14}C data in profile Ságvár I encourage the validity of this age model.

Further age constraints discussed in Chapters 5.4.3 and 5.4.4 derive from a comparison between malacological data in Hungary (Sümegi, 2005; Sümegi and Krolopp, 1995, 2002) and serve as a reference. Without further geochronological analysis (radiocarbon or luminescence dating) it is not possible to gain a more precise age model that covers both sections at Ságvár completely.

5.4.3. Paleoenvironmental proxy data

5.4.3.1. Discussion of malacology

The analysis of the mollusk fauna of Ságvár I revealed the presence of six malacological zones indicative of the changing paleoclimatic and paleoenvironmental conditions. According to the composition of the fauna (Sümegi, 2005), dust accumulation and loess diagenesis was initiated under arid conditions in a short grassland environment. The first zone contains both cryophilous and thermophilous taxa, suggesting fluctuations between short cold and warm, but dry, climatic phases. Increased temperatures and the elevated numbers of thermophilous taxa in zone 2 refer to a minor change to more temperate conditions compared to the previous zone. Climatic conditions were likely mild and dry. The presence of the *Pupilla triplicata* – *Helicopsis striata* paleoassociation indicates the development of short continental-type dry

grassland vegetation. Based on earlier radiocarbon dated Quaternary malacological material from the loess sections from Hungary (Sümegi, 2005; Sümegi and Krolopp, 1995, 2002) this local malacological zone formed between $26 - 24$ ^{14}C *ka cal BP* and it may be synchronized to the period of Greenland Interstadial GI 2 phase (Andersen et al., 2006; Svensson et al., 2006).

The third zone containing both cold-resistant and cryophilous elements is clearly prevailed by the cold-loving, Northern Asian, xeromontane *Vallonia tenuilabris* (Horsák et al., 2009; Ložek, 1964; Meng, 2009; Sümegi, 2005). This rapid transformation in the composition of the mollusk fauna is typical for the transition at ca. 24 ^{14}C *ka cal BP* in the whole region (Hupuczi and Sümegi, 2010; Sümegi, 2005; Sümegi and Krolopp, 2002; Sümegi et al., 2015) and may also correspond to Heinrich event H2 and the beginning of the LGM. Based on humidity preferences of the examined taxa, the increase of cold-resistant taxa was accompanied by a similar rise in hygrophilous and shade-loving taxa. The peak in the abundance values of the shade-loving *Clausilia dubia*, which prefers closed-forest environments (Horsák et al., 2013; Kerney et al., 1983; Ložek, 1964; Soós, 1943), is very unusual, as there is no major increase in the abundance of ecoton environment dwelling species. On the basis of these characteristics we may postulate the emergence of a unique open parkland (cf. Sümegi et al., 2012a; Willis et al., 2000) studded sporadically by trees and/or scrubs. This environment was composed of alternating mosaics of cold, wet tundra-like, and cold steppe microhabitats at about 24 ^{14}C *ka BP*. Scattered tall herbs and scrubs in certain microhabitats might have provided enough shade for the survival of the shade-loving *Clausilia dubia* during this cold phase of the Late Pleistocene. Mollusk data clearly indicate the presence of a typical and diverse mammoth steppe here (Bocherens, 2003; Bocherens et al., 1996). The presumable lower Gravettian occupation level can also be found in this zone and possibly formed around 24 and 23 ^{14}C *ka cal BP* based on the mass radiocarbon data from this layer (Gábori, 1959, 1965, 1969, 1989; Gábori and Gábori-Csánk, 1957; Gábori-Csánk, 1978; Gáboriné Csánk, 1960; Sümegi and Krolopp, 2002; Vöros, 1982). This third malacological zone formed parallel to the lower and presumable older Gravettian horizon in the section of Ságvár (Gábori and Gábori-Csánk, 1957; Krolopp and Sümegi, 2002).

The fourth malacological zone contains shade-loving and ecoton habitat preferring taxa along with open parkland elements, which are common throughout the investigated period. The mollusk composition points to the presence of alternating cold/cool and wet climatic phases as well as boreal forest/forest steppe vegetation. The *Semilimax kotulai – Punctum pygmaeum - Arianta arbostrum* paleoassociation suggests a formation between 20 and 23 ^{14}C *ka cal BP* ($20 - 17$ *ka BP*) based on radiocarbon data from Hungary (Hupuczi and Sümegi, 2010; Krolopp and Sümegi, 1990, 1991, 1995; Sümegi, 2005; Sümegi and Hertelendi, 1998; Sümegi and Krolopp, 1995, 2000, 2002; Sümegi et al., 1998a, 2015).The composition of the mollusk fauna from the charcoal-rich loess layer indicates the development of mosaic vegetation - a continental forest steppe with tundra spots - in this phase. According to our findings, taxa requiring denser vegetation cover underwent an expansion between 23 and 22 ^{14}C *ka cal BP* in the areas of the Danube bend, the foothills of the Hungarian Upland, as well as the southern parts of Transdanubia, the Tiszántúl and the Danube-Tisza Interfluve (Hupuczi and Sümegi,

2010; Sümegi, 2005; Sümegi and Hertelendi, 1998; Sümegi and Krolopp, 1995, 2000, 2002; Sümegi et al., 2015). This local malacological zone developed parallel with the younger Upper Gravettian archeological layer, which can be clearly seen in the analyzed loess profile with small bones and burnt charcoal. The malacological data and their relation to the archeological layers suggest that the second and younger Gravettian horizon can be found at the transition between the fifth and the fourth local Quaternary malacological zones (Fig. 5.4).

The fifth zone marks drier and colder conditions. Biostratigraphically, it can be assigned to the *Pupilla sterri* zone in other profiles, which is suggested to be younger than 20 ^{14}C *ka cal BP* (17 *ka BP*) on the basis of radiocarbon dated mollusk faunas from loess profiles in the Carpathian Basin (Krolopp and Sümegi, 1992; Sümegi, 1995, 2005; Sümegi and Krolopp, 1995, 2002; Sümegi and Lóki, 1990; Sümegi et al., 1991, 1992). Also the luminescence data indicates that this zone formed after ~$18 - 22$ *ka* (C-L3789 and C-L3793). However, the *Pupilla sterri* taxon is by no means prevalent in the referred zone at Ságvár. The coldest mean July paleotemperatures are within this zone in the investigated section. This local malacological zone marks the last large-scale appearance of cold-resistant, xerophilous, presently xeromontane mollusk taxa in the central parts of the Carpathian Basin (Sümegi and Krolopp, 1995, 2002; Sümegi et al., 1998a). This period also corresponds to the last significant appearance of cold-loving elements in the mollusk fauna; i.e. the typical loess steppe-dweller elements in the Carpathian Basin. Consequently, the major part of the basin was covered by cold continental steppe with small tundra vegetation spots during this period. In addition some areas were characterized by favorable edaphic microclimatic conditions acting as refugees harboring mixed taiga woodland elements and most likely thermomesophilous arboreal elements as well (Sümegi, 2005, 2012; Sümegi et al., 2012a, 2015).

The sixth zone shows somewhat milder and more humid conditions as well as the last appearance of the loess fauna in the Carpathian Basin. This is also indicated by higher reconstructed mean July paleotemperatures of $13 - 15°C$. In addition, increases in temperature and humidity initiated the formation of continental grassland with tall herbs. Luminescence data suggests that this zone formed after 17.7 ± 1.2 *ka* (C-L3791).

5.4.3.2. Discussion of physical and chemical proxy data

Grain size, rock magnetic and geochemical data point to rather pure loess altered only slightly by pedogenetic processes. The grain size properties of all samples from Ságvár are similar (Fig. A.5). This similarity may be seen as indication of similar paleoenvironmental conditions during a relatively short time span, which is also confirmed by the luminescence chronology. Additionally, the fact that clay does not show a prominent second peak in granulometric volume % (Fig. A.5) may be another indication for rather pure loess (vs. weathered loess and a pedogenic overprint), as reported for the cold phases of the last glacial from other parts of the Carpathian Basin. Here we discuss the rather weak but also clearly present changes in loess composition.

In the Ságvár I profile, the upper part has less coarse components than the lower part, indicating different conditions. At Ságvár II on the other hand, the upper part shows increased amounts of clay. The increased clay content might be related to the pedogenesis of the recent soil above (Fig. 5.5). The grain size distributions have a similar shape as data from several other Hungarian localities (e.g. G. Varga et al., 2012), and are a little coarser than data from Semlac which are interpreted to be non-local (Zeeden et al., 2016c). This and the rather high sand content might indicate local (not distant) sources of Ságvárian loess, potentially in the area of Lake Balaton. The geochemical weathering indices CIA and Ba/Sr ratios have a similar amplitude as in Orlovat (Obreht et al., 2015), indicating paleoenvironmental variability within and similarity between both profiles due to large-scale comparable paleoenvironmental and weathering conditions.

Moreover, rock magnetic results are consistent with rather pure loess, when compared to the glacial background magnetic susceptibility at other sites in the Carpathian Basin and adjacent areas (e.g. Basarin et al., 2014; Buggle et al., 2014; Marković et al., 2011, 2012b, 2014; Zeeden et al., 2011). However, the frequency dependent magnetic susceptibility is relatively high for rather pure loess, compared to other LGM loess data (see e.g. Buggle et al., 2014), and is more indicative for loess deposited in late MIS 3. This may indicate not extremely unfavorable conditions, or more likely a specific source material with elevated frequency dependence. The younger cultural layer shows a peak in the magnetic susceptibility as also seen in Krems (Austria) for burned material (Hambach et al., 2008).

Moreover, the spectrophotometric color analyses give some indications for weak soil formation. At Ságvár I, the color shows darker loess around $60-70$ cm depth, corresponding to a minimum in CaO (cf. Fig 5.5) and a maximum in the Ba/Sr ration, which are all indications for weak pedogenesis. The weak soil formation may indicate slightly more favorable conditions during the presumable older cultural layer, which is located in the same depth. However, human activity may have biased this signal towards a more organic-rich local environment. At Ságvár II, the topmost L* minimum (~$50-80$ cm) is also reflected in enhanced magnetic susceptibility suggesting weak pedogenesis. The L* minimum at ~$110-140$ cm depth, however, corresponds to the interval with dark matter correlated to the younger cultural layer at Ságvár I, and is not visible in any other proxy. This gives further indication that this interval is not affected by pedogenesis, but includes charcoal particles, which led to a darker color.

5.4.4. Integrating proxy data focusing on the cultural layers

Considering the proxy data in combination, we can clearly state that the LGM was not uniformly cold at Ságvár, but that environmental changes are visible in both the mollusk and also physical and chemical proxy data, in agreement with other findings from Hungary (e.g. Sümegi et al., 2012a). In general, we observe a consistent trend towards colder conditions before the occurrence of the archeological layers in multiple proxy data. The presumably older cultural layer was likely formed at the beginning of the LGM in a unique open parkland studded sporadically by trees and/or scrubs with alternating mosaics of cold, wet tundra-like, and cold

steppe microhabitats (if artifact position has not been disturbed post-depositionally). Physical and chemical proxy data indicate a weak pedogenesis in this phase, which was likely related to enhanced moisture availability (as shown by the mollusks). The younger cultural layer is located at the transition of a phase of open landscape and dry and cold climate (malacological zone 4) towards drier and colder conditions (malacological zone 5). Geoscientific data places the occupation a bit higher into the fifth zone. This phase is represented by rather 'pure' loess formation, with no indication of pedogenesis. Pedogenesis was likely hindered due to the dryness of the climate (as shown by malacology). Also in Ságvár II harsh conditions dominated this phase, in accordance with the mollusk assemblages of zone 5. The malacological composition suggests the presumable older Gravettian layer to be formed ~$23 - 24$ ka, while the luminescence chronology as well as malacological data suggests a formation between 20.6 ± 1.4 ka and 18.7 ± 1.3 ka for the younger Gravettian layer.

The malacothermometer and χ_{fd} both show a decreasing trend towards the top of the Ságvár I profile. The high χ_{fd} values in and around the upper cultural layer are an exception and most probably related to burned material. The connection between the mollusk based proxy for paleotemperature and χ_{fd} may be explained by temperatures enhancing soil organic activity and thereby χ_{fd}. Also similarities between the > 63 μm grain size fraction (and also the mode) and the thermophilous snail assemblage can be observed, indicating higher coarse material input being associated with warm phases, as also at e.g. Orlovat (southeastern Carpathian Basin; Obreht et al., 2015). This observation here and at Orlovat may indicate that coarse grain sizes (specifically in the sand fraction) can be related to strong wind intensities during warm phases. Though these similarities between malacological and physical and chemical proxies may not be unexpected, we cannot derive general claims from this dataset. More quantitative comparison between physical, chemical and biological snail proxy data may lead to a better understanding of all proxy data, but will require more data from multiple sites followed by stringent multivariate data analysis.

5.5. Conclusion

This multidisciplinary study of a loess sequence at the last glacial Gravettian site 'Ságvár Lyukas Hill' shows that environmental conditions were not uniform in this time period and that paleoenvironmental changes can be observed even on short (millennial) time scales within rather 'pure' loess formation without visible differences. Both Gravettian layers can be distinguished in the data sets, but disentangling of environmental and anthropogenic signals remains challenging. The luminescence data indicates an accumulation of loess between 21 and 17 ka; comparison of the mollusk species composition to other radiocarbon-dated sections in the Carpathian Basin places Ságvár I possibly between ~25 and 17 ka. The malacological analysis offers a very detailed paleobiological proxy data set that classifies Ságvár I into six malacological zones. These suggest a changing paleoenvironment from short grassland (zone 1-2, ~$25 - 24$ ka), over mosaics of mammoth steppe, forest steppe, continental steppe and tundra (zone 3-5, ~$24 - 18$ ka), to continental grassland (zone 6, after ~18 ka). Additionally, the upper part of Ságvár II (< 18 ka) indicates milder conditions and weak pedogenesis.

This study clearly shows the potential of integrating biological proxy data (here the abundance of different mollusk species) and physical/chemical proxy data. The correlation of physical/chemical sediment proxy interpretations with mollusk assemblage data may be seen as cross-validation of these techniques, more similar studies are required for robust statements. The proxy data show the two cultural layers formed in rather cold climatic phases. This implies that Upper Paleolithic human presence in the Carpathian Basin was not limited to warm or mild phases of the LGM.

6. High-resolution paleoclimatic proxy data from the MIS3/2 transition recorded in northeastern Hungarian loess

Janina Bösken[1], Igor Obreht[1], Christian Zeeden[1], Nicole Klasen[2], Ulrich Hambach[3,4], Pál Sümegi[5], Frank Lehmkuhl[1]
Published in Quaternary International at http://doi.org/10.1016/j.quaint.2017.12.008.

6.1. Introduction

Loess-paleosol sequences have the ability to preserve past environmental and climatic conditions (e.g. Buggle et al., 2013; Derbyshire, 2003; Guo et al., 2002; Heller and Tungsheng, 1984; Krauß et al., 2016; G. J. Kukla, 1977; Kukla et al., 1988; Obreht et al., 2016; Obreht et al., 2017; Smalley and Leach, 1978; Zeeden et al., 2016d). Therefore, these represent a widely used terrestrial archive for the reconstruction of the paleoclimatic dynamics. The loess deposits of the Carpathian Basin have been studied increasingly in recent years for paleoenvironmental studies, but also for geoarcheological investigations (e.g. Bösken et al., 2017b; Chu et al., 2017; Kels et al., 2014). The Danube River has been proposed as route for anatomically modern human dispersal in the Middle and Lower Danube Basin, especially during the Aurignacian (Conard and Bolus, 2003, 2008; Iovita et al., 2014; Mellars, 2011). Additionally, the density of Aurignacian find spots suggests a preference for the Carpathian foothill zone (Hauck et al., 2017). Understanding the paleoenvironmental and paleoclimatological conditions during early modern human dispersal might improve our understanding of past human-climate interactions. In northeastern Hungary, there have been also archeological findings of Gravettian origin such as the Bodrogkeresztúr-Henye site (Dobosi, 2000; Vértes, 1965, 1966). Loess-paleosol sequences can be employed to better understand the environmental context of early modern humans by interpreting proxies of weathering intensity (e.g. Buggle et al., 2011; Obreht et al., 2015; Schatz et al., 2015b; Újvári et al., 2008), pedogenesis (e.g. Bábek et al., 2011; Hao et al., 2008), wind strength and directionality (e.g. Nawrocki et al., 2006; Obreht et al., 2015; Sun et al., 2010; Újvári et al., 2016a; Zeeden et al., 2015), sedimentation rates (e.g. Stevens et al., 2011; Újvári et al., 2010), and changing source material inputs (e.g. Muhs et al., 2013; Obreht et al., 2016; Újvári et al., 2012).

[1]Department of Geography, RWTH Aachen University, Templergraben 55, 52056 Aachen, Germany
[2]Institute of Geography, University of Cologne, Albertus-Magnus-Platz, 50923 Cologne, German
[3]BayCEER & Chair of Geomorphology, University of Bayreuth, Germany
[4]Chair of Physical Geography, Faculty of Sciences, University of Novi Sad, Serbia
[5]Department of Geology and Palaeontology, University of Szeged, Hungary

The present study investigates a loess-paleosol sequence close to the former excavations Bodrogkeresztúr-Henye at the Kopasz Hill (see Fig. 6.1) near Tokaj in northern Hungary. Several proxies (grain size distributions, geochemical analysis, rock magnetic proxies and color measurements) are used to study past environmental changes. Geochronological control is provided by radiocarbon and luminescence dating. The research aim lies in the reconstruction of the paleoenvironmental conditions at the dated loess-paleosol sequence Bodrogkeresztúr (BKT) in order to improve our understanding of the paleoclimatic conditions in northeastern Hungary specifically in MIS 3 and the transition to the cooler MIS 2. A detailed comparison to the close-by loess-paleosol sequence Tokaj (Schatz et al., 2011, 2012, 2015b; Sümegi, 2005; Sümegi and Hertelendi, 1998) aims at detecting local differences in environmental proxies, paleogeography and possibly microclimates. Furthermore, the resolution of the proxy data is increased, which enhances the paleoenvironmental reconstruction.

6.2. Previous investigations

The investigated Bodrogkeresztúr section is located at the northwestern site of the Kopasz Hill, which contains Sarmatian (Miocene) volcanic (including pyroclastic) rocks and is widely covered by loess deposits (Sümegi and Hertelendi, 1998). Previous investigations around the Kopasz Hill have been conducted intensively (Rudner and Sümegi, 2001; Schatz et al., 2011, 2012, 2015b; Sümegi, 2005; Sümegi and Hertelendi, 1998; Sümegi and Krolopp, 2002; Sümegi and Rudner, 2001; Sümegi et al., 2000). The authors constructed a general stratigraphy: the profiles start with a ca. $68-48$ *ka cal BP* 'lower' loess layer, which probably formed during tundra conditions. It is overlain by a dark brown paleosol ($48-41$ *ka cal BP*), which has evolved under a temperate and humid climate. Above, a 'middle' loess layer ($\sim 41-34$ *ka cal BP*) is covered by a reddish brown paleosol that formed during the Upper Weichselian $\sim 34-29$ *ka BP* (Sümegi and Hertelendi, 1998). The Gravettian layer of the Bodrogkeresztúr-Heyne site is also related to this paleosol (Sümegi et al., 2000, 2016). The paleosol is covered by a charcoal bearing white layer indicating the occurrence of extensive (spruce) forest fires under extremely dry conditions $\sim 30-28$ *ka cal BP* (Sümegi, 2005; Sümegi and Hertelendi, 1998; Sümegi and Rudner, 2001; Sümegi et al., 2000). Overlying this soil is the 'upper' loess layer (< 29 *ka cal BP*) that points to continental steppe conditions. Two interstadial phases within the loess layer were determined at $\sim 26-23$ *ka cal BP* and $\sim 20-17$ *ka cal BP* (Sümegi and Hertelendi, 1998), and also two more phases of forest fires occurred around 25 and 20 *ka BP*. Schatz et al. (2011) found two tree-less steppe intervals with strong winds and loess deposition under cool and humid climate. Moreover, five periods with increased tree/shrub vegetation cover were found in this loess layer. Figure 6.1 shows a topographical map with the mentioned investigated sites.

The new site adds a high-resolution paleoenvironmental archive to the previous investigations that is in the vicinity of the archeological site in a comparable geomorphological positions, which allows a reconstruction of the climatological conditions during and after the Gravettian occupation. What is more, the original archeological site and its chronological control is disturbed by erosion of the upper loess layer as well as root penetration into the paleosol (Sümegi and Hertelendi, 1998; Sümegi and Krolopp, 2000; Sümegi et al., 1998b, 2000). The new site at the

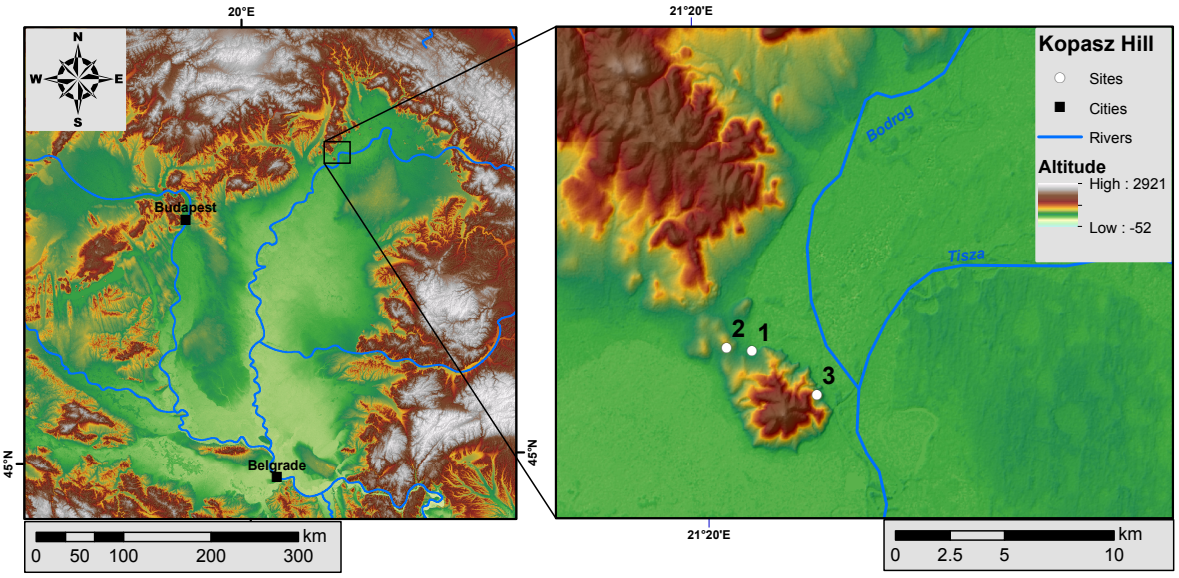

Figure 6.1.: Topographical map showing an overview of the Carpathian Basin (left) and some of the research sites at the Kopasz Hill (right). 1. Bodrogkeresztúr (this study), 2. Bodrogkeresztúr–Henye (e.g. Sümegi, 2005; Sümegi and Rudner, 2001; Sümegi et al., 2016), 3. Tokaj (Schatz et al., 2011, 2012, 2015b; Sümegi, 2005) / Patkó quarry (e.g. Sümegi and Hertelendi, 1998; Sümegi and Krolopp, 2002). Digital elevation model based on SRTM data available from U.S. Geological Survey (Farr et al., 2007).

Bodrogkeresztúr brickyard allows investigating an undisturbed paleosol, which can be connected to the archeological site, and its cover loess. Finally, the investigated sequence is the northernmost loess sequence with a thickness >2 m in this part of the Carpathians highlighting its value for paleoenvironmental studies.

6.3. Methods

6.3.1. Field work

Two loess-paleosol profiles were carefully cleaned, described, and sampled in a former brickyard close to the town of Bodrogkeresztúr in northeastern Hungary. Samples for rock magnetic, sedimentological and color analyses were taken in a resolution of 4 cm, while geochemical analyses were performed in 8 cm resolution. One radiocarbon and three luminescence samples were taken at depths of 1.69 m (C-L3799), 2.9 m (C-L3797), 4.27 m (C-L3795), and 4.51 m (Beta-454081). No further material for ^{14}C dating was observed. Supplementary Figure B.1 shows a photo of the section.

6.3.2. Geochronology

6.3.2.1. Luminescence dating

Equivalent dose (D_e) Sample preparation for D_e determination followed standard laboratory procedures (e.g. Bösken et al., 2017a).

Continuous wave optically stimulated luminescence measurements (CW-OSL) were carried out on a Risø TL/OSL DA 20 reader equipped with a $^{90}Sr/^{90}Y$ β-source and IR LEDs, emitting at 870 nm (FWHM = 40 nm). For signal detection, a 410 nm interference filter was used. The applicability of the pIRIR protocol (Buylaert et al., 2012; Thiel et al., 2011b) was determined by testing different combinations of preheat, first IR, and second IR temperatures on natural and bleached samples (i.e. dose recovery test). First IR stimulation temperature tests on natural samples (cf. Buylaert et al., 2012) were conducted using the $pIRIR_{225}$, $pIRIR_{250}$, $pIRIR_{270}$, and $pIRIR_{290}$ protocols. In a second step, some of these combinations of preheat, first IR stimulation, and second IR stimulation temperatures underwent a dose recovery test, after the aliquots were bleached for 24 h in a Hönle Sol2 solar simulator. Finally, the D_e was determined on a minimum of eight aliquots per sample using an arithmetic mean. The signal was integrated using the first 2.4 s minus a background of the last 25.6 s. Residual doses, after bleaching for 24 hours in a Hönle Sol2 solar simulator, were assessed. Fading rates were measured for one sample after administering a dose of ~115 Gy using storage times between 100 and 800 minutes (following Auclair et al., 2003).

Dose rate Samples for dose rate determination were oven dried ($50°C$), homogenized and packed into plastic cylinders. Radionuclide concentrations were measured on a high-purity germanium gamma-ray spectrometer after a resting period of four weeks (to compensate for radon emanation during pretreatment). Dose rates and ages were calculated in DRAC v.1.2 (Durcan et al., 2015) using the conversion factors of Liritzis et al. (2013), an estimated water content of $15 - 17\%$, and attenuation factors of Bell (1980) and Guérin et al. (2012). The water content was estimated using sample depth and a formula for Hungarian loess sections by Pécsi and Richter (1996). Moreover, a potassium content of $12.5 \pm 0.5\%$ (Huntley and Baril, 1997) and a rubidium content of 400 ± 100 ppm (Huntley and Hancock, 2001) was assumed. The cosmic dose rate was calculated after Prescott and Hutton (1994) considering the geographical position, altitude and sample depth. α-efficiency was determined by giving the samples different α-doses of < 400 Gy in a Freiberg Instruments Lexsyg Research device and recovering this dose with β-irradiation in a Risø-reader, similar to a dose recovery test. It was ensured that the given dose was small enough to be fitted with a linear function.

6.3.2.2. Radiocarbon dating

The charcoal sample was floated to extract the charcoal from the sediment. Dating was performed at the Beta Analytic Radiocarbon Dating Laboratory following the acid/alkali/acid-pretreatment procedure. The content of carbon isotopes was measured by means of accelerator mass spectrometry. Finally, the measured carbon isotope ratios were converted to ^{14}C years and later calibrated using the INTCAL13 calibration curve and the intercept method (Reimer et al., 2013; Talma and Vogel, 1993).

6.3.3. Rock magnetism

The rock magnetic measurements followed procedures outlined in e.g. Baumgart et al. (2013), Buggle et al. (2014), and Zeeden et al. (2011, 2015). Samples were dried and compressed into

plastic boxes with a volume of 6.4 cm^3. Each specimen was measured twice for measurement of the (frequency dependent) magnetic susceptibility (χ_{fd}). Two different frequencies (0.3 and 3 kHz) in a magnetic AC field of 300 Am^{-1} and a MAGNON VFSM susceptibility bridge (sensitivity greater than $5 \cdot 10^{-6}$ SI) were used. Data were corrected for instrument drift and the susceptibility of the container. The frequency dependent magnetic susceptibility is calculated using the following equation:

$$\chi_{fd}\% = ((\chi 0.3kHz - \chi 3kHz)/\chi 0.3kHz) \cdot 100[\%]. \tag{6.1}$$

Oriented sampling of nine specimens were taken at a depth range from about $4.02 - 4.12$ m. Anisotropy of magnetic susceptibility (AMS) measurements follow procedures outlined in Zeeden et al. (2011, 2015). Measurements of the magnetic susceptibility and of the anisotropy of the magnetic susceptibility were made employing an AGICO KLY-3S kappabridge. Data evaluation of magnetic fabric data was done employing the ANISOFT software (version 4.2).

6.3.4. Grain size (GS)

For particle size analysis, all samples were prepared as described in Nottebaum et al. (2015) and Schulte et al. (2016). Particle size was measured with a Laser Diffraction Particle Size Analyzer (Beckman Coulter LS 13 320) calculating the percentaged size frequency of 116 classes within a size range of $0.04 - 2000$ μm (2% error). Accuracy was increased by measuring each sample four times in two different concentrations. The grain size distributions were determined using the Mie theory (ISO International Standard 13320, 2009, Fluid RI: 1.33; Sample RI: 1.55; Imaginary RI: 0.1; Özer et al., 2010; cf. Schulte et al., 2016).

6.3.5. Geochemistry

A Spectro Xepos was used for elemental determination by X-ray fluorescence (EDPXRF). Sample preparation followed procedures described in e.g. Kels et al. (2014) and Obreht et al. (2015, 2016). All samples were measured twice and the arithmetic mean is used for data analysis.

Using elemental data, element ratios, such as Al_2O_3/SiO_2, were calculated to quantify weathering. The Chemical index of alteration was calculated by using the formula

$$CIA = (Al_2O_3/(Al_2O_3 + Na_2O + CaO^*/ + K_2O)) \cdot 100; \tag{6.2}$$

where CaO^* is silicatic CaO (Nesbitt and Young, 1989), as well as the Chemical Proxy of Alteration (CPA, Buggle et al., 2011)

$$CPA = (Al_2O_3/(Al_2O_3 + Na_2O)) \cdot 100. \tag{6.3}$$

Moreover, the Ba/Sr ratio was calculated as indicator for immobile (Ba, bound to clay)/mobile (Sr, similar behavior as Ca and mainly associated with Ca) elements (see Buggle et al., 2011 and references therein). Additionally, an $A - CN - K$ diagram (Nesbitt and Young, 1989) plots the concentrations of Al_2O_3, $Na_2O + CaO^*$, and K_2O in a tertiary diagram.

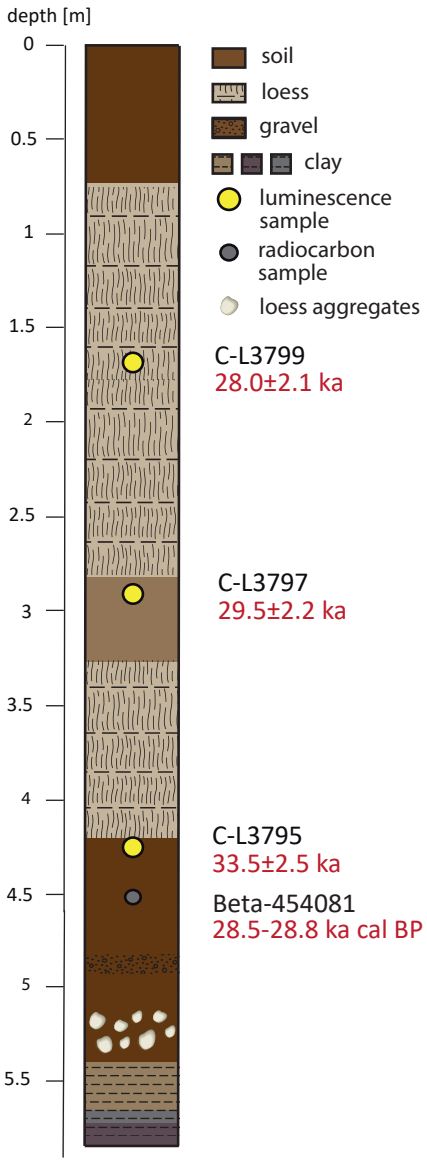

Figure 6.2.: Stratigraphical sketch of the loess-paleosol sequence Bodrogkeresztúr. Location of geochronological samples and their results are also indicated.

6.3.6. Color

Samples were homogenized and dried, the color was determined using a Konica Minolta CM-5 spectrophotometer. The L*a*b* values indicate the extinction of light, on a scale from L* 0 (absolute black) to L* 100 (absolute white), and express color as chromaticity coordinates on red-green (a*) and blue-yellow (b*) scales. Measured colors were plotted using the 'drawProfile.R' R script (Sprafke, 2016; Zeeden et al., 2016a).

6.4. Results

6.4.1. Stratigraphy

The two sampled profiles, about 2 m apart, can be correlated by means of litho- and pedostratigraphy and physical and chemical proxy data. A composite profile will be used for further description (Fig. 6.2). Figure B.1 in the Supplementary Materials shows a photo of the research site.

The bottom of the profile is characterized by dark brown (~$5.7 - 5.84$ m) and dark grey clay ($5.67 - 5.7$ m), followed by light and clay-rich sediment ($5.45 - 5.67$ m). During fieldwork, the clay layers were interpreted as overbank deposits. Complete mollusk shells were found in the paleosol and loess layers. The clay is followed by a chestnut-colored paleosol (~$4.2 - 5.45$ m). Within this horizon, a layer containing fine gravels (~4.75 m) and some thin, flat and lens-like loess aggregates (depth $5.1 - 5.4$ m) can be identified. These embedded flat loess aggregates are from a sedimentological perspective interesting, because theses are atypical for transport over a short distance by water action (cf. Schäfer, 2005). The paleosol is overlain by a horizon of fine grey loess ($3.95 - 4.2$ m) with a transitional zone between soil and loess. On top follows a yellowish and homogenous loess layer (~$3.25 - 3.95$ m) and a weak paleosol ($2.8 - 3.25$ m). The upper part of the profile is characterized by a homogenous yellowish-light brown loess layer ($0.8 - 2.9$ m) and the modern soil ($0 - 0.8$ m).

6.4.2. Geochronology

6.4.2.1. Luminescence data

Thorough testing of the luminescence signal was undertaken on sample C-L3797. First IR stimulation temperature tests are shown in Figure 6.3. Four pIRIR protocols with a second stimulation temperature of $225°C$, $250°C$, $270°C$, and $290°C$ were tested. While preheat temperatures were always $30°C$ higher than second IR stimulation temperatures, different first IR stimulation temperatures were applied: $50°C$, $80°C$, $110°C$, $140°C$ and $180°C$. Additionally, we conducted a dose recovery test (Figure 6.3) for some of the tested protocols, which shows that all tested protocols are able to recover a given dose satisfactorily (recovered/given dose ratios between 0.95 ± 0.02 and 1.02 ± 0.02). In order to keep fading to a minimum and allow a better comparison to other samples measured, we finally used the $pIR_{50}IR_{290}$ protocol for D_e determination. Figure B.2 in the Supplementary Materials shows several shine down and dose response curves. The abanico plots (Fig. B.3) indicate a low relative standard error $< 4\%$ for all D_e distributions. Residual signals after 24 h bleaching are minimal (< 5 Gy) and were not considered for further calculations. Alpha efficiency measurements determined a-values of 0.13 ± 0.02 (C-L3795) and 0.12 ± 0.02 (C-L3797 and C-L3799). The fading measurements determined a mean g_{2days} value of $0.27 \pm 0.76\%$ for sample C-L3797 (Fig. B.4). Dose rates are similar for all samples ~4.1 Gy/ka. Final ages and D_e values increase with depth from 28.0 ± 2.1 ka (115.8 ± 6.0 Gy) to 33.5 ± 2.5 ka (139.8 ± 7.1 Gy). Table 6.1 summarizes the luminescence data.

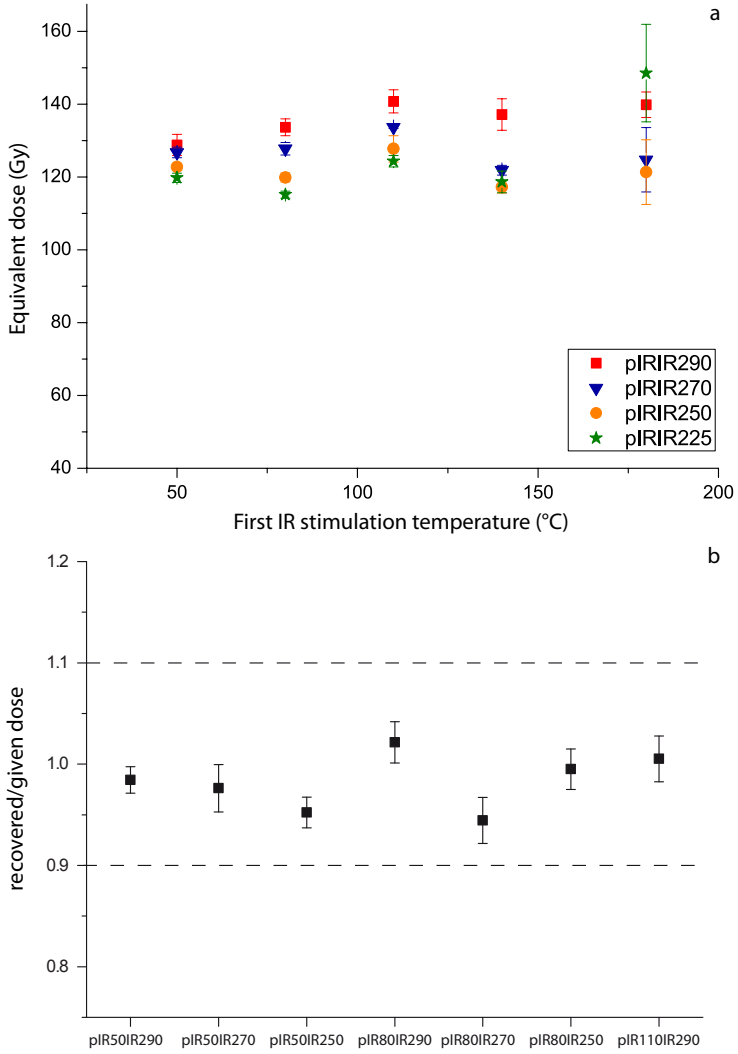

Figure 6.3.: a.) Plot showing the results of the first IR stimulation temperature tests on sample C-L3797. Four different pIRIR protocols were used with second IR stimulation temperatures of $225°C$, $250°C$, $270°C$, and $290°C$. Tested first IR temperatures were $50°C$, $80°C$, $110°C$, $140°C$, and $180°C$. b.) Dose recovery test of sample C-L3797 using different combinations of preheat, first IR and second IR stimulation temperatures. Preheat temperatures were always $30°C$ higher than second IR stimulation temperatures. All tested pIRIR protocols pass the test with an acceptance limit of 1.0 ± 0.1.

Table 6.1.: Luminescence data including radionuclide concentrations, dose rates (DR), equivalent doses, alpha efficiency and age.

Sample Code	**Grain size** (μm)	**Depth** (m)	**No. of aliquots**	D_e (Gy) **mean**	**Residual** (Gy)	U (ppm)	Th (ppm)	K (%)	**Alpha efficiency**	**Water cont.** (%)	**Total DR** (Gy/ka)	**Age** (ka)
C-L3799	4-11	1.69	9/9	115.8 ± 6.0	4.09 ± 0.5	2.51 ± 0.13	10.18 ± 0.6	1.61 ± 0.02	0.12 ± 0.02	15.0 ± 5	4.14 ± 0.2	28.0 ± 2.1
C-L3797	4-11	2.9	9/9	122.5 ± 6.4	4.13 ± 0.3	2.63 ± 0.14	10.29 ± 0.6	1.60 ± 0.02	0.12 ± 0.02	15.8 ± 5	4.14 ± 0.2	29.6 ± 2.2
C-L3795	4-11	4.27	10/10	139.8 ± 7.1	4.73 ± 0.3	2.58 ± 0.14	10.69 ± 0.6	1.53 ± 0.02	0.13 ± 0.02	16.6 ± 5	4.18 ± 0.2	33.5 ± 2.5

6.4.2.2. Radiocarbon dating

Sample Beta-454081 (charcoal) yields a conventional radiocarbon age of $24,580 \pm 90$ BP ($\delta^{13}C = -28.1‰$; calibration with INTCAL13). 2σ-confidence interval of the calibrated age is $28,770 - 28,475$ $cal\ BP$. At a 1σ-confidence interval, the calibrated age estimate is $28,705 - 28,565$ $cal\ BP$.

6.4.3. Rock magnetism

The magnetic susceptibility (χ) of the profile ranges from 30 to $90 \cdot 10^{-8} m^3/kg$ (Fig. 6.4). The lower ~1.5 m of the profile show considerable variability starting with a decrease from $\sim 90 \cdot 10^{-8} m^3/kg$ to $40 \cdot 10^{-8} m^3/kg$ within 30 cm. This is followed by a less rapid increase in χ towards $\sim 70 \cdot 10^{-8} m^3/kg$ (4.6 m depth). Another rapid decrease in χ towards $\sim 35 \cdot 10^{-8} m^3/kg$ is succeeded by a double sigmoidal pattern at a depth from 2.7 to 4.1 m. Above, χ decreases slightly and shows only small variation between 30 and $40 \cdot 10^{-8} m^3/kg$ in the upper part of the profile ($\sim 0.32 - 2.0$ m). The frequency dependent magnetic susceptibility (χ_{fd}) begins with values around 12% in the lower cm, which drops rapidly towards 8-10% ($4.2 - 5.5$ m). After a minimum ~5% ($3.4 - 4.1$ m), the upper 3.4 m show similar values around ~6-7%, however, some variations are observed, especially at 1.2 m and 1.75 m depth.

The magnetic susceptibility is often measured in bulk, but its (an)isotropy can be investigated when turning samples 3-directional in an applied field. This yields a 3-dimensional ellipsoid, which can be fully described by its orientation and three axis lengths of the maximum, medium and minimum susceptibility. In sedimentary systems, anisotropic particles are often lying flat, and also preferential directions can be observed and interpreted.

Here, the axes of maximum susceptibility (k1; circles in Figure 6.5) have a mean declination of 176.4° (±33.2) and inclination of 1.9° (±9.1). The axis of medium susceptibility (k2; triangles) have a mean declination of 266.6° (±33.3) and inclination of 4.7° (±6.1). The minimum (k3; squares) axis of data have a mean declination of 64.8° (± 9.2) and a mean inclination of 84.9° (±6.3).

Confidence in clear separation of a maximum, medium and minimum axis can be reached through parametric (Jelinek, 1977) and nonparametric statistics (Constable and Tauxe, 1990), here the test according to Jelinek (1977) is applied. All tests for anisotropy (mean F-test value is 237), and also rotational anisotropy (mean F test value is 42) show that anisotropy could be determined from all but two (T_2.1; T_6.3) samples. Figure 6.5 shows all data, and encircles the k1 & k2 directions for the two samples where these directions cannot be reliably separated. However, their consistency with remaining samples suggests the correct assignment of k1 and k2 directions.

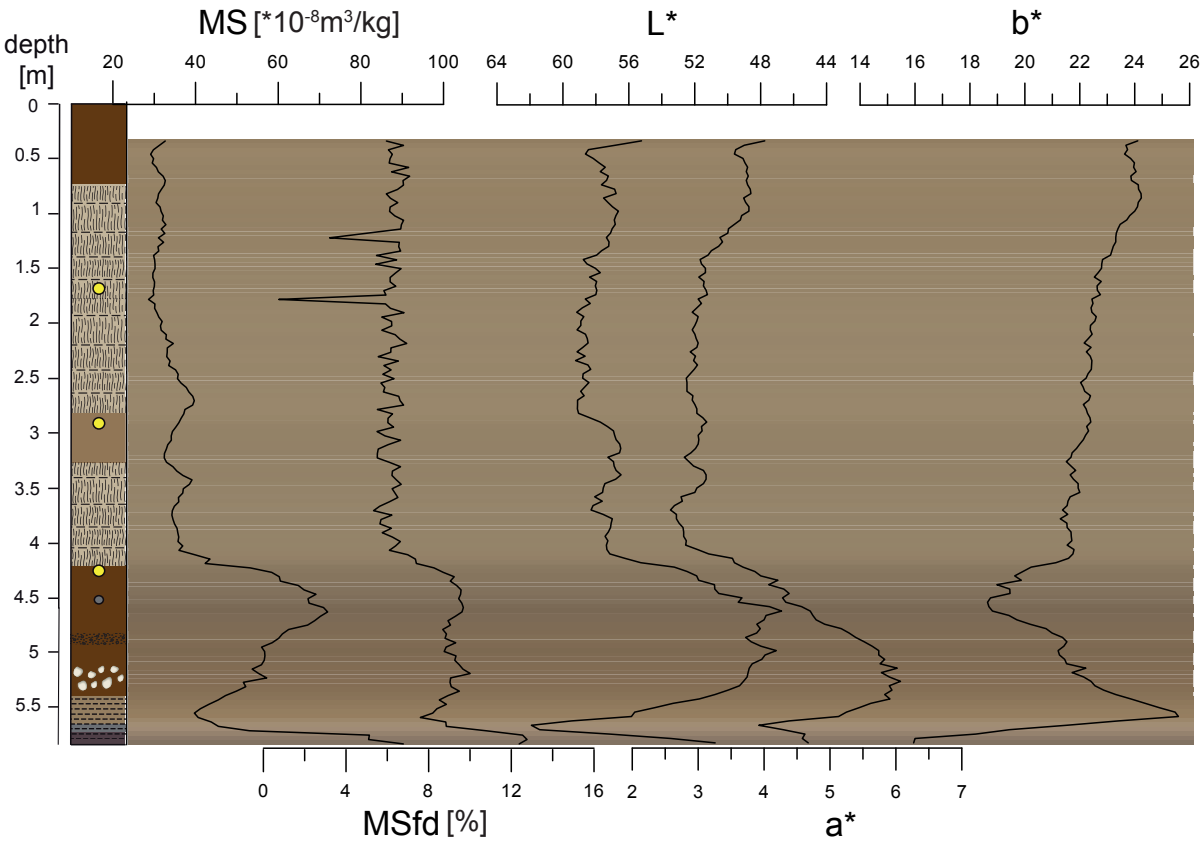

Figure 6.4.: Physical property data of the Bodrogkeresztúr section showing the mangnetic susceptibility (MS), the frequency dependent magnetic susceptibility (MS_{fd}), and the L*, a*, and b* values of the color measurements. In the uppermost part no samples were taken for laboratory analyses. The proxy data are underlain by a representation of dry measured color data.

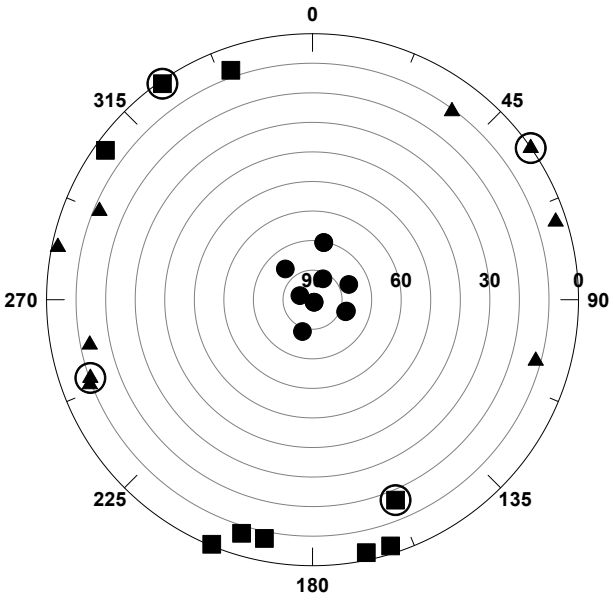

Figure 6.5.: Directions of the anisotropy of the magnetic susceptibility from Bodrogkeresztúr. Circles depict k3 directions, triangles depict k2 directions and squares represent K1 axes. Encircled data indicates that k1 and k2 directions cannot clearly be separated statistically.

6.4.4. Grain size

Figure 6.6 shows the changes in grain size throughout the sequence. At the bottom of the profile fine and coarse silts ($< 5\ \mu m$; $22 - 63\ \mu m$) are the most abundant fractions (~60%), while grains $> 63\ \mu m$ show the smalles proportions of ~5%. Between 3.8 and 5.2 m the coarser fractions increase at varying rates up to 75%, while the finer fractions decrease accordingly. A double sigmoidal pattern is evident for all grain size fractions at $2.8 - 3.8$ m depth. The upper part of the section ($0 - 2.8$ m) is characterized by increasing percentages of the fine grain sizes from ~15% to ~20% ($< 5\ \mu m$) and from 17% to 24% ($5 - 22\ \mu m$; Fig. 6.6). The coarser grain sizes show an decreasing trend in this part (50-45% for $22 - 63\ \mu m$; 19-10% for $> 63\ \mu m$), with a maximum in sand ($> 63\ \mu m$) between 1.3 and 1.8 m.

The U-ratio shows a similar pattern as the coarse grain sizes. It shows a low value of 1.5-2.2 in the bottom of the profile ($4.5 - 5.84$ m). The U-ratio increases rapidly between ~4 and 4.5 m towards 4 and shows the same double sigmoidal pattern as the coarse grain sizes between 2.7 and 4 m. The U-ratio is relatively constant between 2 and ~2.5 m around 3.5 and decreases slowly in the upper 2 m of the profile towards 2.5.

The grain size distribution curves of loess show a bimodal distribution of the sediment with a pronounced peak in the coarse silt fraction and a shoulder in the clay (Fig. 6.7). The well-developed basal paleosol also shows a bimodal grain size distribution, where the pronounced peak has a lower volume and the shoulder in clay has a more pronounced volume. The lowermost 0.2 m of the section are not characterized by bimodal distributions.

6.4.5. Geochemistry

The sediment is dominated by quartz being the major carrier of SiO_2, contributing from 65.8 to 70.7%, except in the lowermost 12 cm of the section where the SiO_2 abundance shows lower values between 56 and 62% (Fig. 6.8). The Al_2O_3 content shows an average of 15.1%. CaO is generally low for Danubean loess (average 4.4%; compare Bösken et al., 2017b; Krauß et al., 2016; Obreht et al., 2015, 2016), with an abundance of ~10%; only in the lower 12 cm values increase up to ~18%. Albeit the general values are low, the lower 20 cm exhibit high fluctuations between 0.9 and 18% (Fig. 6.8). The sediments contain 4.9% FeO with slightly higher values in the lower part (paleosol) of 5-5.5%. The average content of P_2O_5 is 0.2%, its abundance decreases gradually in the paleosol towards 0.11%. Cl shows low values <30 ppm for most of the profile, except in $\sim 2.1 - 2.8$ m, where a sudden increase towards 605 ppm is observed.

Figure 6.9 shows the geochemical ratios and weathering indices. The lowermost ~20 cm show a strong variability in weathering indices. Generally, the weathering indices CIA and CPA follow an upward-decreasing trend with varying values between 64 and 74 (CIA), and $85 - 91$ (CPA). RB/Sr and Ba/Sr follow a similar general pattern. Decreasing values from 5.5 m to 4 m (0.9 for Rb/Sr and 4 for Ba/Sr) are followed by pronounced minima from ca. $4 - 2.4$ m depth. Increasing values occur in the upper ~2.5 m ($0.85 - 0.65$ for Rb/Sr; $4 - 2.8$ for Ba/Sr). The Al_2O_3/SiO_2 ratio is elevated in the paleosol (~0.24) and shows lowest values between 2.8

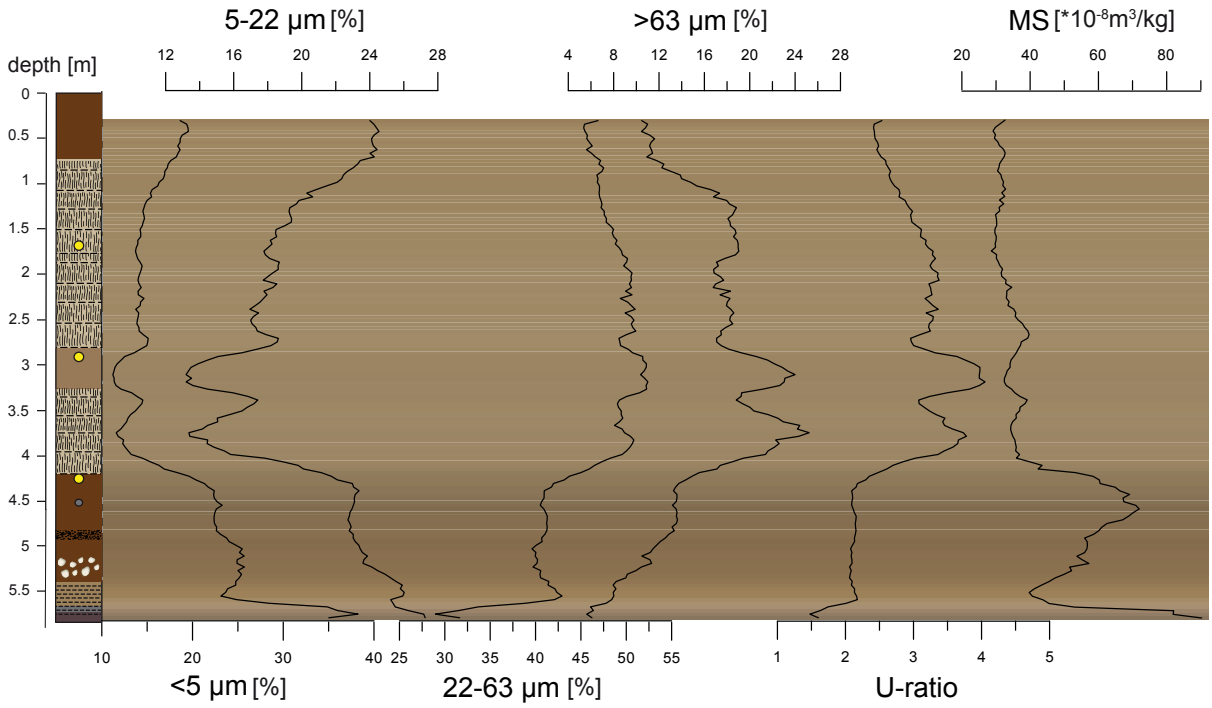

Figure 6.6.: Grain size properties of the Bodrogkeresztúr section showing the $< 5\ \mu m$, $5 - 22\ \mu m$, $22 - 63\ \mu m$, and $> 63\ \mu m$ fractions, as well as the U-ratio. For comparison between the figures the magnetic susceptibility (MS) is shown. In the uppermost part no samples were taken for laboratory analyses.

and 4.2 m ($0.2 - 0.21$). The upper 1.5 m show an increasing trend of Al_2O_3/SiO_2 towards 0.23.

The A–CN–K diagram ($Al_2O_3 - (CaO^* + Na_2O) - K_2O$ diagram; Nesbitt and Young, 1989) in Figure 6.10 informs about weathering and sorting effects of aluminosilicates, as well as the initial composition of the unweathered material (Buggle et al., 2008; Obreht et al., 2015). At the Bodrogkeresztúr section, all samples are clustered on the line parallel to the A-CN join, indicating a domination of the chemical weathering (first-order plagioclase removal, and slight K-feldspar weathering) and an absence of a sediment sorting effect at the section.

6.4.6. Color

Measured colors were plotted in Figure 6.4. Values of L* (extinction of light) and a* (red-green) show a similar pattern (note that L* is plotted from higher to smaller values): L* values range from 48 to 64 with lowest values in the lowermost sample and between 4.2 and 5.3 m. The highest L* values of ~64 occur at a depth of ~5.7 m. In the upper 4 m, L* values range from 54 to 59, with slightly lower values in the interval between 2.8 and 4.1 m. a* shows an opposite pattern with minima around 3 (2.8 – 4.1 m) and a maximum of ~6 (4.9 – 5.3 m). a* shows values ~3 – 3.5 between 1.4 and 4.1 m and increases in the upper 1 m towards 4. b* shows a rapid increase from 15 to 25 between 5.6 m and 5.84 m depth, which is followed by decreasing values towards 18 (4.5 m). b* increases rapidly and then more gradually towards 24 until the top of the section.

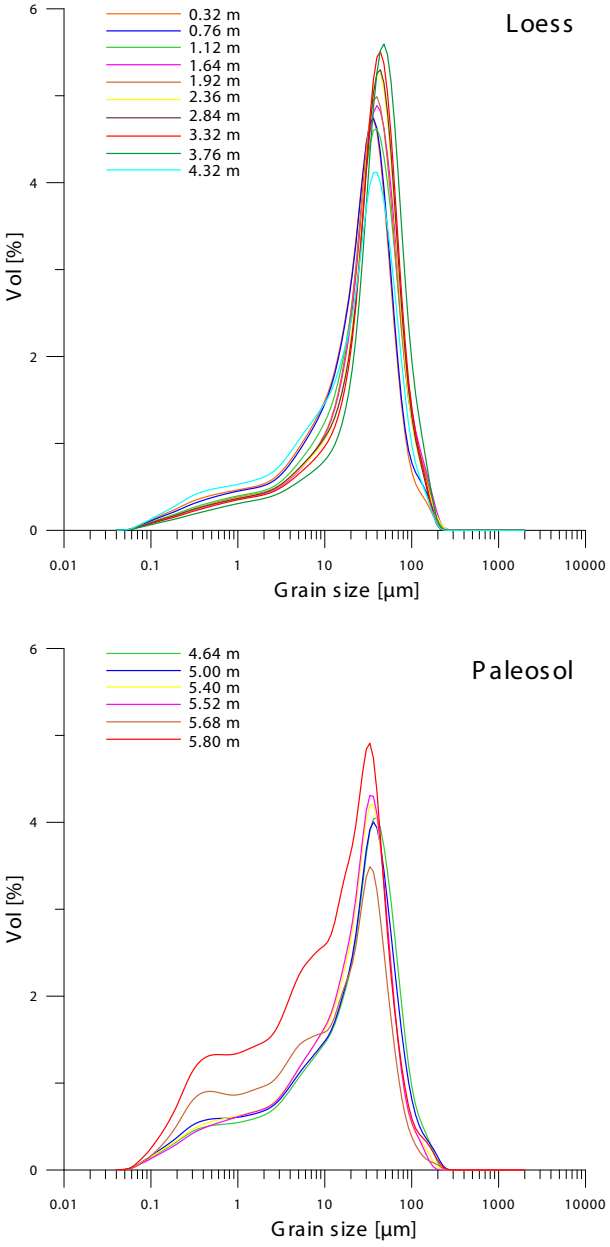

Figure 6.7.: Grain size density distribution curves of representative samples from different stratigraphic depths.

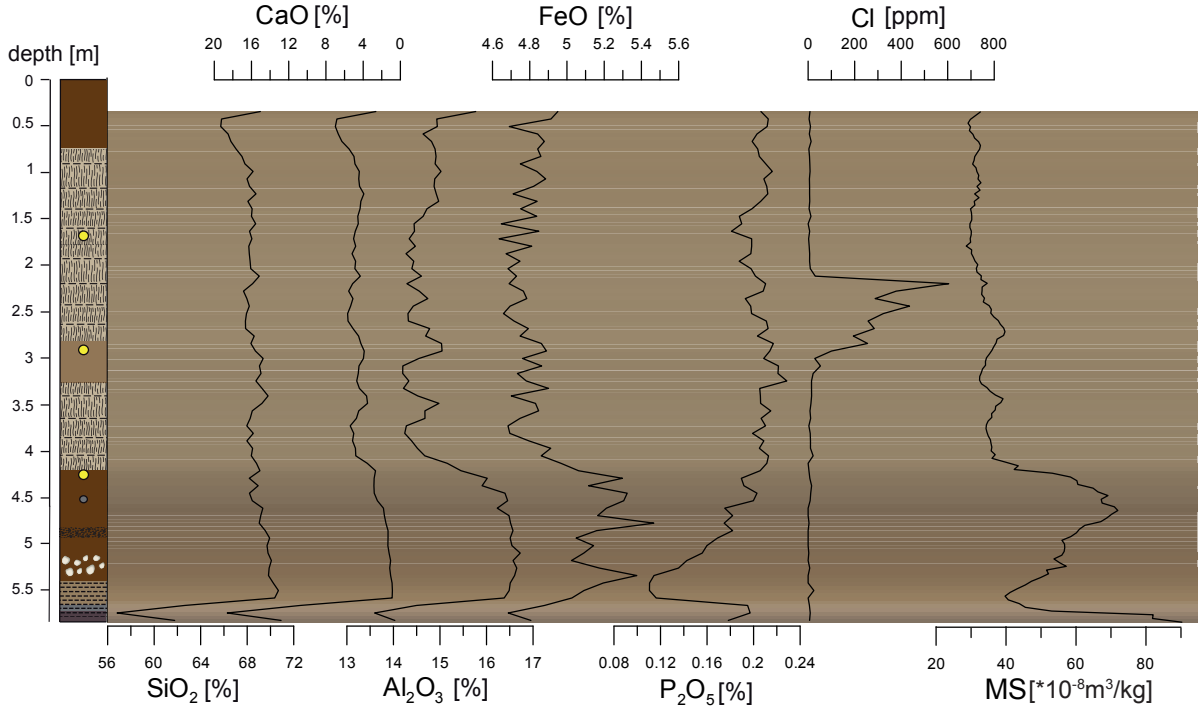

Figure 6.8.: Geochemical properties of the Bodrogkeresztúr section showing the abundance of SiO_2, CaO, Al_2O_3, FeO, P_2O_5, and Cl. For comparison between the figures the magnetic susceptibility (MS) is shown. In the uppermost part no samples were taken for laboratory analyses.

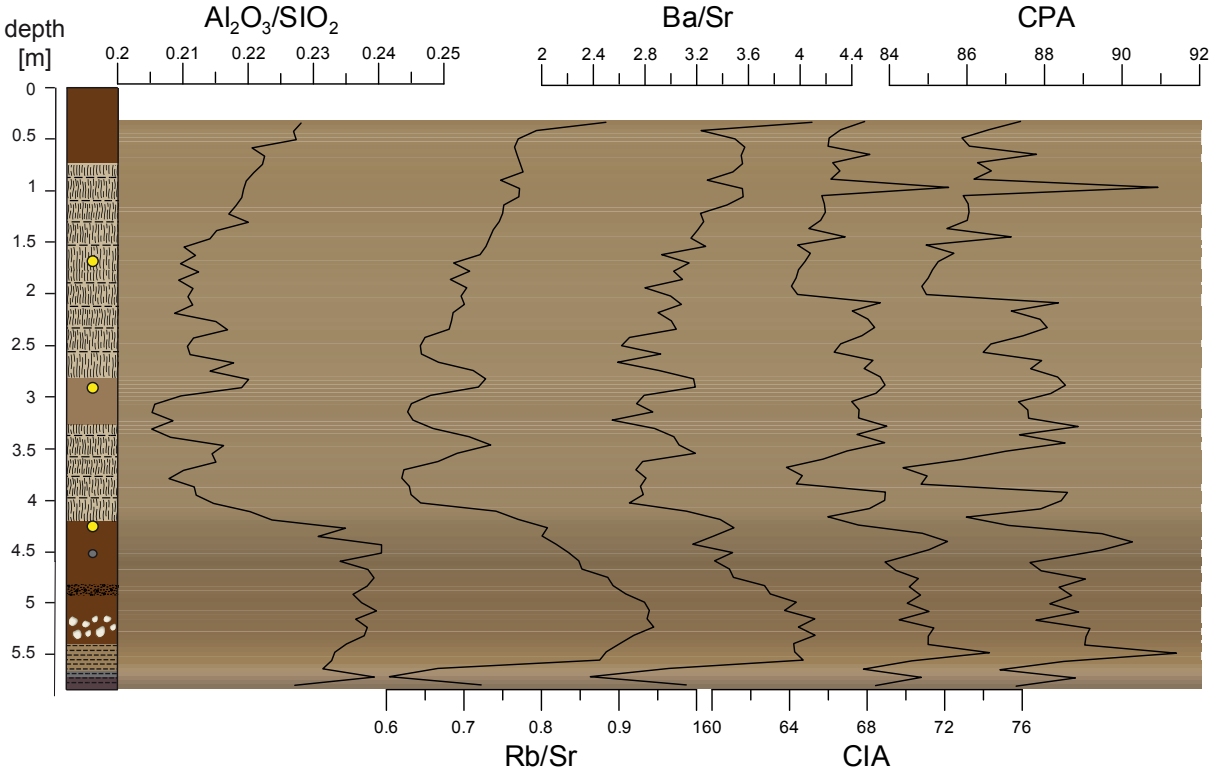

Figure 6.9.: Geochemical weathering indices of the Bodrogkeresztúr section showing the ratios SiO_2/Al_2O_3, SiO_2/K_2O, Rb/Sr, Ba/Sr, the Chemical Index of Alteration (CIA) and the Chemical Proxy of Alteration (CPA).

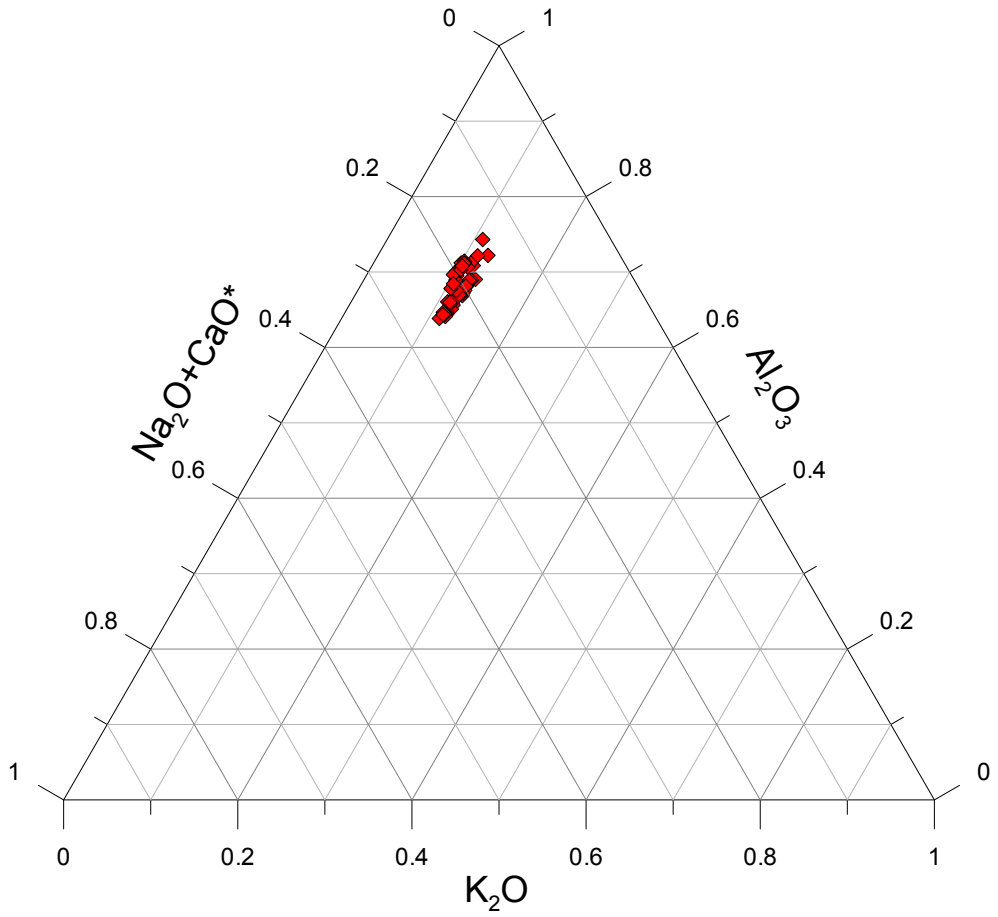

Figure 6.10.: A-CN-K diagram. Sample distribution in the diagram indicates domination of silicate weathering.

6.5. Discussion

6.5.1. Geochronology

The luminescence samples were tested thoroughly to choose the optimal measurement settings. The dose recovery ratios, low fading rates, and low relative standard errors confirm the applicability of the used $pIR_{50}IR_{290}$ protocol. The luminescence data fits well to the radiocarbon chronology of the Kopasz hill (Sümegi and Hertelendi, 1998) and the luminescence chronology of Schatz et al. (2012). The Bodrogkeresztúr section can be linked to the 'upper' paleosol and the 'upper' loess layer found at the other profiles. Our age of 33.5 ± 2.5 *ka* (C-L3795) agrees well with the two $pIRIR_{290}$ ages of 39.2 ± 3.4 *ka* and 30.1 ± 2.7 *ka* of the upper paleosol at Tokaj (Schatz et al., 2012). In addition, the radiocarbon chronology (Sümegi and Hertelendi, 1998) places this paleosol between $29 - 34$ *ka cal BP*. Moreover, the other two ages of 28.0 ± 2.1 and 29.6 ± 2.2 *ka* fall in the same range as the upper loess layer at Tokaj, which is dated to 24.9 ± 2.2 – 27.8 ± 2.5 *ka* (Schatz et al., 2012). The radiocarbon sample gives an age of $28.5 - 28.8$ *ka cal BP* and represents an age estimate of the formation of the paleosol slightly younger than the age of the sedimentation as dated by the luminescence samples. However, this is not surprising as not the same event is dated and age estimates do overlap when their 2σ-uncertainty are considered. Similar observations were made by Újvári et al. (2014a) at the Dunaszekcső loess paleosol sequence where $pIRIR_{290}$ age estimates were consistently older than ^{14}C ages, especially in younger samples.

Even though resulting ages agree well between the BKT and Tokaj profiles, there are considerable differences in the luminescence characteristics, which might speak for different provenance, geochemistry or sedimentary processes prior to deposition. At Tokaj, Schatz et al. (2012) encountered severe problems during the dose recovery measurements related to the optical or thermal pretreatment, while the BKT samples did not show any problematic behavior. Residual doses are higher at Tokaj, but both sections show in general low residuals. In both sections, residual doses increase slightly with the equivalent dose. Dose rates at Tokaj were marginally lower than at BKT, and different a-values were used, which can lead to differences in age of a few thousand years.

6.5.2. Origin of sediments

The bimodal grain size distribution curves of loess with a peak in coarse silt and a shoulder in clay strongly support an eolian origin of the sediments, although a minor contribution of slope wash deposits cannot be ruled out. The well-developed basal paleosol shows a bimodal distribution with exception of the lowermost 0.2 m, suggesting a mixing of loess-like and alluvial deposits here. This is supported by observations in the field and low values of χ (~4.6 m to bottom). Therefore, the part below a depth of 4.6 m should not be interpreted as a paleoclimatic signal.

Wind directions inferred from AMS measurements (e.g. Bradák, 2009; Nawrocki et al., 2006, see Fig. 6.5) speak for a dominant north(west) - south(east) wind direction, or a perpendicular

direction from (south)west - (north)east (for the eolian part of the section). A paleowind direction of north-south direction may also be inferred from landforms in the region and to the south-east in the more open steppe landscape. Here we interpret the data as the material originating from a predominantly northeastern wind direction, because this is most consistent with landforms in the region (visible in topographic maps). This suggests the Tisza floodplain to the northeast to be a main source of sediment, wich is supported by an increased abundance of coarser particles (Fig. 6.6) indicating that the source area was close by (Bösken et al., 2017b; Obreht et al., 2014, 2016). However, the well-developed paleosol shows a high abundance of fine particles, suggesting a strong alteration of primary deposited loess caused by pedogenesis, combiend with a deposition of fine-grained overbank deposits.

Geochemical characteristics (Fig. 6.8) show a composition similar to the Tokaj section, with a higher contribution of SiO_2 and a lower contribution of CaO. This is different to other studied loess sections in Hungary (Bösken et al., 2017b; Újvári et al., 2008; Ujvari, 2014; A. Varga et al., 2011), indicating strong dissolution of CaO from the original sediment, also supported by low Sr values (average 111 ppm). Moreover, χ and χ_{fd} are generally high for Danubean loess, additionally supporting the interpretation of increased weathering intensity caused by relatively high paleo-precipitation. Also low L* and a* values (in comparison to other loess sections in Southeastern Europe, e.g. Bösken et al., 2017b; Lukić et al., 2014; Obreht et al., 2016) indicate a generally high intensity of pedogenesis and weathering.

6.5.3. Weathering indices

Chemical weathering indices have been widely applied to evaluate the intensity of weathering in loess from different regions (Buggle et al., 2011, 2013; Hošek et al., 2015; Krauß et al., 2016; Obreht et al., 2015; Újvári et al., 2014b; A. Varga et al., 2011; Yang et al., 2006). They are based on the concept on mineral alteration, where the selective removal of soluble and mobile elements from a profile section is compared to a relative enrichment of immobile and non-soluble elements. Simple ratios like Ba/Sr or Rb/Sr are suggested to be strongly influenced by $CaCO_3$ content (Buggle et al., 2011), or rarely by MgO content (Obreht et al., 2015). However, Schatz et al. (2015b) reported those ratios to be influenced by the grain size rather than $CaCO_3$ content at Tokaj. Similarly, the Ba/Sr and Rb/Sr ratios from our record show a similar trend like the fine fractions (Fig. 6.9). An explanation of such grain size dependence of geochemical ratios may be related o higher Rb concentrations in clay and enrichment of the Sr in silt (Schatz et al., 2015b; Ujvari, 2014). Nevertheless, additional studies are required for a better understanding of the nature of the Ba/Sr and Rb/Sr ratios as weathering indices. Classical weathering indices like the Chemical Index of Alteration (CIA, Nesbitt and Young, 1989) or the Chemical Proxy of Alteration (CPA, Buggle et al., 2011) are suggested to be more sensitive to the weathering intensity. However, studies with a higher sampling resolution (Krauß et al., 2016; Obreht et al., 2015) demonstrated that the general trends of the CIA and CPA are mostly in agreement with enhanced weathering, but clear deviations are observed in some parts of the profiles. Similarly, the CIA and CPA from the Bodrogkeresztúr section indicate increased weathering in the well-developed paleosol and the upper part of the section, but the values between 2 and 3.5 m show

high values that are not supported by other proxies that represent weathering (cf. Fig. 6.9). A potential explanation for this discrepancy is that weathering indices, such as Rb/Sr and Ba/Sr ratios, may be controlled by grain size and leaching, while CIA and CPA might preferentially reflect Ca and Na removal by plagioclase and feldspar weathering.

6.5.4. Paleoclimatological conditions during late MIS 3

Geochemical characteristics of the Bodrogkeresztúr section show clear differences between loess and paleosol. The well-developed paleosol with a supposed alluvial sediment input at the profile base has higher FeO and Al_2O_3 contents (Fig. 6.8), suggesting strong weathering producing iron oxides and finer particles associated with a higher Al contribution due to post-depositional clay formation.

The unusually well-developed MIS 3 paleosol is a characteristic of both sections, Tokaj and Bodrogkeresztúr, indicating rather humid conditions during MIS 3 in the northern part of the Carpathian Basin. Values of χ in this paleosol (cf. Fig. 6.4) are in the range of the values from interglacial soils in the other parts of the Carpathian Basin (Buggle et al., 2009, 2014; Marković et al., 2011; Stevens et al., 2011; Újvári et al., 2016a; Zeeden et al., 2016d), supporting an interpretation of high humidity and enhanced soil moisture. This is also supported by high values of χ_{fd} in the paleosol (cf. Fig. 6.4). Moreover, dark soil color suggests a high concentration of humic material and therefore, strong pedogenesis over this period.

Lower values of weathering indices at the Tokaj section, when compared to Bodrogkeresztúr, also indicate weaker weathering at the higher geomorphological position. Consequently, the different geomorphologically situated sections of Tokaj and Bodrogkeresztúr did experience slightly different local paleoenvironmental conditions; however, both profiles show that paleoclimatic conditions were more humid than in the remaining Carpathian Basin.

6.5.5. Paleoclimatological conditions during early MIS 2

The χ_{fd} also shows higher values in loess (MIS 2) in comparison to other loess sections of the same period. Values are in the range usually found in MIS 3 paleosols of the Carpathian Basin, or even higher (Basarin et al., 2014; Buggle et al., 2014; Marković et al., 2014). The values of the close-by Tokaj section are notably lower, but still higher than other sections in the Carpathian Basin (Basarin et al., 2014; Bösken et al., 2017b; Buggle et al., 2014; Marković et al., 2014; Obreht et al., 2015; Zeeden et al., 2016d). High χ and χ_{fd} for loess sediments, supported by low L*, high a* values and low CaO content, proves generally wetter/milder conditions at the Kopasz Hill also during periods of loess formation.

Although milder conditions at the Bodrogkeresztúr section are recorded, two layers at ~$280-320$ cm and ~$360-390$ cm clearly show a high contribution of coarse particles indicating rather high wind intensities or a shorter transport distance (cf. Fig. 6.6). These layers may relate to Heinrich Event 3 and/or 2, reported from (south)eastern European loess (Shi et al., 2003; Sümegi et al., 2012a; Zeeden et al., 2016b). In particular, Heinrich event 2 has been sug-

gested to be associated with high eolian sedimentation rates (Bokhorst et al., 2011). Although the possible events might be covered by the OSL ages of samples C-L3795 and C-L3797, the large uncertainties of ages estimates do not allow a straightforward assignment. In the lower layer with high coarse particles content, all other proxies show low values (χ, χ_{fd}, a* and weathering indices) indicating cold and dry conditions. The layer with high content of coarse particles between ~280 and 320 m is represented by indications of a weak paleosol development. Moreover, χ and χ_{fd} do show a slight decrease, but are still generally high for MIS 2 loess (Fig. 6.4). This indicates that the general soil humidity was still relatively high, while the eolian dynamics were more intensive or the source area was characterized by coarser particles (e.g. due to stronger river discharge). At the Tokaj section, modeling results of n-alkanes suggest MIS 2 as a period with higher soil moisture, but two dry periods are also observed (Schatz et al., 2011). Relying only on luminescence dating it is challenging to conclude if those two layers of dryer conditions at the Tokaj section are related to two layers with higher sand content at the Bodrogkeresztúr section. However, the vicinity and consistency of their occurrence suggests so, and also points towards a more widely occurring signal related to north Atlantic cold events.

The loess at BKT shows a generally homogeneous geochemical composition. However, a part of the profile between ~210 and 280 cm shows surprisingly high Cl values (cf. Fig. 6.8). Such high Cl values may be related to a tephra layer (Obreht et al., 2016), but no glass shards were found after detailed microscopic sample examination. This may indicate further contribution from an additional or different source during the formation of this loess layer, and suggests a change in sediment properties. Moreover, the characteristic stratigraphic shape of the anomaly with an abrupt but low amplitude beginning and a following increase ending in a maximum peak, which is abruptly ceased, speaks for the relocation of parental material with high Cl content. A different composition is further supported by the opposing trends of χ and χ_{fd}, suggesting that the contribution from the additional source might have had a higher bulk χ than the main source area, while the climatic conditions were unfavorable for the formation of fine magnetic grains and χ_{fd} decreased. Without further proof we refrain from an interpretation.

6.5.6. Erosion of uppermost loess (late MIS 2)

Another interesting feature of the section investigated at the Kopasz Hill is that the upper loess deposition seems to have ended around 20 ka or was eroded and/or overprinted by Holocene pedogenesis (Schatz et al., 2012). Although we did not date the uppermost part of the profile, one can assume a similar behavior as at Bodrogkeresztúr, since sample C-L3799 can be considered rather old in comparison to its depth of 1.69 m. It is noteworthy that stratigraphy and ages compare well between Bodrogkeresztúr and Tokaj, although the geomorphological setting is different (this study: position low in the landscape on the northern side of the Kopasz Hill vs. Schatz et al.: position higher in the landscape on the eastern side of the same hill).

6.6. Conclusion

The investigated loess-paleosol sequence in northeastern Hungary was dated to $33.5 \pm 2.5 - 28.0 \pm 2.1$ *ka* and ~2.5 m of loess accumulated in the dated time frame. While the lowermost part needs to be disregarded in the paleoclimatological investigation due to the (partial) input of alluvial sediments, the remaining section shows several interesting features. It is suggested that the loess originates dominantly from the Tisza River floodplain and that sediment was transported predominantly from a north-eastern direction. We conclude that the general climatic conditions during late MIS 3 and early MIS 2 were more humid than in most of the Carpathian Basin. However, short relatively dry periods are recorded as well. This supports an overall observation based on mollusk results from the Carpathian Basin that the northern part was more humid (but colder), and that the paleoenvironmental evolution was more dynamic (Bösken et al., 2017b; Rudner and Sümegi, 2001; Sümegi and Krolopp, 2002). Contrarily, temperatures were higher but the general humidity was lower in the southern Carpathian Basin, suggesting steppic environmental conditions (Marković et al., 2007, 2015). Additionally, we highlight that the foothill areas apparently provided unique microclimatic conditions in the Carpathian Basin that were more humid and with higher biomass production than in the basin itself, at least during the last ~$30 - 50$ *ka* (also supported by Schatz et al., 2011). This may be related to an increased occurrence of Upper Paleolithic findings along the foothill areas around the Carpathian Basin, as suggested for the Aurignacian (e.g. Floss et al., 2016), supporting a more favorable environment in these elevated positions. Also, Sümegi et al. (2016) point out that the local environment of the oldest Gravettian sites occur along creek valleys and mixed taiga woodlands and loess-covered hills of spruce and steppe forests. The absence of discovered artifacts outside of the foothill area and the occurrence of camp sites repeatedly within spruce forests within this period (Sümegi et al., 2016), may be interpreted as highlighting a selective preference of the Gravettian population for these environments.

7. Geochronology of the Aurignacian open-air site of Crvenka-At (Serbia)

7.1. Introduction

The previous chapters dealt with paleoclimatic reconstructions of loess-paleosol sequences in context of Gravettian findings. In this chapter, the geochronology of a site with Aurignacian artifacts is investigated. The Crvenka-At site is located in northern Serbia, in the Banat, a historic region in Central Europe currently divided between Romania, Serbia and Hungary. There are several Aurignacian open-air sites in this region (cf. Figure 3.3, Anghelinu et al., 2012; Chu et al., 2014; Chu et al., 2016; Kels et al., 2014; Léonard, 2016; C. Schmidt et al., 2013; Sitlivy et al., 2012, 2014), showing its importance for the emergence of the Upper Paleolithic in Europe. After the discovery of a human mandible in the Peştera cu Oase, several sites were reinvestigated in recent years. The remains at Peştera cu Oase comprise the earliest securely dated human remains of anatomically modern human in Europe ($37 - 42$ *ka cal BP*, Trinkaus et al., 2003). The reinvestigation included the open-air sites of Romaneşti-Drumbrăviţa, Coşava and Tincova (Anghelinu et al., 2012; Chu et al., 2016; Léonard, 2016; Sitlivy et al., 2012, 2014) and some paleoenvironmental records (Kels et al., 2014; C. Schmidt et al., 2013). As highlighted before, most archeological sites within the Middle Danube Basin are located at geographically elevated positions such as Romaneşti-Drumbrăviţa, Eger-Köporos, and Tincova (Hauck et al., 2017). In contrast to the the Crvenka-At site that is located in the lowlands. Artifacts were found in a depth of ~5 m, which might explain why there are only a few findings in lowland positions so far.

The Crvenka-At sites (45° 08'126"N, 21° 16'820"E) are located in the southern belt of the Middle Danube Basin, ca. 3 km north of the town of Vršac and the Vršac Mountains. The archeological sites are all located within a sand ridge of ~1 km length (up to 93 m a.s.l) that separates the depressions north of Vršac and east of Alibunar. Previous excavations were conducted by R. Rašajski (1952–1978; Mihailović et al., 2011), and by Radovanović (1986). Mihailović (1992) divided the found assemblages in 'typical' Aurignacian layers and 'Krems' style Aurignacian layers (according to Chu et al., 2014). Due to the unsystematic nature of the excavation of some of these artifacts, as well as the relatively small assemblage numbers collected during excavation, Chu et al. (2014) re-excavated the Aurignacian Crvenka-At site. Preliminary data indicates two levels containing possibly Aurignacian finds at multiple locations. Further chronological investigations will be presented here.

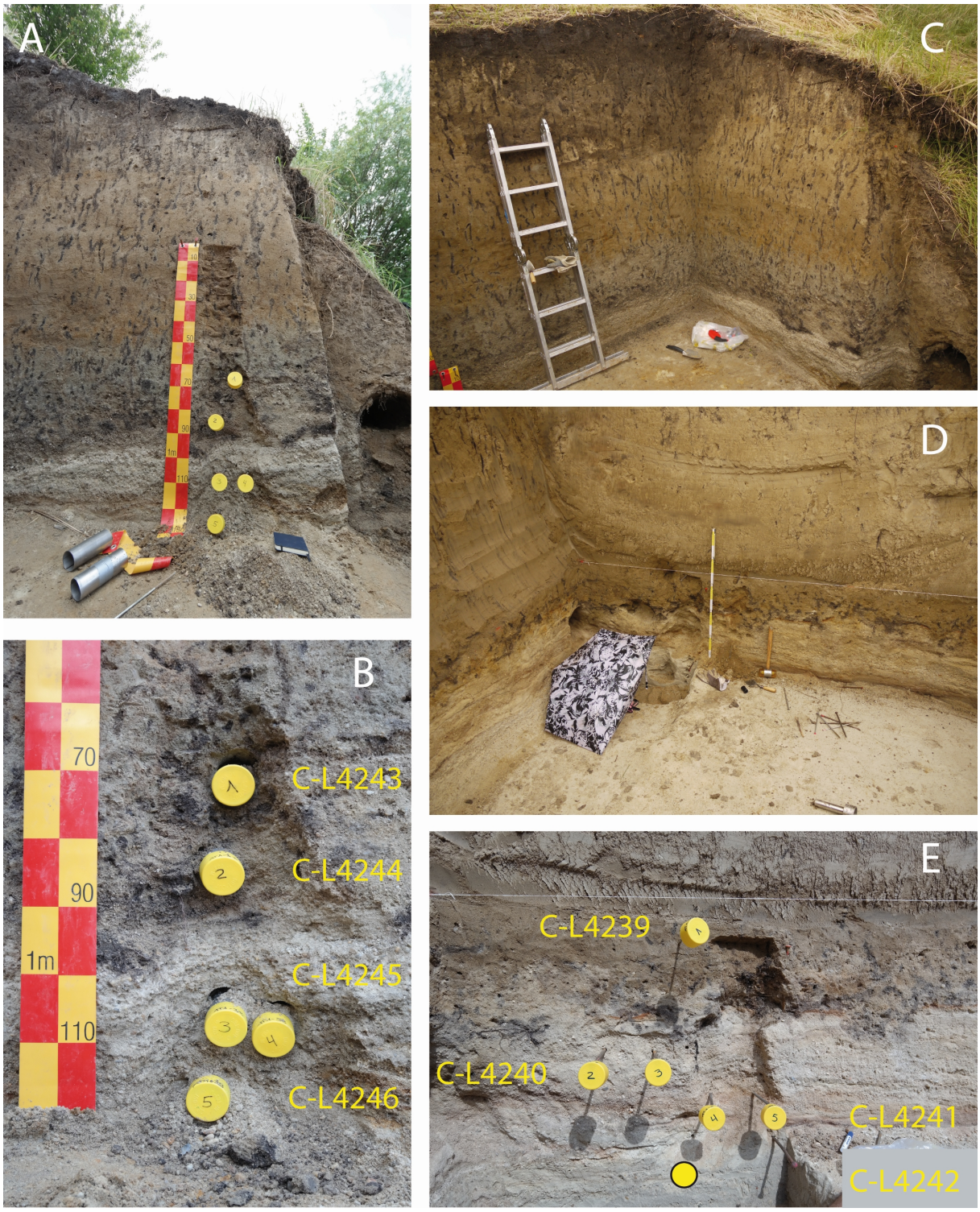

Figure 7.1.: Photos of the field sites $At1_{3B}$ (A, B, C) and $At1_5$ (D, E) showing the position and names of the luminescence samples. For some samples two cylinders were taken due to the coarseness of the sediment.

7.2. Methods

During the field campaigns in 2014 and 2015, two sites were excavated - At1 and At2 (cf. Chu et al., 2014). Within At1 four luminescence samples were taken within trench 3B ($At1_{3B}$) and another four luminescence samples were taken within trench 5 ($At1_5$) by hammering and extracting 15 cm long metal tubes into the previously cleaned sediment wall (Fig. 7.1). To determine radionuclide concentrations further samples were taken within each stratigraphical unit in the surrounding of the luminescence samples.

Samples for equivalent dose (D_e) determination were extracted from the metal tubes under subdued red light conditions; the outer 2 cm of sediment were removed. Samples were oven dried ($50°C$), the water content was determined (water content over dry mass) and samples were then treated with 10% hydrochloric acid, 10% hydrogen peroxide and 0.01 N sodium oxalate to remove carbonates, organic matter, and to dissolve aggregates. After thoroughly removing the chemicals, samples were separated into a $100 - 150\ \mu m$ and a $150 - 200\ \mu m$ fraction, only for sample C-L4241 grain sizes between $100 - 250\ \mu m$ were used due to a low amount of sample material. Via density separation quartz and kalifeldspar grains were extracted. The quartz fraction underwent further etching in hydrofluoric acid (HF).

Continuous wave optically stimulated luminescence measurements (CW-OSL) were carried out on a Risø TL/OSL DA 20 reader. The reader is equipped with a $^{90}Sr/^{90}Y$ β source, blue light emitting diodes (LEDs), emitting at 470 nm (FWHM = 20 nm), and IR LEDs, emitting at 870 nm (FWHM = 40 nm). Signals of quartz were detected through a Hoya U-340 filter and signals of kalifeldspars were detected through a 410 nm interference filter. A single aliquot regenerative dose (SAR) protocol (cf. Murray and Wintle, 2000, 2003) was applied for quartz. Sensitivity changes, recycling ratios and recuperation were monitored by the SAR protocol (Murray and Wintle, 2000). A preheat plateau test (e.g. Murray and Wintle, 2000) and a dose recovery test (e.g. Murray and Wintle, 2003) were performed on sample C-L4240 prior to D_e measurements to assess the proper measurement settings. Preheat plateau tests (PHTs) with different preheat and cutheat temperatures between $160°C$ and $280°C$ were carried out. Cutheat temperatures were always $20°C$ lower than preheat temperatures. Dose recovery tests (DRTs) included optical stimulation for 100 s and laboratory irradiation to create a known laboratory dose. The chosen irradiation dose was equal to the expected D_e. The signal was integrated from the first 0.8 s of the 40 s stimulation minus a background of the last 8 s.

For kalifeldspar measurements, the $pIRIR_{290}$ and $pIRIR_{225}$ SAR protocol were tested (Buylaert et al., 2009; Thiel et al., 2011b). Prior IR stimulation temperature tests were performed (cf. Buylaert et al., 2012). Furthermore, DRTs using bleached samples (24 h Hönle Sol2 solar simulator) were conducted. These tests were carried out on samples C-L4239 - C-L4242. Finally, the equivalent dose was determined on a minimum of 28 aliquots per sample using an arithmetic mean. A late background subtraction for dose response curve fitting was used for kalifeldspar measurements. The signal was integrated using the first 2.4 s minus a background of the last 40 s (of 200 s total stimulation). Residual doses were assessed after bleaching the

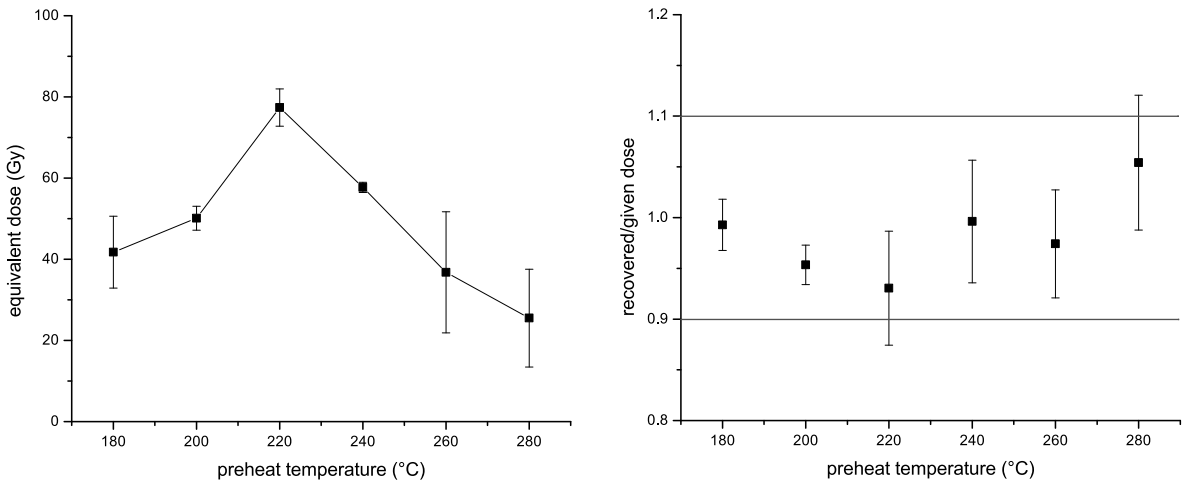

Figure 7.2.: Preheat plateau test (left) and dose recovery test (right) of quartz sample C-L4240. Solely 8 mm aliquots for the PHT and both 2 mm and 8 mm aliquots for the DRT were used. The horizontal lines in the DRT indicate that recovered/given dose ratios between 1.1 and 0.9 are acceptable.

aliquots for 24 hours in a solar simulator. Fading tests were conducted on sample C-L4240. For these tests, doses of 100 Gy were given and the normalized luminescence signals were measured after different storage times between 100 and 800 minutes.

Samples for dose rate determination were oven dried ($50°C$); the water content was determined, and samples were homogenized and packed into plastic cylinders for radionuclide measurements. Additionally, the saturation water content of one sample representative for the sand layer was determined by centrifuging and adding water until the sediment reached its maximum absorption capacity (following the example of Nelson and Rittenour, 2015). The samples for radionuclide measurements rested for four weeks to compensate for radon emanation during pretreatment. Afterwards, radionuclide concentrations were measured on a high-purity germanium gamma-ray spectrometer. The dose rates and ages were calculated using the Adele software. Within the software, the cosmic radiation was determined by the longitude, latitude and altitude of the sample location and the density of the sediments. For the internal dose rate a potassium content of $12.5 \pm 0.5\%$ was assumed (Huntley and Baril, 1997). For the external dose rate the radionuclide concentrations of the over- and underlying sediment layers and the estimated water contents were taken into account. Moreover, an alpha efficiency of 0.11 ± 0.02 was assumed for kalifeldspars (Kreutzer et al., 2014).

7.3. Results

7.3.1. Stratigraphy

Figure 7.1 shows some pictures of the At1 site and the sample locations. The stratigraphies are described in the following. The stratigraphy at $At1_5$ starts with fine white sands containing a few coarser sands and some mica flitters ($4.1 - 4.25$ m depth). At a depth of 4.12 m some organic (root?) coatings are present. On top of this layer, a horizon of layered orange and white sands

and fine gravels with diameters up to 4 mm has accumulated (4.03 – 4.1 m). It is followed by a horizon containing coarser sands and gravels of a little lighter color than below (3.95 – 4.03 m). Above from 3.86 – 3.95 m, beige sands with only a few occasional gravels deposited. This is followed by a homogeneous horizon of beige sands and some silts (3.77 – 3.86 m). At a depth of 3.77 m some organic material can be found in a lateral position. The horizon from 3.45 – 3.77 m is characterized by dark brown sands and silts. The silt abundance is increasing towards the top of the sampled part of the profile, while the abundance of sand is decreasing. The upper ~3.45 m of the profile belong to the same stratigraphic unit of dark brown silts, but were not investigated in detail.

Profile $At1_{3B}$ has a generally similar composition, but it is characterized by immense root channels throughout the profile. The stratigraphy starts with a horizon of sandy loam that contains mica (3.72 – 3.9 m). The abundance of mica increases greatly in the horizon above (3.62 – 3.72 m). On top, a layer of white sands and pebbles accumulated (3.48 – 3.62 m). This is followed by a grey redoxidation horizon of sands and pebbles (3.19 – 3.48 m), which is coarser in the upper half. Above, a reddish oxidation layer that contains sand and clay is located (2.6 – 3.19 m). The transition between both layers is inclined and occurs between 3.11 m and 3.19 m. Horizontal root channels are located at ~3.47 m, 3.38 m, and 3.31 m. The following 10 cm of the investigated profile contain carbonate-rich sands and a few pebbles (2.5 – 2.6 m). The upper 88 cm of the profile is characterized by an increasing amount of root channels and was therefore not investigated in great detail. Approximately 1.6 m of sediment is missing on top due to agricultural activities (deduced from the maxmimum height measured at the outcrop using a total station). See also the stratigraphic layers indicted in Figure 7.7.

7.3.2. Measurements on quartz

The measurement results of the quartz fraction were highly variable. Some aliquots (2-8 mm) approached saturation and a few also exhibited a small IR signal, although no feldspars were detected under the microscope. The measurements focused on the $100 - 150\ \mu m$ grain size fraction. The preheat plateau test of sample C-L4240 does not show a plateau, but the dose recovery test behaved satisfactorily with recovered/given dose ratios between 0.95 ± 0.02 and 1.05 ± 0.07 (Fig. 7.2). The different characteristics of the single aliquots are demonstrated in Figure 7.3, which depicts shine down and dose response curves of three quartz aliquots from sample C-L4240. D_e measurements were undertaken with a preheat temperature of $240°\ C$. However, the abanico plot in Figure 7.4 demonstrates the wide spread in the data. Only 43.6% of the data points lie in a 2σ-range. Due to this problematic behavior, it was decided to refrain from further investigation of the quartz fraction.

7.3.3. Measurements on kalifeldspar using the $pIRIR_{290}$ and $pIRIR_{225}$ protocols

The kalifeldspar fraction of samples C-L4239 - C-L4243 were investigated using grain sizes of $150 - 200\ \mu m$ (only for C-L4241 gains sizes between $100 - 250\ \mu m$ were used). A first IR stimulation temperature test was conducted using the $pIRIR_{290}$ and the $pIRIR_{225}$ protocols (see Fig. 7.5). For the prior, no plateau region can be identified satisfactorily, but the latter

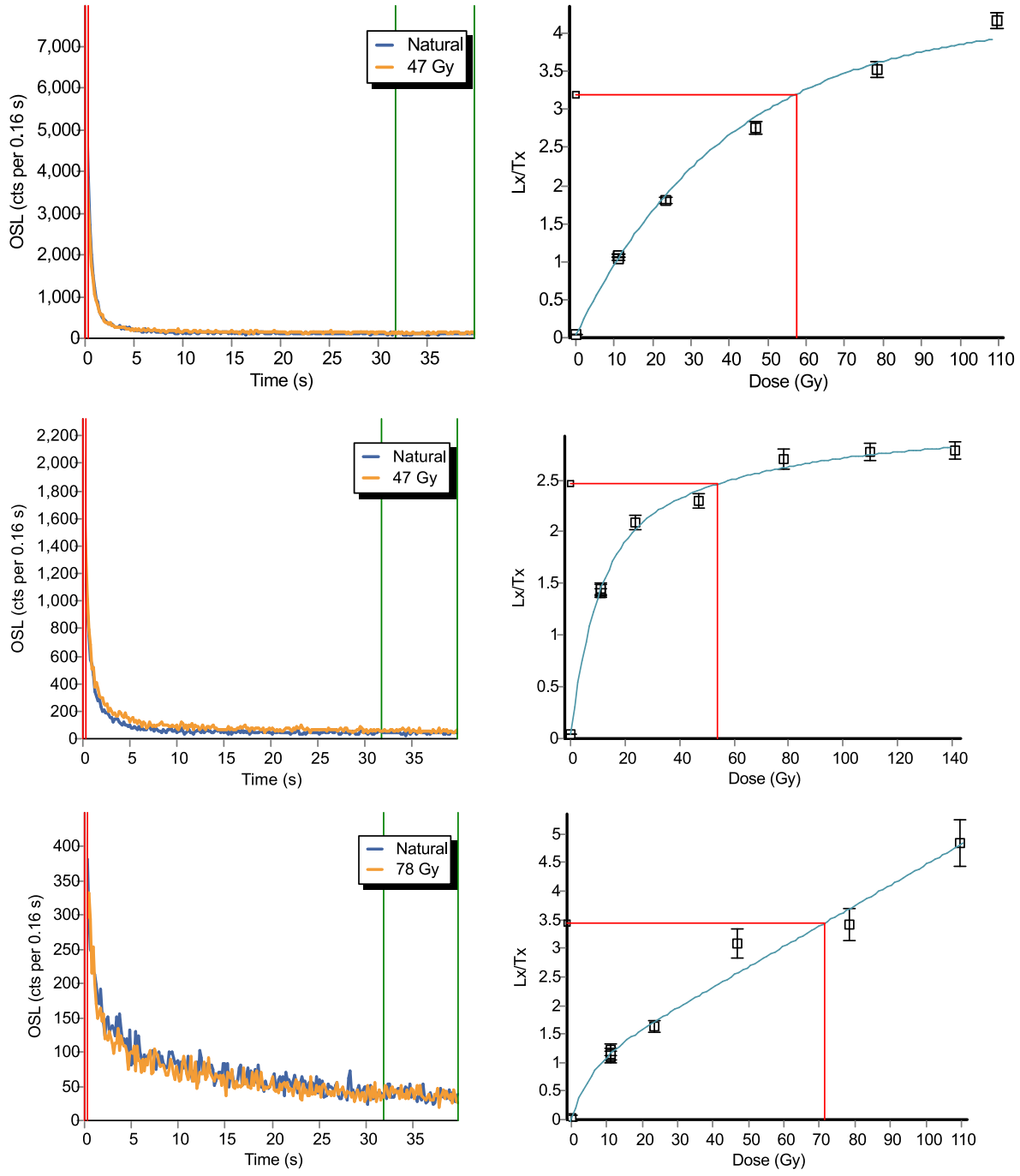

Figure 7.3.: Shine down curves (left) and dose response curves (right) of quartz sample C-L4240 showing three aliquots with different signal characteristics. The uppermost aliquot was fitted with a single saturating exponential function, the one below with a single saturating exponential plus linear function, and the lowermost aliquot was fitted with two saturating exponential functions. The second aliquot is approaching saturation, while the lowermost aliquot exhibit a very small signal. Analyst version 4.14.6 was used to generate the plots (Duller, 2015a).

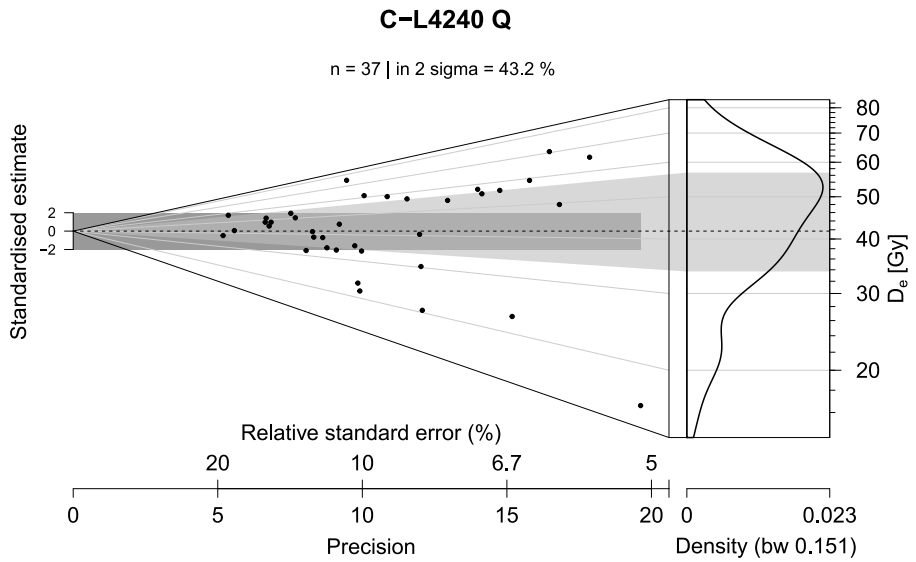

Figure 7.4.: Abanico plot showing the D_e distribution of 2 mm quartz aliquots of sample C-L4240. The plots were generated in the R luminescence package using the '*plot_AbanicoPlot*'-function according to Dietze et al. (2016)

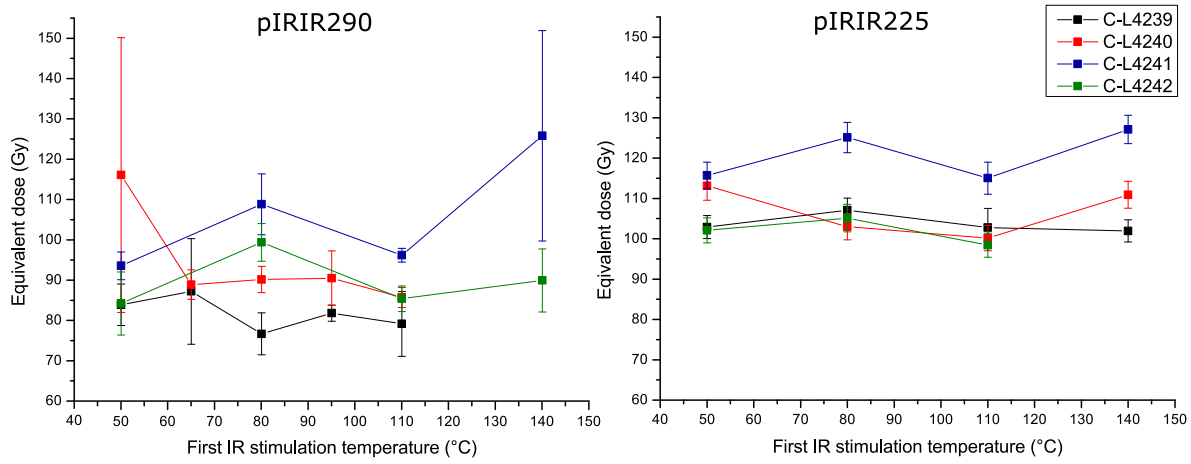

Figure 7.5.: First IR stimulation temperature test of samples C-L4239 - C-L4243 using the $pIRIR_{290}$ (left) and $pIRIR_{225}$ (right) protocols. The measurements show much more scatter using the $pIRIR_{290}$ protocol.

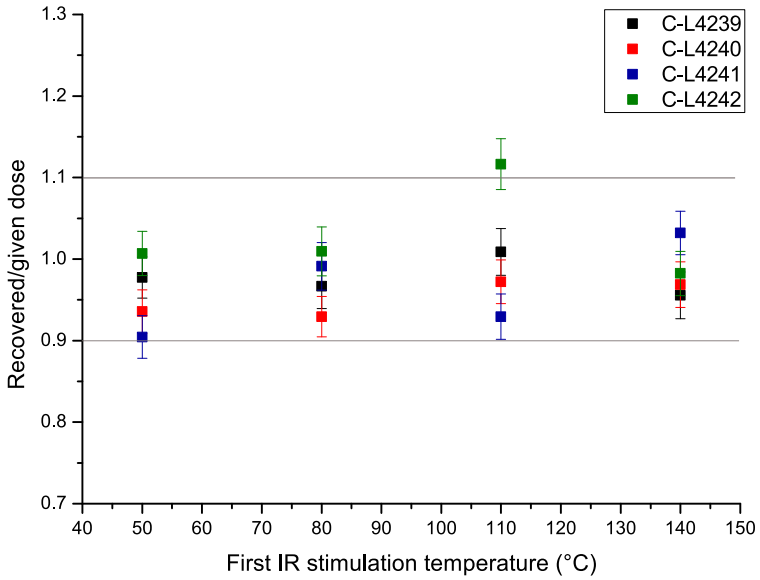

Figure 7.6.: Dose recovery test of samples C-L4239 - C-L4243 using the pIRIR$_{225}$ protocol. All samples except for two lie well within the desired 1.0 ± 0.1-ratio. For the measurements that applied the pIR$_{80}$IR$_{225}$ protocol ratios cluster closest together around 0.97 ± 0.02.

shows much less scatter with a first IR stimulation temperature plateau between all tested temperatures. Therefore, a dose recovery test was applied using solely the pIRIR$_{225}$-protocol. Figure 7.6 shows recovered to given dose ratios between 0.96 ± 0.03 and 1.12 ± 0.03. Fading measurements indicate low fading rates of $g_{2days} = 0.08 \pm 0.21$ (pIR$_{50}$IR$_{225}$), $g_{2days} = 0.01 \pm 0.07$ (pIR$_{80}$IR$_{225}$), and $g_{2days} = 0.21 \pm 0.75$ (pIR$_{110}$IR$_{225}$) (see also Fig. C.1). Due to the satisfactory behavior of the measurements using the pIR$_{80}$IR$_{225}$ protocol within the first IR stimulation temperature test, dose recovery test, and fading experiment, the D_e measurements were also carried out with this protocol. Figures C.2 and C.3 present exemplary shine down and growth curves for all measured samples of both trenches, which show bright luminescence signals. Figures C.4 and C.5 depict the corresponding abanico plots. There is some spread and variability in the data, but this can be expected from small aliquot sizes (2 mm) and fluvial sediments. A summary of the luminescence and age data is shown in Table 7.1, and the dose rate data of the different sediment layers is summarized in Table 7.2. The saturation water content measurements indicate a value of ~24% for the sandy layer. To cover a wide range (50%) of possible moisture conditions a water content of $12 \pm 6\%$ was applied to all samples in the age calculations. Only for sample C-L4242 a higher water content of 20±8% was assumed because here the present water content was also much higher than within the other samples. An error of 8% was applied to also cover the estimated water contents of the other samples. Figure 7.7 shows age-depth plots of the two profiles At1$_{3B}$ and At1$_5$ and highlights the good consistency between the obtained ages. The Aurignacian artifacts have been found between samples C-L4240 and C-L4241, and C-L4244 and C-L4245 (darker shaded area in Fig. 7.7), indicating a deposition between 33.9 ± 2.9 *ka* and 41.3 ± 3.4 *ka*. It should be noted that the timing can be pinpointed more precisely at At1$_5$, but more artifacts have been found at At1$_{3B}$.

Table 7.1.: Summary of the luminescence data of the $At1_5$ and $At1_{3B}$ profiles. The measured (W_m) and used (W_{used}) water contents, cosmic (D_{cosmic}) and total dose rates (D_{total}), residual doses, equivalent doses (D_e) and ages are shown.

Sample	**Mineral**	**Grain size** (μm)	**Depth** (m)	n	$W_measured$ (wt. %)	W_{used} (wt. %)	D_{cosmic} (mGy/ka)	D_{total} (Gy/ka)	**Residual** (Gy)	D_e (Gy)	**Age** (ka)
C-L4239	KFS	150-200	3.6	28/34	8	12±6	143	3.33±0.34	1.4±0.1	100.62±5.25	30.2±2.6
C-L4240	KFS	150-200	3.9	43/46	3	12±6	139	2.81±0.28	1.3±0.2	103.6±5.67	36.8±3.1
C-L4241	KFS	100-250	4.1	28/34	1	12±6	136	2.85±0.28	1.3±0.1	118.0±6.11	41.3±3.4
C-L4242	KFS	150-200	4.3	30/31	20	20±8	133	2.57±0.27	1.4±0.1	100.04±5.12	38.9±3.5
C-L4243	KFS	150-200	3.15	36/37	8.3	12±6	150	3.25±0.35	1.25±0.18	113.1±6.83	34.8±3.2
C-L4244	KFS	150-200	3.3	39/40	3.8	12±6	148	3.25±0.33	1.36±0.12	110.05±5.96	33.9±2.9
C-L4245	KFS	150-200	3.55	51/55	5.7	12±6	144	3.85±0.41	1.39±0.1	158.84±9.24	41.3±3.6
C-L4246	KFS	150-200	3.7	32/34	13.4	12±6	142	3.3±0.34	1.32±0.09	118.23±6.45	35.8±3.1

Table 7.2.: Summary of the dose rate data shown for the individual stratigraphic layers of the $At1_5$ and $At1_{3B}$ profiles at Crvenka-At.

Layer	U (Bq/kg)	Th (Bq/kg)	K (Bq/kg)
At1-5 A	20.71±1.01	25.34±1.31	636.29±9.46
At1-5 B	4.93±0.43	6.96±0.51	647.13±9.49
At1-5 C	5.51±0.42	6.66±0.48	686.17±9.98
At1-5 D	4.58±0.35	5.85±0.46	645.46±9.52
At1-3B A	20.91±1.07	23.97±1.3	613.94±9.15
At1-3B B	12.43±0.72	15.76±0.94	713.57±10.38
At1-3B C	6.62±0.54	10.12±0.71	1024.52±14.37
At1-3B D	12.68±0.73	17.89±1.02	712.63±10.49

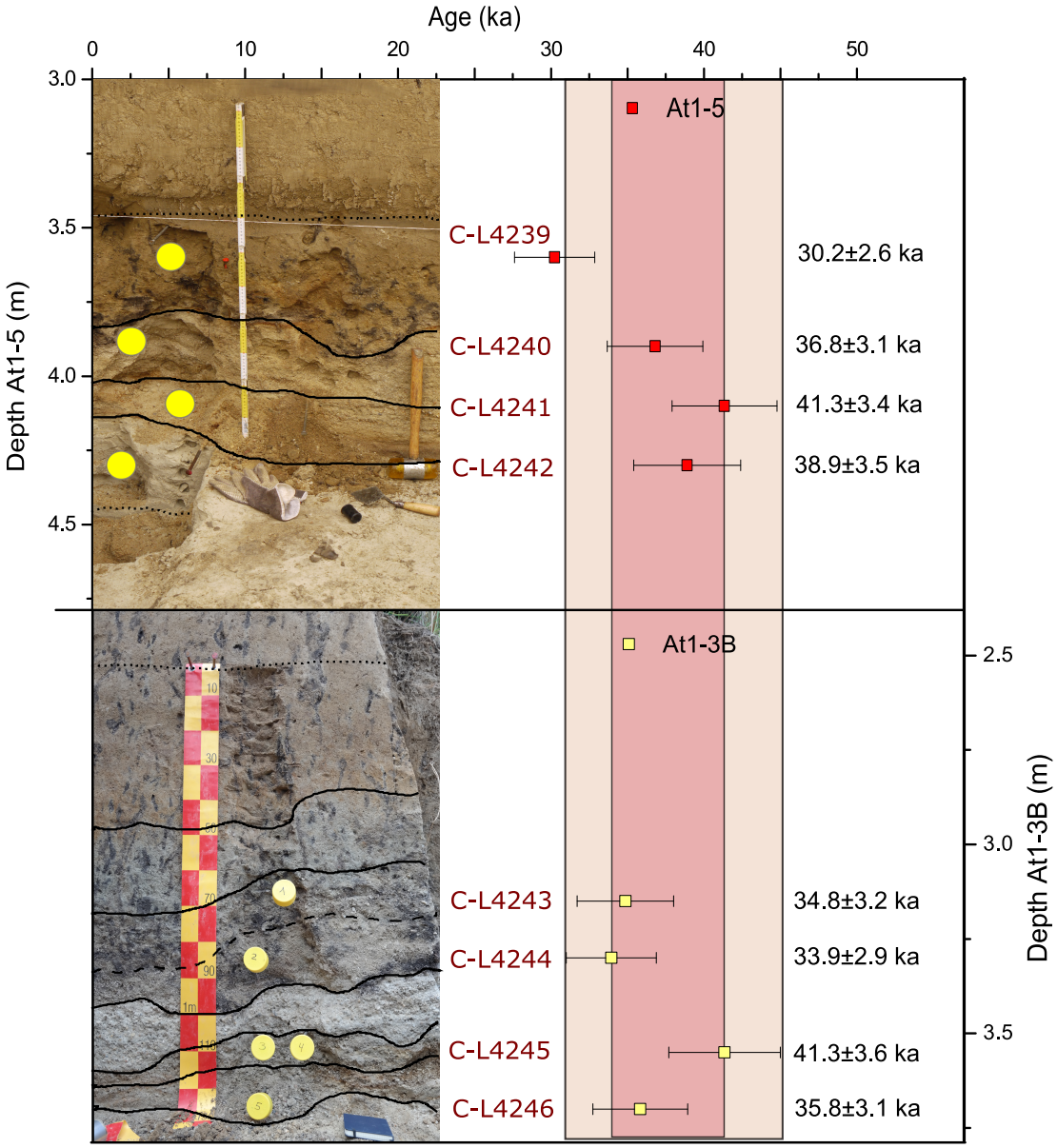

Figure 7.7.: Age-depth plot depicting both trenches at At1, the location of luminescence samples and their ages. Shaded area in the background indicates the age of the different sand layers, highlighting the consistency between the two profiles. The darker shaded area highlights the possible age range of the sediments in which the Aurignacian artifacts have been found. Stratigraphic layers described in section 7.3.1 are indicated on the photos.

7.4. Discussion and conclusion

After thorough investigation of the quartz and kalifeldspar luminescence characteristics, it was shown that the $pIR_{80}IR_{225}$ protocol using kalifeldspars is most suitable for D_e measurements. Surprisingly, the samples exhibit no fading, although fading rates have been reported in literature (Buylaert et al., 2009; Smedley et al., 2015; Vasiliniuc et al., 2012). Residual doses are $< 1.5\ Gy$, so no correction for residual doses was needed. Some uncertainty is likely introduced by the estimation of the moisture content. Therefore, the saturation water content was determined to achieve a better estimate of the average moisture conditions since deposition. Nevertheless, some uncertainty remains because this was only done for one sample. This uncertainty might also explain why in both profiles the lowermost samples, which originate from a different stratigraphical layer, have slightly younger ages than the samples above. The saturation water content sample contains the same material as the samples above and below the archeological findings, which ensures a proper age estimate for the archeological context. Although first IR stimulation temperature test, dose recovery tests and fading experiments were only carried out on the samples of $At1_5$, the geochronologies of both profiles agree well with each other, further supporting the robustness of the age model. Nevertheless, the abanico plots (Figs. C.4 and C.5) show slightly more scatter in the D_e distributions of the samples from $At1_{3B}$, which is probably connected to post-depositional mixing due to the development of roots (as observed in the field). However, most distributions resemble a normal distribution, and only samples C-L4240 and C-L4245 show a slightly skewed distribution towards higher $D_e s$. This can be expected in a fluvial environment, where not all grains might have been completely bleached prior to deposition. However, this does not affect the average D_e greatly and only a few outliers are present.

The Aurignacian artifacts were found in sediments with an age between $33.9 \pm 2.9\ ka$ and $41.3 \pm 3.6\ ka$ at $At1_{3B}$. The geochronology of $At1_5$ even points to a more precise age of sediment deposition between $36.8 \pm 3.1\ ka$ and $41.3 \pm 3.4\ ka$. This age range fits well to other dated Aurignacian findings in the Banat region. A human mandible at Peştera cu Oase has a radiocarbon-age of $37 - 42\ ka\ cal\ BP$ (Trinkaus et al., 2003). Also the thermoluminescence ages of heated artifact at the Early Upper Paleolithic site Romaneşti-Drumbrăviţa fit well with the new OSL ages at Crvenka-At. C. Schmidt et al. (2013) determined that the last heating of the artifacts at Romaneşti-Drumbrăviţa occurred at $40.6 \pm 1.5\ ka$. This points to a more widespread occurrence of anatomically modern humans in the Banat region during this time-frame than previously thought. It demonstrates that not only the upland regions, but also lowland areas were attractive for Early Modern Human hunters and gatherers and it furthermore highlights that exploration in the lowlands of the Banat region might yield potential for future (geo)archeological research.

8. New luminescence-based geochronology framing the last two glacial cycles at the southern limit of European Pleistocene loess in Stalać (Serbia)

Janina Bösken[1], Nicole Klasen[2], Christian Zeeden[1], Igor Obreht[1], Slobodan B. Markovic[3], Ulrich Hambach[3,4], Frank Lehmkuhl[1]
Published in Geochronometria at http://dx.doi.org/10.1515/geochr-2015-0062.

8.1. Introduction

Loess-paleosol sequences (LPS) are terrestrial archives containing information about paleoenvironmental conditions during the Quaternary (see e.g. Antoine et al., 2009; Bösken et al., 2017b; Frechen et al., 2003; Muhs et al., 2008; Sun et al., 2006; Zeeden et al., 2016b). In Southeastern Europe, LPS can be several tens of meters thick representing well preserved and high-resolution archives (see e.g. Marković et al., 2008, 2015; Obreht et al., 2014; Stevens et al., 2011; Zeeden et al., 2016d). In contrast to extensively studied LPS along the Danube River, deposits further to the south in the Central Balkan region have been poorly investigated so far (Basarin et al., 2011; Kostić and Protić, 2000; Obreht et al., 2014). The studied section Stalać is located in this region south of the typical loess distribution area of the Carpathian Basin (Middle Danube Basin) and the Lower Danube Basin, and it is especially important for an integral view on paleoenvironments in the yet poorly investigated interior of the Balkans. This region was under much stronger influence of the Mediterranean climate in the past, suggesting a very dynamic climatic evolution of this region. Thus, the area where the Stalać section is located seems to be potentially extraordinary sensitive to past and present climatic changes (Bösken et al., 2014).

Dating of the sediments is crucial to place the climatic information of a loess-paleosol record into a temporal context. The most commonly used dating technique in LPS is luminescence dating. Loess samples consisting of fine grains of quartz are thought to be the ideal material for optically stimulated luminescence (OSL) dating (Roberts, 2008), but recent studies indicate that this is not necessarily correct. Timar-Gabor et al. (2012, 2015b) found varying dose response curve (DRC) shapes for different grain sizes of quartz that led to age discrepancies.

[1]Department of Geography, RWTH Aachen University, Templergraben 55, 52056 Aachen, Germany
[2]Institute of Geography, University of Cologne, Albertus-Magnus-Platz, 50923 Cologne, Germany
[3]Laboratory for Paleoenvironmental Reconstruction, Faculty of Sciences, University of Novi Sad, Serbia
[4]BayCEER & Chair of Geomorphology, University of Bayreuth, Germany

Moreover, disagreements between natural and laboratory-induced DRCs (e.g. Chapot et al., 2012; Timar-Gabor et al., 2015a) raise questions about the reliability of equivalent dose (D_e) estimates within the high dose range, as natural DRCs saturate earlier than expected from the D_0-value (cf. Wintle and Murray, 2006).

Especially for older samples, the application of infrared stimulated luminescence (IRSL) of (coarse-grained) feldspars or (fine-grained) polyminerals is an alternative technique for dating loess deposits. In particular, post-infrared-IRSL methods (pIRIR) are interesting, as these only show negligible fading rates in contrast to conventional IRSL methods (Buylaert et al., 2012; Murray et al., 2009; Thiel et al., 2011b; Thomsen et al., 2008; Vasiliniuc et al., 2012; Zhang et al., 2015). For protocols with elevated preheat and stimulation temperatures fading rates <1%/decade are observed (Zhang et al., 2015), which were suggested to be a laboratory artifact (Vasiliniuc et al., 2012).

The major aim of this study is to construct a reliable luminescence chronology for the Stalać section in the Central Balkan region as a cornerstone for paleoenvironmental investigations (cf. Obreht et al., 2016) by focusing on polymineral $pIR_{50}IR_{290}$ and quartz OSL dating of fine grains ($4-11\ \mu m$).

8.2. Regional setting

The Stalać section is located in central Serbia (43°40.64812'N, 21°25.06967'E), close to the city of Kruševac (Fig. 8.1). It is exposed in an active brickyard at the village of Stalać on the east side of the Južna (South) Morava River, ca. 3 km from the confluence of the Južna Morava and the Zapadna (West) Morava Rivers into the Velika (Great) Morava River. Due to the geological setting of those river catchments, transported sediments contain large amounts of igneous and metamorphic detritus, as reported from the Belotinac section located ca. 80 km south of Stalać (Basarin et al., 2011; Obreht et al., 2014). This is also reflected in the geophysical characteristics and geochemistry of the section, showing extraordinary high magnetic susceptibility and several times higher values of Ni and Cr (Obreht et al., 2016) when compared to other LPS in Southeastern Europe (e.g. Buggle et al., 2008, 2009; Marković et al., 2015; Obreht et al., 2015; Újvári et al., 2008; Zeeden et al., 2016b). This clearly points to a mainly local source of the material from the surrounding rivers at the Stalać section.

The loess deposits at Stalać are formed as a plateau-like structure covering the eastern slopes of the tectonically controlled Morava-floodplain-basin. Geomorphology and present day land-use-patterns indicate that widespread and thick Middle and Late Pleistocene loess is restricted to the eastern slopes of this basin north of the confluence of the Južna Morava and the Zapadna (West) Morava Rivers indicating prevailing north-western winds. Southeast to northwest trending 2 to 3 km long valleys are cut into the plateau. The depositional pattern of the loess-paleosol-sequence argues for their potentially constant activity throughout the time of loess deposition. Shorter maximum 1 km long valleys occur as tributaries of the main valleys and seem to be formed as gullies during single and dramatic erosional events and later filled up

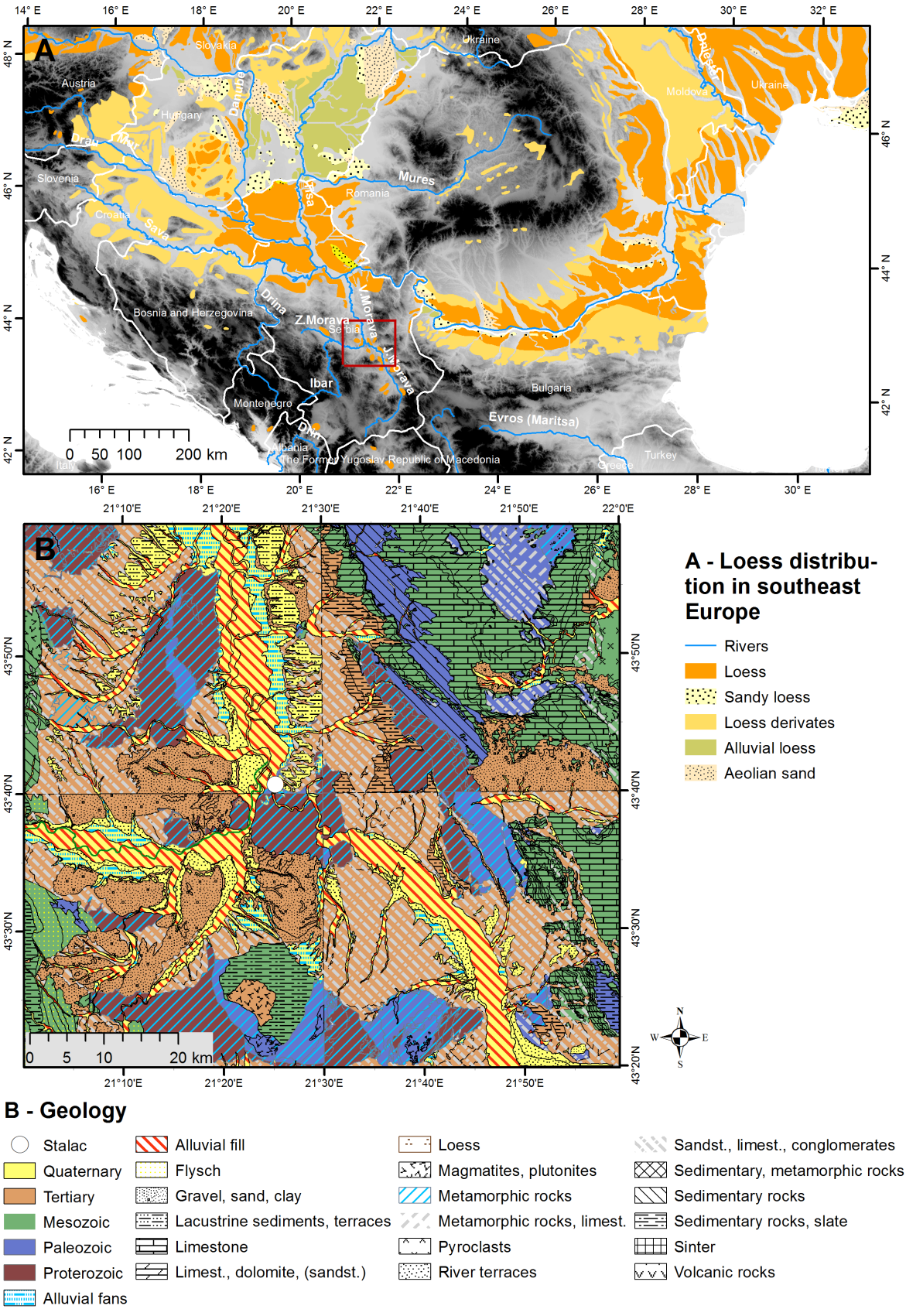

Figure 8.1.: Distribution of loess and loess derivates modified after Haase et al. (2007), Lindner et al. (2017), and Vandenberghe et al. (2014) (A). Red square indicates the extent and location of map B. Map B shows a simplified geological map (Dolić et al., 1980; Krstić et al., 1978; Rakić et al., 1975; Vojnogeografski Institut, 1968). The location of the Stalać section is indicated by a white circle. Digital elevation model based on SRTM data available from U.S. Geological Survey (Farr et al., 2007).

with eolian loess. The northwest trending depth line of such a structure is presently located just 200 m to the South of the sampled outcrop wall and might form the base-level of the observed erosional surface in the loess sequence.

The current climatic conditions are characterized with moderate continental conditions. From 1981 to 2010, the mean annual temperature (with a high interannual variability) was 11.4°C at a nearby climate station in Kruševac; the mean annual precipitation was 628 mm and exhibits precipitation maxima in June and November (RHMS, 2016).

Fig. 8.1 shows the loess distribution of Southeastern Europe and the location of the section. Moreover, it displays a simplified geological map. The geological map (Dolić et al., 1980; Vojnogeografski Institut, 1968) indicates Cenozoic clays, sandstones, conglomerates, slates; Mesozoic limestones, sandstones, marls, and dolomites; and Proterozoic slates, shales and schists exposed in the mountains and a Holocene fluvial landscape development in the valleys. Also, Quaternary sediments formed by erosional processes and alluvial fans are present. The location of the Stalać brickyard is mapped as Pleistocene lake sediments on top of Miocene clay, sandstones, and conglomerates; moreover, proterozoic hornfels, schists and migmatite are exposed. The sampled loess deposits are not indicated in the regional geological maps.

Kostić and Protić (2000) undertook a first paleopedological and mineralogical investigation at the Stalać section. Based on their grain-size, clay minerology and carbonate content results, they showed that the climatic dynamics of this region gradually shifted from a dominated Mediterranean climate towards a more continental climate. This was characterized with decreasing precipitation and possible overall cooling from the Middle to Late Pleistocene. However, no numerical dating was applied, thus their interpretation is based on solely correlative stratigraphy, and will be evaluated by our geochronological investigations.

8.3. Sampling and stratigraphy

The section is exposed in a northeast to south-westward direction. Fig. D.1 shows photos of the site. The section contains a compacted profile in the northeast (not shown in photos), and four dipping profiles on the slope in the southwest. It is possible to track the sediment layers between the profiles. For this study the four profiles on the slope were sampled, as this allowed sampling in a higher stratigraphic resolution. The profiles were carefully cleaned. Sediment, paleosol and tephra layers including their characteristics were recorded and correlated within the individual sub-profiles. Six luminescence samples were taken by hammering and extracting 15 cm long metal tubes into the previously cleaned sediment wall, and by collecting the surrounding material in a radius of 30 cm for dose rate determination.

For a better overview, a composite profile was made out of the four individual profiles using the paleosol and tephra layers (Fig. 8.2). Stratigraphic labeling followed the scheme proposed by Marković et al. (2015), in which the loess and paleosol stratigraphic units were designated as ‘L’ and ‘S’ and numbered in order of increasing age.

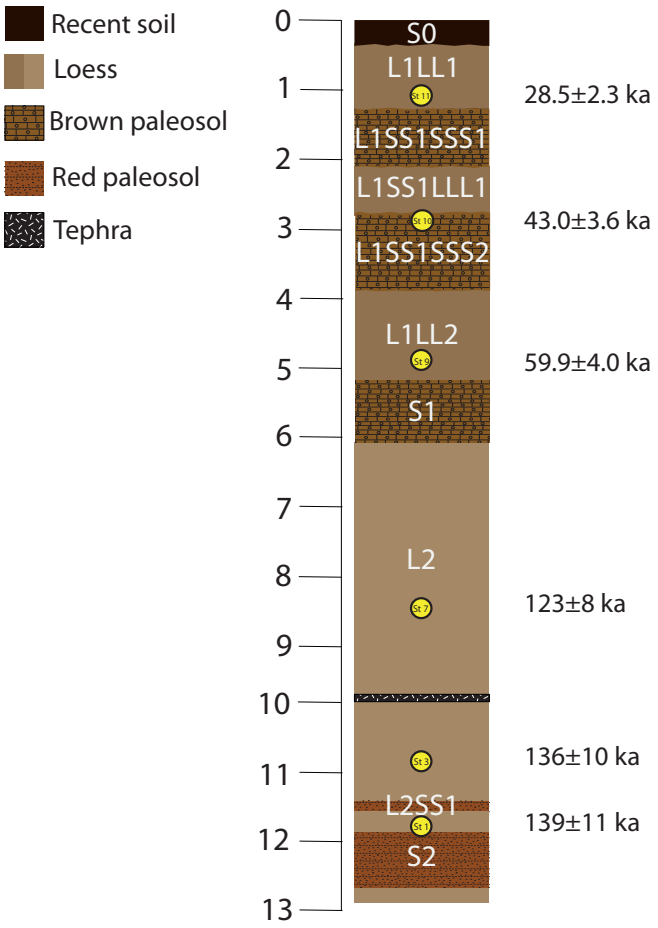

Figure 8.2.: Sketch of a composite profile, showing the nomenclature of paleosols and loess (after Marković et al., 2015) and the investigated luminescence samples.

The bottom of the profile starts with a 20 cm thick loess layer. On top, a reddish cambisol (11.9 – 12.7 m), and a 2 m thick pale yellow loess layer (L2) is exposed. The loess layer is intercalated by a deep-red vertic (11.45 – 11.6 m, L2SS1) and two weak brown humic horizons (10.8 – 10.9 m, 10.43 – 10.55 m). At ca. 10 m depth on the composite profile a tephra with a thickness of ca. 5 cm is exposed. Above the tephra follows a thick loess layer (ca. 3.85 m, L2) containing some carbonate concretions in the lower part. The loess layer is intercalated by clearly visible organic layers at ca. 6.6 – 6.7 m and 7.05 – 7.15 m. This layer is overlain by a kastanozem-like pedocomplex (S1) with calcareous root channels (5.2 – 6.05 m). Above, another loess layer (3.9 – 5.2 m) is exposed, which contains a few darker layers at 4.7 – 4.85 m and around 4.4 m. On top of this loess layer a second kastanozem-like paleosol (L1SS1SSS2) with a thickness of 1.1 m can be found (2.8 – 3.9 m). At a depth of 2.1 – 2.8 m a loess layer (L1SS1LLL1) is located, on top of which a third 80 cm thick kastanozem-like paleosol developed (1.3 – 2.1 m, L1SS1SSS1). Physical and chemical proxy data (Obreht et al., 2016) revealed the existence of a crypto tephra mixed within the L1SS1LLL1 loess layer at ca. 2.4 – 2.8 m. Above, a brown loess layer (0.3 – 1.3 m, L1LL1) is located. On top, the recent soil (S0) is exposed. A more detailed stratigraphy is presented in Obreht et al. (2016).

8.4. Methodology

8.4.1. D_e Equivalent dose measurements

Samples for equivalent dose (D_e) determination were extracted from the metal tubes under subdued red light conditions; the outer 2 cm of sediment were removed. Samples were oven dried ($50°C$), the water content was determined (water content over dry mass) and samples were then treated with 10% hydrochloric acid, 10% hydrogen peroxide and 0.01 N sodium oxalate to remove carbonates, organic matter, and to dissolve aggregates. Where needed, 30% hydrogen peroxide was used. After thoroughly removing the chemicals, samples were separated into the $4 - 11\ \mu m$ fraction. One part of each fraction was etched in 34% hexafluorosilicic acid for one week to extract fine-grained quartz minerals. The other part remained as a polymineral fraction.

Continuous wave optically stimulated luminescence measurements (CW-OSL) were carried out on a Risø TL/OSL DA 20 reader. The reader is equipped with a $^{90}Sr/^{90}Y$ β source, blue light emitting diodes (LEDs), emitting at 470 nm (FWHM = 20 nm), and IR LEDs, emitting at 870 nm (FWHM = 40 nm). Signals of quartz were detected through a Hoya U-340 filter and signals of polymineral fine grains were detected through a 410 nm interference filter. A single aliquot regenerative dose (SAR) protocol (cf. Murray and Wintle, 2000, 2003) was applied for quartz. Sensitivity changes, recycling ratios and recuperation were monitored by the SAR protocol (Murray and Wintle, 2000). A preheat plateau test (e.g. Murray and Wintle, 2000) and a dose recovery test (e.g. Murray and Wintle, 2003) were performed on sample C-L3787 prior to D_e measurements to assess the proper measurement settings. This sample was used for testing after preliminary geochemical results were available. These showed similarities between samples C-L37781 and C-L3787, which is why the tests were done on one sample only. Preheat plateau tests (PHTs) with different preheat and cutheat temperatures between $160°C$ and $280°C$ were carried out. Cutheat temperatures were always $20°C$ lower than preheat temperatures. Dose recovery tests (DRTs) included optical stimulation for 100 s and laboratory irradiation to create a known laboratory dose. The chosen irradiation dose was equal to the expected D_e. We used an early background subtraction for equivalent dose calculation (Ballarini et al., 2007). The signal was integrated from the first 0.48 s of the 40 s stimulation minus a background of the following 1.28 s.

For polymineral fine grain measurements the $pIR_{50}IR_{290}$ SAR protocol was used (Thiel et al., 2011b). A prior IR stimulation temperature test was performed (cf. Buylaert et al., 2012). Furthermore, a DRT using bleached samples (24 h Hönle Sol2 solar simulator) with the favorable prior IR stimulation temperature was applied. These tests were carried out on C-L3780, C-L3784 and C-L3787. These three samples were chosen based on preliminary sedimentological results indicating different units in the profiles. Finally, the equivalent dose was determined on a minimum of ten aliquots per sample using the arithmetic mean. Polymineral feldspar measurements used a late background subtraction for the dose response curve fitting (e.g. Banerjee et al., 2000). The signal was integrated using the first 2.4 s minus a background of the last 25.6 s (total stimulation length was 200 s). Residual doses were assessed after bleaching the

aliquots for 24 hours in a solar simulator. Fading tests were conducted on samples C-L3780 and C-L3787. For these, doses of 650 Gy and 187 Gy were given and the normalized luminescence signals were measured after different storage times between 100 and 800 minutes.

8.4.2. Dose rate measurements

Samples for dose rate determination were oven dried ($50°C$); the water content was determined, and samples were homogenized and packed into plastic cylinders for radionuclide measurements. After a resting period of four weeks to compensate for radon emanation during pretreatment, radionuclide concentrations were measured on a high-purity germanium gamma-ray spectrometer. The dose rates and ages were calculated using DRAC, v.1.2 (Durcan et al., 2015). Conversion factors of Guérin et al. (2011) and the measured water content (W) were included. In order to cover possible fluctuations in water content a wide error range of $\pm 0.5 * W$ was assumed. The internal β dose rate contribution of the polymineral samples was calculated by assuming a potassium content of $12.5 \pm 0.5\%$ (Huntley and Baril, 1997). Beta attenuation factors of Brennan (2003) and Mejdahl (1979) were used. The cosmic dose rate was calculated following Prescott and Hutton (1994) considering the geographical position, altitude and sample depth. A value of 0.036 ± 0.003 (Kreutzer et al., 2012a) was assumed for α-efficiency of the fine grain quartz samples. The α-efficiency for the polymineral samples was determined by bleaching the aliquots thermally by heating to $480°C$ and administering α-doses < 200 Gy in a Freiberg Instruments Lexsyg Research device; afterwards the laboratory dose of the samples was determined using β-irradiation in a Risœ reader (pIRIR protocol); the α-efficiency is the ratio of the measured β-dose divided by the given α-dose (cf. Kreutzer et al., 2014). A linear function was used for fitting.

After the age calculation, ages bracketing the paleosols and the tephra were combined to one density function per layer, of which an estimate for the ages of the layers themselves including uncertainties was calculated. This was done conservatively by determining 1- and 2-sigma uncertainties of the combined densities.

8.5. Results and discussion of the luminescence data

8.5.1. Investigation of the quartz samples

8.5.1.1. Preheat dependency and dose recovery tests

First, we investigated the dependency of the equivalent dose on the preheat temperature and the ability to recover a given dose (Fig. 8.3). Equivalent doses are decreasing with increasing preheat temperature and no plateau was observed. Several aliquots showed sensitivity changes (recycling ratios between 1.11 and 1.13; see Fig. 8.4 for more detail), but recuperation was negligible (values below 0.77%). All D_e-values are smaller than $2 * D_0$ and do not depend on the signal integration interval (see $D_e(t)$-plot in Fig. D.2). Laboratory doses were recovered within 10% of unity for all preheat temperatures except for a preheat temperature of $240°C$ (see Fig. 8.3 bottom). IR depletion ratios of 1.06 ± 0.05 (PHT) and 1.00 ± 0.04 (DRT) indicated that the quartz fraction was not contaminated by feldspar. Examples of DRCs can be

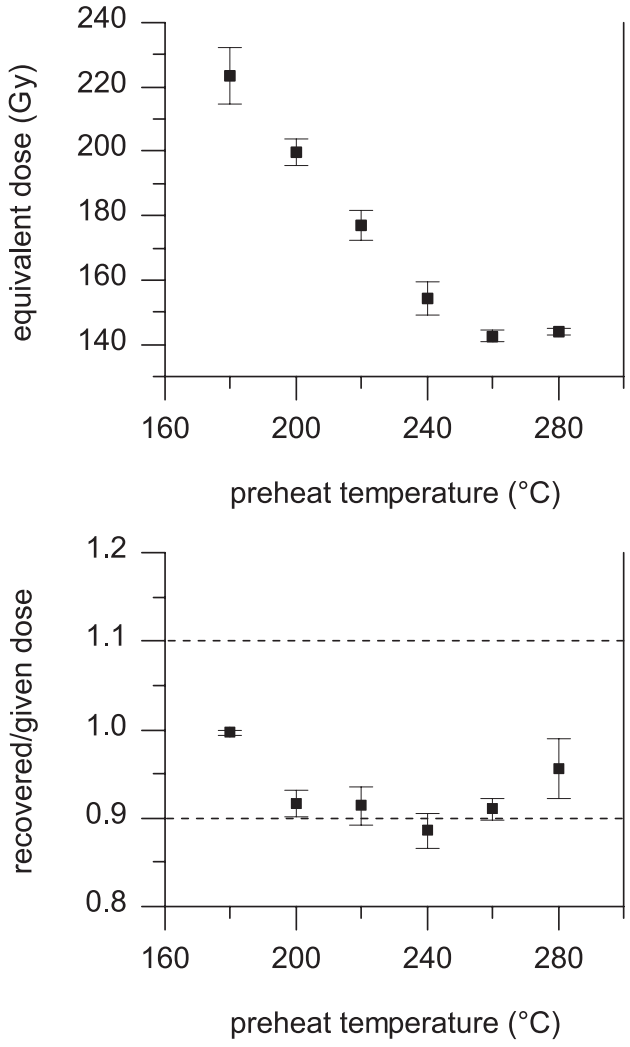

Figure 8.3.: Top shows a plot of D_e as a function of preheat temperature for five aliquots per temperature of the quartz fraction of sample C-L3787. The standard error is shown. Bottom shows a dose recovery test of the same sample using different preheat temperatures. Aliquots were bleached and given a dose of $\sim 150\ Gy$. Area between dashed lines displays the desired ratio. Error bars show standard deviation.

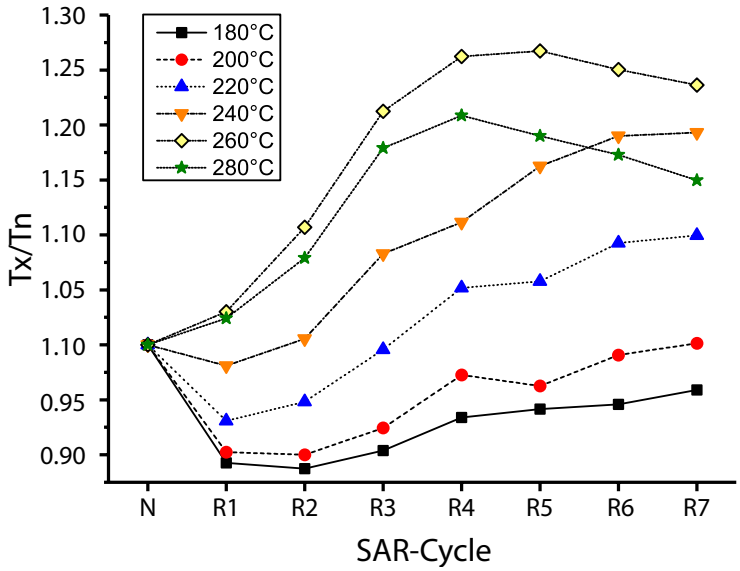

Figure 8.4.: Response to a testdose (T_x) normalized to the testdose response of the natural signal (T_n) throughout the PHT measurements of sample C-L3787 showing the sensitivity changes occurring during the SAR-cycle.

viewed in Fig. D.3 A and B.

8.5.1.2. Natural and regenerated luminescence signal

To further investigate the quartz luminescence behavior, the OSL signal components were fitted (e.g. Fig. D.4). The signal of quartz is known to consist of several components, each having different thermal and optical properties (Bailey, 1997, 2010; Jain et al., 2003; Singarayer and Bailey, 2003). Each component is characterized by a specific photoionization cross section, saturation dose and thermal stability (Bailey, 2010). Using the *fit_CWCurve*-function in the *R* luminescence package (Kreutzer et al., 2012b) showed that most OSL signals consist of the fast, medium, and slow 2 components (cf. Jain et al., 2003). The fast component contributes with $70 - 80\%$ to the total signal in the analyzed sample (Analyst version 4.31.7, Duller, 2015a). The relative contribution of the signals is shifting throughout the SAR-cycle, and is also not similar between aliquots or preheat temperatures. Fig. 8.5 shows the ratios of medium and slow components to the fast component: $\sigma_{medium}/\sigma_{fast}$ and $\sigma_{slow}/\sigma_{fast}$; and the expected values by Jain et al. (2003). While $\sigma_{medium}/\sigma_{fast}$ is greater than expected in most signals (independent of preheat temperature or SAR-cycle step), there are also some signals that do not exhibit a medium component at all (e.g. L3 180°C in Fig. 8.5). Sometimes also a slow 1 component is present (see L3 180°C in Fig. 8.5). In general, most differences can be seen between the natural and the regenerated signals.

This difference becomes also evident in the $NR(t)$ plots in Fig. D.5 (following the example of Steffen et al., 2009; using the *plotNRt*-function in the R luminescence package, Burow et al., 2016). To create these plots the natural OSL signal (N) is divided by the regenerated OSL

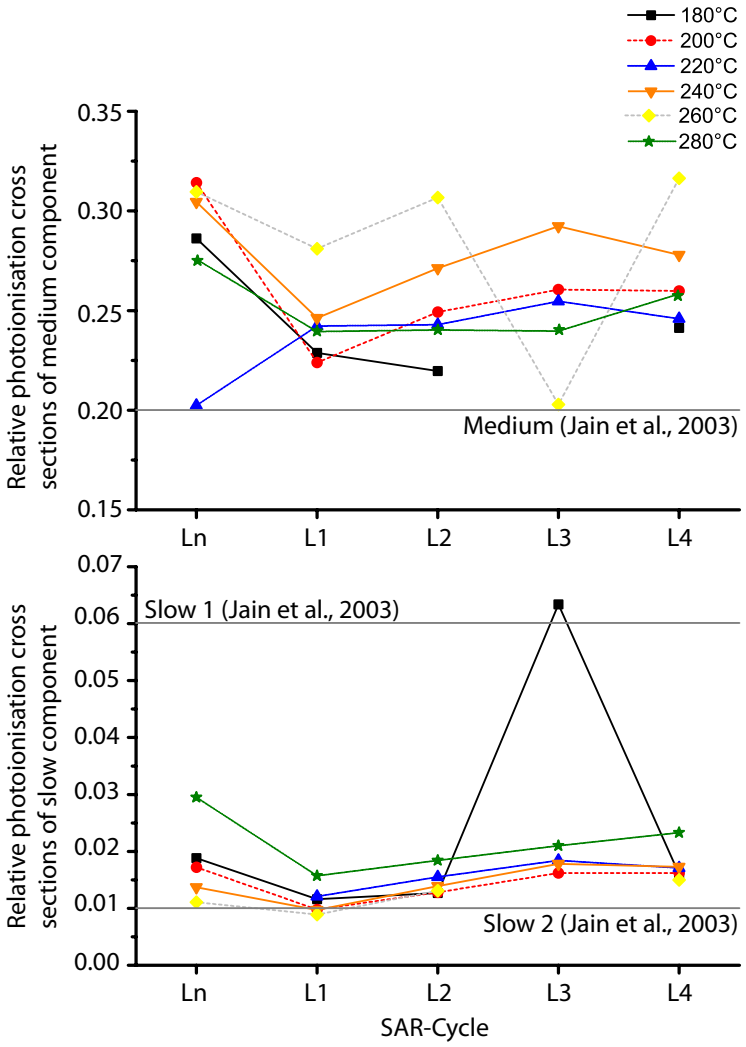

Figure 8.5.: Relative photoionisation cross sections of medium (top) and slow (bottom) components with regard to the fast component at different preheat temperatures during the PHT of C-L3787. Note that only one aliquot per preheat temperature is shown and that aliquots do not behave equally. Horizontal lines show the values observed by Jain et al. (2003).

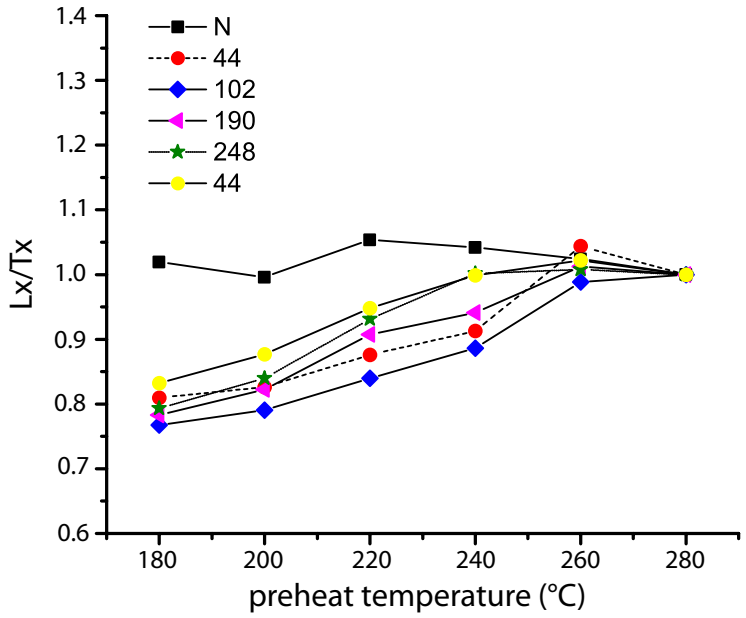

Figure 8.6.: Normalized luminescence signal (L_x/T_x) of the natural signal (N) and the regeneration dose points (indicted in Gy) during the different preheat temperature measurements. All points are normalized to the $280°C$ data point.

signal (R) and scaled to 1. A N/R ratio below 1, therefore, indicates that the natural signal is decaying faster than the regenerated one. This is the case for all preheat temperatures.

Furthermore, the observed difference between natural and regenerated signals is also visible in Fig. 8.6, which presents the normalized luminescence signal (L_x/T_x) plotted against the preheat temperature (cf. Roberts, 2006): while the natural signal (L_n/T_n) remains constant, the regenerated signal (L_x/T_x) is increasing with higher preheat temperatures (with regard to the $280°C$ dose point). A steeper dose response curve results in lower D_e values, which were evident in the preheat plateau test (Fig. 8.3).

8.5.1.3. Evaluation of the quartz characteristics

The variation within the contribution of different signal components and the sensitivity changes are not very large (<30%), and the SAR-protocol was able to correct for this at least partially (recycling ratios within $0.9-1.1$ for most aliquots). Part of the preheat temperature dependency of the equivalent dose can be explained by the fact that the fast component contributes to the signal with only $70-80\%$, but it remains unclear if this is the reason for the quartz behavior. Similar observations with decreasing preheat plateaus were also observed by Roberts (2006) and interpreted as thermal transfer of charge from a trap between cutheat and preheat temperatures into the OSL trap. Moreover, their study showed that falling preheat plateaus are particularly problematic for older loess samples, although the signal is not saturated. We observed the same behavior for the Stalać sample, which has equivalent doses between $140-220\ Gy$ depending on the preheat temperature used. This might also hint towards another process within quartz OSL measurements, which is not yet understood. Especially considering the differences between grain

sizes (cf. Timar-Gabor and Wintle, 2013; Timar-Gabor et al., 2015b) and differences between natural and laboratory growth curve shapes (e.g. Chapot et al., 2012; Timar-Gabor et al., 2015a), which both seem to start around $100-150\ Gy$, this problem becomes evident. Until the underlying processes are better understood, it is advisable to investigate the quartz OSL signal thoroughly, apply preheat plateau tests routinely, and abandon the dating of samples that show a preheat dependency, especially for samples with high paleodoses. Therefore, we do not report quartz OSL ages from this profile at Stalać.

8.5.2. Investigation of the polymineral samples

First, the dependency of the temperature of prior IR stimulation on the equivalent dose was investigated: the D_e is independent from prior IR stimulation temperatures for sample C-L3780 between 50 and $110°C$, for sample C-L3784 between 50 and $140°C$, and for sample C-L3787 between 50 and $170°C$ (Fig. 8.7 top). Accordingly, we continued the measurements with a first IR stimulation temperature of $50°C$, which exhibit higher signal intensities. We applied test doses of ~30% of the equivalent dose. DRTs gave recovered/given dose ratios of 0.97 ± 0.004 (C-L3780), 1.07 ± 0.02 (C-L3784), and 0.96 ± 0.02 (C-L3787) as depicted in Fig. 8.7. For these ratios the residual doses were subtracted.

D_e measurements were carried out on at least ten aliquots per sample and all aliquots passed the SAR quality checks. No residual doses were subtracted for D_e calculations, as suggested by Kars et al. (2014). Fig. D.3 and D.6 show examples of a growth and decay curves, while Fig. D.7 depicts abanico plots of the D_e distributions. Table 8.1 summarizes the D_e and age data. Recycling ratios were between $0.96 - 1.06$ and recuperation was smaller than 1.6%. Residual doses were generally low, ranging from $4-7\ Gy$, i.e. less than 2.5% of the equivalent dose. Also, fading rates were determined for samples C-L3780 and C-L3787. Fading rates (g-values) vary greatly and also negative g-values are observed, which is why no age correction was undertaken. The average g-value of C-L3780 and C-L3787 are $g_{2days} = 1.99 \pm 0.73\%$ and $g_{2days} = -1.56 \pm 2.4\%$ (see Fig. D.8).

In fact, the measurements show optimal performance: all SAR criteria were met, dose recovery ratios were within 10% of unity and prior IR stimulation temperature plateaus were present for all samples tested. Therefore, we used the equivalent doses of the $pIR_{50}IR_{290}$ measurements of the polymineral samples for the final age assessment.

8.5.3. Dose rate and age calculation

Table 8.1 shows a summary of the dose rate measurements, equivalent doses and age estimates of the studied section. We used the measured water content to calculate the total (wet) dose rate. Ages are based on the polymineral samples using the $pIR_{50}IR_{290}$ protocol. The α-efficiency was determined giving values between 0.102 ± 0.013 (C-L3786) and 0.149 ± 0.015 (C-L3784). Ages are all in stratigraphic order, ranging from $28.5 \pm 2.3\ ka$ to $139 \pm 11\ ka$. These ages might be considered as falling in Marine Isotope Stages (MIS) 2, 3, 4 and 6. The ages of samples C-L3778 ($139 \pm 11\ ka$), C-L3780 ($136 \pm 10\ ka$), and C-L3784 ($123 \pm 8\ ka$) highlight a presumably high

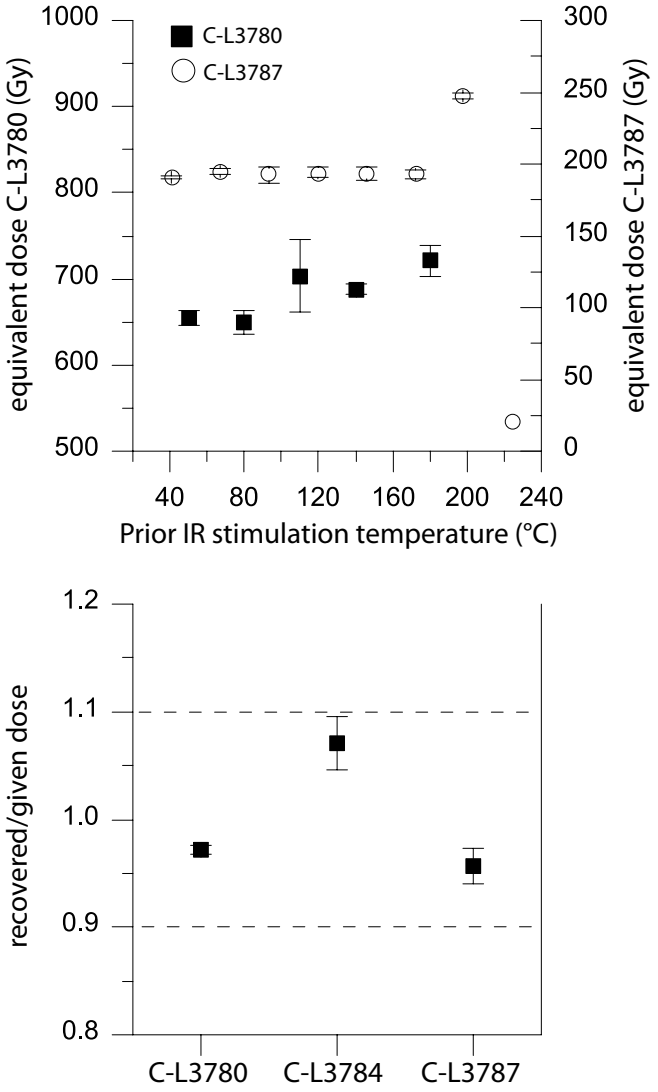

Figure 8.7.: Top shows prior IR stimulation temperature plotted against measured dose. Dose of C-L3787 can be viewed at the right hand axis, while dose of C-L3780 can be viewed at the left hand axis. Standard errors are shown. Bottom shows dose recovery tests of C-L3780, C-L3784 and C-L3787. Recovered to given doses are depicted as mean and standard error of at least three aliquots per sample. Given doses were $194\ Gy$ for C-L3787, $617\ Gy$ for C-L3784 and $645\ Gy$ for C-L3780. Residual doses, after bleaching for 24 h in a solar simulator, were subtracted.

Table 8.1.: Summary of the D_e, dose rate and age data. Water content is the one obtained in the laboratory. For alpha efficiency a 10% error was applied when standard deviation was smaller than 10%, otherwise standard deviation was used. Dose rates were calculated as described in section 8.4.2. Standard errors are indicated. Ages are expressed with a 1-sigma error range.

Sample name	Lab Code	Grain size (μm)	Depth (m)	Water cont. (%)	U (Bq/kg)	Th (Bq/kg)	K (%)	Cosmic DR (Gy/ka)	Alpha efficiency	Total DR (Gy)	No. of aliquots	D_e (Gy) mean	Age (ka)
St 1	C-L3778	4-11	7	14.5 ± 7.3	33.78 ± 1.58	44.44 ± 2.26	1.69 ± 0.03	0.101 ± 0.01	0.134 ± 0.013	3.77 ± 0.2	10	630 ± 32	139 ± 11
St 3	C-L3780	4-11	6	11.8 ± 5.9	34.23 ± 1.62	45.86 ± 2.35	1.83 ± 0.03	0.111 ± 0.01	0.128 ± 0.013	4.07 ± 0.2	13	650 ± 36	136 ± 10
St 7	C-L3784	4-11	4.5	8.6 ± 4.3	33.49 ± 1.6	42.96 ± 2.21	1.76 ± 0.03	0.13 ± 0.01	0.149 ± 0.015	4.06 ± 0.2	13	622 ± 32	123 ± 8
St 9	C-L3786	4-11	6.3	8.0 ± 4.0	30.88 ± 1.63	42.65 ± 2.49	1.48 ± 0.02	0.108 ± 0.01	0.102 ± 0.013	3.71 ± 0.2	10	245 ± 12	59.9 ± 4.0
St 10	C-L3787	4-11	7	10.7 ± 5.4	30.42 ± 1.73	48.07 ± 2.9	1.75 ± 0.02	0.101 ± 0.01	0.108 ± 0.026	3.97 ± 0.2	14	191 ± 10	43.0 ± 3.6
St 11	C-L3788	4-11	5	7.8 ± 3.9	36.06 ± 1.68	45.82 ± 2.34	1.77 ± 0.03	0.123 ± 0.01	0.143 ± 0.03	4.26 ± 0.2	10	149 ± 8	28.5 ± 2.3

accumulation rate in this time range (although the slope position should not be disregarded).

Probability density functions of the ages of over- and underlying samples were combined to assess the ages of paleosol and tephra layers. This results in an age of 127 and 148 ka at a 1σ confidence level for L2SS1 ($116-159$ ka, 2σ); and an age of $118-141$ ka at 1σ ($109-152$ ka, 2σ) for the tephra. Although the samples bracketing the tephra are not in close stratigraphic distance, the difference in age is small. We restrain from this calculation for S1 because of the age differences between samples C-L3784 and C-L3786. Combining the probability density functions for the L1 paleosols gives ages of $41-62$ ka 1σ ($37-66$ ka, 2σ) for L1SS1SSS2 and $27-45$ ka 1σ ($25-49$ ka, 2σ) for L1SS1SSS1.

8.6. Stratigraphical implications

Generally, LPS have been investigated intensively in Southeastern Europe, but only some were OSL-dated in high-resolution (Constantin et al., 2014; Fitzsimmons and Hambach, 2014; Fuchs et al., 2008; Marković et al., 2014; Murray et al., 2014; E. D. Schmidt et al., 2010; Stevens et al., 2011; Zeeden et al., 2016b); mainly data concerning physical/chemical properties have been reported. Marković et al. (2015) give an extensive overview. Most sections are located in the Carpathian Basin and the Lower Danube Basin, in contrast to Stalać being situated south of the common loess distribution, giving it special importance due to its distinct geochemical character (see Chapter 8.2).

The previous investigation at the Stalać section has established a correlative age model (Kostić and Protić, 2000). They correlated the cambisol (S2) to the Riss/Würm interglacial (MIS 5), while three weaker kastanozem-like paleosols above were correlated to the last glacial soil developments (S1, L1SS1SSS2, L1SS1SSS1). However, our investigation demonstrates that such a correlation is challenging and in this case very likely incorrect. Based on the luminescence data (Table 8.1), we show that the two younger kastanozem-like paleosols developed during MIS 3 (C-L3787 and C-L3780) and the oldest kastanozem-like paleosol (S1, see Fig. 8.2) formed during MIS 5, while the cambisol (S2) probably developed during the penultimate interglacial (C-L3778, C-L3784, C-L3786). This fundamentally changes the conclusion from the Kostić and Protić (2000) study. It furthermore reveals that the environmental conditions during the last two interglacials were remarkably different. Adapting the data by Kostić and Protić (2000) with respect to the new age-model suggests stronger weathering during the formation of the S2 paleosol and an upward trend of decreasing precipitation. A trend of gradual aridization was also discussed by Buggle et al. (2013) for the Lower and Middle Danube Basins. They furthermore suggested a westward expansion of the Eurasian Steppe belt since the Early Pleistocene. Moreover, physical similarities in the S1 pedocomplex and the two paleosols L1SS1SSS2 and L1SS1SSS1 indicate relatively similar environmental conditions during their formation, which is in contrast to the sections in the Carpathian Basin (e.g. Antoine et al., 2009; Buggle et al., 2008; Marković et al., 2008, 2015), where the soil development during L1SS1 is clearly weaker. This might indicate a generally different environmental and climatic evolution of the Central Balkan and the Carpathian Basin during the last glacial, also suggested by Obreht et al. (2016).

Geochemical analyses of glass shards found in the L1SS1LLL1 layer indicate the existence of cryptotephra layer (Obreht et al., 2016), which is related to the Campanian Ignimbrite / Y-5 tephra. This tephra is $^{40}Ar/^{39}Ar$ dated to 39.28 ± 0.11 *ka* (De Vivo et al., 2001), which fits well to the age of 43.0 ± 3.6 *ka* (C-L3787) below this loess layer.

Another tephra was dated to $109 - 152$ *ka* ($118 - 141$ *ka*, 1σ) by means of samples C-L3780 and C-L3784. Though samples bracketing the L2 tephra were not closely spaced in the profile, their ages overlap within 1σ errors. Wacha and Frechen (2011) dated a tephra in Croatian loess to 139 ± 9 *ka* (above) and 145 ± 12 *ka* (below), which is consistent with the L2 tephra found at Stalać. Moreover, a tephra in Lake Ohrid with an $^{40}Ar/^{39}Ar$-age of 133.5 ± 2 *ka* (Leicher et al., 2016; Satow et al., 2015) might correlate to this L2 tephra. Unfortunately, the glass shards from this layer were weathered, and consequently this tephra cannot be identified geochemically. However, the consistency between the tephra ages gives further confidence in the pIRIR ages obtained in this study.

Finally, the lowermost sample (C-L3778) places the beginning of the L2 loess accumulation phase at 139 ± 11 *ka*. However, the top of the S2 soil in Eurasian loess is usually placed at ~190 *ka* (e.g. Basarin et al., 2011). This suggests that either this pIRIR age might be underestimated, or that the correlative stratigraphy may need adjustment.

Additionally, we dated a pedogenic horizon (L2SS1) at $11.45 - 11.6$ m within the L2 loess to $126 - 148$ *ka* (1σ, C-L3778 and C-L3780). Also several other Balkan LPS reveal a weakly developed pedogenic layer within the L2 (Marković et al., 2009, 2015), fitting our interpretation of a brief period of soil formation. To our knowledge, this 'embryonic paleosol' has not been dated before. However, the possibility of an age underestimation suggested for sample C-L3778, which is based on regional correlative stratigraphy, might also affect this age estimate. This issue needs to be further studied in the future, e.g. by dating a sample below the S2 soil, or by comparison to independent age control or other proxy data.

8.7. Conclusion

In contrast to earlier views, fine quartz grains with high equivalent dose values are not always the ideal material for OSL dating, as was also shown in this study. The importance of a thorough investigation was demonstrated, underlining the necessity of a preheat plateau test and the usefulness of a plot of the normalized luminescence signal versus preheat temperature. High-dosed quartz with falling preheat plateaus remains unsuitable for OSL dating until the underlying processes that cause these problems are better understood.

A reliable chronology of the Stalać LPS covering the last two glacial cycles was established by dating the polymineral fine-grain fraction. The good behavior of the polymineral samples made them ideal for measurements with the $pIR_{50}IR_{290}$ protocol and support the validity of the obtained ages. The wide time range enhances our understanding on the timing of LPS south of

the typical loess distribution. Moreover, the previous chronology by Kostić and Protić (2000) was corrected by means of the new ages, highlighting the importance of luminescence dating to contribute to chronological questions in LPS. This revealed a quite different paleoenvironmental evolution of the Carpathian Basin and the Central Balkan region during the last interstadial, which shows stronger pedogenesis at Stalać. Finally, the tephra found in L2 was dated to $118 - 142$ ka (1σ), contributing to the establishment of a reliable loess chronology of the penultimate glaciation in Southeastern Europe.

9. Luminescence dating of the Urluia loess-paleosol sequence in the Lower Danube Basin - geochronology and challenges

9.1. Introduction

The importance of luminescence dating in building chronologies for paleoenvironmental reconstructions or archeological investigations has been shown in the previous chapters. Absolute dating is essential for the understanding of the timing of environmental change and the correlation between archives. Also the benefit of applications in geoarcheological context was demonstrated. This chapter presents the geochronology of an archive in the Dobrogea region, thereby extending the research area to the Lower Danube Basin. The Urluia loess-paleosol sequence was investigated by dating 13 luminescence samples with the aim to construct a robust geochronology for the region. The challenges that can occur in such investigations are presented in the following.

9.2. Study site

The Urluia loess-paleosol sequences (44°05.650'N, 27°54.186'E, 125 m a.s.l) is located in the Dobrogea plateau in southeastern Romania, ca. 15 km south of the Danube. The outcrop contains thick packages of loess and several well preserved paleosols. Figure E.1 in the Supplementary Materials shows a photo of the outcrop. The investigated loess-paleosol sequence is 16 m high comprising mainly loess and one paleosol. The loess-paleosol sequence (LPS) overlies Cretaceous-Tertiary limestone, which was uplifted in the early-mid Quaternary (Fitzsimmons and Hambach, 2014; Fitzsimmons et al., 2013; Munteanu et al., 2008). Previous studies at another part in the outcrop presented a luminescence chronology and environmental magnetic analyses (Fitzsimmons and Hambach, 2014). Another study deals with the impact of the Campanian Ignimbrite eruption on human evolution using the CI/Y-5 tephra found at the section (Fitzsimmons et al., 2013). First paleoclimatic and geochronological results of the section under investigation here will be published by Obreht et al. (2017) revealing mild paleoclimatic conditions during middle MIS 3 ($50 - 40$ ka) followed by a trend of general continentalization with drier and colder climatic conditions between 40 and 27 ka likely related to a change in atmospheric circulation patterns. Also early MIS 2 and the LGM indicate dry and cold paleoclimatic conditions, while the onset of deglactiation was probably accompanied by increased humid conditions. Their interpretations are based on a luminescence chronology of the upper 7 m, dating the section from 21.0 ± 1.6 to 54.2 ± 4.1 ka. This geochronological data is also included in the discussion here to present a complete luminescence data set of the ~16 m long

Urluia section.

9.3. Stratigraphy

The upper 1.0 m of the Urluia sequence contains the recent soil, which overlies homogenous yellow-brownish loess ($1.2-3.6$ m). The loess horizon contains some loess dolls from $1.5-2.5$ m and becomes more yellow downprofile ($\sim 2-3$ m). The upper 2.5 m of the profile show signs of bioturbation. Between 3.0 and 3.5 m the loess exhibits grey color that changes abruptly around $3.5-3.7$ m. Here, the loess is getting coarser and darker than above, until ~5.2 m. Between 5.2 and 5.5 m brown loess with humic root channels and some krotovinas is present, followed by an ochre horizon (5.5−5.7 m). Between 5.7 and 8 m a horizon of grey-yellow loess has been deposited that gets a bit redder around 7.4 m. Obreht et al. (2017) point out that at 6.16 m a hardly visible tephra layer is exposed, which is prominently present in the profile investigated by Fitzsimmons and Hambach (2014). At 8 m a sharp border towards grey loess ($8.0-11.2$ m) was observed. Between 11.2 and 12.1 m the deposited loess becomes darker (weakly brown) and overlies a humic horizon ($12.1-12.4$ m). Within the following grey-yellow loess layer ($12.4-15.1$ m) another humic horizon was observed ($13.1-13.2$ m). This is underlain by a chestnut brown Ah horizon showing $2-6$ mm aggregates indicative of rainworm activity. The lowermost 30 cm exhibit calcareous grey loess containing some dark humic brown krotovinas. The occurrence of krotovinas, loess dolls and carbonate is marked in the schematic profile drawing (Figure 9.1).

9.4. Methods

9.4.1. Equivalent dose measurements

Samples for D_e determination were prepared under subdued red illumination in the Cologne Luminescence Lab (CLL). The outer 2 cm were removed when the samples were extracted from the cylinders. The gravimetric water content was determined and the dried samples were treated with 10% hydrochloric acid, 10% hydrogen peroxide and 0.01 N sodium oxalate to remove carbonates, organic matter, and to disperse sediment aggregates. The $4-11$ μm grain size fraction was isolated using Stokes' law and by removing the clay fraction (< 4 μm) via centrifuging.

Continuous wave optically stimulated luminescence measurements (CW-OSL) were carried out on a Risø TL/OSL DA 20 reader. The reader is equipped with a $^{90}Sr/^{90}Y$ β-source, infrared (IR) LEDs emitting at 870 nm (FWHM = 40 nm), and blue LEDs emitting at 470 nm (FWHM = 20 nm). A 410 nm interference filter was used for signal detection of feldspars, a Hoya U-340 filter was used for signal detection of quartz. The $pIR_{50}IR_{290}$ SAR protocol was used (Buylaert et al., 2012; Thiel et al., 2011b). Additionally to the pIRIR signal, also the luminescence signal of the first IR stimulation was extracted from the pIRIR measurements. The signals were integrated using the first 2.4 s of the stimulation curve minus a background derived from the last 25.6 s. Prior IR stimulation temperature tests (cf. Buylaert et al., 2012) were performed on samples C-L3706 and C-L3713. Furthermore, several dose recovery tests (DRTs) with the

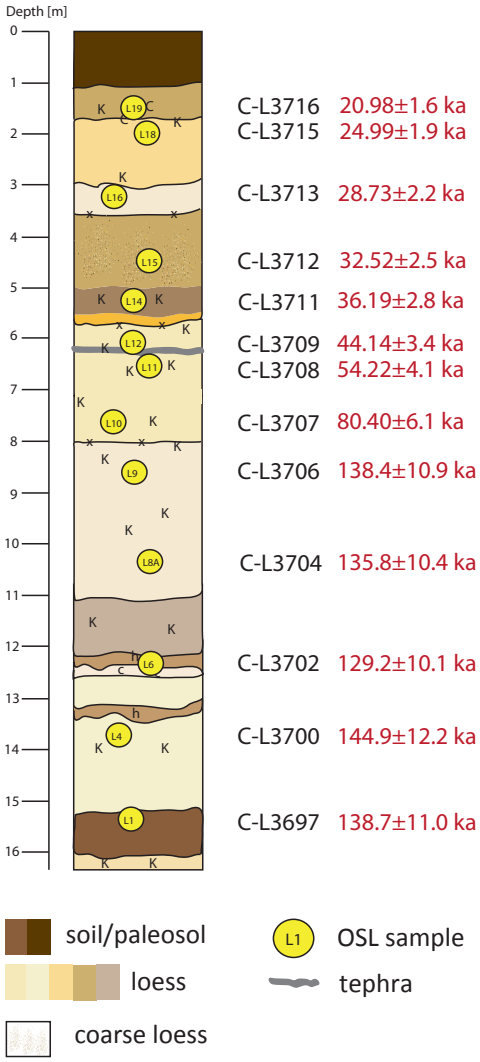

Figure 9.1.: Profile sketch of the Urluia LPS showing different layers of loess, paleosols, humic horizons (h), krotovinas (K), and carbonated horizonts (c). The position of the tephra layer is also indicated. Sharp borders are indicated with 'x'. Note that the upper part shows yellow loess, while the lower part is characterized by more whitish loess.

favourable prior IR stimulation temperature were performed using bleached samples (24 h Hönle Sol2 solar simulator). Moreover, residual doses of polyminerals were assessed after bleaching the aliquots in the same manner. Fading tests were conducted on samples C-L3704 and C-L3711. For these, laboratory beta doses of 602 and 186 Gy were used and the normalized luminescence signals were measured after different storage times between 100 and 800 minutes.

For quartz measurements, the single aliquot regenerative dose (SAR) protocol (cf. Murray and Wintle, 2000, 2003) was applied. Preheat plateau tests (e.g. Murray and Wintle, 2000) were performed on samples C-L3700, C-L3707, C-L3709 and C-L3711. A dose recovery test (Murray and Wintle, 2003) was performed on samples C-L3709. Early background subtraction (Ballarini et al., 2007) was used for all quartz measurements (first 0.48 s of the stimulation minus a background of the following 1.28 s). Finally, mean equivalent doses of polymineral and quartz fractions were determined using the central age model (CAM) and the common age model (COM) (Galbraith et al., 1999).

For data analysis the R 'luminescence' package (Dietze et al., 2013, 2016; Kreutzer et al., 2012b) and Analyst v. 4.31.7 (Duller, 2015a) were used.

9.4.2. Dose rate measurements

Samples for dose rate determination were oven dried at $50°C$ for at least 48 h, homogenized and packed into plastic cylinders for radionuclide measurements. Radionuclide concentrations were measured on a high-purity germanium gamma-ray spectrometer after a resting period of four weeks to compensate for radon emanation during pretreatment. The dose rates and ages were calculated using DRAC, v.1.2 (Durcan et al., 2015). Conversion factors of Liritzis et al. (2013) and an estimated water content of $10 \pm 5\%$ were included. The internal β dose rate contribution of the polymineral samples was calculated by assuming a K content of $12.5 \pm 0.5\%$ (Huntley and Baril, 1997) and a Rb content of 400 ± 100 ppm (Huntley and Hancock, 2001). Attenuation factors of Bell (1980) and Guérin et al. (2012) were used. The cosmic dose rate was calculated following Prescott and Hutton (1994) considering the geographical position, altitude, sample depth and density of the overlying sediments. The α-efficiency of the polyminerals was determined for six aliquots of two samples. Aliquots were thermally annealed ($480°C$) before administering α-doses of up to 200 Gy in a Freiberg Instruments Lexsyg Research device. The laboratory dose of the samples was determined using β-irradiation in a Risø reader (pIRIR protocol). Finally, the a-value was calculated as the ratio of the measured β-dose divided by the given α-dose (cf. Kreutzer et al., 2014). A linear function was used for fitting. A mean a-value was used for all polymineral samples. For quartz samples, an a-value of 0.036 ± 0.003 was assumed (Kreutzer et al., 2012a).

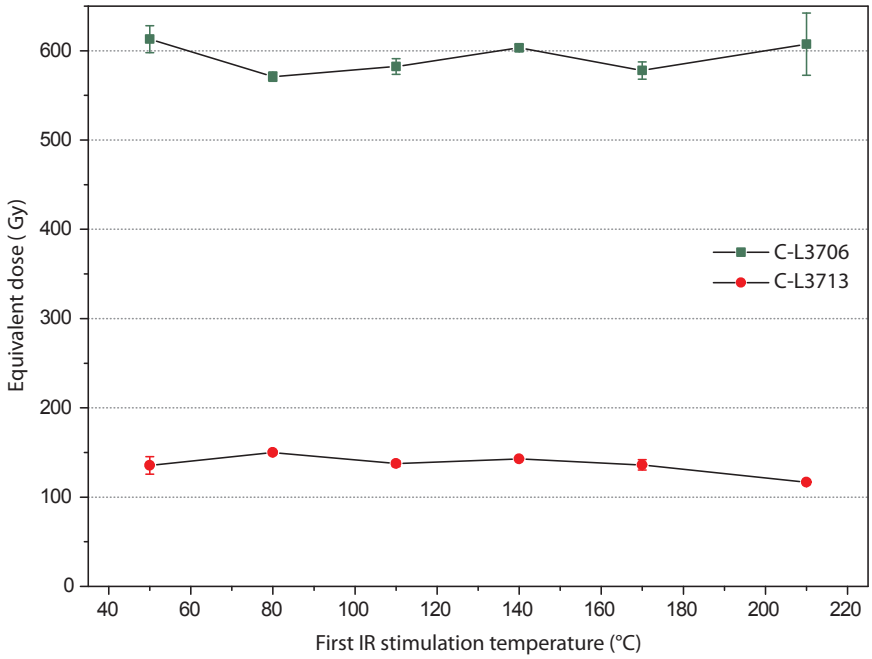

Figure 9.2.: First IR stimulation temperature tests of samples C-L3706 and C-L3713 show plateaus between first IR stimulation temperatures of $50°C$ and $210°C$.

9.5. Geochronology

9.5.1. Polymineral measurements (pIRIR)

The first IR stimulation temperature tests on samples C-L3713 (Obreht et al., 2017) and C-L3706 showed that equivalent doses are independent of the used first IR stimulation temperatures (Figure 9.2). To avoid too stringent measurement procedures, it was decided to do all further measurements with a first IR stimulation temperature of $50°C$. Dose recovery tests were conducted on nearly all samples and showed recovered/given dose ratios within 10% of unity for all samples but C-L3697, which has a ratio of 1.25 ± 0.06 (Table 9.1). Residual doses measured after bleaching for 24 h in a Sönle Sol2 solar simulator are $< 10\ Gy$, i.e. <7% of D_e. Fading measurements (see Supplementary Figure E.2) scatter greatly between aliquots. Mean g_{2days}-values are $-0.9 \pm 0.7\%$ for C-L3711 and $1.2 \pm 1.5\%$ for C-L3704; no fading corrections were undertaken (cf. Buylaert et al., 2012).

Equivalent doses increase with depth in the upper 8 m from $84.3 \pm 4.3\ Gy$ to $625.4 \pm 35.2\ Gy$. In the lower 7 m, D_es do not increase greatly anymore; the highest D_e was measured in sample C-L3700 with $708.9 \pm 45.3\ Gy$. Supplementary Figure E.3 shows examples of shine down and growth curves; abanico plots are depicted in Supplementary Figure E.4, E.5, and E.6. Total dose rates range from $4.02 \pm 0.22\ Gy/ka$ in the uppermost sample to $5.26 \pm 0.29\ Gy/ka$ in sample C-L3711. Looking at the age depth plot in Figure 9.3 one can see that the luminescence ages range from $20.98 \pm 1.6\ ka$ to $144.9 \pm 12.2\ ka$. They appear to increase rather constantly in the upper half, but then much more rapidly between ~7 and 9 m and reach values around $140\ ka$ in the lower five samples.

Table 9.1.: Summary of luminescence data for samples from Urluia (URL1). For sample C-L3711 only the results of aliquots within the preheat plateau (C-L3711$_p$) are depicted for comparison between quartz (Q) and polymineral (PM) fraction. Number of accepted in comparison to measured aliquots (n) and radionuclide concentrations are indicated; as well as the measured (W_m) and used (W_{used}) water contents, total dose rates (D_{total}), dose recovery ratios (DRT ratio), residual doses, values of overdispersion (OD), and luminescence ages.

Sample	Mineral	Depth (m)	n	U (ppm)	Th (ppm)	K (%)	W_m (%)	W_{used} (%)	D_{cosmic} (Gy/ka)	D_{total} (Gy/ka)	DRT ratio	Residual (Gy)	D_e (Gy)	OD (%)	Age (ka)
C-L3716	PM	1.5	10/10	2.4 ± 0.13	8.83 ± 0.54	1.3 ± 0.01	-	10 ± 5	0.18 ± 0.02	4.02 ± 0.22	-	-	84.27 ± 4.29	0.0 ± 0.0	20.98 ± 1.6
C-L3715	PM	2	24/24	2.86 ± 0.14	9.41 ± 0.49	1.45 ± 0.03	14.4	10 ± 5	0.14 ± 0.01	4.48 ± 0.24	0.91 ± 0.01	7.1 ± 0.28	111.93 ± 6.05	9.36 ± 1.55	24.99 ± 1.9
C-L3713	PM	3.3	10/10	3.0 ± 0.14	11.24 ± 0.52	1.54 ± 0.03	11	10 ± 5	0.12 ± 0.01	4.73 ± 0.26	0.99 ± 0.04	6.98 ± 0.1	135.9 ± 7.01	0.59 ± 6	28.73 ± 2.2
C-L3712	PM	4.5	10/10	3.22 ± 0.15	11.35 ± 0.57	1.67 ± 0.03	8.3	10 ± 5	0.12 ± 0.01	5.11 ± 0.28	0.96 ± 0.02	6.36 ± 0.44	166.27 ± 8.72	2.52 ± 2.21	32.52 ± 2.5
C-L3711	PM	5.2	20/20	3.43 ± 0.16	11.75 ± 0.59	1.64 ± 0.03	9	10 ± 5	0.11 ± 0.01	5.26 ± 0.29	1.02 ± 0.00	6.64 ± 0.29	190.25 ± 9.84	4.15 ± 1.32	36.19 ± 2.8
C-L3711$_p$	Q	5.2	13/13	3.43 ± 0.16	11.75 ± 0.59	1.64 ± 0.03	9	10 ± 5	0.11 ± 0.01	3.75 ± 0.14	-	-	156.17 ± 8.63	0.0 ± 0.0	44.01 ± 2.8
C-L3709	PM	6	10/10	3.24 ± 0.15	10.94 ± 0.55	1.62 ± 0.03	9.6	10 ± 5	0.11 ± 0.01	5.01 ± 0.28	1.07 ± 0.02	6.18 ± 0.37	221.01 ± 11.67	3.1 ± 2.07	44.14 ± 3.4
C-L3709	Q	6	9/9	3.24 ± 0.15	10.94 ± 0.55	1.62 ± 0.03	9.6	10 ± 5	0.11 ± 0.01	3.59 ± 0.14	1.01 ± 0.01	-	175.30 ± 9.18	0.0 ± 0.0	48.78 ± 3.2
C-L3708	PM	6.9	11/11	3.0 ± 0.14	10.85 ± 0.54	1.51 ± 0.03	-	10 ± 5	0.1 ± 0.01	4.76 ± 0.26	-	-	258.24 ± 13.3	1.05 ± 3.41	54.22 ± 4.1
C-L3707	PM	7.7	13/13	2.82 ± 0.12	10.15 ± 0.61	1.49 ± 0.02	-	10 ± 5	0.09 ± 0.01	4.53 ± 0.25	-	-	364.58 ± 19.09	3.87 ± 1.6	80.40 ± 6.1
C-L3706	PM	8.65	8/10	2.91 ± 0.14	9.72 ± 0.49	1.5 ± 0.03	6.4	10 ± 5	0.08 ± 0.01	4.52 ± 0.25	0.99 ± 0.01	8.52 ± 0.32	625.41 ± 35.21	0.0 ± 0.0	138.4 ± 10.9
C-L3704	PM	10.43	9/16	3.03 ± 0.14	10.29 ± 0.52	1.55 ± 0.03	9.3	10 ± 5	0.08 ± 0.01	4.7 ± 0.26	1.05 ± 0.02	8.67 ± 0.54	638.43 ± 33.95	0.0 ± 0.0	135.8 ± 10.4
C-L3702	PM	12.56	6/11	3.03 ± 0.14	10.39 ± 0.53	1.57 ± 0.03	8.6	10 ± 5	0.07 ± 0.01	4.73 ± 0.26	1.03 ± 0.0	5.61 ± 0.52	610.76 ± 33.91	3.64 ± 2.7	129.2 ± 10.1
C-L3700	PM	13.7	6/20	3.01 ± 0.15	10.89 ± 0.56	1.69 ± 0.03	9.8	10 ± 5	0.06 ± 0.01	4.89 ± 0.27	1.08 ± 0.01	9.53 ± 0.43	708.9 ± 45.32	8.18 ± 3.35	144.9 ± 12.2
C-L3697	PM	15.33	14/18	3.62 ± 0.17	10.95 ± 0.55	1.51 ± 0.03	14.4	10 ± 5	0.05 ± 0.01	5.01 ± 0.29	1.25 ± 0.06	7.58 ± 0.60	705.04 ± 37.78	0.0 ± 0.0	138.7 ± 11.0

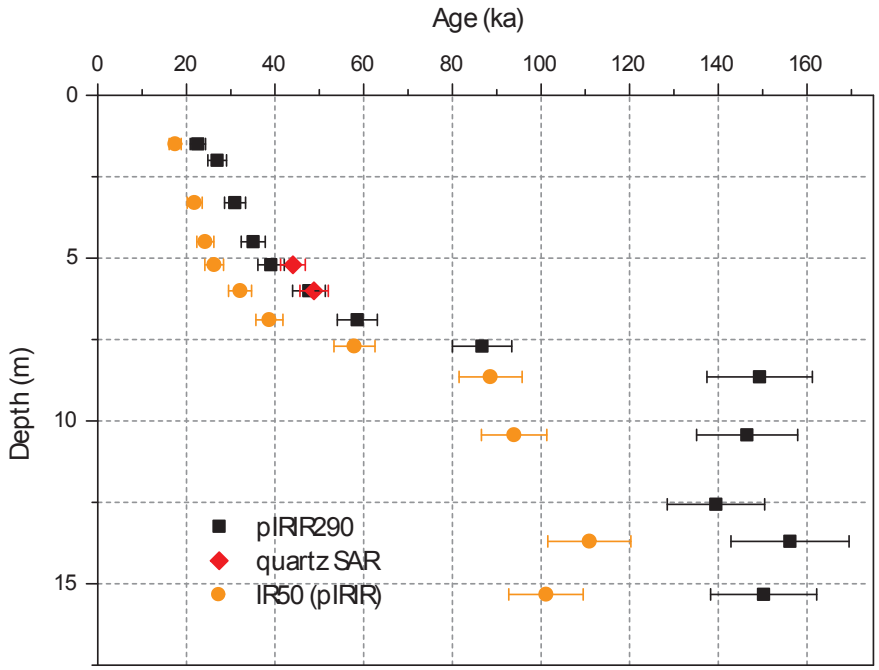

Figure 9.3.: Age-depth plot of the Urluia section showing polymineral $pIRIR_{290}$, quartz OSL and polymineral IR_{50} (from pIRIR measurement) ages and associated uncertainties. No fading corrections were undertaken. It should be noted that IR_{50} aliquots did not pass the dose recovery tests and should therefore be considered with caution.

It is furthermore noteworthy that several aliquots of the lower samples show signs of saturation if the $D_e < 2 * D_0$ criterion (cf. Wintle and Murray, 2006), which is commonly used for quartz, is applied. For sample C-L3706 only one aliquot is in saturation, for sample C-L3704 6/10 aliquots are in saturation; sample C-L3700 has 13/20 aliquots in saturation, and sample C-L3697 has 4/18 aliquots in saturation. For the lowermost sample, even the dose recovery test shows signs of saturation if the quartz criterion is used. This further underlines that the lowermost ages are only minimum ages. All luminescence data are summarized in Table 9.1.

9.5.2. Polymineral IRSL measurements

To further investigate the polymineral measurements, the signals of the first IR stimulation (IR_{50}) were also analyzed. The same signal and background integration intervals were used. All samples but C-L3713 failed the dose recovery test, which indicates that the age results are not reliable and should be considered with caution. Also for the IR_{50} signal fading rates are highly variable, with mean values of $g_{2days} = 2.4 \pm 1.5\%$ for C-L3711 and $g_{2days} = 4.1 \pm 1.1\%$ for C-L3704. Due to the wide spread between samples and the failing DRTs, no fading corrections were undertaken. Table 9.2 shows a summary of the IR_{50} data. For comparison, Figure 9.3 also shows ages resulting from the first IR stimulation, but these are no considered reliable age estimates. Nevertheless, they show the same trends of increasing D_e as the pIRIR data.

Table 9.2.: Summary of luminescence data of the first IR stimulation from the Urluia (URL1) samples. Number of accepted in comparison to measured aliquots (n) and radionuclide concentrations are indicated; as well as the measured (W_m) and used (W_{used}) water contents, total dose rates (D_{total}), dose recovery ratios (DRT ratio), residual doses, values of overdispersion (OD), and luminescence ages. Note that these 'ages' are only for comparison and are not reliable, due to the poor dose recovery ratios. No fading correction was done.

Sample	Mineral	Depth (m)	n	U (ppm)	Th (ppm)	K (%)	W_m (%)	W_{used} (%)	D_{cosmic} (Gy/ka)	D_{total} (Gy/ka)	DRT ratio	Residual (Gy)	D_e (Gy)	OD (%)	Age (ka)
C-L3716	PM	1.50	10/10	2.4±0.13	8.83±0.54	1.3±0.01	-	10±5	0.18±0.02	3.42±0.2	-	-	84.27±3.08	0.0±0.0	17.45±1.3
C-L3715	PM	2.00	4/24												
C-L3713	PM	3.30	10/10	3.0±0.14	11.24±0.52	1.54±0.03	11.00	10±5	0.12±0.01	4.01±0.23	0.71±0.01	4.95±0.22	57.60±74.56	0.15±30.28	21.83±1.7
C-L3712	PM	4.50	10/10	3.22±0.15	11.35±0.57	1.67±0.03	8.30	10±5	0.12±0.01	4.33±0.25	0.76±0.01	4.44±0.08	105.08±5.74	5.11±2.11	24.26±1.9
C-L3711	PM	5.20	12/20	3.43±0.16	11.75±0.59	1.64±0.03	9.00	10±5	0.11±0.01	4.43±0.26	0.97	4.71±0.43	116.35±6.3	5.23±2.01	26.24±2.1
C-L3709	PM	6.00	10/10	3.24±0.15	10.94±0.55	1.62±0.03	9.60	10±5	0.11±0.01	4.24±0.25	0.83±0.04	4.39±0.45	135.01±7.48	5.83±2.0	32.12±2.6
C-L3708	PM	6.90	10/11	3.0±0.14	10.85±0.54	1.51±0.03	-	10±5	0.1±0.01	4.02±0.24	-	-	155.82±8.17	2.22±2.51	38.72±3.1
C-L3707	PM	7.70	13/13	2.82±0.12	10.15±0.61	1.49±0.02	-	10±5	0.09±0.01	3.84±0.22	-	-	222.47±12.1	6.38±1.84	57.91±4.6
C-L3706	PM	8.65	10/10	2.91±0.14	9.72±0.49	1.5±0.03	6.40	10±5	0.08±0.01	3.83±0.22	0.76±0.04	5.48±0.25	339.23±18.66	5.28±2.23	88.61±7.1
C-L3704	PM	10.43	16/16	3.03±0.14	10.29±0.52	1.55±0.03	9.30	10±5	0.08±0.01	3.98±0.23	0.79±0.04	5.1±0.19	373.85±19.41	2.97±1.84	93.95±7.4
C-L3702	PM	12.56	2/11												
C-L3700	PM	13.70	10/16	3.01±0.15	10.89±0.56	1.69±0.03	9.80	10±5	0.06±0.01	4.15±0.24	0.8±0.02	5.96±0.31	460.40±28.35	8.5±3.35	110.9±9.4
C-L3697	PM	15.33	17/18	3.62±0.17	10.95±0.55	1.51±0.03	14.40	10±5	0.05±0.01	4.23±0.26	0.89±0.05	-	427.56±23.82	8.59±2.04	101.1±8.4

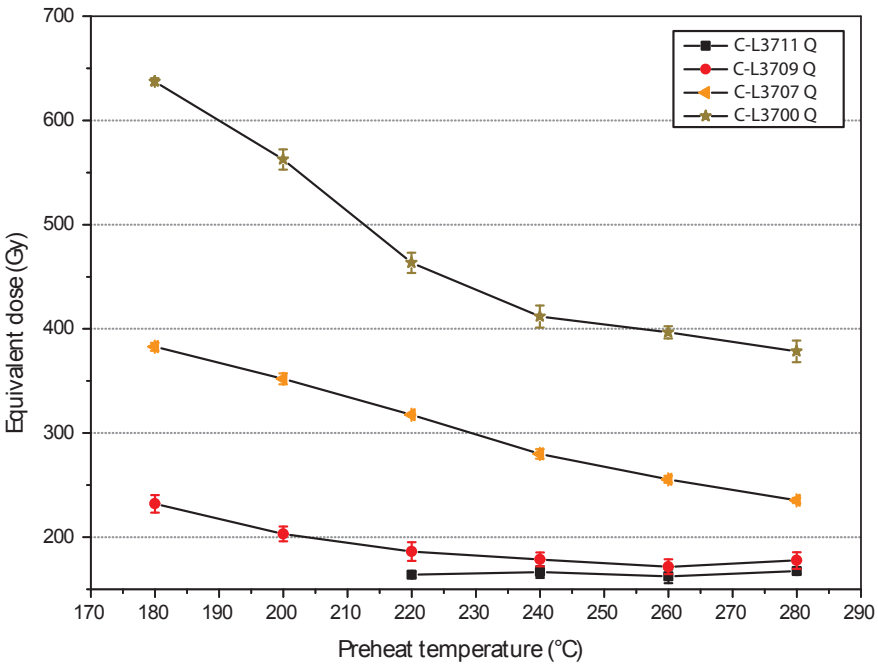

Figure 9.4.: Preheat plateau test of four quartz samples. While the equivalent doses of C-L3700 and C-L3707 are dependent on preheat temperature, a preheat plateau is present between $220°C$ and $280°C$ for samples C-L3709 and C-L3711.

9.5.3. Quartz SAR measurements

The quartz fraction of four samples was investigated to validate the pIRIR ages. Therefore, firstly preheat plateau tests were conducted. Figure 9.4 demonstrates that preheat plateaus ($220 - 280°C$) were only found for the two younger samples (C-L3709 and C-L3711), while the two older ones (C-L3700 and C-L3707) exhibit a strong dependency of preheat temperature on equivalent dose. Since these samples contain very high $D_e s$ for quartz, this is not very surprising (Bösken et al., 2017a; Chapot et al., 2012; Timar-Gabor et al., 2015a) and makes these samples unsuitable for dating. A dose recovery test on sample C-L3709 gave a recovered/given dose ratio of 1.01 ± 0.01. Unfortunately, there was not enough sample material left to conduct dose recovery tests and D_e measurements on sample C-L3700. Table 9.1 shows the results of C-L3707 with a D_e of 175.30 ± 9.18 Gy and an age of 48.78 ± 3.2 ka. The table also shows the results of the PHT for sample C-L3711, but this serves only for comparison and should be considered with caution. Nevertheless, both ages agree well with the pIRIR ages, supporting the pIRIR geochronology at least in the upper 6 m of the profile. Supplementary Figure E.6 depicts the two abanico plots of the quartz samples. Supplementary Figure E.7 shows examples of shine down and growth curves.

9.6. Discussion

9.6.1. Luminescence characteristics

The luminescence samples were investigated thoroughly. First IR and dose recovery tests define the measurement settings of the pIRIR protocol and show that results are reproducible. In

addition, the residual signals are low and cannot affect the ages greatly. The pIRIR protocol is not supposed to be prone to fading (e.g. Buylaert et al., 2012; Thiel et al., 2011b), which was also shown here with very scattered g-values. Scattered g-values are also observed for other sections (Bösken et al., 2017a,b, see Chapters 5 and 8; Murray et al., 2014; Thiel et al., 2011a).

The age obtained on the quartz sample (C-L3709) agrees well with the pIRIR ages and supports their chronology at least in the upper 6 m of the profile. Other tested quartz samples with higher doses show a dependency of preheat temperature on D_e, which indicates that they cannot be dated reliably. Similar problematic behavior was also found at Stalać (Chapter 8), where the importance of a preheat plateau test in detecting this behavior was demonstrated. The unreliability of these quartz samples is not very surprising considering their doses. Other studies demonstrated that the shapes of natural and laboratory growth curves of quartz deviate starting around $100 - 150\ Gy$, giving a further indicator that quartz above this dose range should not be dated (Chapot et al., 2012; Timar-Gabor et al., 2015a).

Interestingly, the lowermost polymineral samples show signs of saturation in the pIRIR measurements. Although the $D_e < 2 * D_0$ criterion is usually applied to quartz measurements, we used it here to have a critical look at the pIRIR ages. Four samples show aliquots in saturation; for the lowermost sample some aliquots are even within the dose recovery test in saturation. This is very surprising, considering that the pIRIR protocol should be able to date feldspars up to very high doses. Murray et al. (2014) dated a Serbian loess-paleosol sequence and determined an upper datable limit for a D_e of ~1000 Gy, which is not reached in the Urluia samples. Nevertheless, they found 8 samples in laboratory and field saturation, i.e. ages did not increase anymore with depth. The highest dose they obtained without encountering saturation problems was $519 \pm 21\ Gy$, which is in the same range as the sudden D_e increase at Urluia. This suggests that also here field saturation is reached, although only some of the aliquots show laboratory saturation.

9.6.2. Geochronological and stratigraphical implications

The pIRIR geochronology of the upper ca. 7 m of the Urluia section is supported by the age of the quartz sample. In addition, the age of sample C-L3709 ($44.14 \pm 3.4\ ka$) at a depth of 6 m is in accordance with the age of the Campanian Ignimbrite / Y-5 tephra ($39.28 \pm 0.11\ ka$, De Vivo et al., 2001) when a 2σ-error is considered. The samples of the upper ca. 7 m were also compared in Obreht et al. (2017) with a correlative age model based on correlation of frequency dependent magnetic susceptibility and grain size variation patterns to the Greenland $\delta^{18}O$ record (Andersen et al., 2004). Although some luminescence samples show slightly older ages of $2 - 3\ ka$, luminescence ages and correlative age model overlap within 2σ for all samples. The good agreement between the age models further supports the luminescence chronology of the upper part of the Urluia section.

The luminescence data in the lower part of the profile is rather unexpected. It shows a rapid increase in ages between ca. $7 - 9$ m, followed by similar ages in the lower ca. 7 m of the section.

There are several hypotheses (or a combination of those) that might explain this behavior:

1. High loess accumulation around $130 - 140$ ka, followed by an erosional event that erased around 60 ka of loess accumulation and paleosol formation.

2. Field saturation is reached for doses > 600 Gy and ages in the lower 7 m comprise minimum ages.

3. The sediments were insufficiently bleached prior to deposition, thereby inheriting a dose. The paleodose cannot be determined satisfactorily.

4. Between ~130 and 80 ka no loess accumulated or no loessification took place.

The first possibility would suggest a major erosional event, such as a landslide, that was powerful enough to erode the MIS 5 paleosol complex. This seems rather unlikely as no erosional discrepancy was observed in the field. Nevertheless, Fitzsimmons et al. (2013) described a paleotopographic depression approximately 20 m to the northwest of the section and the Campanian Ignimbrite / Y5 tephra layer is inclining along the outcrop from northwest to southeast. This suggests that the surface was inclined in the past, which might be related to valley incision or might be an indicator for a possible event of erosion. Topographic maps show indications of (ephemeral/paleo) stream incision, supporting this possibility. Also Lauer et al. (2017) report several chronological hiati in the Agh Band loess-paleosol sequence (northern Iran) that were not detected during fieldwork. They interpret these events as phases of minor loess sedimentation and/or erosion. A major hiatus in the sediments between 170 ka and 100 ka is explained by an intensive period of erosion. Interestingly, the two samples above and below the hiatus are only 130 cm apart and samples above the hiatus show $D_es < 380$ Gy and samples below the hiatus have $D_es > 600$ Gy, which is in the same range as the samples at Urluia. Nevertheless, at Agh Band D_es below the hiatus increase slightly up to ~800 Gy, although most of them overlap within error and several age inversions are present.

The second possibility was already suggested in the previous section. Although this proposes that saturation is reached with lower doses than e.g. at Stari Slankamen (Murray et al., 2014), it can be expected that different sediments have differing luminescence behavior and the beginning saturation within the Urluia samples is obvious. On the other hand, this would imply minimum ages for these samples, which would consequently infer an even greater hiatus.

The third possibility suggests that the samples of the lower half of the section have not been completely bleached prior to deposition. Although theoretically possible, this is rather unlikely, since the section is composed of eolian deposits. Eolian transport is widely accepted to bleach even signals that are more difficult to bleach, such as the pIRIR signals. Additionally, this would imply extremely big residual doses, which is even more unlikely.

The last possibility – no loess accumulation between 130 and 80 ka – is extremely unlikely. Numerous loess-paleosol sequences within this time-frame indicate that loess deposition took place rather constantly in the Dobrogea. Additionally, this hypothesis cannot explain why no

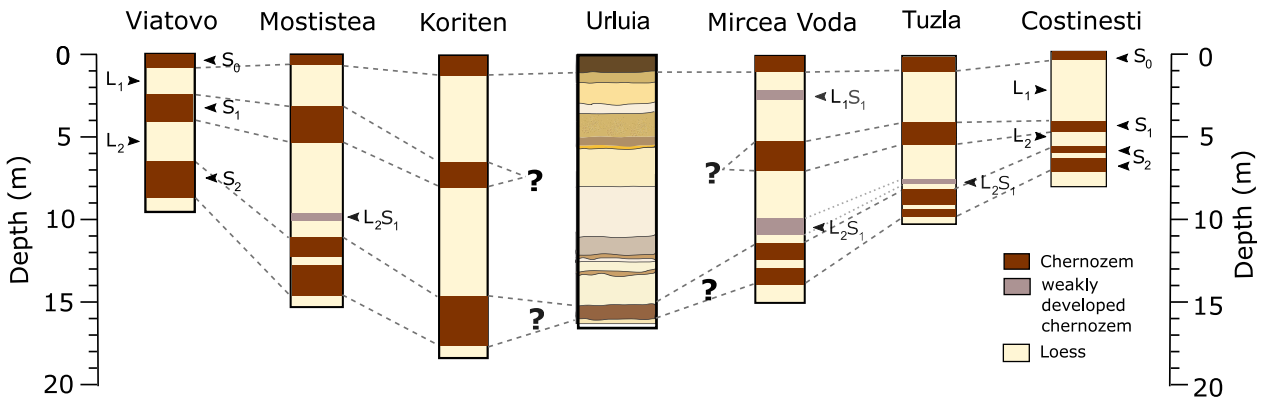

Figure 9.5.: Stratigraphies of various loess-paleosol sequences in the Lower Danube Basin including Viatovo (Jordanova et al., 2007a), Mostistea (e.g. Balescu et al., 2010; Vasiliniuc et al., 2012), Koriten (Jordanova and Petersen, 1999), Urluia (this study), Mircea Voda (Balescu et al., 2010; Buggle et al., 2009), Tuzla (Balescu et al., 2003), and Costineşti (e.g. Constantin et al., 2014; Tugulan et al., 2016). For Urluia, the color scheme of Figure 9.1 was used, while the other profiles show a simplified stratigraphy according to units of loess, chernozem and weakly developed chernozems. The location of the profiles is depicted in Figure 9.6.

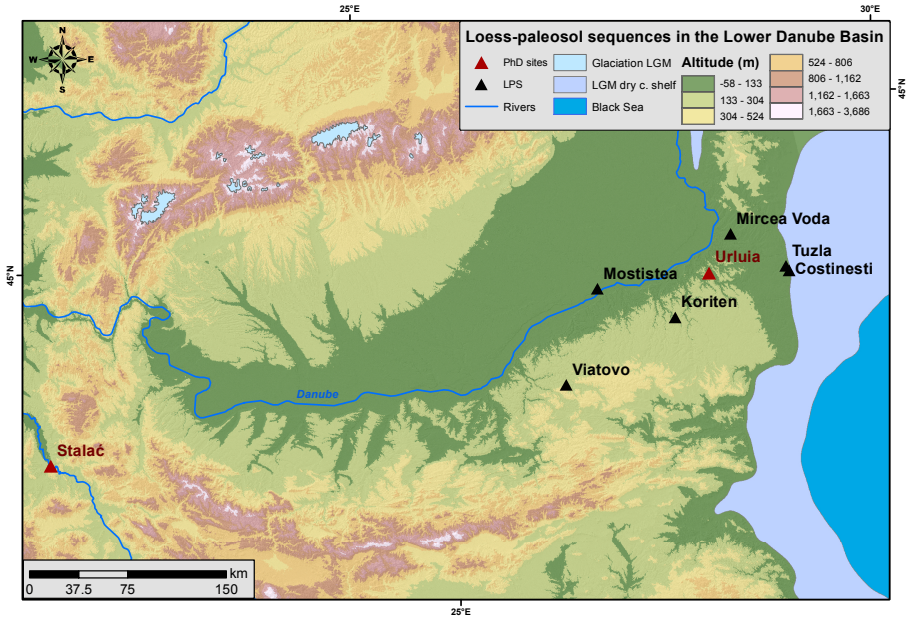

Figure 9.6.: Location of the loess-paleosol sequences presented in Figure 9.5. Digital elevation model based on SRTM data available from U.S. Geological Survey (Farr et al., 2007).

MIS 5 paleosol was found at the section. Moreover, the age of the lowermost sample in the paleosol (138.7 ± 11 *ka*) does not fit any interglacial age expectations. However, one should keep in mind that this age is not considered reliable due to the failed dose-recovery test and might underestimate the true age.

Figure 9.5 shows the stratigraphies of six sequences in ca. 100 km proximity to the Urluia section. All profiles show chernozem-type soils for the S_1 and S_2 pedocomplexes, which are usually related to MIS 5 and MIS 7. Some profiles exhibit several S_2 paleosols, while others also show weakly developed paleosols within L_1 and L_2. Generally, the Urluia profile fits rather well to the stratigraphy of the other sections (except for the fact that no S_1 paleosol is present). Although stratigraphic depth and the thickness of loess deposits are dependent on the geomorphological position, the distance to the source area, and prevailing wind strength and directionality, one might assume the assignment of the lower paleosol to S_2 (MIS 7), which is also suggested by the $pIR_{50}IR_{290}$ ages. Moreover, the ages of samples C-L3697 - C-L3706 compare well to other luminescence samples dated in L_2 loess in the Lower Danube Basin (e.g. Balescu et al., 2003, 2010; Constantin et al., 2014; Timar-Gabor and Wintle, 2013; Vasiliniuc et al., 2012).

At this point, the stratigraphical challenges cannot be solved. The most likely scenarios involve erosion of the MIS 5 paleosol (hypothesis 1) or more fundamental challenges related to the saturation characteristics within polymineral samples using pIRIR protocols (hypothesis 2). To investigate this issue further, it is necessary to compare the age model to independent age control or extend the correlative age model. Moreover, the possibility of a true hiatus within other proxy data needs to be explored. Furthermore it would be interesting to investigate the saturation characteristics of luminescence samples below the paleosol in the current profile. It might be also possible to explore other luminescence signals, but also here comparison to independent age control is indispensable.

9.7. Conclusion

The investigations at the Urluia loess-paleosol sequence demonstrates the challenges in dating samples with high equivalent doses. The section was dated from 20.98 ± 1.6 *ka* to 144.9 ± 12.2 *ka*. While the upper 7 m of the section yielded a reliable chronology, which was shown by independent age control in form a the Campanian Ignimbrite / Y-5 tephra and a comparison to a correlative age model (in Obreht et al., 2017), the lower part of the sequence remains less well constrained. A rapid increase in ages between ~7 and 9 m is followed by rather constant ages > 130 *ka* in the lower 7 m of the profile. These ages are in contrast with the expectation of a well developed MIS 5 paleosol in the lowermost part of the section. Several hypothesis trying to explain these findings were explored, but could not be solved satisfactorily. Nevertheless, the geochronology fits well to other sections in the Lower Danube Basin, although the hiatus cannot be explained. The most likely scenario comprises massive erosion including the MIS 5 paleosol, which is also supported by topographical depressions and stream incisions found at the outcrop. Nevertheless, the saturation characteristics of polymineral samples using the $pIRIR_{290}$ need further study to

validate the geochronology found at Urluia.

10. Synthesis

In this doctoral dissertation four loess-paleosol sequences and one fluvial section in the Middle and Lower Danube catchments were investigated. They cover various time frames from the penultimate interglacial (MIS 7) to the Holocene. The loess sediments at Ságvár were deposited during the last glacial maximum (LGM), the sediments of the Bodrogkeresztúr section cover the MIS 3/2 transition, and the material of the Crvenka-At section accumulated during MIS 3. The sediments at the two longer sections Stalać and Urluia date back to ~150 *ka* (MIS 6), but luminescence data implies a hiatus within the Urluia section. The overall research goal of the presented doctorate dissertation was to increase ones understanding of the environmental conditions in the Middle and Lower Danube catchments during the last 150 *ka*. The methodological approach focused on optically stimulated luminescence dating, but for some of the sections the geochronological methods were combined with physical, biological, and geochemical proxy data to reconstruct the paleoenvironmental conditions. For other sections these paleoenvironmental aspects were published separately (Obreht et al., 2016; Obreht et al., 2017). Those results are taken into account here as well in order to create a more complete picture of the paleoenvironment. In the following sections, the research questions presented in Chapter 1.3 are addressed.

How can luminescence dating techniques aid reconstructions of the paleoenvironment? Where are its limitations and challenges?

Luminescence dating is a frequently used tool used in studies of paleoenvironmental conditions and (geo)archeology. Geochronologies are essential to understand the paleoenvironmental changes over time, or to date archeological artifact and occupation layers. For instance, the investigations at the Stalać section demonstrated how a previous study (Kostić and Protić, 2000), which was based solely on a correlative stratigraphy, misinterpreted the paleoenvironmental information. By means of the new geochronology, the paleoenvironmental data was interpreted within the proper chronological context. At the Crvenka-At site, the dating of sand layers was used to pinpoint Aurignacian presence in the Banat region. Additionally, luminescence dating can also be used to correlate archives of paleoclimate and/or archeological occupation between different profiles, as demonstrated for the Bodrogkeresztúr section.

In order to build robust age models, a detailed investigation of the conducted samples is needed. It was shown that the characteristics of the luminescence signal need to be examined thoroughly. For quartz samples, this comprises preheat plateau and dose recovery tests. Furthermore, one needs to be aware of sensitivity changes, saturation characteristics, and the possibility of thermal transfer. The investigations at Stalać (Chapter 8) demonstrated the importance of a preheat plateau test to reveal unsuitable signal behavior. Component fitting of the

luminescence signals revealed an inconsistent contribution of the signal components throughout the SAR cycle. The largest differences were found between natural and regenerated signals. These findings might be related to thermal transfer and demonstrate that high-dosed quartz should not be dated without thorough investigation. Also at Urluia (Chapter 9), the importance of a preheat plateau test was pointed out. While two quartz samples with lower doses could be dated reliably, two samples with higher doses showed falling D_e plateaus indicating their unsuitability for this dating approach. But not only high-dosed quartz can be problematic, as was demonstrated for the At samples (Chapter 7). Here, small aliquots of coarse quartz grains exhibited tremendous scatter within the D_e distribution and numerous aliquots reached saturation already at 40 Gy. Finally, the quartz fraction of these samples could not be dated. Other problems regarding quartz that have been under investigation recently are the varying dose response curve shapes and saturation characteristics for different grain sizes that led to age discrepancies (Timar-Gabor et al., 2012, 2015b, 2017), and the disagreement between natural and laboratory-induced dose response curves (e.g. Chapot et al., 2012; Timar-Gabor et al., 2015a). These issues highlight the necessity for careful examination of the quartz luminescence characteristics.

Similarly, polymineral and kalifeldspar samples need to be investigated in detail. In this dissertation, first IR stimulation temperature tests, dose recovery tests, fading experiments, and residual dose measurements were undertaken. While none of the samples exhibited noteworthy residual doses, fading rates were highly variable between the aliquots. This might indicate that either fading rates are too small to be detected properly during the fading experiments or that the fading measurements are not appropriate to detect fading using pIRIR protocols. It is likely that the fading rates are too low to be detected satisfactorily within the usually applied 2-day measurements, thus it might be useful to conduct longer measurements in future research. Another important test determines the appropriate first IR stimulation temperature. It comprises a useful tool to decide on the most suitable measurement protocol. For most samples investigated in this dissertation, the $pIRIR_{290}$ protocol was applied, but e.g. in case of the At samples (Chapter 7) the $pIRIR_{225}$ protocol was more appropriate. Moreover, it is crucial to conduct dose recovery tests since they ensure that laboratory measurement results are reproducible.

The investigations at Urluia and Stalać demonstrated that while it is possible to date polymineral (and kalifeldspar) samples with higher doses than quartz samples, it remains unclear up to which dose range age estimates are reliable. The age estimate of the lower two samples at Stalać underestimate the accepted correlative stratigraphy, although the luminescence signals have not reached saturation. At Urluia, the lowermost samples begin to approach saturation, which would indicate an increasing age underestimation downprofile. Nevertheless, resulting ages do not increase anymore with depth and overestimate the known pedostratigraphy. The geochronology indicates a hiatus within the profile, which has not been detected by other proxy data. This demonstrates that further research is needed to ensure the reliability of pIRIR protocols for doses > 600 Gy.

Another important aspect that has been pointed out in the doctoral dissertation is the discrepancy between measured values of α-efficiency (a-value) and the often applied literature value (which has been determined for the $IRSL_{50}$ protocol). E.g. at Ságvár ages decreased by ~15% when the measured values were used. This indicates that the a-value should be determined for each sample or set of samples, and one should refrain from using a-values that have been determined with another measurement protocol. Future research should test the possibility of a common a-value for the different pIRIR protocols (cf. Kreutzer et al., 2014).

General age uncertainties in luminescence dating are related to the estimation of the water content and the usage of mean dose rates. To cover possible fluctuations in the water content since time of deposition, water contents with wide error bars were used for the calculation in this doctoral dissertation. For the At section (Chapter 7), the saturation water content was also determined to further improve the estimation. It might be useful to determine the saturation water content routinely in future research, but studies on paleohydrological changes within different sediment archives are also needed. Finally, future research in the field of luminescence dating should focus on increasing the accuracy of the age estimate by improving the precision of dose rate determination, possibly even towards a single grain level.

Which local paleoenvironmental and paleoclimatological conclusions can be drawn from the studied sections?

At **Ságvár** in the central part of the Middle Danube Basin two short loess-paleosol sequences were investigated. The sections were divided into paleoenvironmental zones. The first zone indicates climatic fluctuations between short cold and warm, but dry climatic phases, followed by more temperate mild and dry conditions in zone 2. This zone ($26-24\ ^{14}C\ ka\ cal\ BP$) is likely associated with short continental-type dry grassland vegetation. The third zone (~beginning of the local LGM, ca. $24\ ^{14}C\ ka\ cal\ BP$) is characterized by an unique open parkland studded sporadically by trees and/or shrubs. The fourth zone (ca. $23-20\ ^{14}C\ ka\ cal\ BP$) indicates alternating cold/cool and wet conditions as well as boreal forst/forest steppe vegetation. This is followed by drier and colder climatic conditions after ca. $20\ ^{14}C\ ka\ cal\ BP$. The last phase suggests milder and more humid conditions during the formation of continental grassland with tall herbs. The multidisciplinary study shows that environmental conditions in the Middle Danube Basin were not uniform during MIS 2 and that paleoenvironmental changes can be observed even on short (millennial) time scales within rather 'pure' loess formation.

The **Bodrogkeresztúr** section in the northern Middle Danube Basin is characterized by a well-developed MIS 3 paleosol indicating humid paleoclimatic conditions. Also during loess deposition, relatively mild paleoclimatic conditions prevailed. Sediment accumulation rates were very high, in particular between 33.5 ± 2.5 and $28.0 \pm 2.1\ ka$. The loess likely originated from the Tisza floodplain and was transported to the section from a northeastern wind direction. Although milder condition at the Bodrogkeresztúr section are recorded during MIS 2, two layers indicate phases with high wind intensities. One of the layers is also characterized by weak pedogenesis indicating that the general soil humidity was still relatively high, while the eolian

dynamics were more intensive or the source area was characterized by coarser particles. The sediments of late MIS 2 were not preserved at the section.

The **Stalać** loess-paleosol sequence is located in the Central Balkan region, south of the typical loess distribution. It contains four paleosols and two tephra layers and dates back to MIS 7. With the new geochronology, it was shown that the lowermost paleosol (MIS 7) was characterized by stronger weathering indicating more humid and warmer paleoenvironmental conditions. The paleoclimate changed from a Mediterranean influence to more continental conditions with a trend of decreasing precipitation. During MIS 5 and MIS 3 similar climatic conditions prevailed, which is shown by the formation of three kastanozems. Also Obreht et al. (2016) point out that the climatic conditions during the last glacial were unexpectedly warm and humid in comparison with those of previous glaciations. This might be related to a decreasing extent of glaciers in the Dinarides. During previous glaciations incoming relatively warm and moist air masses from the south and southwest were probably blocked. This barrier ceased during the last glacial leading to increased humidity in the Central Balkan region.

The **Urluia** loess-paleosol sequence in the Lower Danube Basin delivered a robust geochronology for the last ~50 ka, but the establishment of a reliable chronology in the lower half of the 16 m long sequence was challenging. A rapid increase in ages between ~7 and 9 m is followed by rather constant ages in the lower 7 m of the profile. Several hypothesis trying to explain these findings were explored, but could not be solved satisfactorily. A possible explanation comprises massive erosion (including the MIS 5 paleosol), which is also supported by topographical depressions and stream incisions found at the outcrop. Nevertheless, this needs further study before the paleoclimatic conditions can be determined in this part of the section. The upper part was investigated by Obreht et al. (2017) indicating enhanced moisture conditions with moderate wind dynamics between $50-40$ ka, followed by stronger wind intensities with dryer and colder climatic conditions during late MIS 3 ($40-27$ ka). MIS 2 was characterized by pronounced arid and cold climate, and a sudden increase in humidity at the offset of the deglaciation (Obreht et al., 2017).

What are the overall environmental and climatological implications for the Middle and Lower Danube Basins and how do these relate to anatomically modern human occupation?

In the Central Balkan region, at the southern part of the Middle Danube catchment, paleoclimatic conditions changed from a Mediterranean influence to continental climatic conditions from the penultimate interglacial (MIS 7) to the last interglacial (MIS 5). A continentalization with a trend of decreasing precipitation persisted during the last glacial cycle. During MIS 5 and MIS 3 similar climatic conditions prevailed. A trend of gradual aridization was also suggested for the Middle and Lower Danube Basins (Buggle et al., 2013), accompanied by a westward expansian of the European steppe belt since the Early Pleistocene. However, paleosols in the central part of the Middle and Lower Danube Basins indicate continental climatic conditions also during the penultimate interglacial (Marković et al., 2015), in contrast to the findings at

Stalać. Moreover, the MIS 3 paleosols in the central part of the Middle and Lower Danube Basins are usually less developed than the MIS 5 paleosol formation, which suggests a generally different environmental and climatic evolution of the Central Balkans and the central parts of the Middle and Lower Danube Basins. Obreht et al. (2016) relate this to the existence of a climatic boundary between those regions. They also showed that the Mediterranean climate influence weakened progressively in southeastern Europe as a whole.

The Lower Danube Basin was characterized by stronger wind intensities with dryer and colder climatic conditions during late MIS 3 ($40 - 27$ ka), in contrast to the Middle Danube Basin, where conditions were warmer and more humid during this period. Obreht et al. (2017) proposed an increased influence of the Eurasian high-pressure system (Siberian High) to be responsible for a shift of the Westerlies southward, which in turn induced warmer and moister air to the Middle Danube Basin in late MIS 3. The humid conditions did not reach the Lower Danube Basin because it was (and still is) located in the rain shadow of the Carpathian Mountains. Nevertheless, both regions were not as humid as the Central Balkans, as suggested above.

In the Middle Danube Basin three sites were investigated. The Crvenka-At site is the only research site that contains fluvial sediments. At the Crvenka-At site Aurignacian artifacts were found in sand layers that deposited between 33.9 ± 2.9 ka and 41.3 ± 3.6 ka, and between 36.8 ± 3.1 ka and 41.3 ± 3.4 ka. This age range fits well with other Aurignacian sites in the Banat region, such as the Peştera cu Oase ($37 - 42$ ka cal BP, Trinkaus et al., 2003) and Romaneşti-Drumbrăviţa (40.6 ± 1.5 ka, C. Schmidt et al., 2013; cf. Kels et al., 2014). The human mandible found at Peştera cu Oase is the oldest directly dated anatomically modern human fossil in Europe, highlighting the importance of other Aurignacian findings within this time frame. The new geochronology of the Crvenka-At site points to a more widespread occurrence of anatomically modern humans in the Banat region than previously thought. Moreover, it demonstrates that not only the upland regions, but also lowland areas were attractive for Early Modern Humans. Finally, it highlights the need for further exploration in the lowlands of the Banat region.

Paleoenvironmental investigations in the Middle Danube Basin revealed that the foothill region in the northern part of the basin was more humid during late MIS 3 and early MIS 2 than the areas in the central parts of the basin. However, the southern parts of the basin were most likely characterized by warmer climate suggesting steppic environmental conditions (Marković et al., 2007, 2015). Although conditions during early MIS 2 were relatively mild, two phases of colder and dryer climate with increased eolian dynamics were also discovered. The investigation at the Bodrogkeresztúr and adjacent sections generally highlight favorable climatic conditions in the foothill region with higher biomass production between $\sim 30 - 50$ ka, which might be the reason for the occurrence of Upper Paleolithic findings in these areas. Sümegi et al. (2016) point out that the local environment of the oldest Gravettian sites were rather similar and occur along creek valleys and mixed taiga woodlands and loess-covered hills of spruce

and steppe forests. The occurrence of sites repeatedly within spruce forests within this period (Sümegi et al., 2016), may be interpreted as highlighting a selective preference of the Gravettian population for these environments. Contrarily, later Gravettian occupation at Ságvár in the central parts of the Middle Danube Basin took place during a 'typical' cold LGM phase. The occupation occurred during two phases characterized by dry climate. A consistent trend towards colder conditions before the occurrence of the archeological layers was observed in multiple proxy data. The older Gravettian layer was likely formed at the beginning of the local LGM ($\sim 23-24$ *ka*) in a unique open parkland studded sporadically by trees and/or shrubs with alternating mosaics of cold, wet tundra-like, and cold steppe microhabitats. The younger Gravettian layer occurred between 20.6 ± 1.4 *ka* and 18.7 ± 1.3 *ka* within rather 'pure' loess, with no indication of pedogenesis. Malacological data suggests a transition of a phase of open landscape and dry and cold climate towards even drier and colder conditions. This implies that Upper Paleolithic human presence in the Middle Danube Basin was not limited to warm or mild phases.

Overall, this doctoral dissertation highlights the importance of luminescence dating in paleoenvironmental and geoarcheological studies. It was demonstrated how the combination and integration of multiple proxy data enhances the paleoenvironmental interpretations, and identifies remaining challenges. The paleoclimatic dynamics in the Middle and Lower Danube catchments were discussed, highlighting the complexity of southeastern European climate at the junction of Atlantic, Mediterranean and continental climatic regimes. Finally, paleoenvironmental conditions during phases of Upper Paleolithic occupation were equally diverse demonstrating anatomically modern humans' ability to adapt to changing paleoenvironments.

Acknowledgments with regard to the content of the published articles

All investigations were carried out in the context of the CRC 806 "Our way to Europe", subproject B1 "The Eastern Trajectory: Last Glacial Paleogeography and Archeology of the Eastern Mediterranean and of the Balkan Peninsula", supported by the DFG (Deutsche Forschungsgemeinschaft, Grant number INST 216/596-2).

Chapter 5

The physical and chemical data obtained in this study are available in the Pangaea database at https://doi.pangaea.de/10.1594/PANGAEA.868368. Rock magnetic data were measured in the Laboratory for Palaeo- and Environmental Magnetism (PUM), Bayreuth. We thank Ulrich Hambach for supervision and discussing the data. The luminescence samples were measured at the Cologne Luminescence Lab. We thank Anja Zander for the assessment of the radionuclide concentrations and her help in the laboratory. We thank Marianne Dohms and her team from the sedimentological Lab at the RWTH Aachen University for the measurements of the sedimentological and geochemical samples. Further, the authors would like to thank Christa Loibl for help during fieldwork, and Igor Obreht and Philipp Schulte for fruitful discussions. Moreover, we thank Kathrin Emunds and Heiko Lindner for the compilation of Figure 5.1.

Chapter 6

The physical and chemical data obtained in this study are available in the CRC806 database (see Bösken et al., 2017c). We thank Anja Zander for the assessment of the radionuclide concentrations and her help in the Cologne Luminescence Laboratory. We thank Marianne Dohms and her team from the sedimentological Laboratory at the RWTH Aachen University for the measurements of the sedimentological and geochemical samples. Further, the authors would like to thank David Molnar for help during fieldwork, and Philipp Schulte and Daniel Veres for fruitful discussions. Finally, we thank Wei Chu for his assistance in the field, his advice on the manuscript and the preparation of the radiocarbon samples.

Chapter7

I thank Anja Zander for the assessment of the radionuclide concentrations and her help in the Cologne Luminescence Laboratory. I thank Nicole Klasen and Christian Zeeden for their support and discussions. I thank Wei Chu and the whole research team including Frank

Lehmkuhl for making this research possible.

Chapter 8

Logistical and scientific support was provided by our Serbian colleagues. We thank Christa Loibl and Nikola Bačević for their help with sampling. Moreover, we thank the colleagues in the Cologne Luminescence Laboratory, especially Anja Zander for gamma spectrometry measurements and analysis, Christoph Burow for his help with R, and Georgina King and Melanie Bartz for support and feedback. Finally, we thank Lydia Krauß for reading the manuscript carefully.

Chapter 9

I thank Anja Zander for the assessment of the radionuclide concentrations and her help in the Cologne Luminescence Laboratory. I thank Christoph Burow, Dominik Brill, and Nicole Klasen for their input, help and discussions. I thank Christian Zeeden and Igor Obreht for support and the whole research team including Daniel Veres, Ulrich Hambach, and Frank Lehmkuhl for making this project possible. Finally, I thank the students that were involved in some of the preparation and measurements.

Acknowledgments

Hiermit möchte ich mich bei jedem bedanken, der mich in den letzten drei Jahren begleitet hat oder dazu beigetragen hat, dass ich hier gelandet bin. Ich weiß gar nicht wo ich anfangen soll or in which language to write this.

Vielleicht sollte ich mit meiner Familie anfangen, ohne die ich sicher nicht so weit gekommen wäre. Ich danke meiner Mutter Marly für ihre Intelligenz und dass sie mich zu einer so fleißigen und pflichtbewussten Person erzogen und mich immer unterstützt hat. An dieser Stelle möchte ich auch meiner Oma danken, die mit mir schon mit 6 Jahren Schach spielte und die meinen Geist stets trainierte. Ich danke meinem Vater Theo für die Gelassenheit, die nötig ist, um zwischen all den abstrakten Daten nicht unterzugehen und nicht aufzugeben und dafür, dass er mir vermittelt hat wie wichtig Balance im Leben ist. Ohne einige Stunden Pause mit einem kopje koffie hätte ich die langen Arbeitstage sicher nicht überstanden. Ich danke meinem Stiefvater Walter für sein Engagement im Klimaschutz und dafür, dass er mir gezeigt hat, wie man gesellschaftliche Probleme direkt selber angehen kann und letztendlich danke ich ihm auch dafür, dass ich zu einer so starken Frau herangewachsen bin. Ich danke meiner Stiefmutter Petra dafür, dass sie mich nie vergessen lässt, wie wichtig Quatsch und Lebensfreude sind (und heiße Waschmaschinen :). Ich danke meinem Bruder Michael und seiner Verlobten Bianca, die das Leben mit Erfolg und Freude und gemeinsam meistern und mir ein unglaubliches Vorbild setzen.

I am thankful for the love of my life, my moon and stars, Jan, without whom I would not have managed to keep going and who taught me the importance of serenity and leisure. He was grounding me when the stress level got too high and he was my home when I was without.

Hier wil ik ook iedereen bedanken die ik in Amsterdam heb leren kennen. Mijn tijd in Amsterdam was erg belangrijk voor mijn persoonlijke ontwikkeling en gaf mij het zelfvertrouwen wat nodig was om mijn phd te beginnen.

An dieser Stelle möchte ich mich auch bei meinen Freunden bedanken, für ihr Verständnis für die Abende, an denen ich mal wieder keine Zeit hatte oder zu abgedriftet in meine Forschung war. I promise to make up for this :)

I am thankful for the support and help from all my colleagues and friends in Aachen and Cologne, especially for Lydia, Igor and Joerg. Gefangen im selben Boot, konnten wir uns gegenseitig unterstützen. I thank Lydia for the unicorns and dreams and for believing in me. I thank Igor for being the sweetest Serb there is and for helping me understand southeastern (eating and drinking) culture. For his help in the field, even when we tried sampling cement

and for never complaining no matter what difficulties we faced. Ich bedanke mich bei Joerg für die konstruktive und produktive Arbeitsatmosphäre in unserm Büro und dafür, dass du es mir nicht übel genommen hast auch wenn ich mal etwas zuviel geredet habe :D Besonders bedanke ich mich, dass du mich immer unterstützt und zu mir gehalten hast.

Ich bin dankbar für die Diskussionen und Gespräche aller Kollegen des PGG, besonders Philipp, Veit, Martin, Georg und Kaifeng und ich bedanke mich für jeden Tag bei dem nicht nur über Fußball geredet wurde. Ich bin dankbar für die IT-Unterstützung von Gernot und die GIS-Unterstüzung von Isa, Heiko, Arne, Kathrin und Janek. Ich danke Arne dafür, dass er niemals aufgeben hat, egal wie oft die Koordinaten geändert wurden. I am thankful for the help in the field by Stephan and for the girlpower of Kathrin and Beate, and for not being the only female in the field. And last but not least, bedanke ich mich bei Marianne und Anja K., ohne die hier überhaupt nichts laufen würde.

I am very thankful for the scientific and non-scientific support of my postdocs Nicole and Christian without whom I never would have understood what I am actually doing and who prepared me well for the scientific world. I also thank them for believing in me and supporting me when it got difficult.

Finally and maybe most of all I thank my Doktorvater Frank Lehmkuhl for giving me the chance to work in science and to prove my abilities and for supporting me in all the fieldtrips, workshops and conferences I wanted to visit to satisfy my hunger for knowledge.

I thank my colleagues in Cologne Anja Z., Christoph, Dominik, David, Franz, and Melanie for their help in the lab and for teaching me how to use *R* and for always having a desk for me to work. I thank Anja G. for helping me with the sample preparation, and never complaining no matter how much mica we needed to remove. I am thankful for Melanie and Svenja who are as crazy about luminescence as I am. I am still impressed with your networking skills (or boldness). Ich freu mich schon auf unsere Zeit in Südafrika und bin froh, dass wir das mit der Planung dann doch noch geschafft haben :)

I am thankful for all the IRTG people. It was an unbelievable time and I am happy we shared it all. I thank everyone who made the meetings, workshops and lectures possible. Jasmijn en Thomas, ik wil jullie bedanken dat jullie mij hebben helpen herinneren aan de Nederlandse cultuur en 'gezelligheid' en aan wat belangrijk is in het leven. Ook dank ik Ine en Wei voor de mooie samenwerking en het avontuurlijke veldwerk.

Finally, I thank all my colleagues 'abroad' in Hungary, Serbia, Romania, and Bayreuth for teaching me during fieldwork, for being sampling machines, for analyzing mollusc, magnetic and tephra samples, for writing and reading manuscripts. I am glad to have gotten to know the loess kings of Serbia and Romania and for all the language skills I could not master.

Ich bedanke mich beim SFB806 für 3,5 Jahre Forschung und bei der DFG für die Finanzierung all unserer Vorhaben. I acknowledge the USGS, who made the SRTM data freely available, which were used in the digital maps shown in this thesis. I hope that this service will be preserved.

I thank all the people that proof-read this dissertation, especially Jess, Jan, Maarten, Lisa, and Jenni for trying. I hope you will enjoy the chocolate from the Aachener Lindt factory :)

Last but not least I thank all the reviewers, especially Frank Lehmkuhl and Helmut Brückner for taking their time and knowledge to improve the articles and the dissertation.

Thank you all, dankeschön, muchas gracias en hartstikke bedankt!

A. Supplementary figures to the manuscript ‘Investigating the last glacial Gravettian site ‘Ságvár Lyukas Hill’ (Hungary) and its paleoenvironmental and geochronological context using a multi-proxy approach’

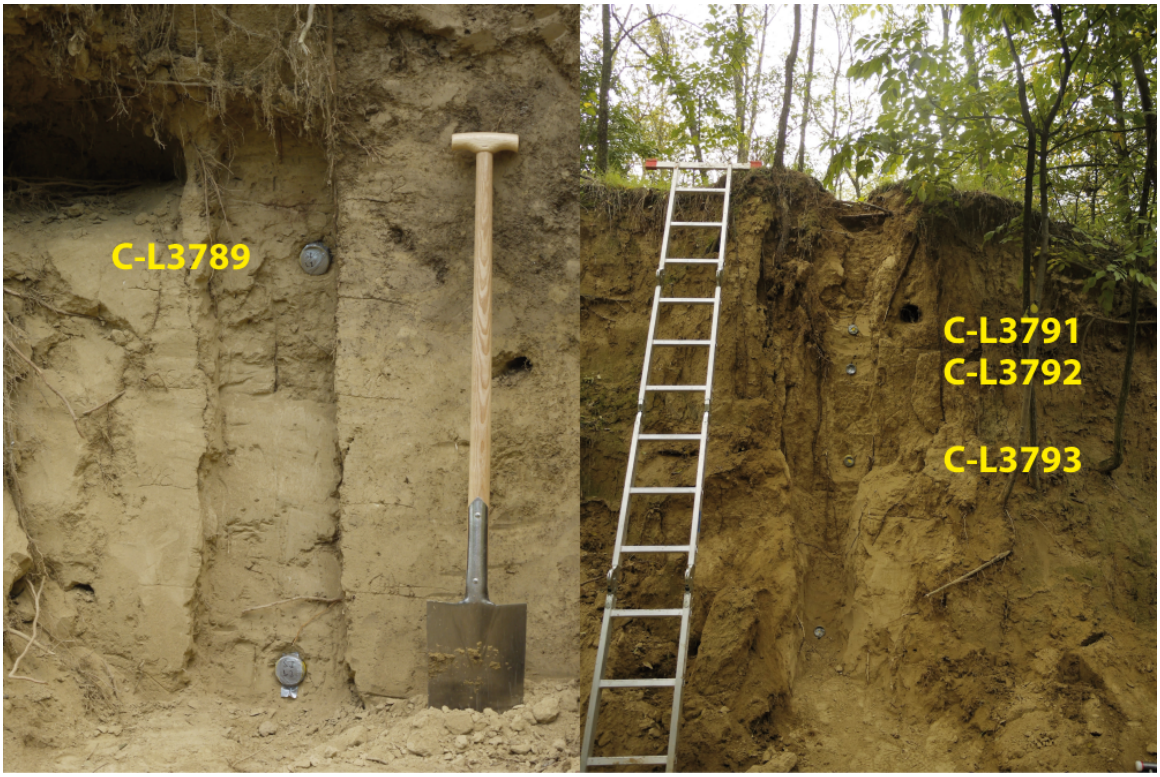

Figure A.1.: Photos of Ságvár I (with cylinders for luminescence dating in the wall) and Ságvár II (right).

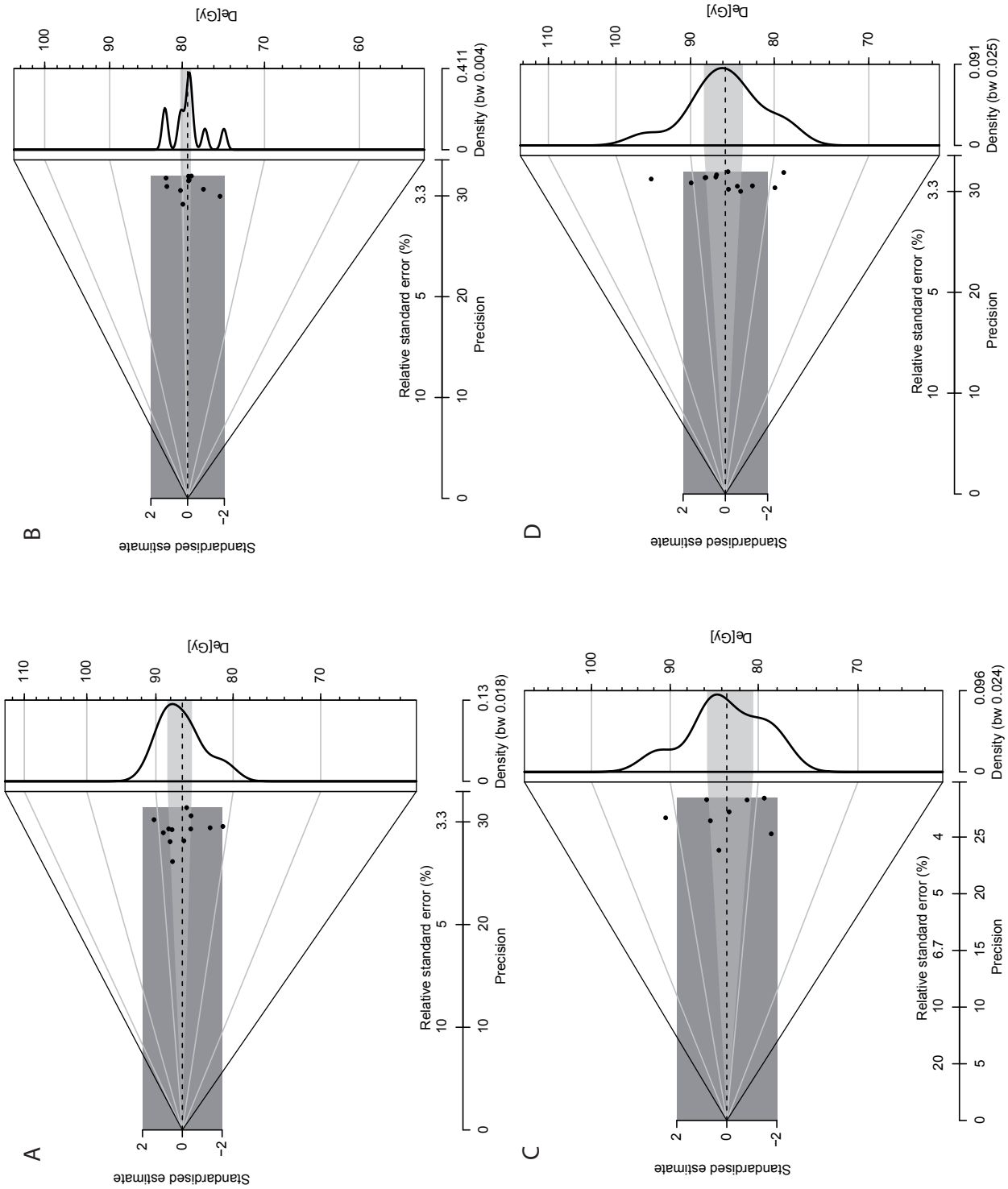

Figure A.2.: Abanico plots of D_e distributions of samples C-L3789 (A), C-L3791 (B), C-L3792 (C), C-L3793 (D), generated using the R luminescence package (Dietze et al., 2016).

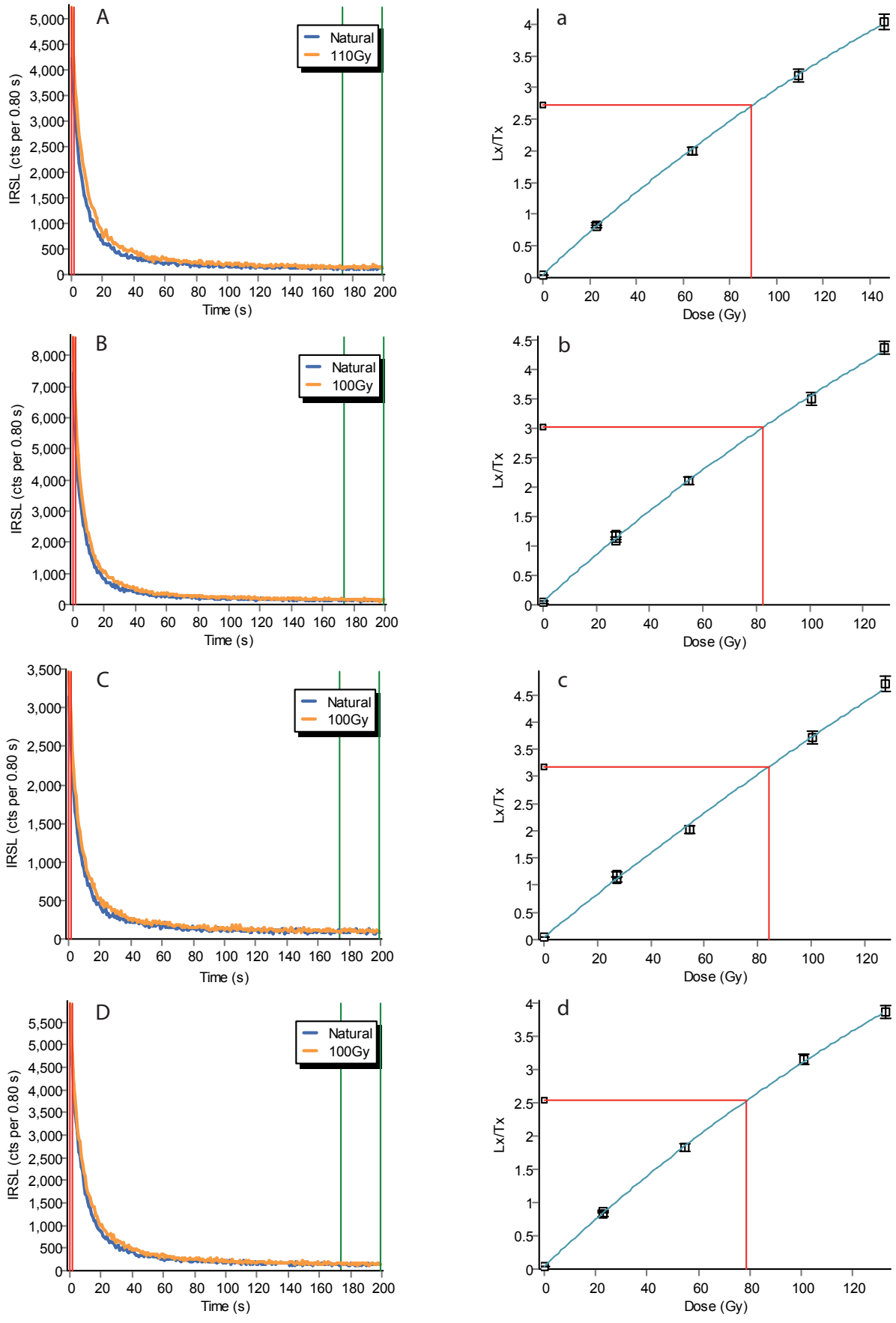

Figure A.3.: Shine down and growth curves of samples C-L3789 (A/a), C-L3791 (B/b), C-L3792 (C/c), and C-L3793 (D/d). Exponential fitting used. Plots were generated with Analyst v. 4.31.7 (Duller, 2015a).

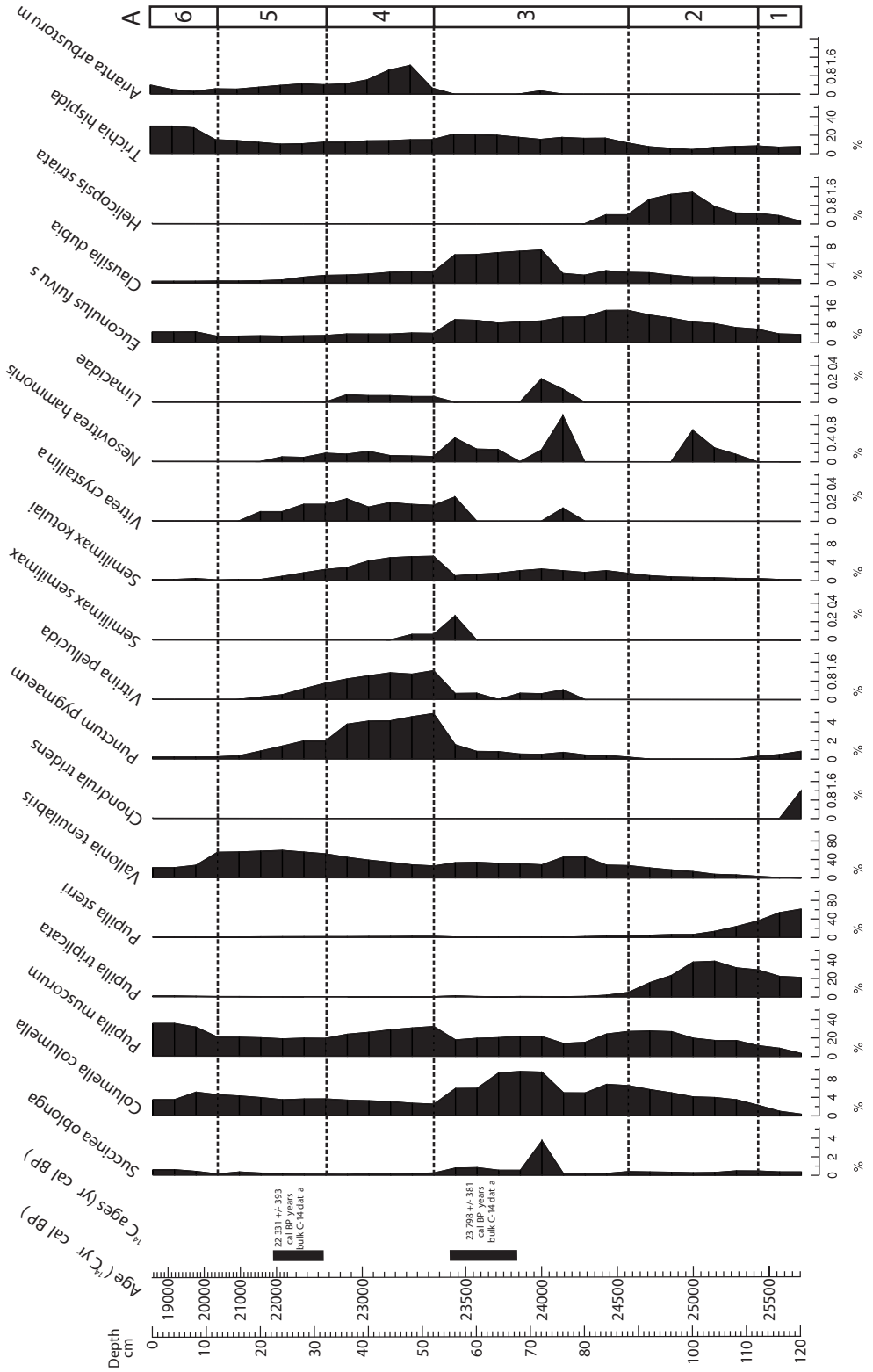

Figure A.4.: Abundance of different Mollusk taxa identified in Ságvár I (in %). 'A' indicates the local malacological zones. As a reference a time-scale is given that is based on two radiocarbon ages (Krolopp and Sümegi, 2002) and a comparison to other radiocarbon-dated malacological sections in Hungary.

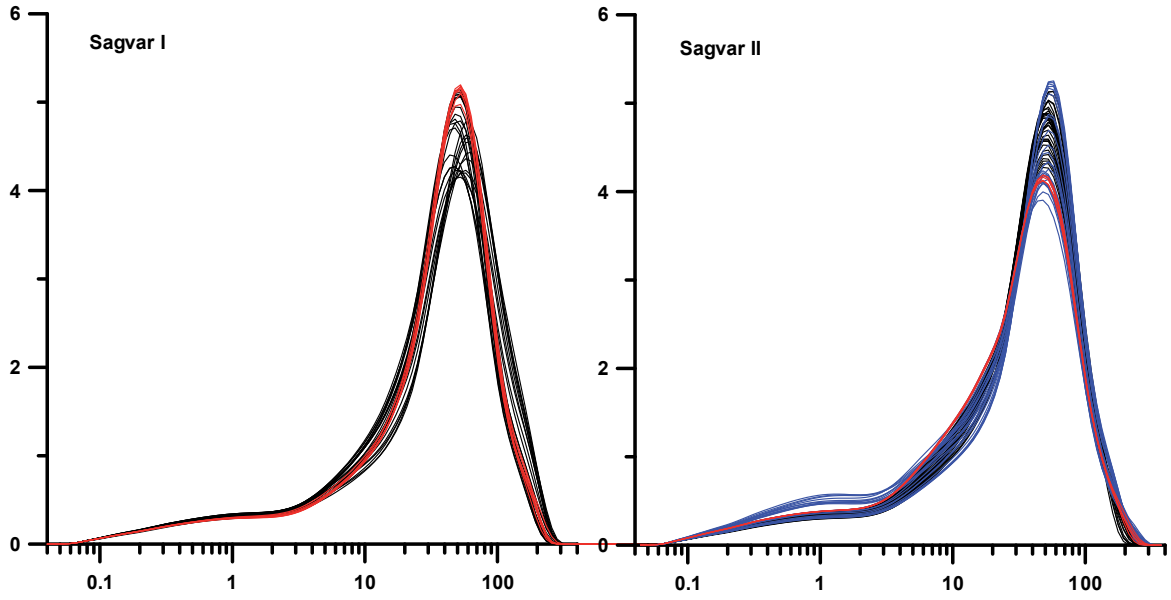

Figure A.5.: Grain size distributions of the Ságvár profiles 1 and 2. Samples from Ságvár I are plotted on the left with samples from 26 cm upwards (the upper part including the younger cultural layer) plotted in red. For Ságvár II samples from the level correlated to the younger cultural layer ($100 - 120$ cm) are also plotted in red, while the lower part from $120 - 256$ cm is black and the upper part (until 100 cm) is plotted in blue.

B. Supplementary figures to the manuscript 'Paleoenvironmental conditions during the MIS3/2 transition recorded at a loess-paleosol sequence in northeastern Hungary and its significance for spatial paleosol formation patterns'

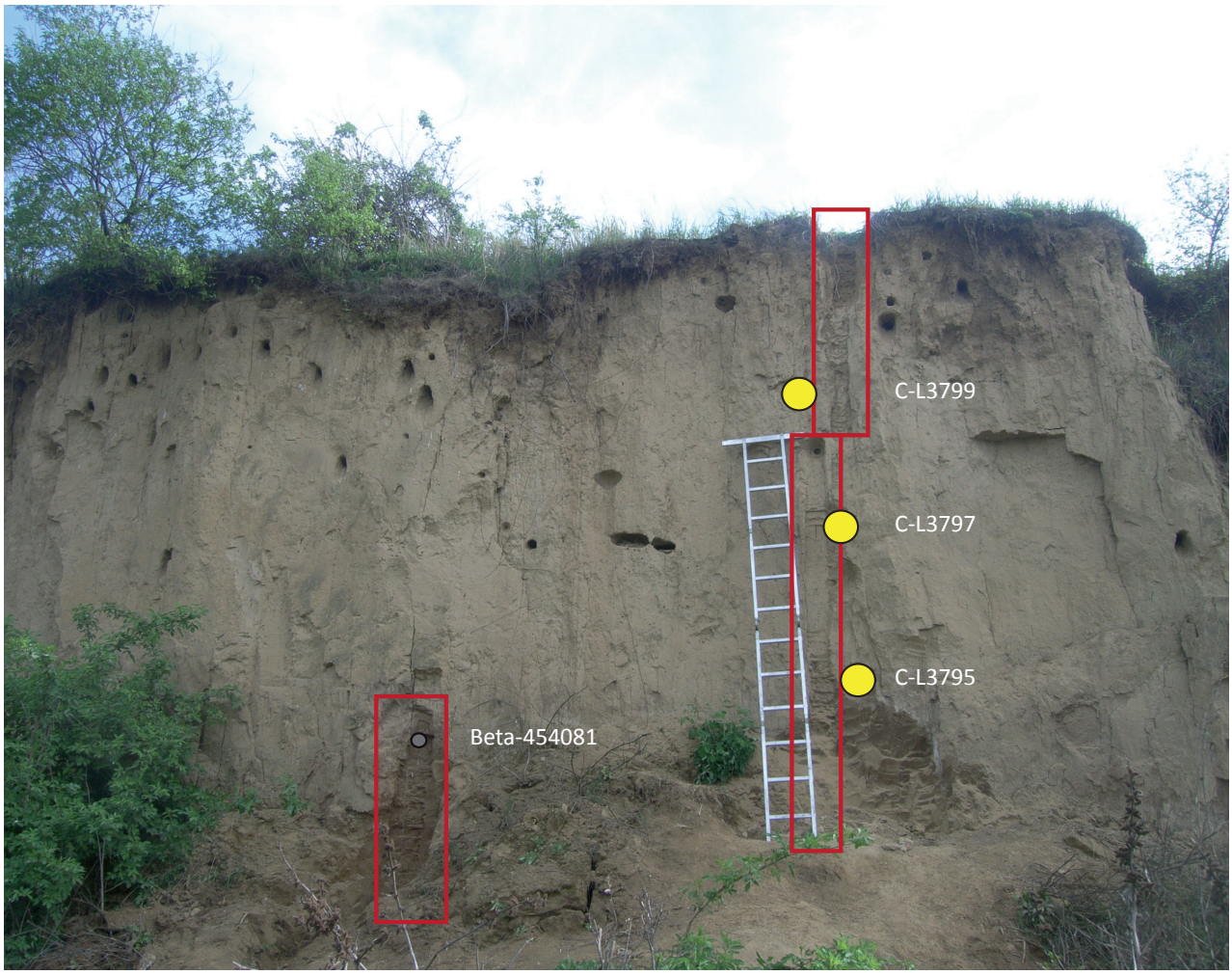

Figure B.1.: The photograph shows the Bodrogkeresztúr section with the locations of the sediment samples (red squares), luminescence samples (yellow circles) and the radiocarbon sample (grey circle).

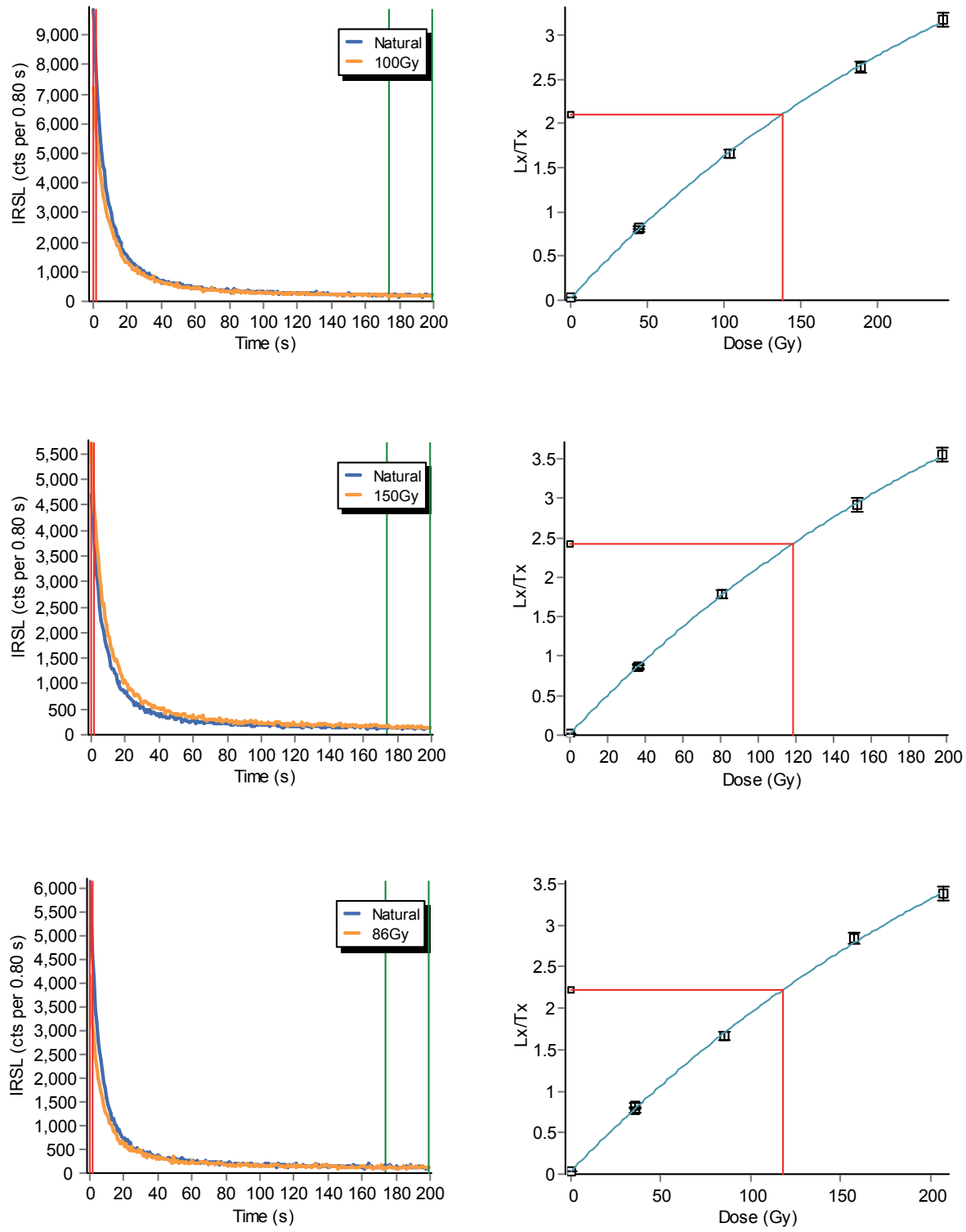

Figure B.2.: Shine down curves (left) and dose response curves (right) for samples C-L3795 (top), C-L3797 (middle), and C- L3799 (bottom). Analyst version 4.14.6 was used to generate the plots (Duller, 2015a).

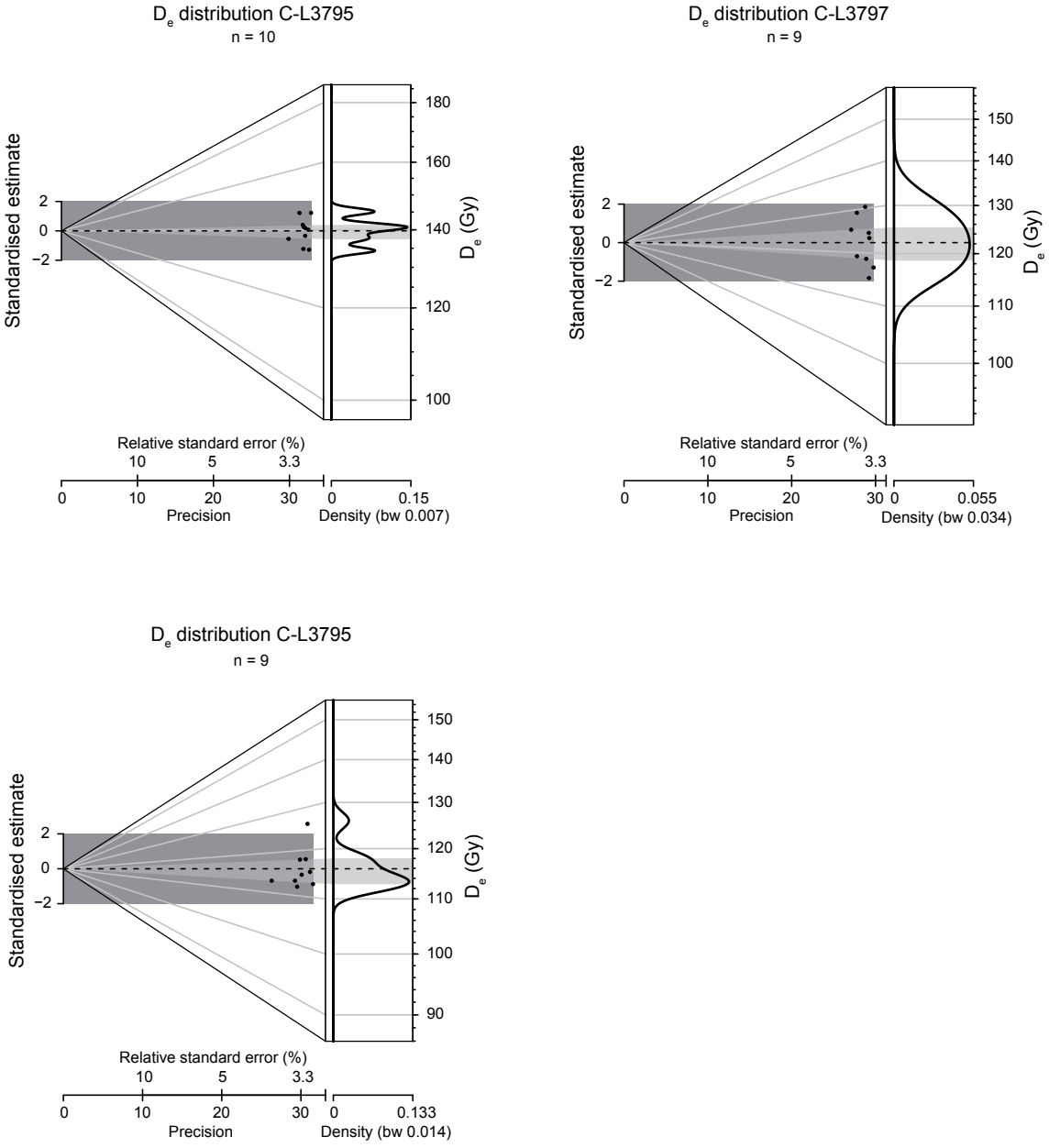

Figure B.3.: Abanico plots showing the D_e distribution of the three samples. The plots were generated in the R luminescence package using the '*plot_AbanicoPlot*'-function according to Dietze et al. (2016).

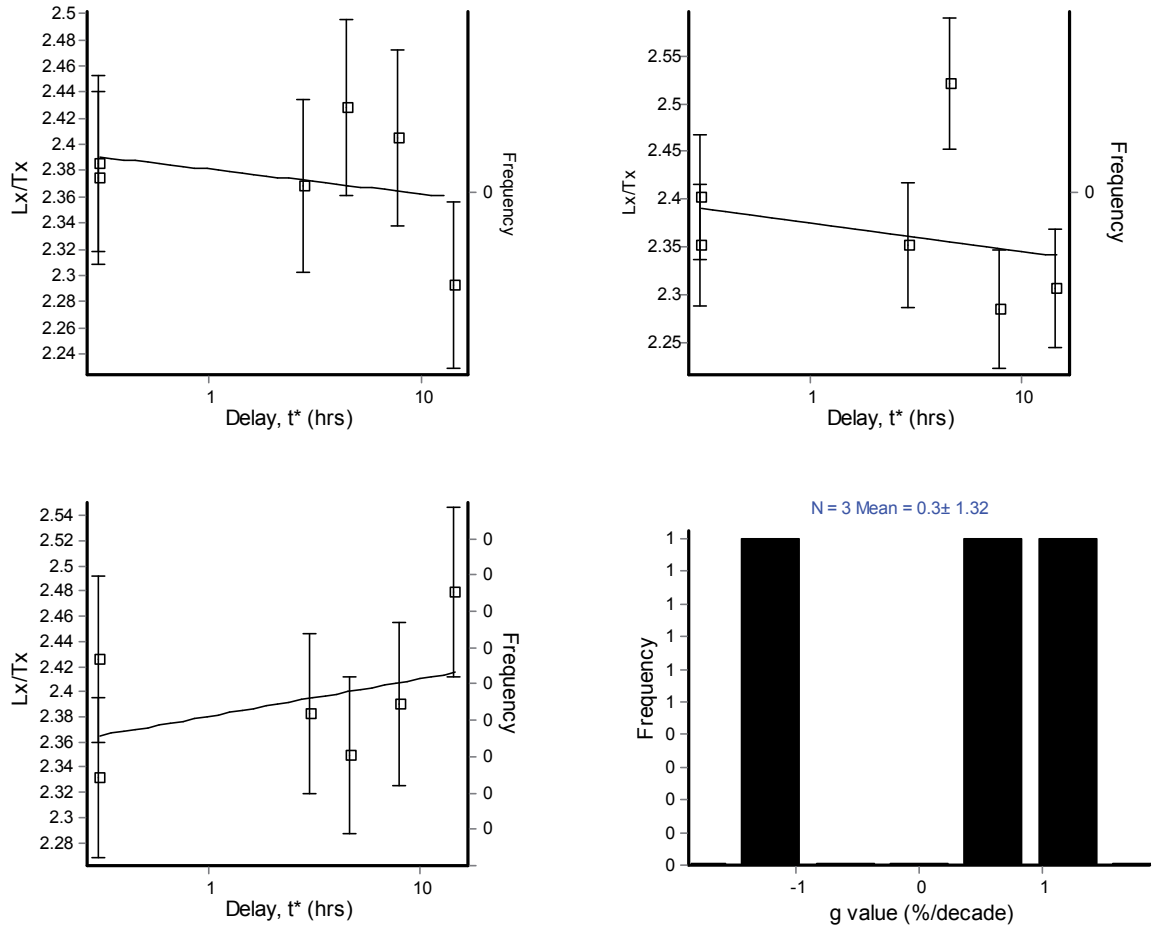

Figure B.4.: Fading measurements of sample C-L3797 show varying fading rates between $-1.2 \pm 1.7\%$ and $1.3 \pm 1.8\%$. Mean and standard error are $0.27 \pm 0.76\%$. The bottom right diagram indicates the mean value and its standard deviation.

C. Supplementary figures to the chapter 'Geochronology of the Aurignacian open-air site of Crvenka-At (Serbia)'

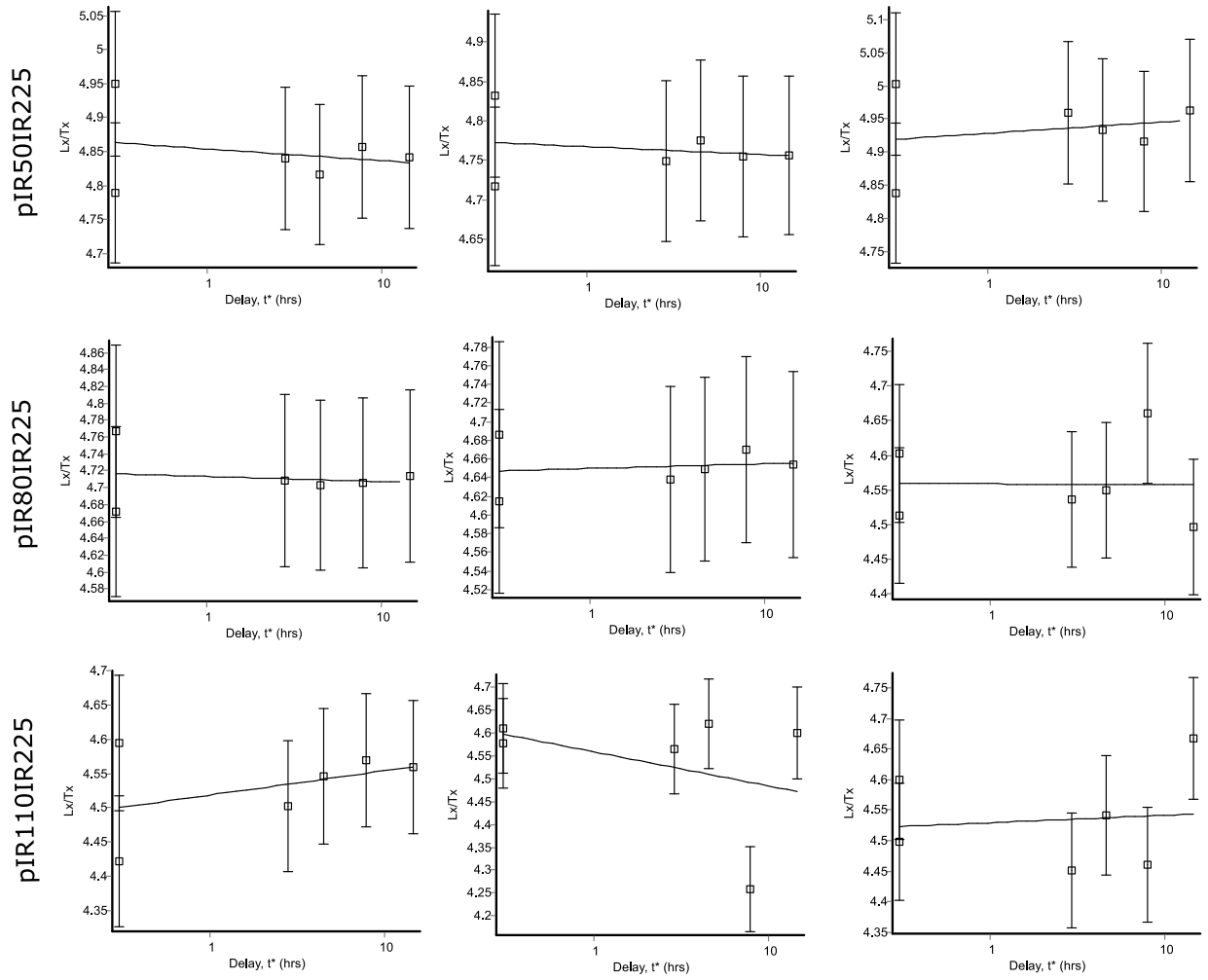

Figure C.1.: Fading measurements of sample C-L4240 for the $pIR_{50}IR_{225}$, the $pIR_{80}IR_{225}$ (middle), and the $pIR_{50}IR_{225}$ (bottom) protocols. Mean and standard error indicate fading rates of $g_{2days} = 0.08 \pm 0.21$, $g_{2days} = 0.01 \pm 0.07$, and $g_{2days} = 0.21 \pm 0.75$. Analyst version 4.14.6 was used to generate these plots (Duller, 2015a)

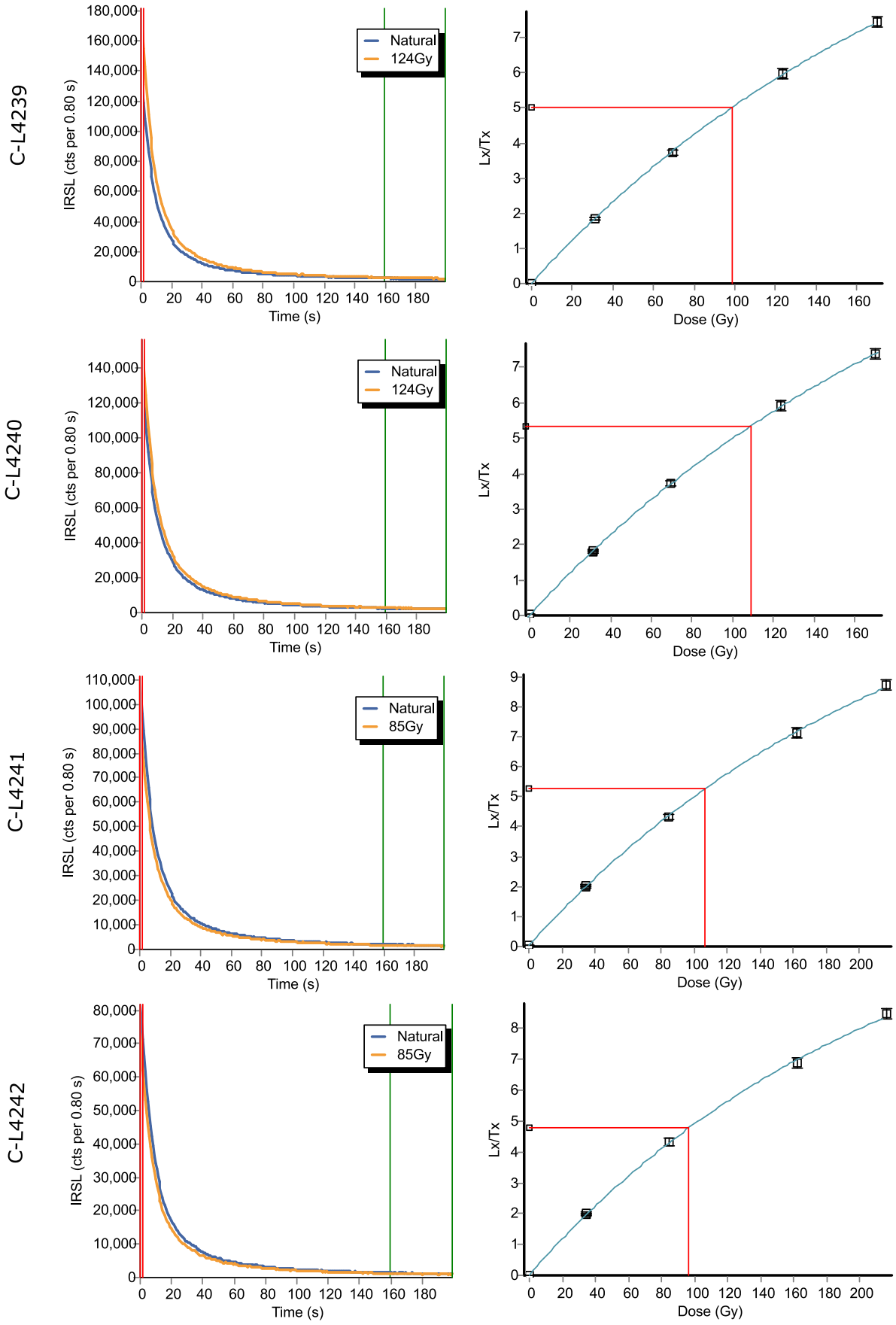

Figure C.2.: Shine down curves (left) and dose response curves (right) for samples C-L4239 - C-L4242. Analyst version 4.14.6 was used to generate the plots (Duller, 2015a).

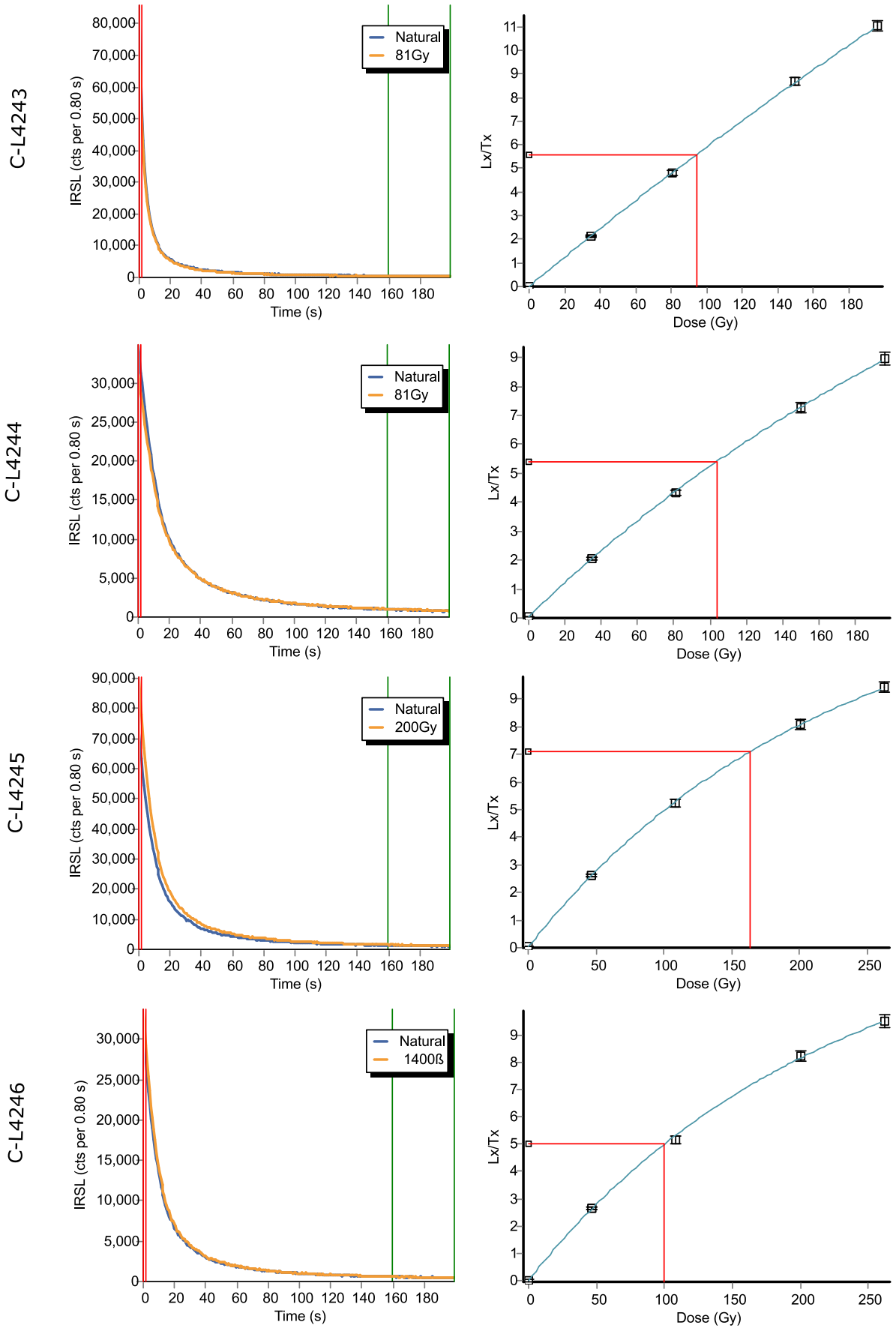

Figure C.3.: Shine down curves (left) and dose response curves (right) for samples C-L4243 - C-L4246. Analyst version 4.14.6 was used to generate the plots (Duller, 2015a).

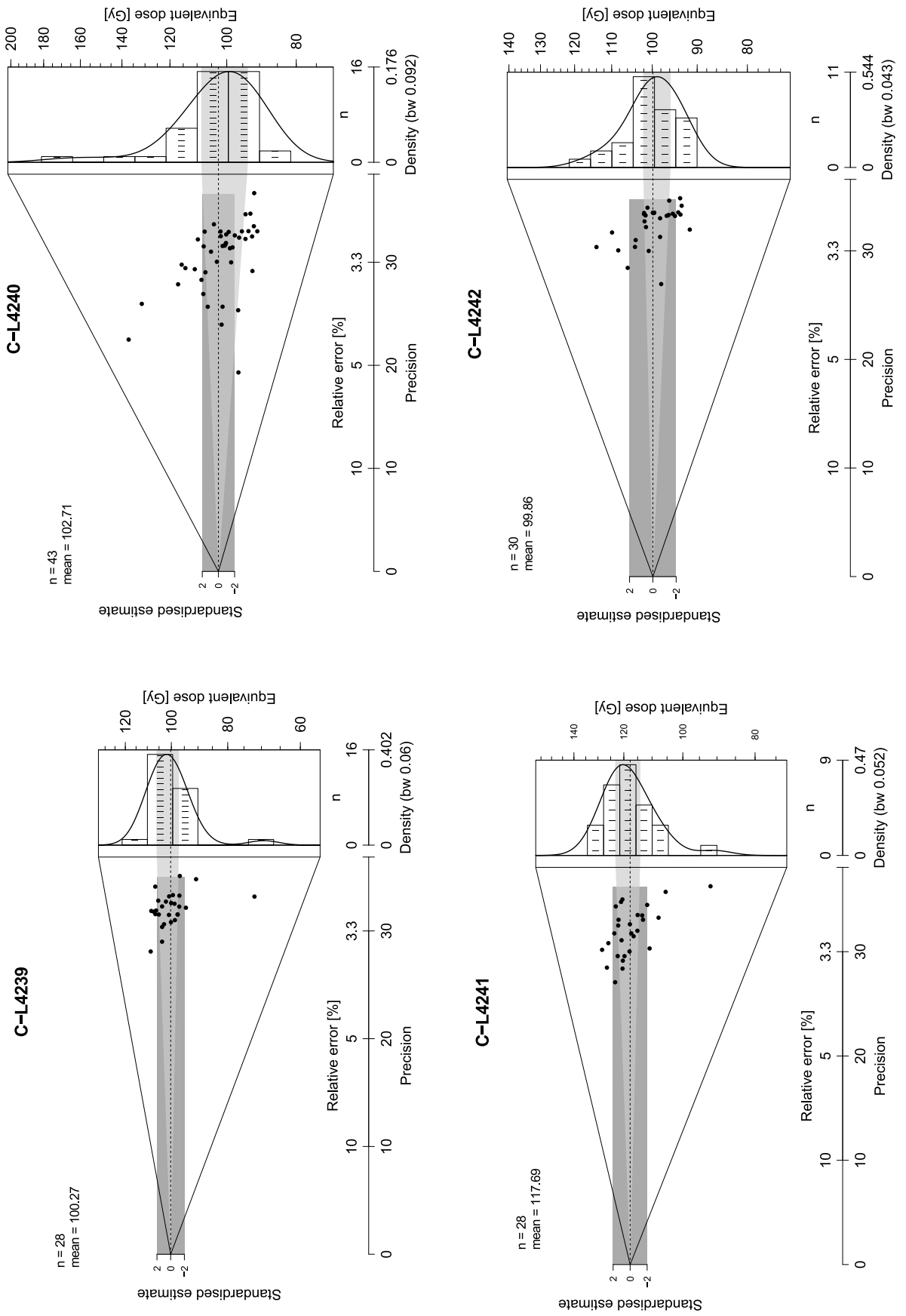

Figure C.4.: Abanico plots howing the D_e distribution of samples C-L4239 - C-L4242. The plots were generated in the R luminescence package using the '*plot_AbanicoPlot*'-function according to Dietze et al. (2016).

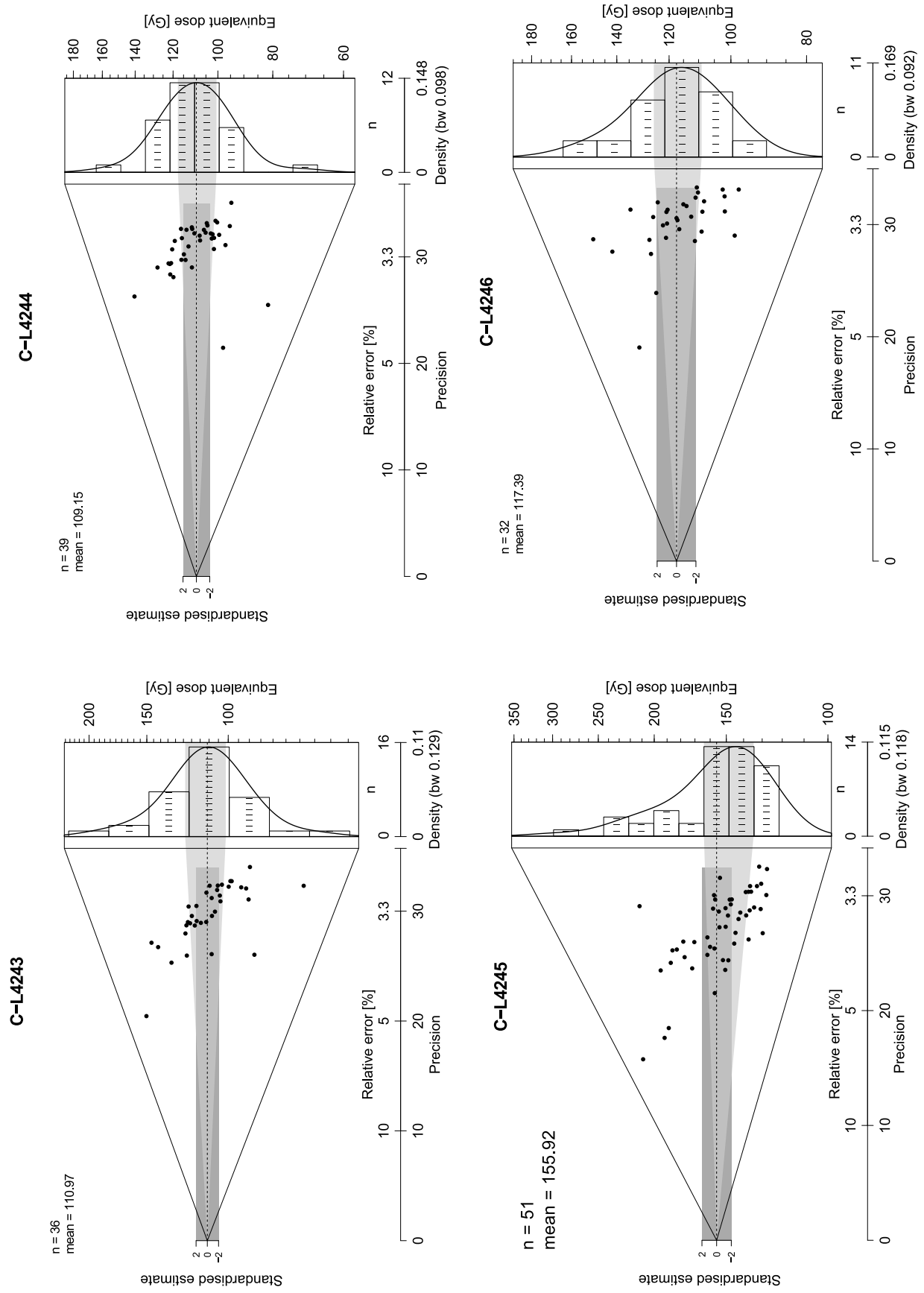

Figure C.5.: Abanico plots howing the D_e distribution of samples C-L4243 - C-L4246. The plots were generated in the R luminescence package using the '*plot_AbanicoPlot*'-function according to Dietze et al. (2016).

D. Supplementary figures to the manuscript 'A new luminescence-based geochronology framing the last two glacial cycles at the southern limit of European Pleistocene loess in Stalać (Serbia)'

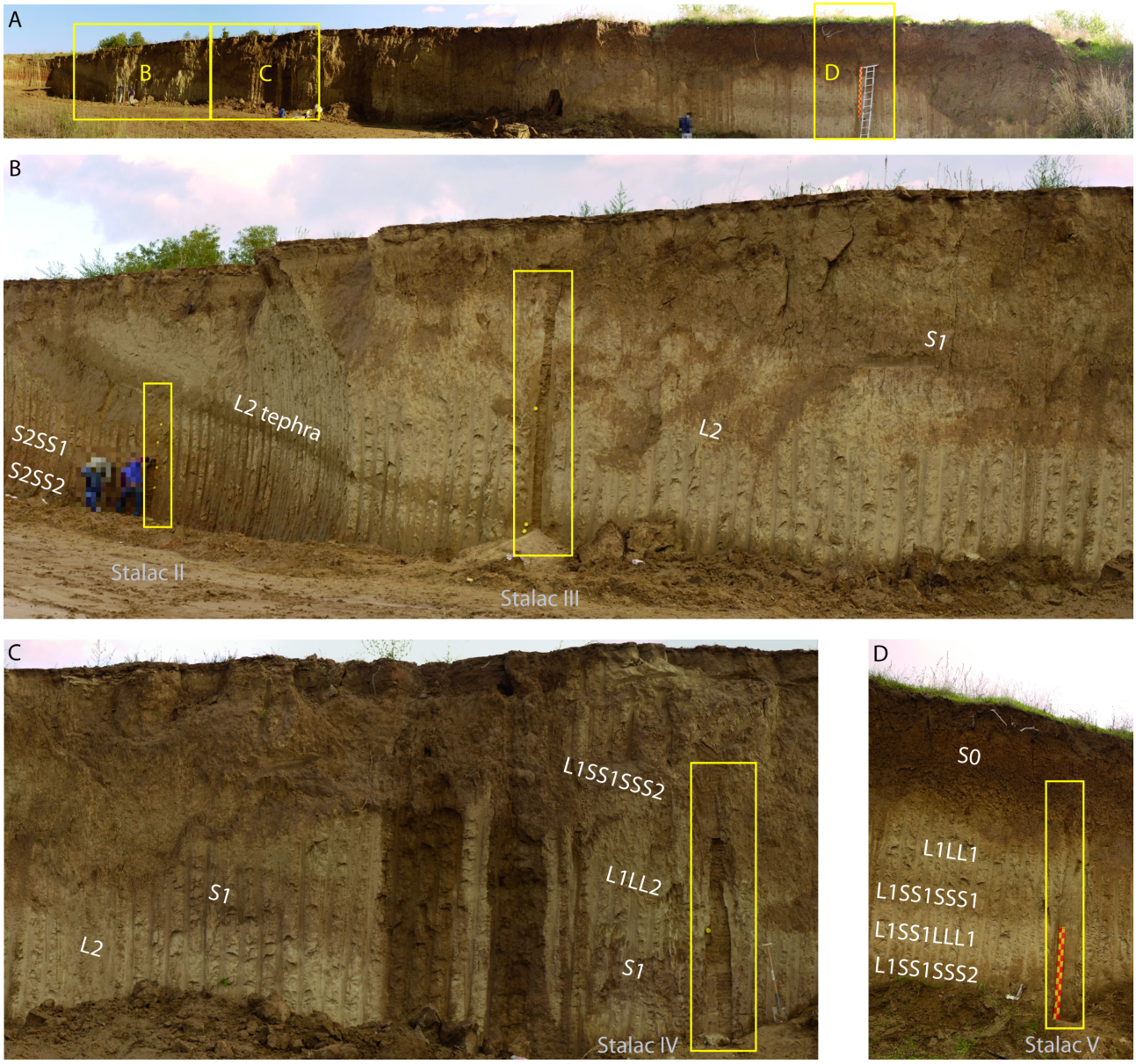

Figure D.1.: Photos from the field site showing sampled sections and stratigraphical units (after Marković et al., 2015). An overview is given in A. The boxes in B, C, and D show the sampled areas.

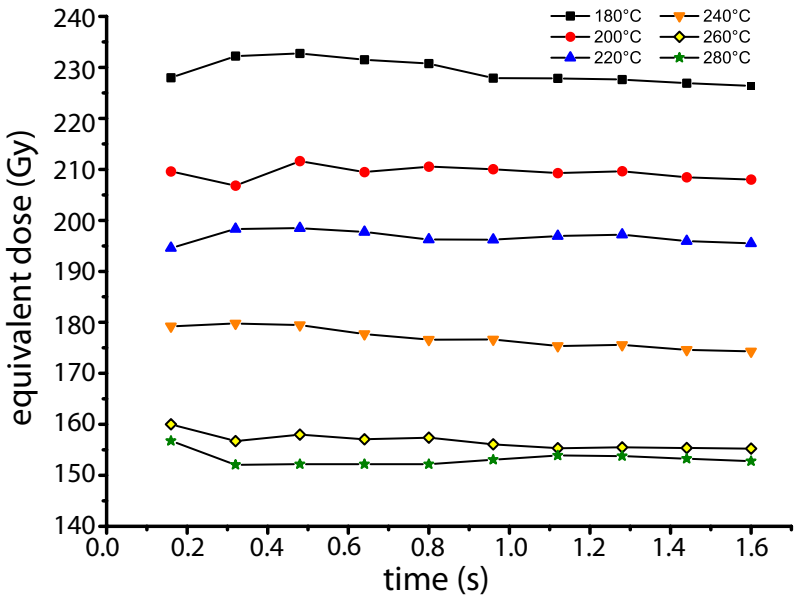

Figure D.2.: The $D_e(t)$-plot presents the equivalent dose as a function of the signal integration interval shown on the time-axis. Here, late background subtraction was used. Each line corresponds to another preheat temperature of samples C-L3787.

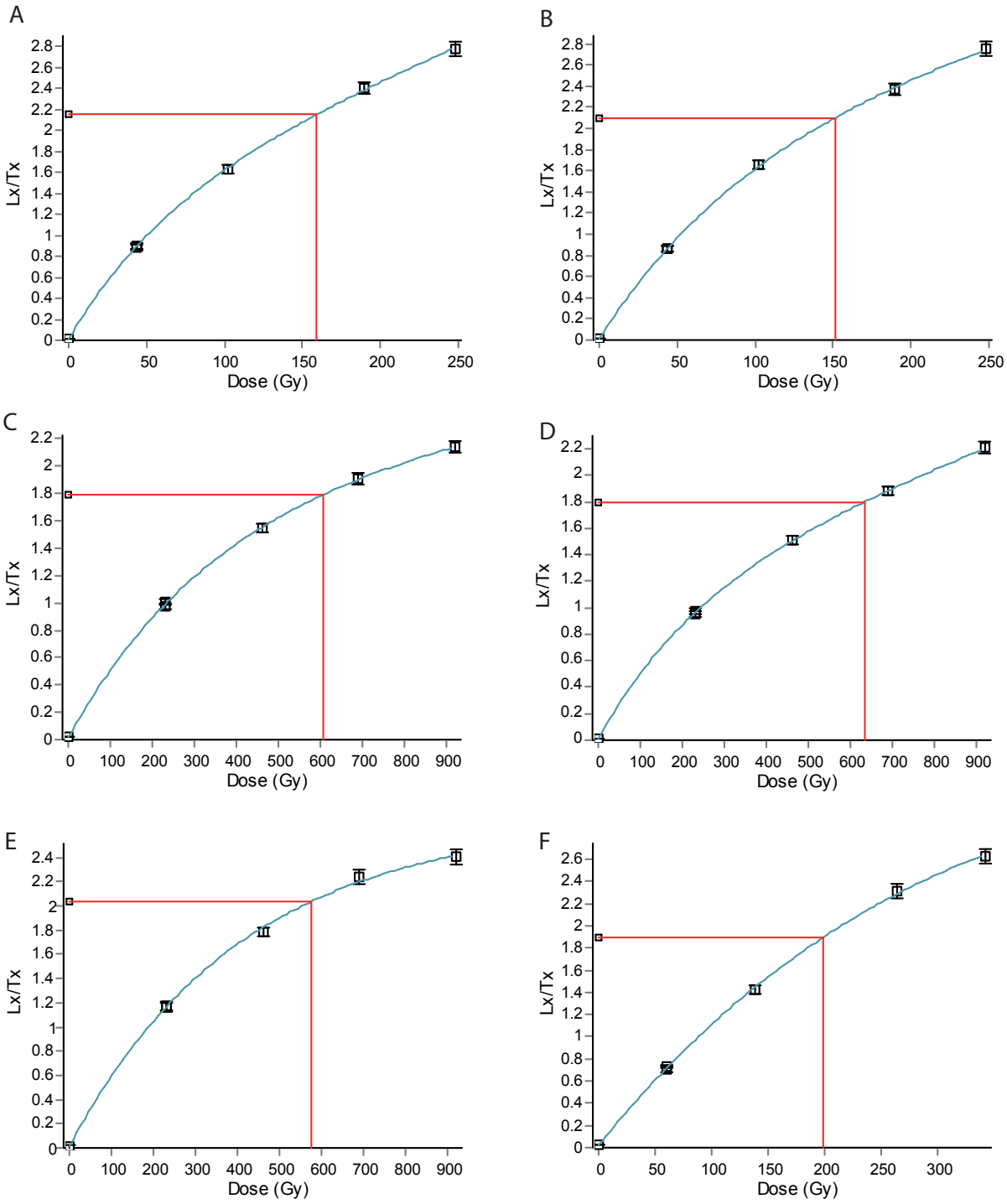

Figure D.3.: Fitted dose response curves of C-L3787 with a preheat temperature of $260°C$ (A) and $280°C$ (B) of the quartz fraction; and DRCs of C-L3778 (C), C-L3780 (D), C-L3784 (E), and C-L3787 (F) of the polymineral fraction.

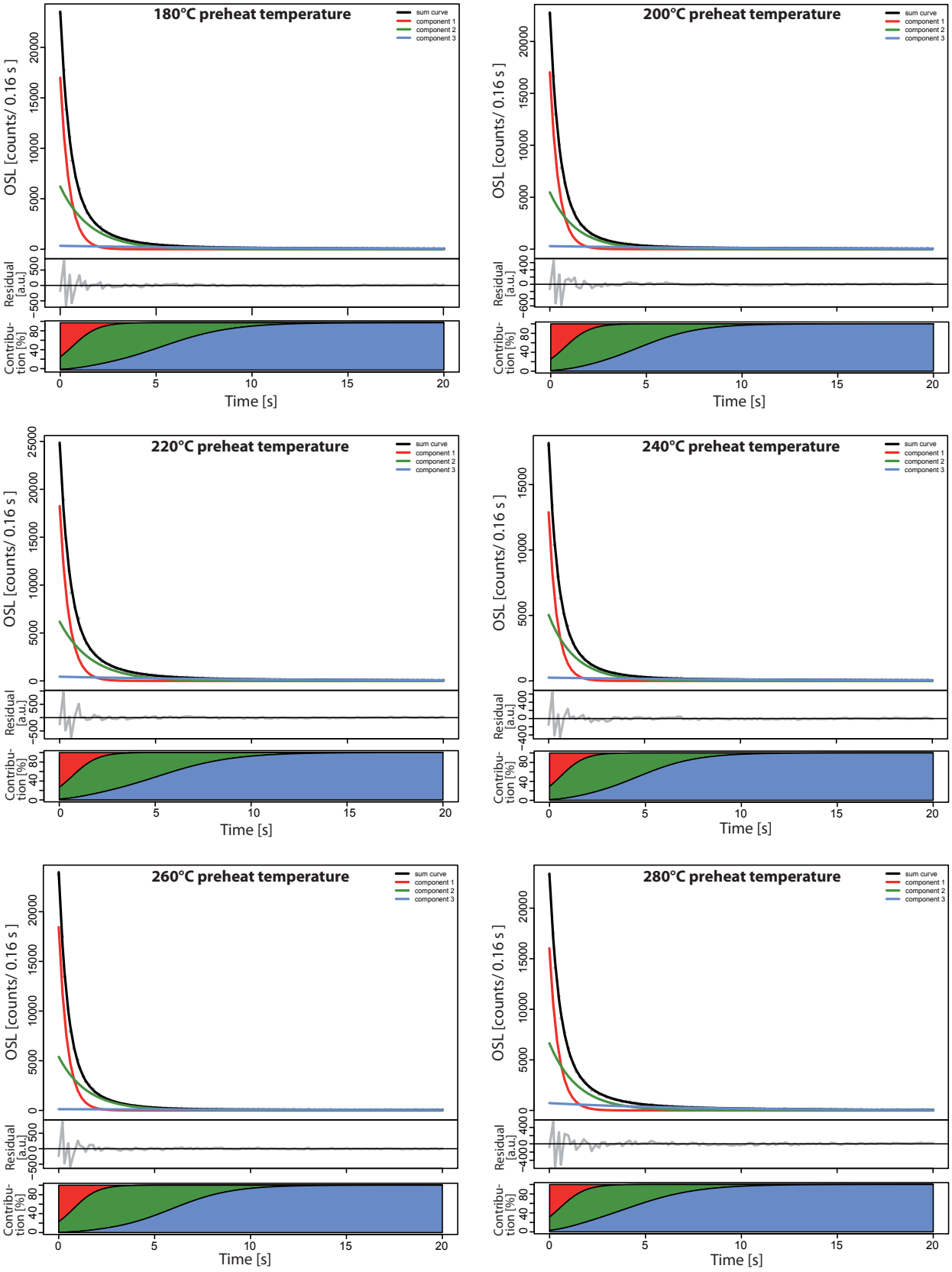

Figure D.4.: Fitted decay curves with their residual and signal components of the quartz fraction of C-L3780. One curve per preheat temperature is shown. Curves were made using the *fit_CWCurve*-function in the R luminescence package (Kreutzer et al., 2012b). Colors indicate the sum curve (black), component 1 (red), component 2 (green), and component 3 (blue).

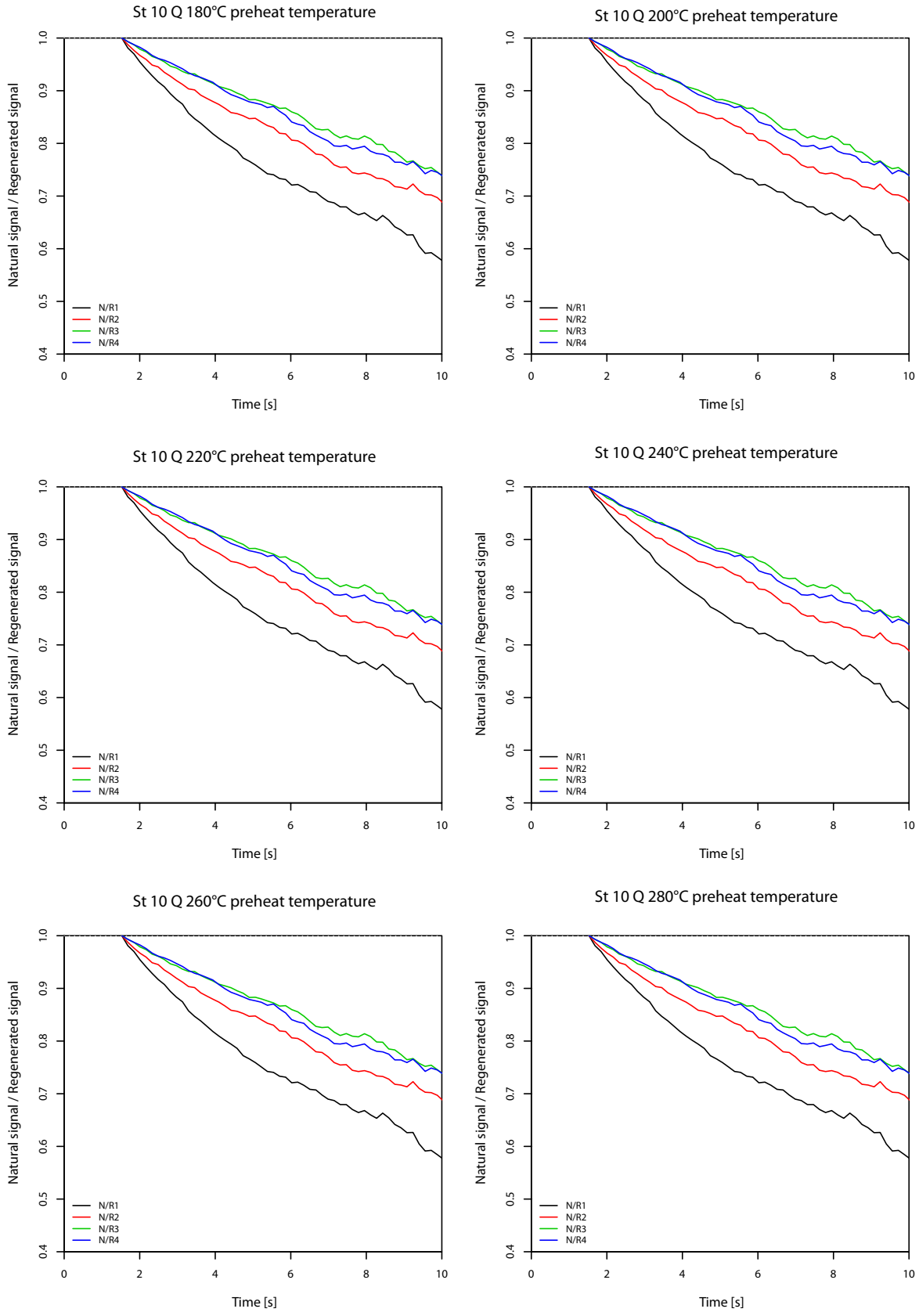

Figure D.5.: Ratio of the natural signal to several regenerated signals of one aliquot per preheat temperature of the C-L3787 quartz sample (Steffen et al., 2009). Each plot shows four lines that correspond to four regenerated dose points. Plots were generated using the *plot_NRt*-function of the R Luminescence package (Burow et al., 2016; Kreutzer et al., 2012b).

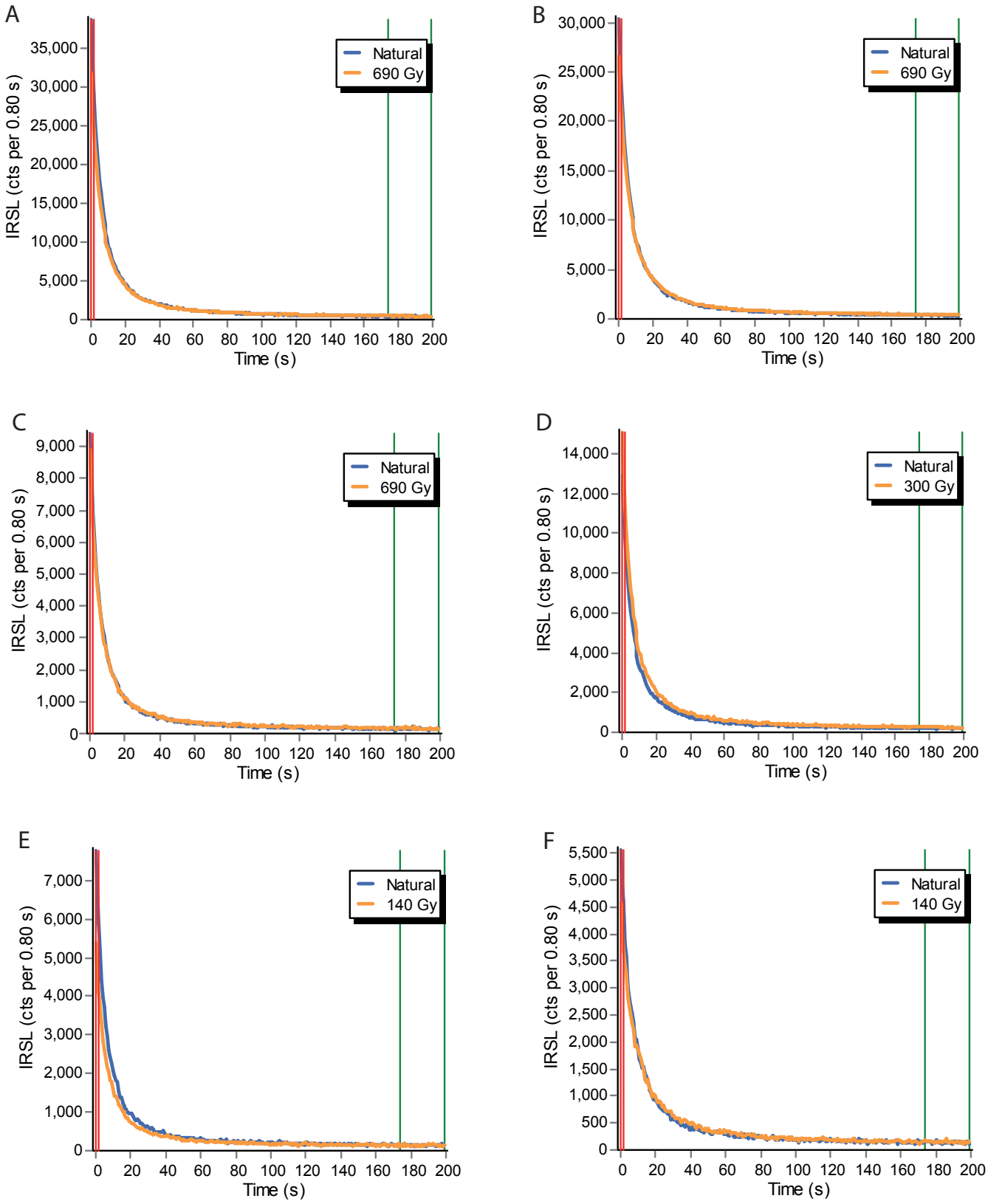

Figure D.6.: Decay curves of the pIRIR measurements. One curve per sample is shown: C-L3778 (A), C-L3780 (B), C-L3784 (C), C-L3786 (D), C-L3787 (E), and C-L3788 (F).

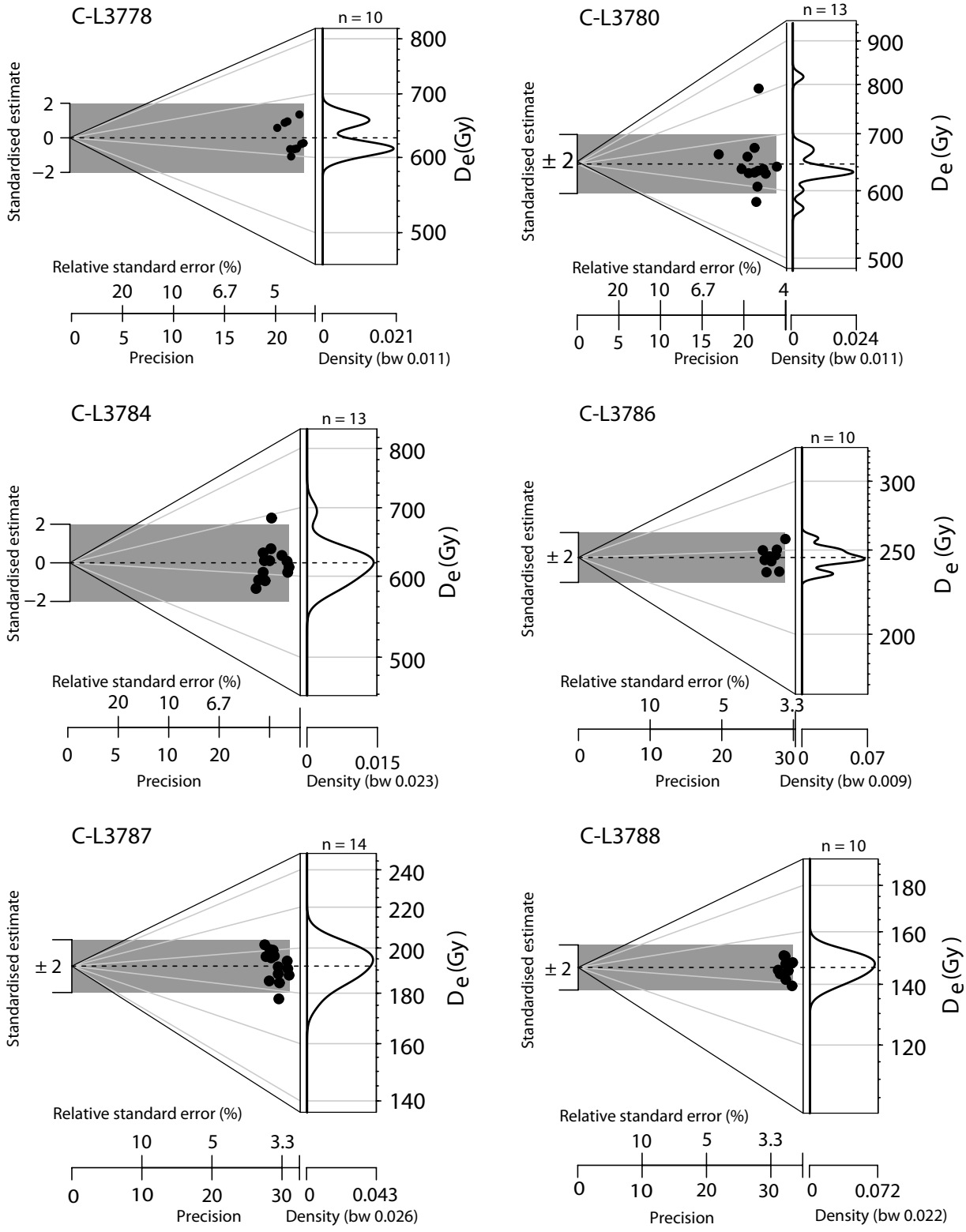

Figure D.7.: Abanico plots showing the D_e distributions of the pIRIR D_e measurements.

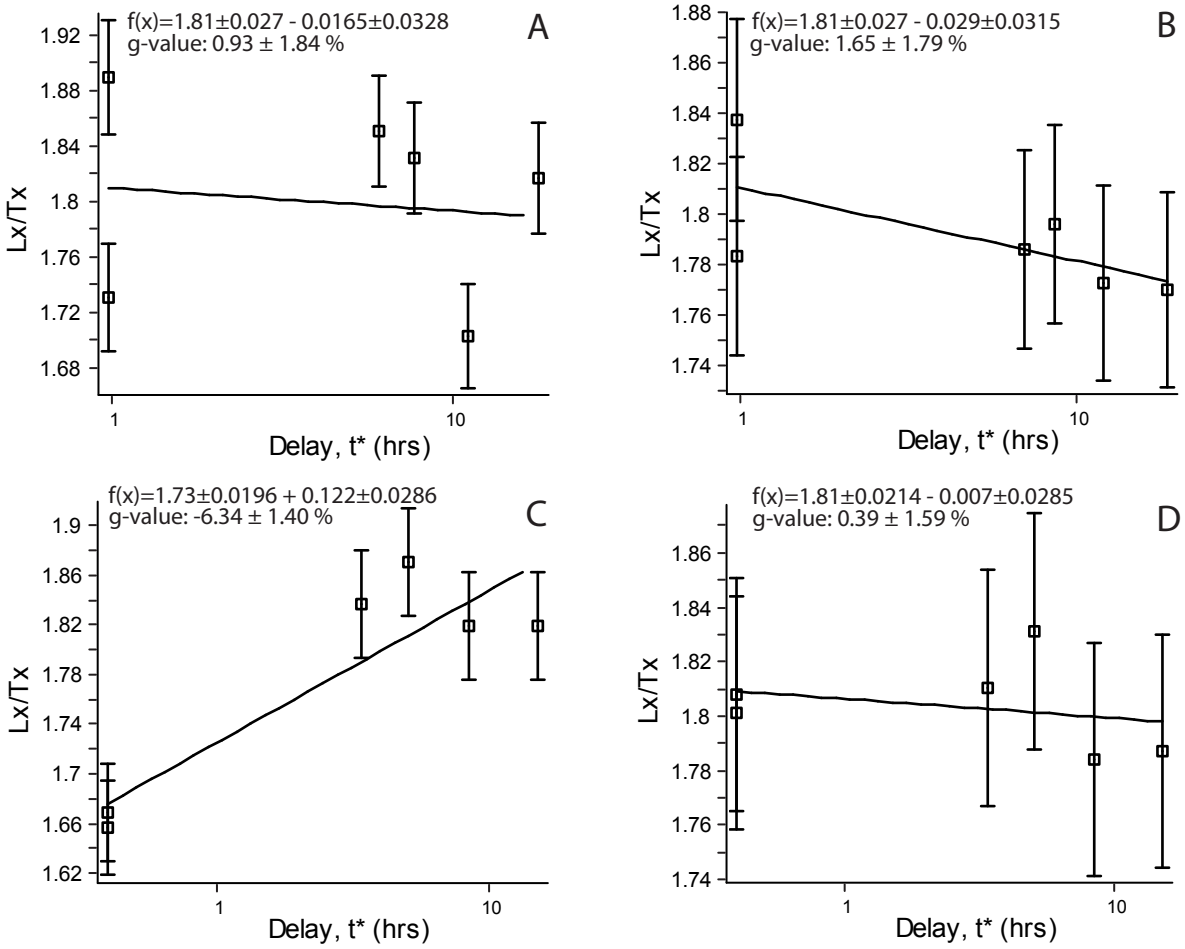

Figure D.8.: Plots showing the fading experiments. The normalized luminescence signal (L_x/T_x) is plotted against delay time. The linear functions used for fitting and the resulting g-values (fading rate) are shown. A and B show two aliquots of sample C-L3780; C and D show two aliquots of sample C-L3787.

E. Supplementary figures to the chapter ‘Luminescence dating of the Urluia loess-paleosol sequence in the Lower Danube Basin - geochronology and challenges’

Figure E.1.: The photograph shows the Urluia outcrop with the here investigated study site in blue and the location of previous investigations by (Fitzsimmons and Hambach, 2014; Fitzsimmons et al., 2013) in yellow.

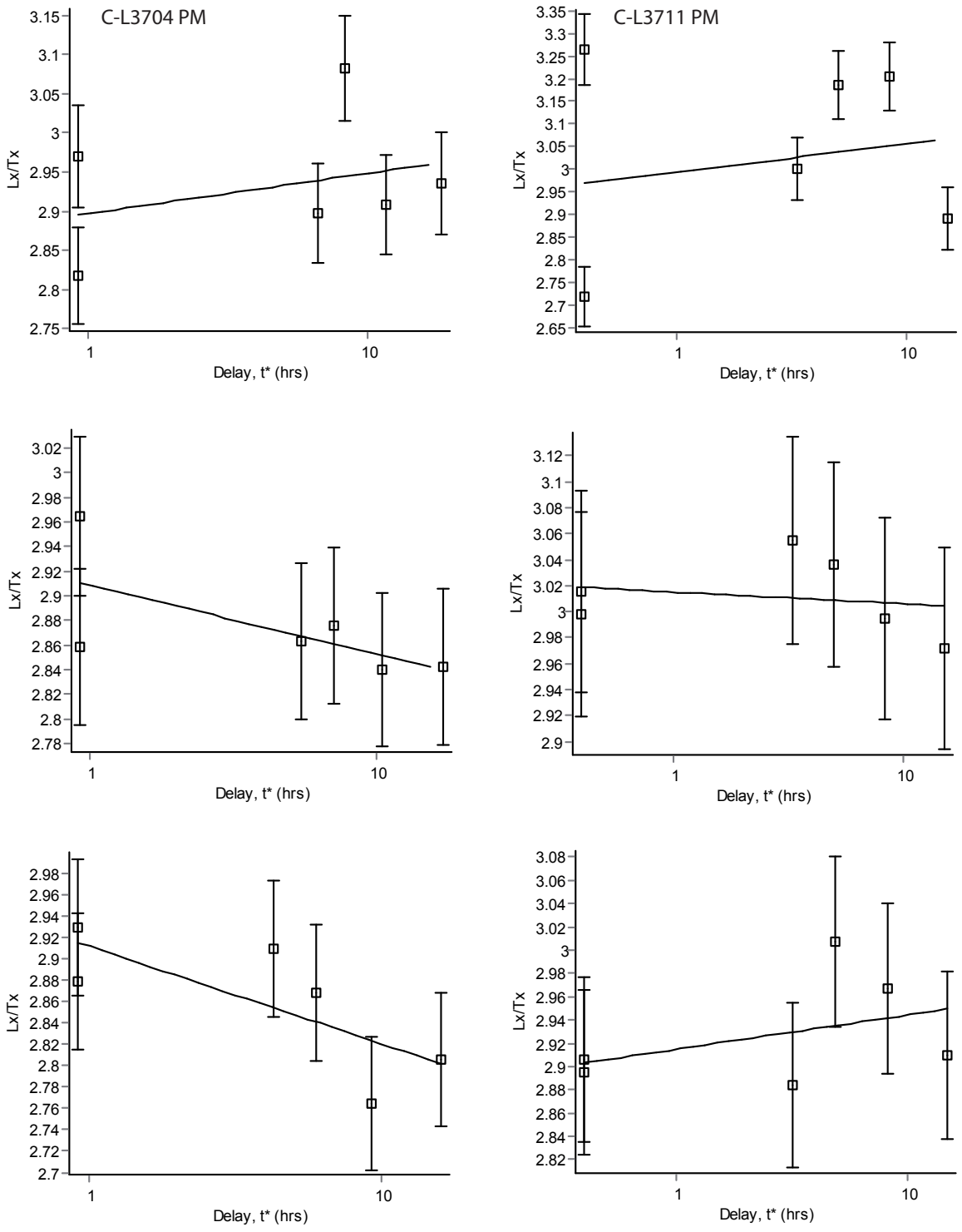

Figure E.2.: Plots showing the fading experiments. The normalized luminescence signal (L_x/T_x) is plotted against delay time. A linear function was used for fitting. The plots on the left hand side show three measurements of C-L3704, while the plots on the right hand side show three measurements of C-L3711. Analyst version 4.14.6 was used to generate the plots (Duller, 2015a).

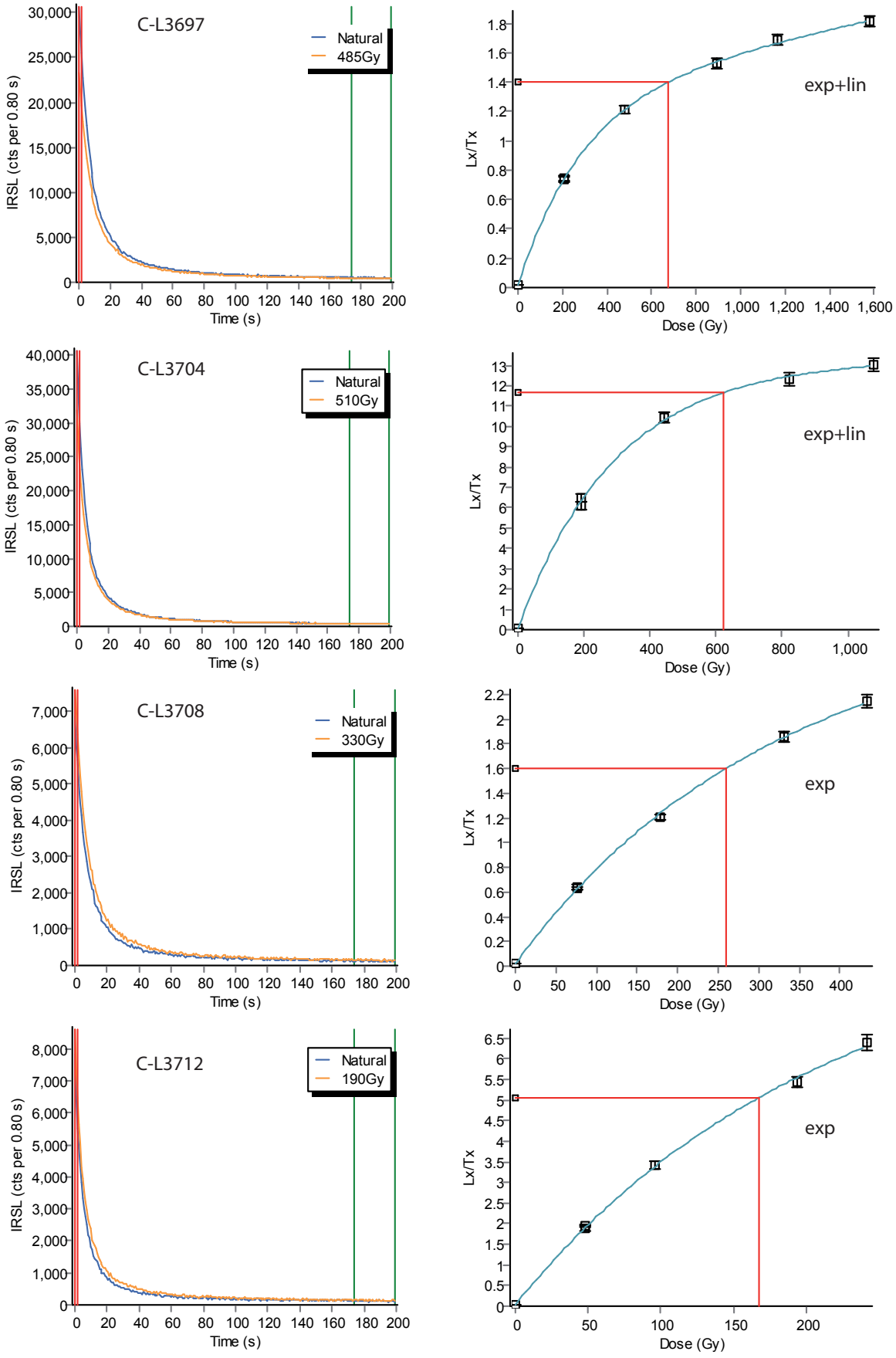

Figure E.3.: Shine down and growth curves of the polymineral fraction of samples C-L3697, C-L3704, C-L3708, and C-L3712. Single saturating exponential (exp) or exponential plus linear functions (exp+lin) were used for fitting the growth curves. Plots were generated with Analyst v. 4.31.7 (Duller, 2015a).

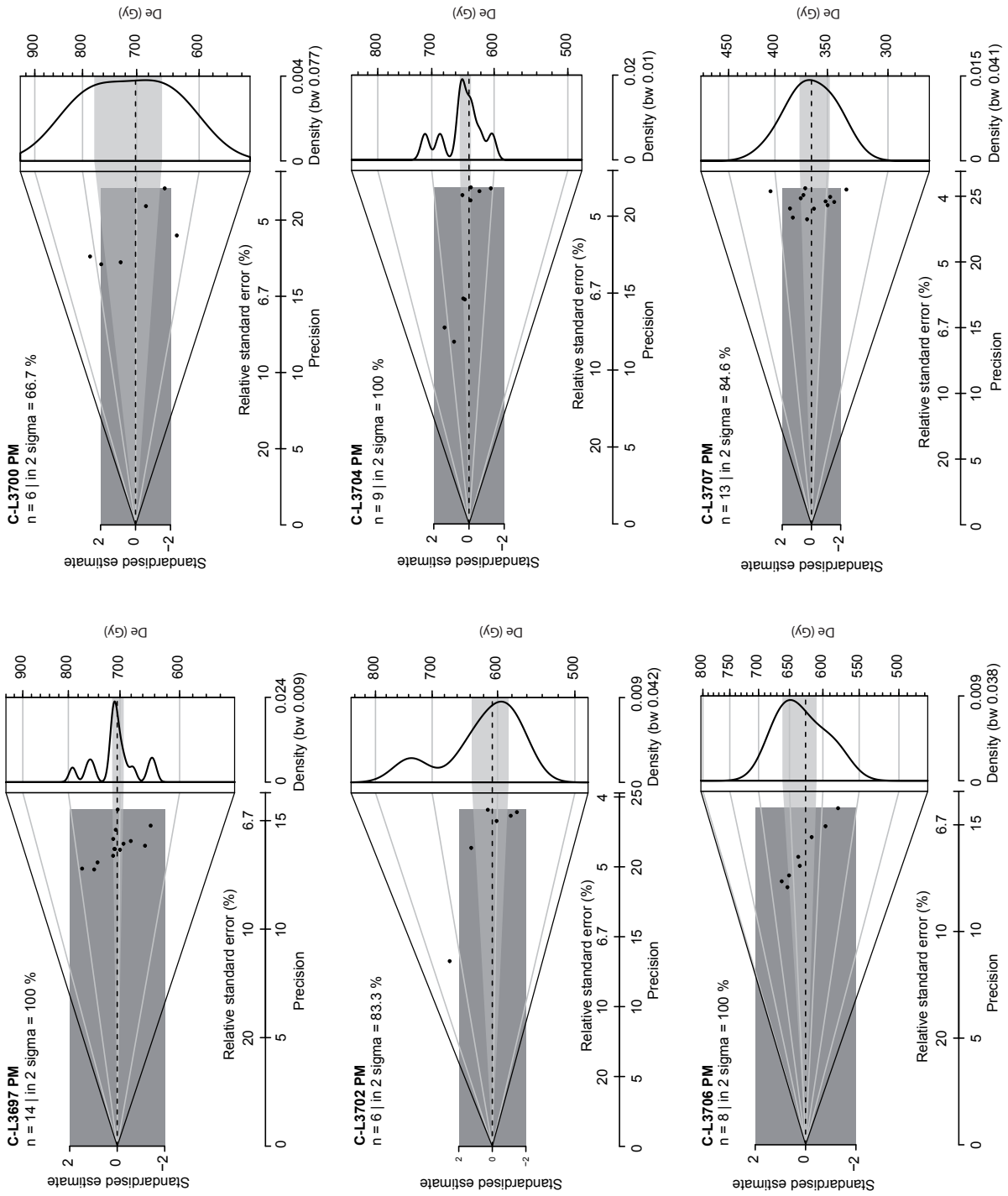

Figure E.4.: Abanico plots of D_e distributions of the polymineral samples C-L3697, C-L3700, C-L3702, C-L3704, C-L3706, and C-L3707 generated using the R luminescence package (Dietze et al., 2016).

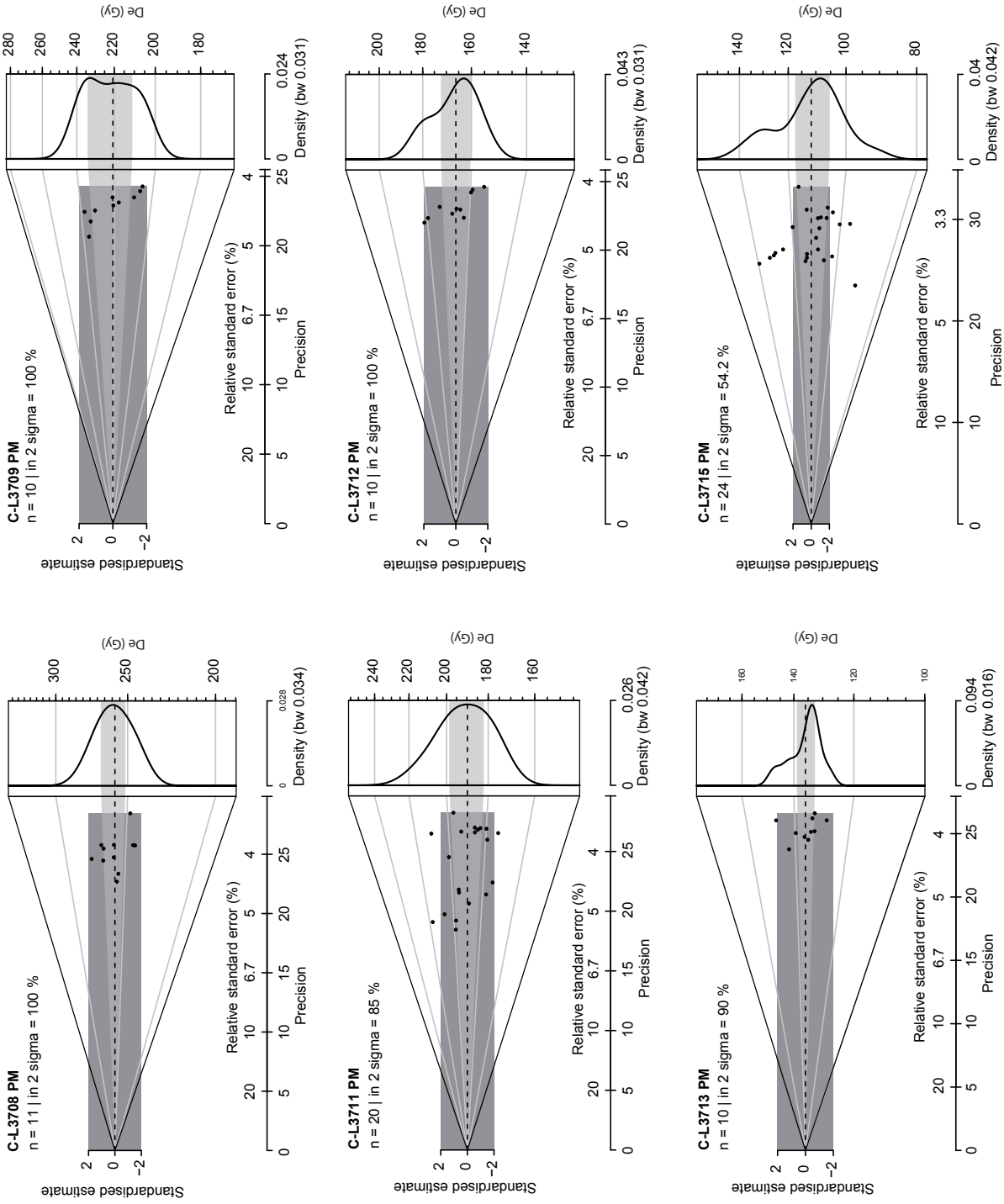

Figure E.5.: Abanico plots of D_e distributions of the polymineral samples C-L3708, C-L3709, C-L3711, C-L3712, C-L3713, and C-L3715 generated using the R luminescence package (Dietze et al., 2016).

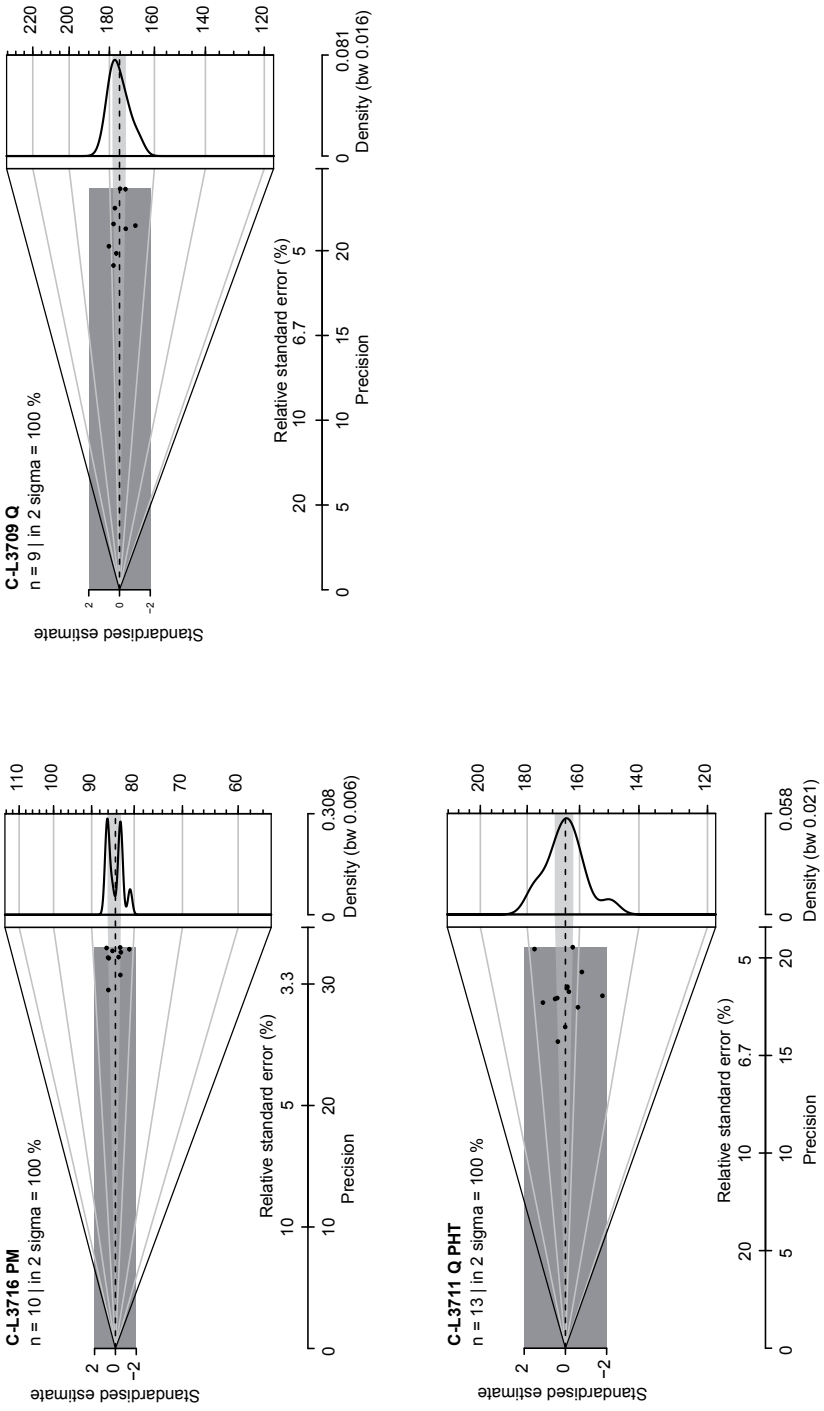

Figure E.6.: Abanico plots of D_e distributions of the polymineral sample C-L3716, and the quartz samples C-L3709, and C-L3711 generated using the R luminescence package (Dietze et al., 2016). The latter one depicts the aliquots within the plateau in the preheat plateau test.

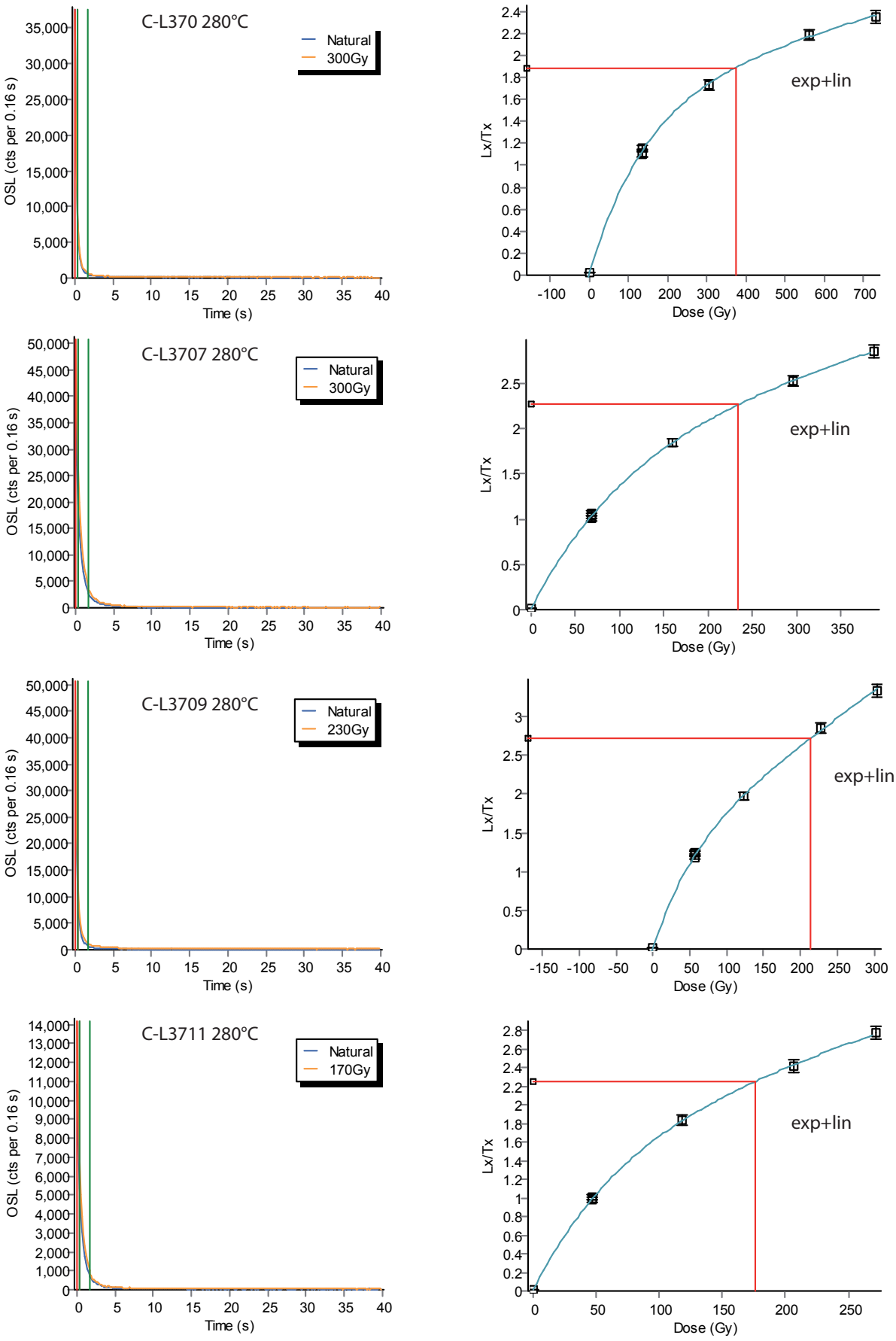

Figure E.7.: Shine down and growth curves of the quartz fraction of samples C-L3700, C-L3707, C-L3709, and C-L3711. All examples show measurements with a preheat temperature of $280°C$. Exponential plus linear functions were used for fitting the growth curves. Plots were generated with Analyst v. 4.31.7 (Duller, 2015a).

Bibliography

Adams, B. (2007). Gulyás archaeology: the Szeletian and the Middle to Upper Palaeolithic transition in Hungary and Central Europe. *BAR International Series* 1620, pages 91–110.

Aitken, M. J. (1985a). Alpha particle effectiveness: numerical relationship between systems. *Ancient TL* 3, pages 22–25.

Aitken, M. J. (1985b). *Thermoluminescence dating*. Academic press, London. 359 pages.

Aitken, M. J. (1997). Luminescence Dating. In: *Chronometric Dating in Archaeology*. Edited by R. E. Taylor and M. J. Aitken. Advances in Archaeological and Museum Science 2. Springer US, pages 183–216. DOI: 10.1007/978-1-4757-9694-0_7.

Aitken, M. J. (1998). *An introduction to optical dating: the dating of Quaternary sediments by the use of photon-stimulated luminescence*. Oxford University Press, New York. 267 pages.

Allen, J. R. L. and Thornley, D. M. (2004). Laser granulometry of Holocene estuarine silts: effects of hydrogen peroxide treatment. *The Holocene* 14 (2), pages 290–295. DOI: 10.1191/0959683604hl681rr.

Andersen, K. K. et al. (2004). High-resolution record of Northern Hemisphere climate extending into the last interglacial period. *Nature* 431, pages 147–151. DOI: 10.1038/nature02805.

Andersen, K. K. et al. (2006). The Greenland Ice Core Chronology 2005, 15–42 ka. Part 1: constructing the time scale. *Quaternary Science Reviews* 25 (23), pages 3246–3257. DOI: 10.1016/j.quascirev.2006.08.002.

Anghelinu, M., Niţă, L., Sitlivy, V., Uthmeier, T., and Băltean, I. (2012). Looking around Peştera Cu Oase: The beginnings of Upper Paleolithic in Romania. *Quaternary International* 274, pages 136–157. DOI: 10.1016/j.quaint.2012.01.012.

Ankjærgaard, C. (2010). Understanding optically stimulated charge movement in quartz and feldspar using time-resolved measurements. PhD thesis. Technical University of Denmark. Risø National Laboratory for Sustainable Energy. 230 pages.

Ant, H. (1963). *Faunistische, ökologische und tiergeographische Untersuchungen zur Verbreitung der Landschnecken in Nordwestdeutschland*. Landesmuseum für Naturkunde. 125 pages.

Antoine, P., Rousseau, D.-D., Fuchs, M., Hatté, C., Gauthier, C., Marković, S. B., Jovanović, M., Gaudenyi, T., Moine, O., and Rossignol, J. (2009). High-resolution record of the last climatic cycle in the southern Carpathian Basin (Surduk, Vojvodina, Serbia). *Quaternary International* 198 (1), pages 19–36. DOI: 10.1016/j.quaint.2008.12.008.

Auclair, M., Lamothe, M., and Huot, S. (2003). Measurement of anomalous fading for feldspar IRSL using SAR. *Radiation Measurements* 37 (4), pages 487–492. DOI: 10.1016/S1350-4487(03)00018-0.

Bábek, O., Chlachula, J., and Grygar, T. M. (2011). Non-magnetic indicators of pedogenesis related to loess magnetic enhancement and depletion: Examples from the Czech Republic

and southern Siberia. *Quaternary Science Reviews* 30 (7), pages 967–979. DOI: 10.1016/j.quascirev.2011.01.009.

Bailey, R. (1997). Partial bleaching and the decay form characteristics of quartz osl. *Radiation Measurements* 27 (2), pages 123–136.

Bailey, R. (2010). Direct measurement of the fast component of quartz optically stimulated luminescence and implications for the accuracy of optical dating. *Quaternary Geochronology* 5, pages 559–568. DOI: 10.1016/j.quageo.2009.10.003.

Balescu, S., Lamothe, M., Mercier, N., Huot, S., Balteanu, D., Billard, A., and Hus, J. (2003). Luminescence chronology of Pleistocene loess deposits from Romania: testing methods of age correction for anomalous fading in alkali feldspars. *Quaternary Science Reviews* 22 (10), pages 967–973. DOI: 10.1016/S0277-3791(03)00056-8.

Balescu, S., Lamothe, M., Panaiotu, C., and Panaiotu, C. (2010). La chronologie IRSL des séquences lœssiques de l'est de la Roumanie. *Quaternaire* 21 (2), pages 115–126. DOI: 10.4000/quaternaire.5488.

Ballarini, M., Wallinga, J., Wintle, A., and Bos, A. (2007). A modified SAR protocol for optical dating of individual grains from young quartz samples. *Radiation Measurements* 42 (3), pages 360–369. DOI: 10.1016/j.radmeas.2006.12.016.

Bălteanu, D., Jurchescu, M., Surdeanu, V., Ionita, I., Goran, C., Urdea, P., Rădoane, M., Rădoane, N., and Sima, M. (2012). Recent Landform Evolution in the Romanian Carpathians and Pericarpathian Regions. In: *Recent Landform Evolution: The Carpatho-Balkan-Dinaric Region*. Springer, pages 249–286.

Banerjee, D., Bøtter-Jensen, L., and Murray, A. S. (2000). Retrospective dosimetry: estimation of the dose to quartz using the single-aliquot regenerative-dose protocol. *Applied Radiation and Isotopes* 52 (4), pages 831–844.

Barry, R. (2008). *Mountain weather and climate*. Cambridge University Press, Cambridge. 506 pages.

Bartz, M., Rixhon, G., Kehl, M., El Ouahabi, M., Klasen, N., Brill, D., Weniger, G.-C., Mikdad, A., and Brückner, H. (2017). Unravelling fluvial deposition and pedogenesis in ephemeral stream deposits in the vicinity of the prehistoric rock shelter of Ifri n'Ammar (NE Morocco) during the last 100 ka. *CATENA* 152, pages 115–134. DOI: 10.1016/j.catena.2016.12.007.

Basarin, B., Vandenberghe, D. A. G., Marković, S. B., Catto, N., Hambach, U., Vasiliniuc, Ş., Derese, C., Rončević, S., Vasiljević, D. A., and Rajić, L. (2011). The Belotinac section (Southern Serbia) at the southern limit of the European loess belt: Initial results. *Quaternary International* 240 (1), pages 128–138. DOI: 10.1016/j.quaint.2011.02.022.

Basarin, B., Buggle, B., Hambach, U., Marković, S. B., Dhand, K. O., Kovačević, A., Stevens, T., Guo, Z., and Lukić, T. (2014). Time-scale and astronomical forcing of Serbian loess–paleosol sequences. *Global and Planetary Change* 122, pages 89–106. DOI: 10.1016/j.gloplacha.2014.08.007.

Baumgart, P., Hambach, U., Meszner, S., and Faust, D. (2013). An environmental magnetic fingerprint of periglacial loess: Records of Late Pleistocene loess–palaeosol sequences from Eastern Germany. *Quaternary International* 296, pages 82–93. DOI: 10.1016/j.quaint.2012.12.021.

Bell, W. (1980). Alpha dose attenuation in quartz grains for thermoluminescence dating. *Ancient TL* 12, pages 4–8.

Bennett, K. D., Tzedakis, P. C., and Willis, K. J. (1991). Quaternary Refugia of North European Trees. *Journal of Biogeography* 18 (1), page 103. DOI: 10.2307/2845248.

Berg, L. (1916). The origin of loess [in Russian]. *Izv. Russ. Geog. Obsh.* 52, pages 579–646.

Berger, G. W. (1991). The use of glass for dating volcanic ash by thermoluminescence. *J. Geophys. Res.* 96 (B12), pages 19705–19720. DOI: 10.1029/91JB01899.

Biswas, R. H., Williams, M. A. J., Raj, R., Juyal, N., and Singhvi, A. K. (2013). Methodological studies on luminescence dating of volcanic ashes. *Quaternary Geochronology* 17, pages 14–25. DOI: 10.1016/j.quageo.2013.03.004.

Bocherens, H. (2003). Isotopic biogeochemistry and the paleoecology of the mammoth steppe fauna. *Deinsea* 9, pages 57–76.

Bocherens, H., Pacaud, G., Lazarev, P. A., and Mariotti, A. (1996). Stable isotope abundances (13C, 15N) in collagen and soft tissues from Pleistocene mammals from Yakutia: Implications for the palaeobiology of the Mammoth Steppe. *Palaeogeography, Palaeoclimatology, Palaeoecology* 126 (1-2), pages 31–44. DOI: 10.1016/S0031-0182(96)00068-5.

Bokhorst, M., Vandenberghe, J., Sümegi, P., Łanczont, M., Gerasimenko, N., Matviishina, Z., Marković, S. B., and Frechen, M. (2011). Atmospheric circulation patterns in central and eastern Europe during the Weichselian Pleniglacial inferred from loess grain-size records. *Quaternary International* 234 (1), pages 62–74. DOI: 10.1016/j.quaint.2010.07.018.

Bösken, J., Klasen, N., Zeeden, C., Obreht, I., Marković, S. B., Hambach, U., and Lehmkuhl, F. (2017a). New luminescence-based geochronology framing the last two glacial cycles at the southern limit of European Pleistocene loess in Stalać (Serbia). *Geochronometria* 44, pages 150–161. DOI: 10.1515/geochr-2015-0062.

Bösken, J., Obreht, I., Zeeden, C., Klasen, N., Sümegi, P., Marković, S. B., and Lehmkuhl, F. (2014). Environmental conditions on the corridor of human migration between 40,000 and 14,000 a BP in the Balkan region. A multi-proxy approach on loess-paleosol profiles. In: *Late Pleistocene and Holocene Climatic Variability in the Carpathian-Balkan Region*. Marcel Mindrescu & Ionela Gradinaru (Eds.) Cluj-Napoca, Romania, pages 11–15.

Bösken, J., Sümegi, P., Zeeden, C., Klasen, N., Gulyás, S., and Lehmkuhl, F. (2017b). Investigating the last glacial Gravettian site 'Ságvár Lyukas Hill' (Hungary) and its paleoenvironmental and geochronological context using a multi-proxy approach. *Palaeogeography, Palaeoclimatology, Palaeoecology*.

Bösken, J., Zeeden, C., Klasen, N., Obreht, I., Hambach, U., Sümegi, P., and Lehmkuhl, F. (2017c). Paleoclimatic proxy data from the MIS3/2 transition recorded at the Bodrogkeresztúr loess-paleosol sequence in Northeast Hungary. *CRC806-Database*. DOI: 10.5880/SFB806.38.

Bøtter-Jensen, L., McKeever, S. W. S., and Wintle, A. G. (2003). *Optically Stimulated Luminescence Dosimetry*. Elsevier, Amsterdam, The Netherlands. 355 pages.

Bradák, B. (2009). Application of anisotropy of magnetic susceptibility (AMS) for the determination of paleo-wind directions and paleo-environment during the accumulation period of Bag Tephra, Hungary. *Quaternary International* 198 (1), pages 77–84. DOI: 10.1016/j.quaint.2007.11.005.

Brennan, B. (2003). Beta doses to spherical grains. *Radiation Measurements* 37 (4), pages 299–303. DOI: 10.1016/S1350-4487(03)00011-8.

Brill, D., Jankaew, K., and Brückner, H. (2015). Holocene evolution of Phra Thong's beach-ridge plain (Thailand) — Chronology, processes and driving factors. *Geomorphology* 245, pages 117–134. DOI: 10.1016/j.geomorph.2015.05.035.

Buggle, B., Glaser, B., Zöller, L., Hambach, U., Marković, S. B., Glaser, I., and Gerasimenko, N. (2008). Geochemical characterization and origin of Southeastern and Eastern European loesses (Serbia, Romania, Ukraine). *Quaternary Science Reviews* 27 (9), pages 1058–1075. DOI: 10.1016/j.quascirev.2008.01.018.

Buggle, B., Hambach, U., Glaser, B., Gerasimenko, N., Marković, S. B., Glaser, I., and Zöller, L. (2009). Stratigraphy, and spatial and temporal paleoclimatic trends in Southeastern/Eastern European loess–paleosol sequences. *Quaternary International* 196 (1), pages 86–106. DOI: 10.1016/j.quaint.2008.07.013.

Buggle, B., Glaser, B., Hambach, U., Gerasimenko, N., and Marković, S. B. (2011). An evaluation of geochemical weathering indices in loess–paleosol studies. *Quaternary International* 240 (1), pages 12–21. DOI: 10.1016/j.quaint.2010.07.019.

Buggle, B., Hambach, U., Kehl, M., Marković, S. B., Zöller, L., and Glaser, B. (2013). The progressive evolution of a continental climate in southeast-central European lowlands during the Middle Pleistocene recorded in loess paleosol sequences. *Geology* 41 (7), pages 771–774. DOI: 10.1130/G34198.1.

Buggle, B., Hambach, U., Müller, K., Zöller, L., Marković, S. B., and Glaser, B. (2014). Iron mineralogical proxies and Quaternary climate change in SE-European loess–paleosol sequences. *CATENA* 117, pages 4–22. DOI: 10.1016/j.catena.2013.06.012.

Burow, C., Zens, J., Kreutzer, S., Dietze, M., Fuchs, M. C., Fischer, M., Schmidt, C., and Brückner, H. (2016). Exploratory data analysis using the R package 'Luminescence' - towards data mining in OSL applications. In: UK Luminescence and ESR Meeting 2016. Liverpool, page 38.

Buylaert, J.-P., Murray, A. S., Thomsen, K., and Jain, M. (2009). Testing the potential of an elevated temperature IRSL signal from K-feldspar. *Radiation Measurements* 44 (5), pages 560–565. DOI: 10.1016/j.radmeas.2009.02.007.

Buylaert, J.-P., Jain, M., Murray, A. S., Thomsen, K. J., Thiel, C., and Sohbati, R. (2012). A robust feldspar luminescence dating method for Middle and Late Pleistocene sediments: Feldspar luminescence dating of Middle and Late Pleistocene sediments. *Boreas* 41 (3), pages 435–451. DOI: 10.1111/j.1502-3885.2012.00248.x.

Chapot, M. S., Roberts, H. M., Duller, G. A. T., and Lai, Z. P. (2012). A comparison of natural- and laboratory-generated dose response curves for quartz optically stimulated luminescence signals from Chinese Loess. *Radiation Measurements* 47 (11), pages 1045–1052. DOI: 10.1016/j.radmeas.2012.09.001.

Chu, W., Lengyel, G., Zeeden, C., Péntek, A., Kaminská, Ľ., and Mester, Z. (2017). Early Upper Paleolithic surface collections from loess-like sediments in the northern Carpathian Basin. *Quaternary International*. DOI: 10.1016/j.quaint.2017.05.017.

Chu, W., Hauck, T., and Mihailovic, D. (2014). Crvenka-At– preliminary results from a lowland Aurignacian site in the middle Danube catchment. In: *Palaeolithic and Mesolithic Research in the Central Balkans*. Belgrade, pages 69–75.

Chu, W., Zeeden, C., and Petrescu, S. (2016). The Early Upper Paleolithic of the Banat and recent research at the Paleolithic site of Tincova. *Banatica* 26, pages 51–72.

Conard, N. J. and Bolus, M. (2003). Radiocarbon dating the appearance of modern humans and timing of cultural innovations in Europe: new results and new challenges. *Journal of human Evolution* 44 (3), pages 331–371.

Conard, N. J. and Bolus, M. (2008). Radiocarbon dating of the late Middle Paleolithic and the Aurignacian of the Swabian Jura. *Journal of Human Evolution* 55, pages 886–897. DOI: 10.1016/j.jhevol.2008.08.006.

Constable, C. and Tauxe, L. (1990). The bootstrap for magnetic susceptibility tensors. *Journal of Geophysical Research* 95 (B6), pages 8383–8395. DOI: 10.1029/JB095iB06p08383.

Constantin, D., Begy, R., Vasiliniuc, Ş., Panaiotu, C., Necula, C., Codrea, V., and Timar-Gabor, A. (2014). High-resolution OSL dating of the Costineşti section (Dobrogea, SE Romania) using fine and coarse quartz. *Quaternary International* 334-335, pages 20–29. DOI: 10.1016/j.quaint.2013.06.016.

Constantin, D., Cameniţă, A., Panaiotu, C., Necula, C., Codrea, V., and Timar-Gabor, A. (2015). Fine and coarse-quartz SAR-OSL dating of Last Glacial loess in Southern Romania. *Quaternary International* 357. DOI: 10.1016/j.quaint.2014.07.052.

Csongrádiné, B. (1997). Ságvár – késői felsőpaleolit telep (a kőeszközkészlet tipológiai vizsgálata). *FolArch* 46, pages 17–46.

Csontos, L., Nagymarosy, A., Horváth, F., and Kovac, M. (1992). Tertiary evolution of the Intra-Carpathian area: a model. *Tectonophysics* 208 (1), pages 221–241.

Curie, D. (1963). *Luminescence in crystals [translated from the French edition (1960) by G. F. J. Garlick.]* Methuen, London; Wiley, New York. 332 pages.

De Vivo, B., Rolandi, G., Gans, P. B., Calvert, A., Bohrson, W. A., Spera, F. J., and Belkin, H. E. (2001). New constraints on the pyroclastic eruptive history of the Campanian volcanic Plain (Italy). *Mineralogy and Petrology* 73 (1), pages 47–65. DOI: 10.1007/s007100170010.

Derbyshire, E. (2003). Loess, and the Dust Indicators and Records of Terrestrial and Marine Palaeoenvironments (DIRTMAP) database. *Quaternary Science Reviews* 22 (18), pages 1813–1819. DOI: 10.1016/S0277-3791(03)00209-9.

Dietze, M., Kreutzer, S., Fuchs, M. C., Burow, C., Fischer, M., and Schmidt, C. (2013). A practical guide to the R package Luminescence. *Ancient TL* 31 (1), pages 11–18.

Dietze, M., Kreutzer, S., Burow, C., Fuchs, M. C., Fischer, M., and Schmidt, C. (2016). The abanico plot: Visualising chronometric data with individual standard errors. *Quaternary Geochronology* 31, pages 12–18. DOI: 10.1016/j.quageo.2015.09.003.

DIN ISO 11277 (2002). Soil Quality - Determination of particle size distribution in mineral soil material - method by sieving and sedimentation. *International Organization for Standardization, Geneva.*

Ding, Z. L., Ranov, V., Yang, S. L., Finaev, A., Han, J. M., and Wang, G. A. (2002). The loess record in southern Tajikistan and correlation with Chinese loess. *Earth and Planetary Science Letters* 200 (3), pages 387–400. DOI: 10.1016/S0012-821X(02)00637-4.

Dobosi, V. T. (2000). Archaeological investigations at Bodrogkeresztúr-Henye. *Bodrogkeresztur-Henye, NE Hungary, Upper Palaeolithic Site. Magyar Nemzeti Múzeum.*

Dolić, D., Kalenić, M., Lončarević, Č., and Hadži-Vuković, M. (1980). *Paraćin.* Savezni geološki zavod, Laboratorija za metode geološkog kartiranja Rudarsko, geološkog fakulteta, Vojnogegrafski institute, Belgrade, Serbia.

Duller, G. (2003). Distinguishing quartz and feldspar in single grain luminescence measurements. *Radiation Measurements* 37 (2), pages 161–165. DOI: 10.1016/S1350-4487(02)00170-1.

Duller, G. (2004). Luminescence dating of Quaternary sediments: recent advances. *Journal of Quaternary Science* 19 (2), pages 183–192.

Duller, G. (2015a). *Analyst User Manual v4.31.7.* Aberystwyth Luminescence Research Laboratory, Aberystwyth University.

Duller, G. (2015b). Luminescence Dating. *Encyclopedia of Scientific Dating Methods*, pages 390–404. DOI: 10.1007/978-94-007-6326-5_125-1.

Durcan, J. A., King, G. E., and Duller, G. A. (2015). DRAC: Dose Rate and Age Calculator for trapped charge dating. *Quaternary Geochronology* 28, pages 54–61. DOI: 10.1016/j.quageo.2015.03.012.

Evans, J. G. (1972). *Land snails in archaeology.* Seminar Press, London. 436 pages.

Farr, T. G. et al. (2007). The Shuttle Radar Topography Mission. *Reviews of Geophysics* 45 (2). DOI: 10.1029/2005RG000183.

Feurdean, A., Perşoiu, A., Tanţău, I., Stevens, T., Magyari, E. K., Onac, B. P., Marković, S. B., Andrič, M., Connor, S., Fărcaş, S., et al. (2014). Climate variability and associated vegetation response throughout Central and Eastern Europe (CEE) between 60 and 8 ka. *Quaternary Science Reviews* 106, pages 206–224.

Fitzsimmons, K. E. and Hambach, U. (2014). Loess accumulation during the last glacial maximum: Evidence from Urluia, southeastern Romania. *Quaternary International* 334-335, pages 74–85. DOI: 10.1016/j.quaint.2013.08.005.

Fitzsimmons, K. E., Hambach, U., Veres, D., and Iovita, R. (2013). The Campanian Ignimbrite Eruption: New Data on Volcanic Ash Dispersal and Its Potential Impact on Human Evolution. *PLoS ONE* 8 (6), e65839. DOI: 10.1371/journal.pone.0065839.

Fitzsimmons, K. E., Sprafke, T., Zielhofer, C., Günter, C., Deom, J.-M., Sala, R., and Iovita, R. (2016). Loess accumulation in the Tian Shan piedmont: Implications for palaeoenvironmental change in arid Central Asia. *Quaternary International.* DOI: 10.1016/j.quaint.2016.07.041.

Floss, H., Fröhle, S., and Wettengl, S. (2016). The Aurignacian along the Danube - Its Two-Fold Role as a Transalpine and Cisalpine Passageway of Early Homo Sapiens into Europe. In: *Proceedings of the International Workshop within the Collaborative Research Centres sfb 1070 "RessourcenKulturen", Schloss Hohentübingen, 9th of May 2014.* Southeast Europe before Neolithisation. Universität Tübingen: Krauss, R. and Floss, H. (Eds.), pages 13–39.

Fodor, L., Csontos, L., Bada, G., Györfi, I., and Benkovics, L. (1999). Tertiary tectonic evolution of the Pannonian Basin system and neighbouring orogens: a new synthesis of palaeostress data. *Geological Society, London, Special Publications* 156 (1), pages 295–334.

Forster, T., Evans, M. E., and Heller, F. (1994). The frequency dependence of low field susceptibility in loess sediments. *Geophysical Journal International* 118 (3), pages 636–642. DOI: 10.1111/j.1365-246X.1994.tb03990.x.

Frechen, M., Oches, E. A., and Kohfeld, K. E. (2003). Loess in Europe—mass accumulation rates during the Last Glacial Period. *Quaternary Science Reviews* 22 (18), pages 1835–1857. DOI: 10.1016/S0277-3791(03)00183-5.

Fu, Q. et al. (2015). An early modern human from Romania with a recent Neanderthal ancestor. *Nature* 524 (7564), pages 216–219. DOI: 10.1038/nature14558.

Fuchs, M., Rousseau, D.-D., Antoine, P., Hatté, C., Gauthier, C., Marković, S. B., and Zöller, L. (2008). Chronology of the Last Climatic Cycle (Upper Pleistocene) of the Surduk loess sequence, Vojvodina, Serbia. *Boreas* 37 (1), pages 66–73. DOI: 10.1111/j.1502-3885.2007.00012.x.

Furlan, D. (1977). The climate of Southeast Europe. World Survey of Climatology 6, Climate of central and southern Europe, Elsevier, Amsterdam/Oxford/New York. Edited by C. C. Wallen, pages 185–235.

Gábori, M. (1959). Urjanchaische Waldjäger in der NW-Mongolei und ihre archäologischen Beziehungen. *Acta Archaeologica Academiae Scientiarum Hungaricae* 11.

Gábori, M. (1965). Der zweite paläolithische Hausgrundriss von Ságvár. *Acta Archaeologica Hungaria* 17, pages 111–127.

Gábori, M. (1969). Paläolithische Schneckendepots von Szob. *Acta Archaeologica Hungaria* 29, pages 3–11.

Gábori, M. (1989). Die letzte Phase des Paläolithikums in Ungarn. *Quartär* 39, pages 131–140.

Gábori, M. and Gábori-Csánk, V. (1957). Ètudes archéologiques et stratigraphiques dans les stations de loess paléolithiques de Hongrie. *Acta Archaeologica Hungaria* 8, pages 3–116.

Gábori-Csánk, V. (1978). Une oscillation climatique a la fin du Würm en Hongrie. *Acta Archaeologica Academiae Scientiarum Hungaricae Budapest* 30 (1), pages 3–12.

Gábori-Csánk, V. (1984). A felső paleolithikum nyoma Budapesten (The prints of Upper Paleolithic in Budapest). *Budapest Régiségei* 25, pages 7–14.

Gáboriné Csánk, V. (1960). A ságvári telep abszolút kormeghatározása. *ArchÉrt* 87, pages 125–129.

Galbraith, R. F., Roberts, R. G., Laslett, G. M., Yoshida, H., and Olley, J. M. (1999). Optical dating of single and multiple grains of quartz from jinmium rock shelter, northern australia: part i, experimental design and statistical models*. *Archaeometry* 41 (2), pages 339–364.

Gallus, S. (1936). A nagytétényi neolithikus sír. *Archaeologiai Értesítő* 49, pages 85–86.

Galović, L. (2016). Sedimentological and mineralogical characteristics of the Pleistocene loess/paleosol sections in the Eastern Croatia. *Aeolian Research* 20, pages 7–23. DOI: 10.1016/j.aeolia.2015.10.007.

Gheorghiu, A. and Haas, N. (1954). Date privind omul primitiv de la Baia de Fier: Consideratii paleoantropologice. *Sesiunea Sectiunii de Stiinte Medicale a Academiei RPR* 41, pages 641–63.

Grün, R. (1989). Electron spin resonance (ESR) dating. *Quaternary International* 1, pages 65–109. DOI: 10.1016/1040-6182(89)90010-4.

Grün, R. (2001). Trapped charge dating (ESR, TL, OSL). In: *Handbook of archaeological sciences*. John Wiley & Sons Inc.

Guérin, G., Mercier, N., and Adamiec, G. (2011). Dose-rate conversion factors: Update. *Ancient TL* 29 (1), pages 5–8.

Guérin, G., Mercier, N., Nathan, R., Adamiec, G., and Lefrais, Y. (2012). On the use of the infinite matrix assumption and associated concepts: A critical review. *Radiation Measurements* 47 (9), pages 778–785. DOI: 10.1016/j.radmeas.2012.04.004.

Guo, Z. T., Ruddiman, W. F., Hao, Q. Z., Wu, H. B., Quia, Y. S., Zhu, R. X., Peng, S. Z., Wei, J. J., Yuan, B. Y., and Liu, T. S. (2002). Onset of Asian desertification by 22 Myrs ago inferred from loess deposits in China. *Nature* 416 (6877), pages 159–163.

Gyalog, L. and Síkhegyi, F. (2005). *Magyarország Földtani Térképe 1:100000, a Magyar Àllami Földtani Intézet kiadványa*. Budapest.

Haas, J. (2012). Geological and Tectonic Setting. In: *Recent Landform Evolution: the Carpatho-Balkan-Dinaric Region*. Springer Science & Business Media, pages 3–18.

Haase, D., Fink, J., Haase, G., Ruske, R., Pécsi, M., Richter, H., Altermann, M., and Jäger, K.-D. (2007). Loess in Europe—its spatial distribution based on a European Loess Map, scale 1:2,500,000. *Quaternary Science Reviews* 26 (9), pages 1301–1312. DOI: 10.1016/j.quascirev.2007.02.003.

Haesaerts, P., Borziac, I., Chekha, V. P., Chirica, V., Damblon, F., Drozdov, N. I., Orlova, L. A., Pirson, S., and Plicht, J. v. d. (2009). Climatic Signature and Radiocarbon Chronology of Middle and Late Pleniglacial Loess from Eurasia: Comparison with the Marine and Greenland Records. *Radiocarbon* 51 (1), pages 301–318. DOI: 10.2458/azu_js_rc.51.3492.

Hambach, U., Zeeden, C., Hark, M., and Zöller, L. (2008). Magnetic dating of an Upper Palaeolithic cultural layer bearing loess from the Krems-Wachtberg site (Lower Austria). *Abh. Geol. Bundesanst.* 62, pages 153–157.

Händel, M., Simon, U., Einwögerer, T., and Neugebauer-Maresch, C. (2009). Loess deposits and the conservation of the archaeological record—The Krems-Wachtberg example. *Quaternary International* 198 (1), pages 46–50. DOI: 10.1016/j.quaint.2008.07.005.

Hao, Q., Oldfield, F., Bloemendal, J., and Guo, Z. (2008). Particle size separation and evidence for pedogenesis in samples from the Chinese Loess Plateau spanning the past 22 my. *Geology* 36 (9), pages 727–730.

Harrison, S. P., Kohfeld, K. E., Roelandt, C., and Claquin, T. (2001). The role of dust in climate changes today, at the last glacial maximum and in the future. *Earth-Science Reviews* 54 (1), pages 43–80.

Hauck, T. C., Lehmkuhl, F., Zeeden, C., Bösken, J., Thiemann, A., and Richter, J. (2017). The Aurignacian way of life: Contextualizing early modern human adaptation in the Carpathian Basin. *Quaternary International* xxx. DOI: 10.1016/j.quaint.2017.10.020.

Heller, F., Liu, X., Liu, T., and Xu, T. (1991). Magnetic susceptibility of loess in China. *Earth and Planetary Science Letters* 103 (1), pages 301–310. DOI: 10.1016/0012-821X(91)90168-H.

Heller, F. and Tungsheng, L. (1984). Magnetism of Chinese loess deposits. *Geophysical Journal International* 77 (1), pages 125–141. DOI: 10.1111/j.1365-246X.1984.tb01928.x.

Hertelendi, E., Sümegi, P., and Szöőr, G. (1992). Geochronologic and palaeoclimatic characterization of Quaternary sediments in the Great Hungarian Plain. *Radiocarbon* 34, pages 833–839.

Hervella, M. et al. (2016). The mitogenome of a 35,000-year-old Homo sapiens from Europe supports a Palaeolithic back-migration to Africa. *Scientific Reports* 6. DOI: 10.1038/srep25501.

Hess, M. (1965). Vertical climatic zones in the Polish Western Carpathians. *Zeszyty Naukowe Uniwersytetu Jagiellońskiego, Prace Geograficzne* 11, pages 1–258.

Hess, M. (1971). Piętra klimatyczne w Kawrpatach Północnych i Południowych i ich charakterystyka termiczna (Vertical climatic zones in north and south Carpathians and their thermic characteristics). *Folia Geogr Ser Geogr Phy Kraków* 5, pages 15–23.

Hilgers, A. (2007). The chronology of Late Glacial and Holocene dune development in the northern Central European lowland reconstructed by optically stimulated luminescence (OSL) dating. PhD thesis. Universität zu Köln. 440 pages.

Horsák, M., Juřičková, L., Kintrová, K., and Hájek, O. (2009). Patterns of land snail diversity over a gradient of habitat degradation: a comparison of three Czech cities. *Biodivers Conserv* 18 (13), page 3453. DOI: 10.1007/s10531-009-9654-y.

Horsák, M., Lososová, Z., Čejka, T., Juřičková, L., and Chytrý, M. (2013). Diversity and Biotic Homogenization of Urban Land-Snail Faunas in Relation to Habitat Types and Macroclimate in 32 Central European Cities. *PLOS ONE* 8 (8), e71783. DOI: 10.1371/journal.pone.0071783.

Horváth, F., Bada, G., Szafián, P., Tari, G., Ádám, A., and Cloetingh, S. (2006). Formation and deformation of the Pannonian Basin: constraints from observational data. *Geological Society, London, Memoirs* 32 (1), pages 191–206.

Hošek, J., Hambach, U., Lisá, L., Grygar, T., Horáček, I., Meszner, S., and Knésl, I. (2015). An integrated rock-magnetic and geochemical approach to loess/paleosol sequences from Bohemia and Moravia (Czech Republic): Implications for the Upper Pleistocene paleoenvironment in central Europe. *Palaeogeogr. Palaeoclimatol. Palaeoecol.* 418, pages 344–358. DOI: 10.1016/j.palaeo.2014.11.024.

Huntley, D. and Baril, M. (1997). The K content of the K-feldspars being measured in optical dating or in thermoluminescence dating. *Ancient TL* 15 (1), pages 11–12.

Huntley, D. J., Godfrey-Smith, D. I., and Thewalt, M. L. (1985). Optical dating of sediments. *Nature* 313 (5998), pages 105–107.

Huntley, D. J. and Hancock, R. G. V. (2001). The Rb contents of the K-feldspar grains being measured in optical dating. *Ancient TL* 19 (2), pages 43–46.

Huntley, D. J. and Lamothe, M. (2001). Ubiquity of anomalous fading in K-feldspars and the measurement and correction for it in optical dating. *Canadian Journal of Earth Science* 38 (7), pages 1093–1106. DOI: 10.1139/e01-013.

Hupuczi, J. and Sümegi, P. (2010). The late pleistocene paleoenvironment and paleoclimate of the Madaras section (South Hungary), based on preliminary records from mollusks. *Central European Journal of Geosciences* 2 (1), pages 64–70. DOI: 10.2478/v10085-009-0044-1.

Hütt, G., Jaek, I., and Tchonka, J. (1988). Optical dating: K-feldspars optical response stimulation spectra. *Quaternary Science Reviews* 7 (3), pages 381–385.

Iovita, R., Fitzsimmons, K. E., Dobos, A., Hambach, U., Hilgers, A., and Zander, A. (2012). Dealul Guran: evidence for Lower Palaeolithic (MIS 11) occupation of the Lower Danube loess steppe. *Antiquity* 86 (334), pages 973–989.

Iovita, R., Doboş, A., Fitzsimmons, K. E., Probst, M., Hambach, U., Robu, M., Vlaicu, M., and Petculescu, A. (2014). Geoarchaeological prospection in the loess steppe: Preliminary results from the Lower Danube Survey for Paleolithic Sites (LoDanS). *Quaternary International* 351, pages 98–114. DOI: 10.1016/j.quaint.2013.05.018.

Iriondo, M. H. and Kröhling, D. M. (2007). Non-classical types of loess. *Sedimentary Geology* 202 (3), pages 352–368. DOI: 10.1016/j.sedgeo.2007.03.012.

ISO International Standard 13320 (2009). Particle size analysis — Laser diffraction methods. *International Organization for Standardization, Geneva*.

Jacobs, Z., Duller, G. A. T., and Wintle, A. G. (2003). Optical dating of dune sand from Blombos Cave, South Africa: II—single grain data. *Journal of Human Evolution* 44 (5), pages 613–625. DOI: 10.1016/S0047-2484(03)00049-6.

Jain, M. and Ankjærgaard, C. (2011). Towards a non-fading signal in feldspar: Insight into charge transport and tunnelling from time-resolved optically stimulated luminescence. *Radiation Measurements* 46 (3), pages 292–309. DOI: 10.1016/j.radmeas.2010.12.004.

Jain, M., Murray, A. S., and Bøtter-Jensen, L. (2003). Characterisation of blue-light stimulated luminescence components in different quartz samples: implications for dose measurement. *Radiation Measurements* 37 (4), pages 441–449. DOI: 10.1016/S1350-4487(03)00052-0.

Jelinek, V. (1977). The statistical theory of measuring anisotropy of magnetic susceptibility of rocks and its application. *Geofyzika, Brno* 87 (3), page 4.

Jipa, D. C. (2014). The conceptual sedimentary model of the Lower Danube loess basin: Sedimentogenetic implications. *Quaternary International* 351, pages 14–24. DOI: 10.1016/j.quaint.2013.06.008.

Jordanova, D. and Petersen, N. (1999). Palaeoclimatic record from a loess-soil profile in northeastern Bulgaria—I. Rock magnetic properties. *Geophysical Journal International* 138 (2), pages 520–532. DOI: 10.1046/j.1365-246X.1999.00874.x.

Jordanova, D., Hus, J., and Geeraerts, R. (2007a). Palaeoclimatic implications of the magnetic record from loess/palaeosol sequence Viatovo (NE Bulgaria): Palaeoclimatic implications of the magnetic record. *Geophysical Journal International* 171 (3), pages 1036–1047. DOI: 10.1111/j.1365-246X.2007.03576.x.

Jordanova, D., Jordanova, N., Henry, B., Hus, J., Bascou, J., Funaki, M., and Dimov, D. (2007b). Changes in mean magnetic susceptibility and its anisotropy of rock samples as a result of alternating field demagnetization. *Earth and Planetary Science Letters* 255 (3), pages 390–401. DOI: 10.1016/j.epsl.2006.12.025.

Juhász, G., Pogácsás, G., Magyar, I., and Vakarcs, G. (2007). Tectonic versus climatic control on the evolution of fluvio-deltaic systems in a lake basin, Eastern Pannonian Basin. *Sedimentary Geology* 202 (1), pages 72–95.

Kars, R. H., Reimann, T., Ankjaergaard, C., and Wallinga, J. (2014). Bleaching of the post-IR IRSL signal: new insights for feldspar luminescence dating: Feldspar luminescence dating. *Boreas* 43 (4), pages 780–791. DOI: 10.1111/bor.12082.

Kels, H., Protze, J., Sitlivy, V., Hilgers, A., Zander, A., Anghelinu, M., Bertrams, M., and Lehmkuhl, F. (2014). Genesis of loess-like sediments and soils at the foothills of the Banat Mountains, Romania – Examples from the Paleolithic sites Românești and Coşava. *Quaternary International* 351, pages 213–230. DOI: 10.1016/j.quaint.2014.04.063.

Kerney, M. P., Cameron, R. A., and Jungbluth, J. H. (1983). *Die Landschnecken Nord- und Mitteleuropas*. Parey, Hamburg. 384 pages.

Klasen, N. (2008). Lumineszenzdatierung glazifluvialer Sedimente im nördlichen Alpenvorland. doctoral dissertation. Köln: Universität zu Köln.

Klasen, N., Loibl, C., Rethemeyer, J., and Lehmkuhl, F. (2017). Testing feldspar and quartz luminescence dating of sandy loess sediments from the Doroshivtsy site (Ukraine) against radiocarbon dating. *Quaternary International* (Part A). DOI: 10.1016/j.quaint.2015.05.036.

Kostić, N. and Protić, N. (2000). Pedology and mineralogy of loess profiles at Kapela-Batajnica and Stalać, Serbia. *Catena* (41), pages 217–227.

Krauß, L., Zens, J., Zeeden, C., Schulte, P., Eckmeier, E., and Lehmkuhl, F. (2016). A multi-proxy analysis of two loess-paleosol sequences in the northern Harz foreland, Germany. *Palaeogeography, Palaeoclimatology, Palaeoecology* 461, pages 401–417. DOI: 10.1016/j.palaeo.2016.09.001.

Kreutzer, S., Fuchs, M., Meszner, S., and Faust, D. (2012a). OSL chronostratigraphy of a loess-palaeosol sequence in Saxony/Germany using quartz of different grain sizes. *Quaternary Geochronology* 10, pages 102–109. DOI: 10.1016/j.quageo.2012.01.004.

Kreutzer, S., Schmidt, C., Fuchs, M. C., Dietze, M., Fischer, M., and Fuchs, M. (2012b). Introducing an R package for luminescence dating analysis. *Ancient TL* 30 (1), pages 1–8.

Kreutzer, S., Schmidt, C., DeWitt, R., and Fuchs, M. (2014). The a-value of polymineral fine grain samples measured with the post-IR IRSL protocol. *Radiation Measurements* 69, pages 18–29. DOI: 10.1016/j.radmeas.2014.04.027.

Krolopp, E. and Sümegi, P. (1990). Vorkommen von Vestida turgida (Rossmässler, 1836) in den pleistozänen Sedimenten Ungarns. *Soosiana* 18, pages 5–10.

Krolopp, E. and Sümegi, P. (1991). Dominancia level of species Punctum pymaeum (Draparnaud, 1801): a biostratigraphical and paleoecological key level for the Hungarian loess sediments of the Upper Würm. *Soosiana* 19, pages 17–23.

Krolopp, E. and Sümegi, P. (1992). Pleistocene Vertigo species from Hungary. *Scripta Geologica. Special Issue* 2 (11), pages 263–268.

Krolopp, E. and Sümegi, P. (1995). Palaeoecological reconstruction of the Late Pleistocene, based on Loess Malacofauna in Hungary. *GeoJournal* 36, pages 213–222.

Krolopp, E. and Sümegi, P. (2002). A ságvári lösz-rétegsor csigafaunája (The mollusc fauna of the Ságvár loess profile). *Malakológiai Tájékoztató* 20, pages 7–14.

Krstić, B., Rakić, B., Veselinović, M., Doloć, D., Rakić, M., Anđelković, V., and Baković, V. (1978). *Aleksinac*. Savezni geološki zavod, Laboratorija za metode geološkog kartiranja Rudarsko - geološkog fakulteta, Vojnogeografski institut, Belgrade, Serbia.

Kukla, G. J. (1977). Pleistocene land—sea correlations I. Europe. *Earth-Science Reviews* 13 (4), pages 307–374. DOI: 10.1016/0012-8252(77)90125-8.

Kukla, G. (1987). Loess stratigraphy in central China. *Quaternary Science Reviews* 6 (3), pages 191–219. DOI: 10.1016/0277-3791(87)90004-7.

Kukla, G., Heller, F., Ming, L. X., Chun, X. T., Sheng, L. T., and Sheng, A. Z. (1988). Pleistocene climates in China dated by magnetic susceptibility. *Geology* 16 (9), pages 811–814. DOI: 10.1130/0091-7613(1988)016<0811:PCICDB>2.3.CO;2.

Kulakovska, L., Usik, V., Haesaerts, P., Ridush, B., Uthmeier, T., and Hauck, T. C. (2015). Upper Paleolithic of Middle Dniester: Doroshivtsi III site. *Quaternary International* 359, pages 347–361.

Lambert, F., Delmonte, B., Petit, J.-R., Bigler, M., Kaufmann, P. R., Hutterli, M. A., Stocker, T. F., Ruth, U., Steffensen, J. P., and Maggi, V. (2008). Dust-climate couplings over the past 800,000 years from the EPICA Dome C ice core. *Nature* 452 (7187), pages 616–619.

Lauer, T., Vlaminck, S., Frehen, M., Rolf, C., Kehl, M., Sharifi, J., Lehndorff, E., and Khormali, F. (2017). The Agh Band loess-palaeosol sequence - A terrestrial archive for climatic shifts during the last and penultimate glacialeinterglacial cycles in a semiarid region in northern Iran. *Quaternary International* 429 (Part B), pages 13–30. DOI: 0.1016/j.quaint.2016.01.062.

Laverenz, H. W. (1950). *An Introduction to luminescence of solids*. Dover Publications, New York. 569 pages.

Lazckó, D. (1929). Őstörténeti adatok a Balaton környékéről. A Szent István Akadémia Mennyiségtan- , Természettudományi Osztályának Felolvasásai. 2/5 kö tet. Veszprém.

Leicher, N., Zanchetta, G., Sulpizio, R., Giaccio, B., Wagner, B., Nomade, S., Francke, A., and Del Carlo, P. (2016). First tephrostratigraphic results of the DEEP site record from Lake Ohrid (Macedonia and Albania). *Biogeosciences* 13 (7), pages 2151–2178. DOI: 10.5194/bg-13-2151-2016.

Lengyel, G. (2010). An aspect to the reevaluation of Ságvár (Lyukas–domb) upper Palaeolithic site. *Folia Archaeologica* 54, pages 26–37.

Lengyel, G. (2015). Lithic raw material procurement at Bodrogkeresztúr–Henye Gravettian site, northeast Hungary. *Quaternary International* 359–360, pages 292–303. DOI: 10.1016/j.quaint.2014.07.027.

Lengyel, G. and Mester, Z. (2008). A new look at the radiocarbon chronology of the Szeletian in Hungary. *Dating the Middle to Upper Palaeolithic boundary across Eurasia. Proceedings of Session C* 57, pages 73–83.

Léonard, I. (2016). The settlement and lithic technological organization and lithic raw material procurement strategies during the early Upper Palaeolithic in the Timiş-Bega-Mureş Catchment (Banat, South-western Romania). PhD thesis. University of Cologne.

Leonhard, K. C. von (1823). *Charakteristik der Felsarten*. Heidelberg, Germany: J. Engelmann. 230 pages.

Leroi-Gourhan, A. (1968). Dénomination des oscillations würmiennes. *Bulletin de l'Association française pour l'étude du quaternaire* 5 (4), pages 281–288. DOI: 10.3406/quate.1968.1090.

Lindner, H., Lehmkuhl, F., and Zeeden, C. (2017). Spatial loess distribution in the eastern Carpathian Basin: a novel approach based on geoscientific maps and data. *Journal of Maps* 13 (2), pages 173–181. DOI: 10.1080/17445647.2017.1279083.

Liritzis, I., Stamoulis, K., Papachristodoulou, C., and Ioannides, K. (2013). A re-evaluation of radiation dose-rate conversion factors. *Mediterr. Archaeol. Archaeom* 13 (3), pages 1–15.

Liu, T.-S. (1988). *Loess in China*. second ed. Springer Series in Physical Environment. Springer-Verlag. Berlin & Heidelberg. 224 pages.

Ložek, V. (1964). *Quartärmollusken der Tschechoslowakei: Mit 32 fotographischen Tafeln*. Volume 31. Prague: Geologischen Zentralanstalt im Verlag der Tschechoslowakischen Akademie der Wissenschaften.

Ložek, V. (1965). Das Problem der Lössbildung und die Lössmollusken. *Eiszeitalter und Gegenwart* 15, pages 61–75.

Lóczy, D., Kertész, Á., Lóki, J., Kiss, T., Rózsa, P., Sipos, G., Sütö, L., Szabó, J., and Veress, M. (2012). Recent landform evolution in Hungary. In: *Recent landform evolution: The Carpatho-Balkan-Dinaric Region*. Springer, pages 205–247.

Lukas, S., Spencer, J. Q. G., Robinson, R. A. J., and Benn, D. I. (2007). Problems associated with luminescence dating of Late Quaternary glacial sediments in the NW Scottish Highlands. *Quaternary Geochronology* 2 (1), pages 243–248. DOI: 10.1016/j.quageo.2006.04.007.

Lukić, T., Basarin, B., Buggle, B., Marković, S. B., Tomović, V. M., Raljič, J. P., Hrnjak, I., Timar-Gabor, A., Hambach, U., and Gavrilov, M. B. (2014). A joined rock magnetic and colorimetric perspective on the Late Pleistocene climate of Orlovat loess site (Northern Serbia). *Quaternary International* 334–335, pages 179–188. DOI: 10.1016/j.quaint.2014.03.042.

Lyell, C. (1834). Observations on the loamy deposit called 'loess' of the basin of the Rhine. *Edinburgh New Philosophical Journal* 17 (11), pages 110–122.

Magyar, I., Geary, D. H., and Müller, P. (1999). Paleogeographic evolution of the Late Miocene Lake Pannon in Central Europe. *Palaeogeography, Palaeoclimatology, Palaeoecology* 147 (3), pages 151–167.

Mahowald, N., Kohfeld, K., Hansson, M., Balkanski, Y., Harrison, S. P., Prentice, I. C., Schulz, M., and Rodhe, H. (1999). Dust sources and deposition during the last glacial maximum and current climate: A comparison of model results with paleodata from ice cores and marine sediments. *Journal of Geophysical Research: Atmospheres* 104 (D13), pages 15895–15916.

Marković, S. B., McCoy, W. D., Oches, E. A., Savic, S., Gaudenyi, T., Jovanovic, M., Stevens, T., Walther, R., Ivanisevic, P., and Galic, Z. (2005). Paleoclimate record in the Upper Pleistocene loess-paleosol sequence at Petrovaradin brickyard (Vojvodina, Serbia). *Geologica Carpathica* 56 (6), pages 545–552.

Marković, S. B., Oches, E. A., McCoy, W. D., Frechen, M., and Gaudenyi, T. (2007). Malacological and sedimentological evidence for "warm" glacial climate from the Irig loess sequence, Vojvodina, Serbia. *Geochem. Geophys. Geosyst.* 8 (9), Q09008. DOI: 10.1029/2006GC001565.

Marković, S. B. et al. (2008). Late Pleistocene loess-palaeosol sequences in the Vojvodina region, north Serbia. *Journal of Quaternary Science* 23 (1), pages 73–84. DOI: 10.1002/jqs.1124.

Marković, S. B., Hambach, U., Catto, N., Jovanović, M., Buggle, B., Machalett, B., Zöller, L., Glaser, B., and Frechen, M. (2009). Middle and Late Pleistocene loess sequences at Batajnica, Vojvodina, Serbia. *Quaternary International* 198 (1), pages 255–266. DOI: 10.1016/j.quaint.2008.12.004.

Marković, S. B., Hambach, U., Stevens, T., Kukla, G. J., Heller, F., McCoy, W. D., Oches, E. A., Buggle, B., and Zöller, L. (2011). The last million years recorded at the Stari Slankamen (Northern Serbia) loess-palaeosol sequence: revised chronostratigraphy and long-term environmental trends. *Quaternary Science Reviews* 30 (9), pages 1142–1154. DOI: 10.1016/j.quascirev.2011.02.004.

Marković, S. B. et al. (2012a). Loess in the Vojvodina region (Northern Serbia): an essential link between European and Asian Pleistocene environments. *Netherlands Journal of Geosciences* 91 (1), pages 173–188. DOI: 10.1017/S0016774600001578.

Marković, S. B., Hambach, U., Stevens, T., Basarin, B., O'Hara-Dhand, K., Gavrilov, M. M., Gavrilov, M. B., Smalley, I., and Teofanov, N. (2012b). Relating the Astronomical Timescale to the Loess–Paleosol Sequences in Vojvodina, Northern Serbia. In: *Climate Change*. Edited by A. Berger, F. Mesinger, and D. Sijacki. Springer Vienna, pages 65–78.

Marković, S. B. et al. (2014). Environmental dynamics and luminescence chronology from the Orlovat loess–palaeosol sequence (Vojvodina, northern Serbia). *Journal of Quaternary Science* 29 (2), pages 189–199. DOI: 10.1002/jqs.2693.

Marković, S. B. et al. (2015). Danube loess stratigraphy — Towards a pan-European loess stratigraphic model. *Earth-Science Reviews* 148, pages 228–258. DOI: 10.1016/j.earscirev.2015.06.005.

Marković, S. B., Fitzsimmons, K. E., Sprafke, T., Gavrilović, D., Smalley, I. J., Jović, V., Svirčev, Z., Gavrilov, M. B., and Bešlin, M. (2016). The history of Danube loess research. *Quaternary International* 399, pages 86–99.

Márton, M. and Fodor, L. (2003). Tertiary paleomagnetic results and structural analysis from the Transdanubian Range (Hungary): rotational disintegration of the Alcapa unit. *Tectonophysics* 363 (3), pages 201–224.

McKeever, S. W. S. (1985). *Thermoluminescence of solids*. University Press (New York). 376 pages. DOI: 10.1017/CBO9780511564994.

Mejdahl, V. (1979). Thermoluminescence Dating: Beta-Dose Attenuation in Quartz Grains. *Archaeometry* 21 (1), pages 61–72. DOI: 10.1111/j.1475-4754.1979.tb00241.x.

Mellars, P. (2011). Palaeoanthropology: The earliest modern humans in Europe. *Nature* 479 (7374), pages 483–485. DOI: 10.1038/479483a.

Meng, S. (2009). Rezente zentralasiatische und pleistozäne mitteleuropäische Faunen mit Vallonia tenuilabris (A. Braun, 1843). *Mollusca* 27, pages 61–82.

Mihailović, D. (1992). *Orinjasijenska kremena industrija sa lokaliteta Crvenka-at u blizini vršca*. Filozofski fakultet. University of Belgrade. 52 pages.

Mihailović, D., Mihailović, B., and Lopičić, M. (2011). The Palaeolithic in Northern Serbia. In: *The Prehistory of Banat: The Palaeolithic and Mesolithic.* Edited by N. Tasić, F. Draşovean, and B. Jovanović, pages 77–93.

Miklánek, P. (2012). Rivers. In: *Recent Landform Evolution: The Carpatho-Bakan-Dinaric Region.* Loczy, D., Stankoviansky, M., Kotoarba, A. (eds.) Springer Science & Business Media, pages 31–38.

Moine, O. (2014). Weichselian Upper Pleniglacial environmental variability in north-western Europe reconstructed from terrestrial mollusc faunas and its relationship with the presence/absence of human settlements. *Quaternary International* 337, pages 90–113. DOI: 10.1016/j.quaint.2014.02.030.

Moine, O., Rousseau, D.-D., and Antoine, P. (2005). Terrestrial molluscan records of Weichselian Lower to Middle Pleniglacial climatic changes from the Nussloch loess series (Rhine Valley, Germany): the impact of local factors. *Boreas* 34, pages 363–380. DOI: 10.1111/j.1502-3885.2005.tb01107.x.

Moine, O., Rousseau, D.-D., and Antoine, P. (2008). The impact of Dansgaard–Oeschger cycles on the loessic environment and malacofauna of Nussloch (Germany) during the Upper Weichselian. *Quaternary Research* 70 (1), pages 91–104. DOI: 10.1016/j.yqres.2008.02.010.

Molnár, A. and Sümegi, P. (1990). Classification and ordination methods in the division of the Pleistocene malacological zones of Debrecen I. profile. *Soosiana* 18, pages 11–16.

Molnár, A. and Sümegi, P. (1992). Klasszifikációs és ordinációs módszerek pleisztocén malakológiai zónák lehatárolásához. In: *Fáciesanalitikai, paleobiogeokémiai és paleoökológiai kutatások.* Edited by G. Szöör. MTA Debrecni Bizottsága, pages 37–42.

Muhs, D. R., Bettis III, E. A., Aleinikoff, J. N., McGeehin, J. P., Beann, J., Skipp, G., Marshall, B. D., Roberts, H. M., Johnson, W. C., and Benton, R. (2008). Origin and paleoclimatic significance of late Quaternary loess in Nebraska: Evidence from stratigraphy, chronology, sedimentology, and geochemistry. *Geological Society of America Bulletin* 120 (11/12), pages 1378–1407. DOI: 10.1130/B26221.1.

Muhs, D. R., Bettis III, E. A., Roberts, H. M., Harlan, S. S., Paces, J. B., and Reynolds, R. L. (2013). Chronology and provenance of last-glacial (Peoria) loess in western Iowa and paleoclimatic implications. *Quaternary Research* 80 (3), pages 468–481. DOI: 10.1016/j.yqres.2013.06.006.

Munteanu, M. T., Munteanu, E., Stiuca, E., Macaleti, R., and Dumitrascu, G. (2008). Some aspects concerning the Quaternary deposits in south Dobrogea. *Acta Palaeontologica Romaniae* 6, pages 229–236.

Murray, A. S. and Wintle, A. G. (2000). Luminescence dating of quartz using an improved single-aliquot regenerative-dose protocol. *Radiation Measurements* 32 (1), pages 57–73. DOI: 10.1016/S1350-4487(99)00253-X.

Murray, A. S. and Wintle, A. G. (2003). The single aliquot regenerative dose protocol: potential for improvements in reliability. *Radiation Measurements* 37 (4), pages 377–381. DOI: 10.1016/S1350-4487(03)00053-2.

Murray, A. S., Buylaert, J., Thomsen, K., and Jain, M. (2009). The effect of preheating on the IRSL signal from feldspar. *Radiation Measurements* 44 (5), pages 554–559. DOI: 10.1016/j.radmeas.2009.02.004.

Murray, A. S., Thomsen, K., Masuda, N., Buylaert, J.-P., and Jain, M. (2012). Identifying well-bleached quartz using the different bleaching rates of quartz and feldspar luminescence signals. *Radiation Measurements* 47 (9), pages 688–695. DOI: 10.1016/j.radmeas.2012.05.006.

Murray, A. S., Schmidt, E. D., Stevens, T., Buylaert, J.-P., Marković, S. B., Tsukamoto, S., and Frechen, M. (2014). Dating Middle Pleistocene loess from Stari Slankamen (Vojvodina, Serbia) — Limitations imposed by the saturation behaviour of an elevated temperature IRSL signal. *CATENA* 117, pages 34–42. DOI: 10.1016/j.catena.2013.06.029.

Nawrocki, J., Polechońska, O., Boguckij, A., and Łanczont, M. (2006). Palaeowind directions recorded in the youngest loess in Poland and western Ukraine as derived from anisotropy of magnetic susceptibility measurements. *Boreas* 35 (2), pages 266–271. DOI: 10.1080/03009480600584907.

Necula, C., Panaiotu, C., Heslop, D., and Dimofte, D. (2013). Climatic control of magnetic granulometry in the Mircea Vodă loess/paleosol sequence (Dobrogea, Romania). *Quaternary International* 293, pages 5–14. DOI: 10.1016/j.quaint.2012.03.043.

Nelson, M. S. and Rittenour, T. M. (2015). Using grain-size characteristics to model soil water content: Application to dose-rate calculation for luminescence dating. *Radiation Measurements* 81, pages 142–149. DOI: 10.1016/j.radmeas.2015.02.016.

Nesbitt, H. W. and Young, G. M. (1989). Formation and diagenesis of weathering profiles. *The Journal of Geology* 97 (2), pages 129–147.

Niedźwiedź, T. (2012). Climate. In: *Recent Landform Evolution*. Edited by D. Lóczy, M. Stankoviansky, and A. Kotarba. Springer Geography. Springer, Dordrecht, pages 19–29. DOI: 10.1007/978-94-007-2448-8_2.

NOAA (2017). *Global Summary of the Month (for several years), Station Miskolc, Hungary, generated on 01/27/2017*. U.S. Department of Commerce, National Oceanic & Atmospheric Administration, National Environmental Satellite, Data, and Information Service.

Nottebaum, V., Stauch, G., Hartmann, K., Zhang, J., and Lehmkuhl, F. (2015). Unmixed loess grain size populations along the northern Qilian Shan (China): Relationships between geomorphologic, sedimentologic and climatic controls. *Quaternary International* 372, pages 151–166. DOI: 10.1016/j.quaint.2014.12.071.

Obreht, I. et al. (2014). The Late Pleistocene Belotinac section (southern Serbia) at the southern limit of the European loess belt: Environmental and climate reconstruction using grain size and stable C and N isotopes. *Quaternary International* 334–335, pages 10–19. DOI: 10.1016/j.quaint.2013.05.037.

Obreht, I., Zeeden, C., Schulte, P., Hambach, U., Eckmeier, E., Timar-Gabor, A., and Lehmkuhl, F. (2015). Aeolian dynamics at the Orlovat loess–paleosol sequence, northern Serbia, based on detailed textural and geochemical evidence. *Aeolian Research* 18, pages 69–81. DOI: 10.1016/j.aeolia.2015.06.004.

Obreht, I., Zeeden, C., Hambach, U., Veres, D., Marković, S. B., Bösken, J., Svirčev, Z., Bačević, N., Gavrilov, M. B., and Lehmkuhl, F. (2016). Tracing the influence of Mediterranean climate

on Southeastern Europe during the past 350,000 years. *Scientific Reports* 6 (36334), pages 1–10. DOI: 10.1038/srep36334.

Obreht, I. et al. (2017). Shift of large-scale atmospheric systems over Europe during late MIS3 and implications for Modern Human dispersal. *Nature Scientific Reports* 7 (5484), pages 1–10. DOI: 10.1038/s41598-017-06285-x.

Özer, M., Orhan, M., and Işik, N. S. (2010). Effect of particle optical properties on size distribution of soils obtained by laser diffraction. *Environmental & Engineering Geoscience* 16 (2), pages 163–173.

Pavlović, R., Ćalić, J., Djurović, P., Trivić, B., and Jemcov, I. (2012). Recent Landform Evolution in Serbia. In: *Recent Landform Evolution: The Carpatho-Balkan-Dinaric Region*. Springer, pages 345–375.

Pécsi, M. (1979). Lithostratigraphical subdivision of the loess profiles at Paks. *Acta Geologica Hungarica* 22, pages 409–418.

Pécsi, M. (1990). Loess is not just the accumulation of dust. *Quaternary International* 7, pages 1–21.

Pécsi, M. and Richter, G. (1996). Loess - Herkunft - Gliederung - Landschaften. *Zeitschrift für Geomorphologie, Supplementary Issues* 98. 391 pages.

Podani, J. (1978). A method for clustering of binary (Floristical) data in Vegetation research. *Acta Bot. Acad. Sci. Hung* 24, pages 121–137.

Podani, J. (1979). Association analysis based on the use of mutual information. *Acta bot. hung* 25, pages 125–130.

Prescott, J. and Hutton, J. (1994). Cosmic ray contributions to dose rates for luminescence and ESR dating: Large depths and long-term time variations. *Radiation Measurements* 23 (2), pages 497–500. DOI: 10.1016/1350-4487(94)90086-8.

Pye, K. (1995). The nature, origin and accumulation of loess. *Quaternary Science Reviews* 14 (7), pages 653–667. DOI: 10.1016/0277-3791(95)00047-X.

Pye, K. and Blott, S. J. (2004). Particle size analysis of sediments, soils and related particulate materials for forensic purposes using laser granulometry. *Forensic Science International* 144 (1), pages 19–27. DOI: 10.1016/j.forsciint.2004.02.028.

Radovanović, I. (1986). Vršac-At, palaeolitsko nalazište. *Arheološki pregled* 25, pages 11–12.

Rainer, F. and Simionescu, I. (1942). Sur le premier crâne d'homme Paléolithique trouvé en Roumanie. *Analele Academiei Romane Memoriile Sectiunii Sçtiintifice* 17.

Rakić, M., Hadižvuković, M., Kalenić, M., Marković, V., and Milovanović, L. (1975). *Kruševac*. Savezni geološki zavod, Vojnogeografski institut, Belgrade, Serbia.

Rees-Jones, J. (1995). Optical dating of young sediments using fine-grain quartz. *Ancient TL* 13 (2), pages 9–14.

Reimer, P. J. et al. (2013). IntCal13 and Marine13 Radiocarbon Age Calibration Curves 0–50,000 Years cal BP. *Radiocarbon* 55 (4), pages 1869–1887. DOI: 10.2458/azu_js_rc.55.16947.

RHMS (2016). *Monthly and annual means, maximum and minimum values of meteorological elements for the period 1981 - 2010 in Kruševac*. Republic Hydrometeorological Service of Serbia. URL: http://www.hidmet.gov.rs/eng/meteorologija/stanica_sr.php?moss_id=13383 (visited on 01/15/2016).

Richard, Y., Mihailescu, I.-F., and Planchon, O. (2000). Spatial distribution of the precipitation in Dobruja (Romania/Black Sea). *International Journal of Climatology* 20 (10), pages 1275–1284. DOI: 10.1002/1097-0088(200008)20:10<1275::AID-JOC522>3.0.CO;2-6.

Richthofen, B. F. (1882). II.—On the Mode of Origin of the Loess. *Geological Magazine* 9 (7), pages 293–305. DOI: 10.1017/S001675680017164X.

Roberts, H. M. (2006). Optical dating of coarse-silt sized quartz from loess: Evaluation of equivalent dose determinations and SAR procedural checks. *Radiation Measurements* 41 (7), pages 923–929. DOI: 10.1016/j.radmeas.2006.05.021.

Roberts, H. M. (2008). The development and application of luminescence dating to loess deposits: a perspective on the past, present and future. *Boreas* 37 (4), pages 483–507. DOI: 10.1111/j.1502-3885.2008.00057.x.

Roberts, R. G., Galbraith, R. F., Olley, J. M., Yoshida, H., and Laslett, G. M. (1999). Optical dating of single and multiple grains of quartz from Jinmium rock shelter, northern Australia: part II, results and implications. *Archaeometry* 41 (2), pages 365–395.

Rougier, H. et al. (2007). Peştera cu Oase 2 and the cranial morphology of early modern Europeans. *Proceedings of the National Academy of Sciences* 104 (4), pages 1165–1170. DOI: 10.1073/pnas.0610538104.

Rousseau, D.-D., Limondin, N., Magnin, F., and Puisségur, J.-J. (1994). Temperature oscillations over the last 10,000 years in western Europe estimated from terrestrial mollusc assemblages. *Boreas* 23 (1), pages 66–73.

Rudner, Z. E. and Sümegi, P. (2001). Recurring Taiga forest-steppe habitats in the Carpathian Basin in the Upper Weichselian. *Quaternary International* 76–77, pages 177–189. DOI: 10.1016/S1040-6182(00)00101-4.

Russell, R. J. (1944). Lower Mississippi valley loess. *Geological Society of America Bulletin* 55 (1), pages 1–40.

Satow, C. et al. (2015). A new contribution to the Late Quaternary tephrostratigraphy of the Mediterranean: Aegean Sea core LC21. *Quaternary Science Reviews* 117, pages 96–112. DOI: 10.1016/j.quascirev.2015.04.005.

Schatz, A.-K., Zech, M., Buggle, B., Gulyás, S., Hambach, U., Marković, S. B., Sümegi, P., and Scholten, T. (2011). The late Quaternary loess record of Tokaj, Hungary: Reconstructing palaeoenvironment, vegetation and climate using stable C and N isotopes and biomarkers. *Quaternary International* 240 (1), pages 52–61. DOI: 10.1016/j.quaint.2010.10.009.

Schatz, A.-K., Buylaert, J.-P., Murray, A. S., Stevens, T., and Scholten, T. (2012). Establishing a luminescence chronology for a palaeosol-loess profile at Tokaj (Hungary): A comparison of quartz OSL and polymineral IRSL signals. *Quaternary geochronology* 10, pages 68–74.

Schatz, A.-K., Qi, Y., Siebel, W., Wu, J., and Zöller, L. (2015a). Tracking potential source areas of Central European loess: examples from Tokaj (HU), Nussloch (D) and Grub (AT). *Open Geosciences* 7, pages 678–720. DOI: 10.1515/geo-2015-0048.

Schatz, A.-K., Scholten, T., and Kühn, P. (2015b). Paleoclimate and weathering of the Tokaj (Hungary) loess–paleosol sequence. *Palaeogeography, Palaeoclimatology, Palaeoecology* 426, pages 170–182. DOI: 10.1016/j.palaeo.2015.03.016.

Schäfer, A. (2005). *Klastische Sedimente - Fazies und Sequenzstratigraphie*. Springer Spektrum. 416 pages.

Schmidt, C. et al. (2013). First chronometric dates (TL and OSL) for the Aurignacian open-air site of Românești-Dumbrăviţa I, Romania. *Journal of Archaeological Science* 40 (10), pages 3740–3753. DOI: 10.1016/j.jas.2013.04.003.

Schmidt, E. D., Machalett, B., Marković, S. B., Tsukamoto, S., and Frechen, M. (2010). Luminescence chronology of the upper part of the Stari Slankamen loess sequence (Vojvodina, Serbia). *Quaternary Geochronology* 5 (2), pages 137–142. DOI: 10.1016/j.quageo.2009.09.006.

Schulte, P., Lehmkuhl, F., Steininger, F., Loibl, D., Lockot, G., Protze, J., Fischer, P., and Stauch, G. (2016). Influence of HCl pretreatment and organo-mineral complexes on laser diffraction measurement of loess–paleosol-sequences. *CATENA* 137, pages 392–405. DOI: 10.1016/j.catena.2015.10.015.

Sebe, K. (2013). Ventifacts in the Mecsek region (SW Hungary) – climatic interpretation and tectonic implications. *Zeitschrift für Geomorphologie* 57 (3), pages 305–323. DOI: 10.1127/0372-8854/2013/0103.

Sebe, K., Csillag, G., Ruszkiczay-Rüdiger, Z., Fodor, L., Thamó-Bozsó, E., Müller, P., and Braucher, R. (2011). Wind erosion under cold climate: A Pleistocene periglacial mega-yardang system in Central Europe (Western Pannonian Basin, Hungary). *Geomorphology* 134 (3), pages 470–482. DOI: 10.1016/j.geomorph.2011.08.003.

Shi, C., Zhu, R., Glass, B. P., Liu, Q., Zeman, A., and Suchy, V. (2003). Climate variations since the last interglacial recorded in Czech loess. *Geophysical Research Letters* 30. DOI: 10.1029/2003GL017251.

Singarayer, J. and Bailey, R. (2003). Further investigations of the quartz optically stimulated luminescence components using linear modulation. *Radiation Measurements* 37 (4), pages 451–458. DOI: 10.1016/S1350-4487(03)00062-3.

Sitlivy, V., Chabai, V., Anghelinu, M., Uthmeier, T., Kels, H., Hilgers, A., Schmidt, C., Niţă, L., Băltean, I., and Veselsky, A. (2012). The earliest Aurignacian in Romania: New investigations at the open air site of Românești-Dumbrăviţa I (Banat). *Quartär* 59, pages 85–130.

Sitlivy, V., Chabai, V., Anghelinu, M., Uthmeier, T., Kels, H., Niţă, L., Băltean, I., Veselsky, A., and Ţuţu, C. (2014). Preliminary reassessment of the Aurignacian in Banat (South-western Romania). *Quaternary International* 351, pages 193–212. DOI: 10.1016/j.quaint.2012.07.024.

Smalley, I. J. and Leach, J. A. (1978). The origin and distribution of the loess in the Danube basin and associated regions of East-Central Europe — A review. *Sedimentary Geology* 21 (1), pages 1–26. DOI: 10.1016/0037-0738(78)90031-3.

Smalley, I., O'Hara-Dhand, K., Wint, J., Machalett, B., Jary, Z., and Jefferson, I. (2009). Rivers and loess: The significance of long river transportation in the complex event-sequence approach to loess deposit formation. *Quaternary International* 198 (1), pages 7–18. DOI: 10.1016/j.quaint.2008.06.009.

Smalley, I., Marković, S. B., and Svirčev, Z. (2011). Loess is almost [totally formed by] the accumulation of dust. *Quaternary International* 240 (1), pages 4–11. DOI: 10.1016/j.quaint.2010.07.011.

Smedley, R. K., Duller, G. A. T., and Roberst, H. M. (2015). Bleaching of the post-IR IRSL signal from individual grains of K-feldspar: Implications for single-grain dating. *Radiation Measurements* 79, pages 33–42. DOI: 10.1016/j.radmeas.2015.06.003.

Smith, B. J., Wright, J. S., and Whalley, W. B. (1991). Simulated aeolian abrasion of Pannonian sands and its implications for the origins of Hungarian loess. *Earth Surface Processes and Landforms* 16 (8), pages 745–752.

Smith, B. W. (1988). Zircon from sediments: A combined OSL and TL auto-regenerative dating technique. *Quaternary Science Reviews* 7 (3), pages 401–406. DOI: 10.1016/0277-3791(88)90036-4.

Smith, B. W., Wheeler, G. C. W. S., Rhodes, E. J., and Spooner, N. A. (1991). Luminescence dating of zircon using an imaging photon detector. *International Journal of Radiation Applications and Instrumentation. Part D. Nuclear Tracks and Radiation Measurements* 18 (1), pages 273–278. DOI: 10.1016/1359-0189(91)90122-X.

Soficaru, A., Doboş, A., and Trinkaus, E. (2006). Early modern humans from the Peştera Muierii, Baia de Fier, Romania. *Proceedings of the National Academy of Sciences* 103 (46), pages 17196–17201.

Soficaru, A., Petrea, C., Doboş, A., and Trinkaus, E. (2007). The human cranium from the Peştera Cioclovina Uscată, Romania: context, age, taphonomy, morphology, and paleopathology. *Current Anthropology* 48 (4), pages 611–619.

Sólymos, P. and Sümegi, P. (1999). The shell morpho-thermometer method and its application in palaeoclimatic reconstruction. *Annales Universitatis Scientiarum Budapestiensis, Sectio Geologica* 32, pages 137–148.

Sommerwerk, N., Hein, T., Schneider-Jacoby, M., Baumgartner, C., Óstojić, A., Siber, R., Bloesch, J., Paunović, M., and Tockner, K. (2009). The Danube river basin. In: *Rivers of Europe*. Tockner, K., Uehlinger, U., Robinson, C. (eds.) London: Elsevier, pages 59–112.

Soós, L. (1943). *The mollusc fauna of the Carpathian Basin*. Budapest: Akadémiai Kiadó. 478 pages.

Southwood, T. R. E. (1979). Ecological methods: with particular reference to study of insect populations. *Ecology* 60 (6), page 1290.

Sprafke, T. (2016). Löss in Niederösterreich – Archiv quartärer Klima- und Landschaftsveränderungen. Würzburg University Press. PhD thesis. Würzburg. 272 pages.

Sprafke, T. and Obreht, I. (2016). Loess: Rock, sediment or soil – What is missing for its definition? *Quaternary International* 399, pages 198–207. DOI: 10.1016/j.quaint.2015.03.033.

Steffen, D., Preusser, F., and Schlunegger, F. (2009). OSL quartz age underestimation due to unstable signal components. *Quaternary Geochronology* 4 (5), pages 353–362. DOI: 10.1016/j.quageo.2009.05.015.

Stevens, T., Marković, S. B., Zech, M., Hambach, U., and Sümegi, P. (2011). Dust deposition and climate in the Carpathian Basin over an independently dated last glacial–interglacial cycle. *Quaternary Science Reviews* 30 (5), pages 662–681. DOI: 10.1016/j.quascirev.2010.12.011.

Sümegi, P. (1989). A Hajdúság felsőpleisztocén fejlődéstörénete finomrétegtani (őslénytani, üledékföldtani, geokémiai) vizsgálatok alapján (Upper Pleistocene geohistory of Hajdúság base on fine-stratigraphical (palaeontological, sedimentological, geochemical) ingestigation. Dr. Univ. Thesis. Debrecen: Kossuth University. 96 pages.

Sümegi, P. (1995). Quartermalacological analysis of Late Pleistocene loess sediments of the Great Hungarian Plain. *Quarternary malacostratigraphy in Hungary. Malacological Newsletter. Suppl* 1, pages 79–111.

Sümegi, P. (1996). Comparative palaeoecological and stratigraphical valuation of the NE Hungarian loess-areas. PhD thesis. 120 pp., Kossuth Univ., Debrecen, Hungary.

Sümegi, P. (2005). *Loess and Upper Paleolithic Environment in Hungary: An Introduction to the Environmental History of Hungary.* Aurea. 312 pages.

Sümegi, P. (2012). Multiproxy paleoenvironmental analysis of long-term climatic fluctuations in Southwest Hungary reading terrestrial archives. *Quaternary International* 279–280, page 477. DOI: 10.1016/j.quaint.2012.08.1608.

Sümegi, P. and Hertelendi, E. (1998). Reconstruction of microenvironmental changes in Kopasz Hill loess area at Tokaj (Hungary) between 15,000 - 70,000 BP years. *Radiocarbon* 40, pages 855–863.

Sümegi, P. and Krolopp, E. (1995). Reconstruction of palaeoecological conditions during the deposition of Würm loess formations of Hungary, based on molluscs (in Hungarian). *Földtani Közlöny* 124, pages 125–148.

Sümegi, P. and Krolopp, E. (2000). Paleoecological reconstruction of the sagvar-lauscaux interstadial. *A la recherche de l'Homme préhistorique* E.R.A.U.L. (95), pages 103–111.

Sümegi, P. and Krolopp, E. (2002). Quatermalacological analyses for modeling of the Upper Weichselian palaeoenvironmental changes in the Carpathian Basin. *Quaternary International* 91 (1), pages 53–63. DOI: 10.1016/S1040-6182(01)00102-1.

Sümegi, P. and Lóki, J. (1990). Fine-stratigraphical investigation on the section of the brickyard at Lakitelek. *Acta Geographica, Geologica et Meterologica Debrecina* 14-15, pages 157–167.

Sümegi, P. and Rudner, Z. E. (2001). In situ charcoal fragments as remains of natural wild fires in the upper Würm of the Carpathian Basin. *Quaternary International* 76/77, pages 165–176.

Sümegi, P., Szöőr, G., and Hertelendi, E. (1991). Palaeoenvironmental reconstruction of the last period of the Upper Würm in Hungary, based on malacological and radiocarbon data. *Soosiana* 19, pages 5–12.

Sümegi, P., Lóki, J., Hertelendi, E., and Szöőr, G. (1992). The sedimentological and stratigraphical analyses of the high bluff sequence Tiszaalpár (in Hungarian). *Alföldi Tanulmányok* 14, pages 75–87.

Sümegi, P., Hertelendi, E., Magyari, E., and Molnár, M. (1998a). Evolution of the environment in the Carpathian Basin during the last 30.000 BP years and its effects on the ancient habits of the different cultures. *Hungarian Academy of Sciences (HAS)* 2, pages 183–197.

Sümegi, P., Krolopp, E., and Hertelendi, E. (1998b). A Ságvár-Lascaux interstadiális paleoökológiai rekonstrukciója. *Acta Geogr. Ac Geol. Meterol. Debrecina* 34, pages 165–180.

Sümegi, P., Rudner, E., and Beszeda, I. (2000). Stratigraphical and palaeoecological investigation of the fossil soil comprising Upper Paleolithic tools at Bodrogkeresztúr-Henye. In:

Bodrogkeresztúr-Henye, NE Hungary, Upper Palaeolithic site. Edited by V. T. Dobosi. Budapest, Hungary: Magyar Nemzeti Múzeum, pages 217–220.

Sümegi, P., Gulyás, S., Persaits, G., GergelyPáll, D., and Molnár, D. (2011). The loess-paleosol sequence of Basaharc (Hungary) revisited: Mollusc-based paleoecological results for the Middle and Upper Pleistocene. *Quaternary International* 240 (1), pages 181–192. DOI: 10.1016/j.quaint.2011.05.005.

Sümegi, P., Gulyás, S., Csökmei, B., Molnár, D., Hambach, U., Stevens, T., Marković, S. B., and Almond, P. C. (2012a). Climatic fluctuations inferred for the Middle and Late Pleniglacial (MIS 2) based on high-resolution (ca. 20 y) preliminary environmental magnetic investigation of the loess section of the Madaras brickyard (Hungary). *Central European Geology* 55 (3), pages 329–345.

Sümegi, P., Persaits, G., and Gulyás, S. (2012b). Woodland-grassland ecotonal shifts in environmental mosaics: lessons learnt from the environmental history of the Carpathian Basin (Central Europe) during the Holocene and the last ice age based on investigation of paleobotanical and mollusk remains. In: *Ecotones Between Forest and Grassland*. Edited by R. Myster. Springer, New York, NY, pages 17–57.

Sümegi, P., Magyari, E., Dániel, P., Molnár, M., and Törőcsik, T. (2013). Responses of terrestrial ecosystems to Dansgaard–Oeshger cycles and Heinrich-events: A 28,000-year record of environmental changes from SE Hungary. *Quaternary International* 293, pages 34–50. DOI: 10.1016/j.quaint.2012.07.032.

Sümegi, P., Náfrádi, K., Molnár, D., and Sávai, S. (2015). Results of paleoecological studies in the loess region of Szeged-Öthalom (SE Hungary). *Quaternary International* 372, pages 66–78. DOI: 10.1016/j.quaint.2014.09.003.

Sümegi, P., Törőcsik, T., Náfrádi, K., Sümegi, B., Majkut, P., Molnár, D., and Tapody, R. (2016). Radiocarbon dated complex paleoecological and geoarcheological analyses at the Bodrogkeresztúr-Henye Gravettian site (NE Hungary). *Archeometriai Műhely* 2016/XIII./1.

Sun, Y., Clemens, S. C., An, Z., and Yu, Z. (2006). Astronomical timescale and palaeoclimatic implication of stacked 3.6-Myr monsoon records from the Chinese Loess Plateau. *Quaternary Science Reviews* 25 (1), pages 33–48. DOI: 10.1016/j.quascirev.2005.07.005.

Sun, Y., An, Z., Clemens, S. C., Bloemenda, J., and Vandenberghe, J. (2010). Seven million years of wind and precipitation variability on the Chinese Loess Plateau. *Earth and Planetary Science Letters* 297, pages 525–535. DOI: 10.1016/j.epsl.2010.07.004.

Svensson, A. et al. (2006). The Greenland Ice Core Chronology 2005, 15–42 ka. Part 2: comparison to other records. *Quaternary Science Reviews* 25 (23), pages 3258–3267. DOI: 10.1016/j.quascirev.2006.08.003.

Svirčev, Z., Marković, S. B., Stevens, T., Codd, G. A., Smalley, I., Simeunović, J., Obreht, I., Dulić, T., Pantelić, D., and Hambach, U. (2013). Importance of biological loess crusts for loess formation in semi-arid environments. *Quaternary International* 296, pages 206–215. DOI: 10.1016/j.quaint.2012.10.048.

Talma, A. S. and Vogel, J. C. (1993). A simplified approach to calibrating 14 C dates. *Radiocarbon* 35 (2), pages 317–322.

Tegen, I. (2003). Modeling the mineral dust aerosol cycle in the climate system. *Quaternary Science Reviews* 22 (18), pages 1821–1834.

Terhorst, B., Kühn, P., Damm, B., Hambach, U., Meyer-Heintze, S., and Sedov, S. (2013). Paleoenvironmental fluctuations as recorded in the loess-paleosol sequence of the Upper Paleolithic site Krems-Wachtberg. *Quaternary International* 351, pages 67–82. DOI: 10.1016/j.quaint.2013.03.045.

Thiel, C., Buylaert, J.-P., Murray, A. S., Terhorst, B., Tsukamoto, S., Frechen, M., and Sprafke, T. (2011a). Investigating the chronostratigraphy of prominent palaeosols in Lower Austria using post-IR IRSL dating. *Quaternary Science Journal* 60 (1), pages 137–152. DOI: 10.3285/eg.60.1.10.

Thiel, C., Buylaert, J.-P., Murray, A. S., Terhorst, B., Hofer, I., Tsukamoto, S., and Frechen, M. (2011b). Luminescence dating of the Stratzing loess profile (Austria) – Testing the potential of an elevated temperature post-IR IRSL protocol. *Quaternary International* 234 (1), pages 23–31. DOI: 10.1016/j.quaint.2010.05.018.

Thiel, C., Horváth, E., and Frechen, M. (2014). Revisiting the loess/palaeosol sequence in Paks, Hungary: A post-IR IRSL based chronology for the 'Young Loess Series'. *Quaternary International* 319, pages 88–98. DOI: 10.1016/j.quaint.2013.05.045.

Thompson, L. and Mosley-Thompson, E. (1981). Microparticle concentration variations linked with climatic change: evidence from polar ice cores. *Science* 212, pages 812–815.

Thompson, R. and Oldfield, 1. (1986). *Environmental Magnetism*. Springer, Dordrecht. DOI: 10.1007/978-94-011-8036-8.

Thomsen, K., Murray, A. S., Jain, M., and Bøtter-Jensen, L. (2008). Laboratory fading rates of various luminescence signals from feldspar-rich sediment extracts. *Radiation Measurements* 43 (9), pages 1474–1486. DOI: 10.1016/j.radmeas.2008.06.002.

Timar-Gabor, A. and Wintle, A. G. (2013). On natural and laboratory generated dose response curves for quartz of different grain sizes from Romanian loess. *Quaternary Geochronology* 18, pages 34–40. DOI: 10.1016/j.quageo.2013.08.001.

Timar-Gabor, A., Vasiliniuc, Ş., Vandenberghe, D., Cosma, C., and Wintle, A. (2012). Investigations into the reliability of SAR-OSL equivalent doses obtained for quartz samples displaying dose response curves with more than one component. *Radiation Measurements* 47 (9), pages 740–745. DOI: 10.1016/j.radmeas.2011.12.001.

Timar-Gabor, A., Constantin, D., Buylaert, J. P., Jain, M., Murray, A. S., and Wintle, A. G. (2015a). Fundamental investigations of natural and laboratory generated SAR dose response curves for quartz OSL in the high dose range. *Radiation Measurements* 81. DOI: 10.1016/j.radmeas.2015.01.013.

Timar-Gabor, A., Constantin, D., Marković, S. B., and Jain, M. (2015b). Extending the area of investigation of fine versus coarse quartz optical ages from the Lower Danube to the Carpathian Basin. *Quaternary International* 388. DOI: 10.1016/j.quaint.2014.09.065.

Timar-Gabor, A. et al. (2017). On the importance of grain size in luminescence dating using quartz. *Radiation Measurements* 106, pages 464–471. DOI: 10.1016/j.radmeas.2017.01.009.

Tóthmérész, B. (1993). NuCoSA 1.0: number cruncher for community studies and other ecological applications. *Abstracta Botanica* 17, pages 283–287.

Trinkaus, E., Soficaru, A., Doboş, A., Constantin, S., Zilhão, J., and Richards, M. (2009). Stable isotope evidence for early modern human diet in southeastern Europe: Peştera cu Oase, Peştera Muierii and Peştera Cioclovina Uscată. *Materiale şi Cercetări Arheologice* 5, pages 4–14.

Trinkaus, E. et al. (2003). An early modern human from the Peştera cu Oase, Romania. *Proceedings of the National Academy of Sciences* 100 (20), pages 11231–11236. DOI: 10.1073/pnas.2035108100.

Tugulan, L. C., Duliu, O. G., Bojar, A.-V., Dumitras, D., Zinicovskaia, I., Culicov, O. A., and Frontasyeva, M. V. (2016). On the geochemistry of the Late Quaternary loess deposits of Dobrogea (Romania). *Quaternary International* 399, pages 100–110. DOI: 10.1016/j.quaint.2015.06.062.

Újvári, G., Varga, A., and Balogh-Brunstad, Z. (2008). Origin, weathering, and geochemical composition of loess in southwestern Hungary. *Quaternary Research* 69 (3), pages 421–437. DOI: 10.1016/j.yqres.2008.02.001.

Újvári, G., Kovács, J., Varga, G., Raucsik, B., and Marković, S. B. (2010). Dust flux estimates for the Last Glacial Period in East Central Europe based on terrestrial records of loess deposits: a review. *Quaternary Science Reviews* 29 (23), pages 3157–3166. DOI: 10.1016/j.quascirev.2010.07.005.

Újvári, G., Varga, A., Ramos, F. C., Kovács, J., Németh, T., and Stevens, T. (2012). Evaluating the use of clay mineralogy, Sr–Nd isotopes and zircon U–Pb ages in tracking dust provenance: An example from loess of the Carpathian Basin. *Chemical Geology* 304-305, pages 83–96. DOI: 10.1016/j.chemgeo.2012.02.007.

Újvári, G., Molnár, M., Novothny, Á., Páll-Gergely, B., Kovács, J., and Várhegyi, A. (2014a). AMS 14C and OSL/IRSL dating of the Dunaszekcső loess sequence (Hungary): chronology for 20 to 150 ka and implications for establishing reliable age–depth models for the last 40 ka. *Quaternary Science Reviews* 106. DOI: 10.1016/j.quascirev.2014.06.009.

Újvári, G., Varga, A., Raucsik, B., and Kovács, J. (2014b). The Paks loess-paleosol sequence: A record of chemical weathering and provenance for the last 800ka in the mid-Carpathian Basin. *Quaternary International* 319, pages 22–37. DOI: 10.1016/j.quaint.2012.04.004.

Újvári, G., Kok, J. F., Varga, G., and Kovács, J. (2016a). The physics of wind-blown loess: Implications for grain size proxy interpretations in Quaternary paleoclimate studies. *Earth-Science Reviews* 154, pages 247–278. DOI: 10.1016/j.earscirev.2016.01.006.

Újvári, G., Molnár, M., and Páll-Gergely, B. (2016b). Charcoal and mollusc shell 14C-dating of the Dunaszekcső loess record, Hungary. *Quaternary Geochronology* 35, pages 43–53. DOI: 10.1016/j.quageo.2016.05.005.

Ujvari, G. (2014). Interactive comment on "Paleoclimate and weathering of the Tokaj (NE Hungary) loess-paleosol sequence: a comparison of geochemical weathering indices and paleoclimate parameters" by A.-K. Schatz et al. *Climate of the Past Discussions* 10, pages C19–C26.

Vandenberghe, J. (2013). Grain size of fine-grained windblown sediment: A powerful proxy for process identification. *Earth-Science Reviews* 121, pages 18–30. DOI: 10.1016/j.earscirev.2013.03.001.

Vandenberghe, J., Marković, S. B., Jovanovič, M., and Hambach, U. (2014). Site-specific variability of loess and palaeosols (Ruma, Vojvodina, northern Serbia). *Quaternary International* 334–335, pages 86–93. DOI: 10.1016/j.quaint.2013.10.036.

Varga, A., Újvári, G., and Raucsik, B. (2011). Tectonic versus climatic control on the evolution of a loess–paleosol sequence at Beremend, Hungary: an integrated approach based on paleoecological, clay mineralogical, and geochemical data. *Quaternary International* 240 (1), pages 71–86. DOI: 10.1016/j.quaint.2010.10.032.

Varga, G., Kovács, J., and Újvári, G. (2012). Late Pleistocene variations of the background aeolian dust concentration in the Carpathian Basin: an estimate using decomposition of grain-size distribution curves of loess deposits. *Netherlands Journal of Geosciences* 91 (1), pages 159–171. DOI: 10.1017/S0016774600001566.

Varga, G., Cserháti, C., Kovács, J., and Szalai, Z. (2016). Saharan dust deposition in the Carpathian Basin and its possible effects on interglacial soil formation. *Aeolian Research* 22, pages 1–12.

Vasiliniuc, Ş., Vandenberghe, D., Timar-Gabor, A., Panaiotu, C., Cosma, C., and Haute, P. van den (2012). Testing the potential of elevated temperature post-IR IRSL signals for dating Romanian loess. *Quaternary Geochronology* 10, pages 75–80. DOI: 10.1016/j.quageo.2012.02.014.

Vasiliniuc, Ş., Vandenberghe, D. A. G., Timar-Gabor, A., Cosma, C., and Haute, P. van den (2013). Combined IRSL and post-IR OSL dating of Romanian loess using single aliquots of polymineral fine grains. *Quaternary International* 293, pages 15–21. DOI: 10.1016/j.quaint.2012.01.002.

Vértes, L. (1965). *Az őskőkor és az átmeneti kőkor emlékei Magyarországon. [The remains of the Palaeolithic and Mesolithic ages in Hungary]*. Hungarian. Budapest, Hungary: Akadémiai Kiadó. 385 pages.

Vértes, L. (1966). The Upper Palaeolithic Site on Mt. Henye at Bodrogkeresztúr. *Acta Arch. Acad. Sci. Hung* 18, pages 3–14.

Vogel, J. C. and Waterbolk, H. T. (1964). Groningen Radiocarbon Dates V. *Radiocarbon* 6, pages 349–369. DOI: 10.1017/S0033822200010791.

Vojnogeografski Institut, N. N., editor (1968). *Boljevac*. Geološka i geofizička istraživanja, Belgrade, Serbia.

Vöros, I. (1982). Faunal remains from the Gravettian reindeer Hunters' campsite at Ságvár. *Folia Archaeologica* 33, pages 43–69.

Wacha, L. and Frechen, M. (2011). The geochronology of the "Gorjanović loess section" in Vukovar, Croatia. *Quaternary International* 240 (1), pages 87–99. DOI: 10.1016/j.quaint.2011.04.010.

Walker, M. J. C. (2005). *Quaternary dating methods*. Chisester, England: John Wiley and Sons. 286 pages.

Welter-Schultes, F. W. (2012). *European non-marine molluscs: a guide for species identification*. Planet Poster Ed. 760 pages.

Willis, K. J. and Andel, T. H. van (2004). Trees or no trees? The environments of central and eastern Europe during the Last Glaciation. *Quaternary Science Reviews* 23 (23-24), pages 2369–2387. DOI: 10.1016/j.quascirev.2004.06.002.

Willis, K. J., Rudner, E., and Sümegi, P. (2000). The Full-Glacial Forests of Central and Southeastern Europe. *Quaternary Research* 53 (2), pages 203–213. DOI: 10.1006/qres.1999.2119.

Wintle, A. G. and Murray, A. S. (2000). Quartz OSL: Effects of thermal treatment and their relevance to laboratory dating procedures. *Radiation Measurements* 32 (5), pages 387–400. DOI: 10.1016/S1350-4487(00)00057-3.

Wintle, A. G. and Murray, A. S. (2006). A review of quartz optically stimulated luminescence characteristics and their relevance in single-aliquot regeneration dating protocols. *Radiation Measurements* 41 (4), pages 369–391. DOI: 10.1016/j.radmeas.2005.11.001.

Yang, S., Ding, F., and Ding, Z. (2006). Pleistocene chemical weathering history of Asian arid and semi-arid regions recorded in loess deposits of China and Tajikistan. *Geochimica et Cosmochimica Acta* 70 (7), pages 1695–1709. DOI: 10.1016/j.gca.2005.12.012.

Zeeden, C., Hambach, U., Steguweit, L., Fülling, A., Anghelinu, M., and Zöller, L. (2009). Using the relative intensity variation of the Earth's magnetic palaeofield as correlative dating technique: A case study from loess with Upper Palaeolithic cultural layers at Poiana Cireşului, Romania. *Quartär* 56, pages 175–185.

Zeeden, C., Hambach, U., Steguweit, L., and Anghelinu, M. (2011). Loess stratigraphy using palaeomagnetism: Application to the Poiana Cireşului archaeological site (Romania). *Quaternary International* 240 (1), pages 100–107. DOI: 10.1016/j.quaint.2010.08.018.

Zeeden, C., Hambach, U., and Händel, M. (2015). Loess magnetic fabric of the Krems-Wachtberg archaeological site. *Quaternary International* 372, pages 188–194. DOI: 10.1016/j.quaint.2014.11.001.

Zeeden, C., Krauß, L., Kels, H., and Lehmkuhl, F. (2016a). Digital image analysis of outcropping sediments: Comparison to photospectrometric data from Quaternary loess deposits at Şanoviţa (Romania) and Achenheim (France). *Quaternary International* 429 (B), pages 100–107. DOI: 10.1016/j.quaint.2016.02.047.

Zeeden, C., Hambach, U., Veres, D., Fitzsimmons, K., Obreht, I., Bösken, J., and Lehmkuhl, F. (2016b). Millennial scale climate oscillations recorded in the Lower Danube loess over the last glacial period. *Palaeogeography, Palaeoclimatology, Palaeoecology*. DOI: 10.1016/j.palaeo.2016.12.029.

Zeeden, C., Kels, H., Hambach, U., Schulte, P., Protze, J., Eckmeier, E., Marković, S. B., Klasen, N., and Lehmkuhl, F. (2016c). Sedimentary data from the Semlac loess-paleosol sequence, supplement to: Zeeden, C., Kels, H., Hambach, U., Schulte, P., Protze, J., Eckmeier, E., Marković, S. B., Klasen, N., Lehmkuhl, F. (2016): Three climatic cycles recorded in a loess-palaeosol sequence at Semlac (Romania) - implications for dust accumulation in south-eastern Europe. Quaternary Science Reviews 154, pages 130-142. DOI: 10.1594/PANGAEA.859304.

Zeeden, C., Kels, H., Hambach, U., Schulte, P., Protze, J., Eckmeier, E., Marković, S. B., Klasen, N., and Lehmkuhl, F. (2016d). Three climatic cycles recorded in a loess-palaeosol sequence at

Semlac (Romania) – implications for dust accumulation in south-eastern Europe. *Quaternary Science Reviews* 154, pages 130–142. DOI: 10.1016/j.quascirev.2016.11.002.

Zeeden, C., Krauß, L., Lehmkuhl, F., and Kels, H. (2016e). Supplementary R script for manuscript 'Digital image analysis of outcropping sediments: comparison to photospectrometric data from Quaternary Loess deposits at Sanovita (Romania) and Achenheim (France)'. CRC806-Database. DOI: 10.5880/SFB806.17.

Zhang, J., Tsukamoto, S., Nottebaum, V., Lehmkuhl, F., and Frechen, M. (2015). De plateau and its implications for post-IR IRSL dating of polymineral fine grains. *Quaternary Geochronology* 30 (part B), pages 147–153. DOI: 10.1016/j.quageo.2015.02.003.